The purification and proteomic analysis of α-synuclein-containing inclusions in neurodegenerative disorders

A thesis submitted for the degree of Doctor of Philosophy, July 2013

Amellia McCormack, Bachelor of Science (Honours)

School of Medicine, Faculty of Health Sciences, Flinders University

Table of Contents

Table of Tables

Chapter 1

Chapter 2

Chapter 3

Chapter 4

Chapter 5

Chapter 6

Chapter 7

Table of Figures

Chapter 1

Chapter 2

Chapter 3

Chapter 4

Chapter 5

Chapter 6

Chapter 7

Summary

Neurodegenerative disorders affect a large proportion of the elderly population. A group of disorders, known as the α-synucleinopathies, are characterised by the presence of α-synuclein-containing protein inclusions, such as Lewy Bodies (LBs) found in neurons from Parkinson's Disease (PD) and Dementia with Lewy Bodies (DLB), and Glial Cytoplasmic Inclusions (GCIs) found in oligodendrocytes from Multiple System Atrophy (MSA). Since the discovery of LBs 100 years ago, some major inclusion proteins such as α-synuclein have been identified, but a detailed understanding of their protein composition has yet to be achieved. It is still not known how or why inclusions form and what role they play in the disease process. One hypothesis is that damaged proteins, unable to be degraded by the cell due to underlying proteasomal system or autophagic defects, are selectively targeted to inclusions via vesicle-mediated transport as a protective mechanism.

The analysis of the protein composition of inclusions has been hindered by ineffective methods for isolating the inclusions from the surrounding tissue. This was addressed in this study by optimising a published method for GCI purification by Gai *et al.* (1999) that utilises Percoll gradient density centrifugation combined with magnetic immunocapture. The optimised method gave a 28-fold increase in yield compared to the published method and a 2D-DIGE comparison showed a 3.8-fold increase in α-synuclein enrichment (the major protein in GCIs) and a corresponding 5.2-fold reduction in tubulin contamination. The optimised GCI purification method was then successfully adapted to the purification of LBs from DLB tissue.

A 2D-DIGE comparison of purified GCIs (n=6) and LBs (n=2) revealed that GCIs consist of 11.9% α-synuclein, 2.8% α-β-crystallin and 1.7% 14-3-3 proteins compared to 8.5%, 2.0% and 1.5% in LBs, respectively. A positive linear relationship was found between the relative quantities of α-synuclein and α-β-crystallin in inclusions from each case. The remaining 83-88% of inclusion proteins consists of more than 150 proteins possessing a diverse range of biological functions, including vesicle trafficking, cytoskeletal structure, protein degradation, chaperones, mitochondrial proteins and endoplasmic reticulum proteins.

The GCI protein identifications were performed by sequencing peptides using nanospray Orbitrap mass spectrometry. Peptides were obtained from complex mixtures of trypsin-digested GCI extracts purified from five MSA cases and from trypsin-digested 1-DE gel slices and 2-DE gel spots of GCI proteins. 160 proteins were identified in at least 4 out of the 5 MSA cases analysed. 21% of these 160 proteins were synaptic vesicle-related. The identification of LB proteins was performed by mass spectrometry of complex mixtures of trypsin-digested LB extracts from two DLB cases. Of the 112 proteins identified in both DLB cases and a minimum of 4 out of 5 MSA cases, 25% were synaptic vesicle-related, including synaptosomal-associated protein 25 and V-type proton ATPases.

This study has generated an optimised method for the purification of inclusions to a purity not achieved previously with a yield sufficient for multiple forms of analysis. A comprehensive characterisation of the protein composition of both GCIs and LBs has been performed, including the relative quantification of the major inclusion proteins α-synuclein and α-β-crystallin. The identification of a large set of vesicle-trafficking proteins suggests that α-synuclein may be targeted to LBs and GCIs via a common vesicle trafficking mechanism.

Declaration

I certify that this thesis does not incorporate without acknowledgment any material previously submitted for a degree or diploma in any university; and that to the best of my knowledge and belief it does not contain any material previously published or written by another person except where due reference is made in the text.

Amellia McCormack

Acknowledgements

Firstly, I would like to thank my supervisor, Tim Chataway, for his unwavering support during the last seven years of honours, employment, and finally this PhD. Your guidance on both this project and life in general has been invaluable. Thank you to Flinders University and specifically the Flinders Proteomics Facility for providing the resources to make this project possible and thank you to the FMC Volunteer Service for providing me with my scholarship, with especial thanks to Simon Brookes for providing me with my last four months of funding to make completion possible.

Thank you to my co-supervisor Wei-Ping Gai and to Fariba Chegini for teaching me the original purification technique, to Mark Slee and Malgosia Krupa for their assistance with the Nanozoomer scanning, to Damien Keating for enlightening discussions on vesicle proteins, and to John Power and Daniel Jardine for reading final drafts of my thesis. I would also like to thank the SA Brain Bank, the Human Physiology Department and the Centre for Neuroscience for their support – which really means thank you to Robyn Flook, Karen Price and Kiley MacDonald. Robyn's assistance with brain tissue requests was especially appreciated.

Spending time in the lab wouldn't have been nearly as enjoyable without labmates like Georgia Arentz, Nusha Chegini, and Alex Collela, for discussions of all things science and mostly things that were not. Lastly, thank you to my husband Nigel for his patience during this process and to my mother Susan for looking after our son while I worked and wrote, I couldn't have done this without either of you. And to my darling boy Jake, this thesis has taken me away from you far more than I wanted, so I dedicate it to you and hope you'll understand why one day.

Abbreviations

%	percentage
x g	x gravity
°C	degrees Celcius
µg	microgram
µL	microlitre
µM	micromolar
1°	primary
1-DE	one-dimensional electrophoresis
2°	secondary
2-DE	two-dimensional electrophoresis
2D	two-dimensional
aa	amino acids
ACN	acetonitrile
BSA	bovine serum albumin
CHAPS	3-[3-cholamidopropyl)dimethylammonio]-1-propanesulphonate
CID	collision-induced dissociation
cM	centimeter
Da	Dalton
DAB	3,3'-Diaminobenzidine
DIGE	Difference Gel Electrophoresis
DNA	deoxyribonucleic acid
DTT	dithiothreitol
EDTA	ethylenediaminetetraacetic acid
EtOH	ethanol
FA	formic acid
GE	General Electric
H_2O	water
HCl	hydrochloric acid
HPLC	high performance liquid chromatography
IEF	isoelectric focusing
IPG	immobilised pH gradient

kDa	kilodalton
LB	Lewy body
M	molar
mA	milliampere
mL	milliliter
mm	millimetre
mM	millimolar
mRNA	messenger RNA
MS	mass spectrometry
MS/MS	tandem mass spectrometry
m/Z	mass-to-charge ratio
NaCl	sodium chloride
ng	nanogram
nL	nanolitre
PAGE	polyacrylamide gel electrophoresis
pH	hydrogen ion concentration
pI	isoelectric point
PMSF	phenylmethanesulfonyl fluoride
ppm	parts per million
RNA	ribonucleic acid
rpm	revolutions per minute
SDS	sodium dodecyl sulphate
TBS	tris buffered saline
TBST	tris buffered saline Tween -20
Tris	Tris (hydroxymethyl) aminomethane
V	volts
v/v	volume per volume
W	watts
w/v	weight per volume

1 Introduction

1.1 Synucleopathic neurodegenerative disorders

Parkinson's Disease, Dementia with Lewy Bodies and Multiple System Atrophy are all synucleopathic neurodegenerative diseases. While varying in clinical and pathological presentation, they share a common link – α-synuclein-containing protein inclusions.

1.1.1 Parkinson's Disease

Parkinson's Disease (PD) is a progressive neurological disease that was first described by James Parkinson in 1817 [1-3]. It presents clinically with motor symptoms of a resting tremor, muscular rigidity, bradykinesia (slowness of movement) and postural instability [1, 4-6]. The presence of two of these four cardinal signs normally results in a diagnosis of parkinsonism [2, 5]. The presentation of symptoms can vary broadly, including a wide variety of non-motor symptoms, such as behavioural, cognition, sensory, autonomic, sleep disturbances and fatigue [2].

PD is the most common movement disorder and the second most prevalent neurodegenerative disease in the world (second to Alzheimer's) [5]. Incidence increases with age, from 1% of the population at 65 years of age up to 5% at 85 years of age [1, 5]. It is more prevalent in men than in women [2], with lifetime risks of 2.0% and 1.3%, respectively [7]. While patients can live for 20 years or more after diagnosis is first made, depending on the age of onset [2], quality of life is an issue for PD patients. The early onset form of the disease is the most severe.

PD is neurologically characterised by two main features – the progressive loss of dopaminergic neurons from the substantia nigra (SN) region of the brain [1, 4, 5], and the presence of intracellular proteinaceous inclusions know as Lewy Bodies (LBs) in the surviving neurons [1, 2, 5]. It is the loss of dopamine from the SN that causes the dysregulation of motor circuits, resulting in the clinical manifestations of the disease [1, 2]. The role LBs play in pathology is as yet unknown.

The cause of PD is likely to be a combination of genetic and environmental factors [4-6, 8]. The majority of PD cases are idiopathic [1, 5], with less than 10% of cases due to monogenetic inheritance [1, 4, 8]. The main risk factor for PD is advancing

age [1, 8]. A positive family history is also a risk factor [8], increasing the risk of developing PD by 3 to 4 fold compared to the general population [5]. Mutations in the gene encoding for the lysosomal enzyme glucocerebrosidase (GBA), a deficiency of which causes Gaucher's disease, are also found more frequently in patients with PD than control subjects [9]. Thus, GBA mutations are a risk factor for PD, implicating a link between lysosomal dysfunction and PD onset.

While there is contradicting evidence for environmental risk factors such as rural living, dietary factors and metals exposure, it has been consistently shown that pesticide exposure increases the risk of developing PD [10-12] whereas cigarette smoking is a negative risk factor [13, 14]. Symptomatic parkinsonism can also be caused by environmental insult, such as a tumour, toxins or drugs [2, 5], such as the 1-methyl-4-phenyl-1,2,3,6-tetra-hydropyridine(MPTP)-induced PD seen in some intravenous drug users [4].

No drugs or surgery currently available can slow the progression of PD, but for symptomatic relief, dopamine replacement therapy is the main approach [2]. The treatment of patients with L-dopa, an exogenous dopamine precursor, can help to alleviate motor symptoms [1], although patients can become resistant to treatment. Deep brain stimulation (DBS) of the subthalamic nucleus is an alternative treatment option for levodopa-responsive classical PD patients. DBS reduces the severity of symptoms, although the mechanism of improvement is obscure [15]. While the brain has traditionally been considered one of the most difficult organs to regenerate, neural grafting is also now being considered as a therapy for PD [16]. Fetal nigral cell grafting has been trialled in a clinical setting and these grafted dopaminergic neurons have been shown to survive and increase the uptake of dopamine under limited circumstances [17, 18]. Autologous cell transplantation has also been successfully trialled [19].

1.1.2 Dementia with Lewy Bodies

Dementia with Lewy Bodies (DLB) is a progressive dementing disorder, affecting the elderly [20]. It has previously been described under a variety of names, including Diffuse Lewy Body Disease (DLBD), Lewy Body variant of AD, and Lewy Body dementia [21, 22], but it was defined as DLB at a consensus conference in 1996 [23],

with the adoption of standardised clinical and neuropathological criteria for diagnosis [21].

DLB is the second most frequent neurodegenerative dementia in the elderly, with the most common being Alzheimer's disease [23-25]. It affects 0.7% of the population over 65 years [22], with the average age of onset being 75-80 years [23]. The length of survival for DLB patients is similar to those with Alzheimer's Disease, an average of 8 years from diagnosis [21].

DLB is characterised clinically by fluctuating cognition, visual hallucinations, and parkinsonism [20, 22-25]. The distinction in diagnosis between DLB and Parkinson's Disease with Dementia (PDD) is the timing. If motor symptoms precede the development of cognitive dysfunction by less than a year, the diagnosis is DLB. If dementia does not present until more than a year after the onset of parkinsonism, then a diagnosis of PDD is made [22-25]. Confirmation of diagnosis occurs post-mortem.

As for PD, DLB is characterised pathologically by the presence of Lewy Bodies. In DLB, these are found in the cerebral cortex and brain stem nuclei [2, 20, 23]. Alzheimer's disease pathology is also found to often co-exist in DLB patients [23, 24]. DLB is usually sporadic, but familial forms exist, with similar genes implicated to those in PD [24]. Given the overlap in clinical presentation and pathological features, it is argued that PD, PDD and DLB are a spectrum of LB disorders instead of single disease entities [24, 25].

Neurologically, DLB patients display a reduction in choline acetyltransferase, resulting in low acetylcholine levels in the cortex and decreased cholinergic transmission [23]. This is correlated with the cognitive deficits in DLB patients [25], so acetylcholinesterase inhibitors, such as donepezil, rivastigmine and galantamine, are often used as a first-line therapy for DLB to treat cognitive symptoms [22, 23, 26]. Dopamine deficiencies are also common in DLB, so dopamine replacement therapy in the form of L-dopa can be used for the treatment of motor symptoms [23]. However, DLB patients often display a decreased L-dopa responsiveness compared to PD patients [25].

1.1.3 Multiple System Atrophy

Multiple System Atrophy (MSA) is a sporadic, progressive, adult-onset neurodegenerative disorder. It was established as a single clinicopathological disease entity between 1969 and 1984 [27], incorporating the disorders previous known as striatonigral degeneration (SND), Shy-Drager Syndrome (SDS) and sporadic olivopontocerebellar atrophy (OPCA).

MSA is clinically characterised by parkinsonism, cerebellar ataxia, autonomic failure, and pyramidal signs [28-31]. It is pathologically characterised by the presence of oligodendroglial cytoplasmic inclusions (GCIs) [29-31], which are proteinaceous inclusions similar to LBs, and features neuronal cell loss and gliosis [29, 32]. The most severe neuronal losses are found in the putamen, the substantia nigra, the pontine nuclei, the inferior olivary nuclei, the Purkinje cells and the intermediolateral nuclei of the spinal cord [33]. MSA cases can be classified into two different clinicopathological phenotypes – predominantly parkinsonism (MSA-P) or predominantly cerebellar ataxia (MSA-C), which are SND-predominant and OPCA-predominant, respectively [28, 34].

MSA is less frequent in the population than PD [31] and it appears to be more common in men than in women [33]. The average age of patients at onset is 54-58 years, with an average survival of 6 to 7 years [33, 34]. The MSA-P phenotype is most prevalent in Caucasian populations, whereas the MSA-C phenotype is more common in Japanese and Chinese populations [28, 34].

The cause of MSA is unknown and it is likely that a variety of genetic and environmental factors are responsible, as for PD. While it appears to be sporadic, there has been some familial clustering reported, suggesting genetic causes [31]. Scholz *et al.* [35] have demonstrated an association between MSA risk and single nucleotide polymorphisms (SNPs) in the α-synuclein gene. These genetic risk factors were shown to overlap with those for PD, suggesting a common genetic etiology [35]. There is a higher risk of developing MSA associated with occupational exposure to organic solvents, plastic monomers, pesticides and metals [29] and with an occupational history of farming [36], which would presumably involve exposure to a similar set of substances. As in PD, it appears smoking has a protective effect [37].

1.2 Inclusion bodies

The two principles types of α-synuclein-containing protein inclusions found in synucleopathic neurodegenerative diseases are Lewy Bodies, present in neurons in PD and DLB, and Glial Cytoplasmic Inclusions, present in oligodendrocytes in MSA. However, there are other inclusions present in less abundance, including Lewy Neurites and pale bodies in PD and DLB, and Neuronal Cytoplasmic Inclusions and Neuronal Nuclear Inclusions in MSA.

1.2.1 Lewy Bodies

Lewy Bodies (LBs) were first described by Friederich H. Lewy in 1912 [3, 38]. LBs are eosinophilic aggregates of filamentous structures, resembling neurofilament, and they may also contain vesicular or circular structures [38]. There are two types of LBs – the brainstem (classical) type and the cortical type [38]. Brainstem LBs are found in the cytoplasm, with either single or multiple LBs present in a neuron. They are spherical or elongated in shape, with a dense core and a peripheral halo [38]. In contrast, cortical LBs are poorly defined with an irregular shape, often lacking a central core or conspicuous halo [38].

LBs are widely distributed throughout the central nervous system (CNS), including in the substantia nigra, hypothalamus, nucleus basalis of Meynert, locus ceruleus, dorsal raphe nucleus, intermediolateral nucleus of the spinal cord and sacral autonomic nucleus [38, 39]. Similar inclusions have also been found in the peripheral autonomic nervous system and the enteric system of PD patients [38]. The widespread distribution of LBs may correspond to the variety of motor and non-motor symptoms present in PD [38].

Prior to the formation of a LB, α-synuclein immunoreactivity is not seen in the neuronal cytoplasm [38]. In the first stage of LB formation, a diffuse, pale cytoplasmic staining can be seen in otherwise morphologically normal neurons, and in the second stage of formation a moderately intense, irregular shaped, uneven staining is seen in poorly pigmented neurons [38]. In the third stage of formation, a discrete staining is seen, corresponding to pale bodies (see section 1.2.3), followed by a ring-like staining showing a typical LB with a central core and surrounding halo in the fourth and last stage of formation [38].

While the function of LBs is currently unknown, there are two opposing theories on the relationship between LBs and neuronal loss. The first is that LBs are a toxic aggregation of proteins, that contribute directly to neuronal death [8]. The second is that LBs are a protective mechanism that sequester potentially toxic excess or misfolded α-synuclein that cannot be degraded by the cell [8, 38].

The major constituent of LBs is α-synuclein [1, 8, 38], including truncated, oxidized and phosphorylated variants [6]. The most common modification is a single phosphorylation at Ser129, discovered by Anderson *et al.* [40]. Over 90% of insoluble α-synuclein in DLB brains is phosphorylated at Serine 129, whereas only 4% of normal α-synuclein is phosphorylated at this site [38]. *In vitro*, phosphorylation at Serine 129 accelerates oligomerisation and promotes formation of insoluble filaments, compared to non-phosphorylated α-synuclein, so it is proposed that phosphorylation is a necessary step in LB formation [38]. Phosphorylated α-synuclein is also ubiquitinated [38], and other proteins present in LBs are often highly ubiquitinated as well [1], indicating that they have been targeted for clearance by the ubiquitin-proteasome system but have been unable to be degraded.

There have been more than 70 proteins identified in LBs, including: structural elements of the LB fibrils such as neurofilament and other cytoskeletal proteins such as tubulin; α-synuclein-binding proteins such as 14-3-3 and synphillin-1; components of the ubiquitin-proteasome system; and others [38]. However, an *ad hoc* approach has been taken to the identification of these components and it is not known what relative concentrations they occur in.

Tau, which is present in neurofibrillary tangles in Alzheimer's disease, is also reported to be present in LBs. It may co-aggregate with α-synuclein and together they may interact to promote the formation of α-synuclein fibrils [4]. Detection of Leucine Rich Repeat Kinase 2 (LRRK2) protein in LBs has also been reported [41]. PINK1 protein has been shown with immunohistochemistry to be present in approximately 5-10% of brainstem LBs in sporadic PD [42]. Parkin has been found in LBs [43], with parkin and synphilin-1 proteins showing a colocalisation in the central core of LBs [44]. Synphilin-1 is an α-synuclein binding protein, so parkin and α-synuclein may be linked in a common pathogenic mechanism through their interaction with synphilin-1 [38].

1.2.2 Glial Cytoplasmic Inclusions

Glial cytoplasmic inclusions (GCIs) are found in the cytoplasm of oligodendrocytes. They are filamentous structures, consisting of a loosely packed meshwork of granular-coated fibrils [30, 31]. GCIs can be either sickle, triangular, half moon, oval or conical in shape within the same section of tissue [30, 34]. They are both argyrophilic [30, 34] and eosinophilic [34]. In oligodendrocytes that contain GCIs, the nuclei are slightly larger than in non-GCI bearing cells [27].

GCIs are widely distributed throughout the CNS [27, 30]. They appear more frequently in white matter than in grey matter [27]. Areas of the CNS that contain a higher density of GCIs are the subcortical areas of the motor cortex, pre-motor cortex and supplementary motor areas, and the dorsolateral putamen [27, 34]. The prevalence of GCIs in specific areas of the brain relates to whether the patient has the MSA-P or MSA-C phenotype [27, 45], with GCIs contributing more to the MSA-C phenotype pathology than the MSA-P type [45].

Even in the earliest stages of MSA, GCIs are present. They increase in abundance as the disease progresses, with a correlation between GCI frequency and the severity of olivopontocerebellar degeneration [27, 45]. This is unlike PD and DLB, where the frequency of LBs does not correlate with the degree of striatonigral degeneration [27, 45]. At the advanced stage of MSA, with severe cerebellar devastation, GCIs are absent altogether [27].

α-synuclein is thought to be the most abundant protein present in GCIs [28, 30, 31]. The form present in GCIs is misfolded and relatively insoluble, with predominant oxidative and nitrative modifications [28]. This accumulation of α-synuclein in oligodendrocyte inclusions is unexpected, as α-synuclein is a neuronal protein that is expressed transiently in developing oligodendrocytes but not in the mature cells [46, 47]. The expression of α-synuclein mRNA in oligodendrocytes is negligible or none [48], and there is no increase in α-synuclein mRNA expression between MSA brain tissue and control brain tissue [49]. The presence of full-length α-synuclein in the CSF provides evidence that it is released extracellularly from neurons [50], but it is still unknown how or why it accumulates in GCIs in oligodendrocytes.

Another strong marker for GCIs is tubulin polymerisation promoting protein (TPPP), also known as p25 [51]. TPPP is an oligodendroglia-specific phosphoprotein linked to myelination, as it mediates interactions between myelin binding protein (MBP) and tubulin [31]. It has also been shown *in vitro* to bind to α-synuclein filaments and stimulate α-synuclein aggregation [51].

Others proteins found in GCIs include rab3, which is a member of the Ras family of small GTP-binding proteins, 14-3-3 protein, heat shock protein 90, and DJ-1, which is implicated in PD [28].

1.2.3 Other α-synuclein-containing inclusions in PD, DLB and MSA

Lewy Neurites (LNs) are found concurrently with LBs, but are present in the axonal processes rather than in the main cell body. LNs are usually coarse and round in structure, although they can also extend in an elongated or serpentine fashion [52]. LNs immunostain positive for α-synuclein [52-54].

Pale bodies are distinct inclusions found in neurons in the SN and locus ceruleus, frequently occurring concurrently with LBs [38]. They contain sparse granular and vesicular structures, and filaments identical to those found in LBs [38]. They are well defined, appearing glassy without halos, and are less eosinophilic than LBs [38]. Pale bodies immunostain intensely positive for α-synuclein and weakly positive for ubiquitin [38]. The number of pale bodies is larger than the number of LBs in the early stages of PD, and they are postulated to be closely related to LB formation [38].

Also found in MSA patients are neuronal cytoplasmic inclusions (NCIs) and neuronal nuclear inclusions (NNIs), but the presence of these is less common than GCIs [31, 55]. They are found in the inferior olivary nucleus, pontine nucleus, putamen, and occasionally the cerebral cortex [28]. As for other protein inclusions, their role is not understood [28]. NCIs contain α-synuclein as a major component. [55, 56]. The form of α-synuclein present is phosphorylated at Serine 129 [56]. It has also been reported that some NCIs are α-synuclein negative when immunostaining, but positive for TPPP [55], another major protein component of GCIs.

1.3 Genetic mutations in familial synucleopathies

There have now been seven different loci identified in familial PD (Table 1.1).

Table 1-1: Loci identified in familial PD

Locus	Gene	Inheritance	Present in LBs using IHC
PARK1(4)	α-synuclein	AD	Yes
PARK8	LRRK2	AD	Yes
PARK2	Parkin	AR	Yes
PARK7	DJ-1	AR	Yes
PARK6	PINK1	AR	Yes
PARK5	UCH-L1	AD	Yes
PARK9	ATP13A2	AR	No

AD = autosomal dominant, AR = autosomal recessive

This has led to an interest in identifying common genetic variants of familial PD genes in sporadic PD [4]. However, combination genotype interactions may be more important than single candidate genes [8].

1.3.1 α-synuclein

The α-synuclein gene is found on chromosome 4q21-23 and has an autosomal dominant mode of inheritance [8] with incomplete penetrance [1]. While some studies suggest α-synuclein mRNA is upregulated in sporadic PD [4], mutations have been found lacking in large population studies of sporadic disease [8]. It is interesting that α-synuclein has a major role in sporadic PD, and yet mutations in this gene are a rare cause of PD [1].

In familial inheritance, there are three substitution point mutations commonly known in PD: A53T, A30P and E46K. Although all three of these mutations enhance the aggregation of α-synuclein [39], only the first two of these are associated with an increased propensity to form protofibrils [1]. The A30P mutation is associated with 'classic' PD, the A53T and E46K mutations are associated with the spectrum of PD, PDD and DLB [24]. Very recently, two new point mutations have been discovered. Proukakis *et al.* [57] reported the mutation H50Q, which affects copper coordination, in a single case. Kiely *et al.* [58] reported the mutation G51D in a family with early-onset PD, with clinical symptoms similar to those with A53T and triplication mutations.

The α-synuclein gene can also have duplication and triplication mutations, which cause early onset PD [1, 4, 38]. The enhanced expression of α-synuclein increases its deposition into insoluble aggregates. The age of onset and the severity of symptoms are correlated with the copy number, indicating a gene-dosage effect [1, 4, 6]. Duplications and triplications are also found in DLB patients, with duplications more often associated with 'classic' PD, and triplications associated more often with PDD and DLB [24].

The α-synuclein protein is a member of the synuclein family, which includes β-synuclein, γ-synuclein and synoretin [1]. It has 140 amino acids and a theoretical molecular weight of 14.5 kDa. It has an N-terminal α-helical region, a hydrophobic central component and an acidic C-terminal region [1, 59] (see Figure 1.1). Traditionally is has been considered natively unfolded in solution, adopting an α-helical configuration in lipid containing vesicles and aggregating into β-sheets at high concentrations [8]. More recently, Bartels *et al.* [60] have proposed that endogenous α-synuclein exists largely as a helically folded tetramer of approximately 58 kDa.

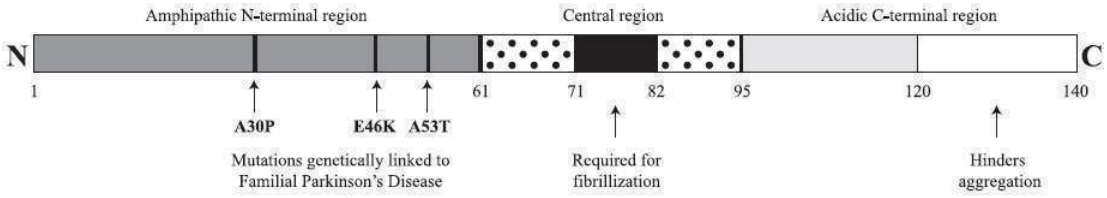

Figure 1-1: Structure of α-synuclein protein [59]
The protein is 140 amino acids long with an amphipathic N-terminal region, hydrophobic central region and acidic C-terminal region.

Aggregated α-synuclein can then take two pathways – the off-fibril pathway, where annular oligomers are formed, or the fibrillar pathway, where oligomers form into protofibrils before forming the long fibril strands that are incorporated into LBs [61] (see Figure 1.2). As LBs contain fibrillar α-synuclein, it is important to understand the properties of these fibrils and the process of their formation [59]. The central hydrophobic region of α-synuclein is necessary for fibrilisation, whereas the negatively charged C-terminal region hinders aggregation [61]. Thus, C-terminal

truncations may promote the aggregation of α-synuclein. α-synuclein truncated at Asp-119 has been found inside LBs, as well as a variety of other C-terminal truncated species [40], which supports this hypothesis.

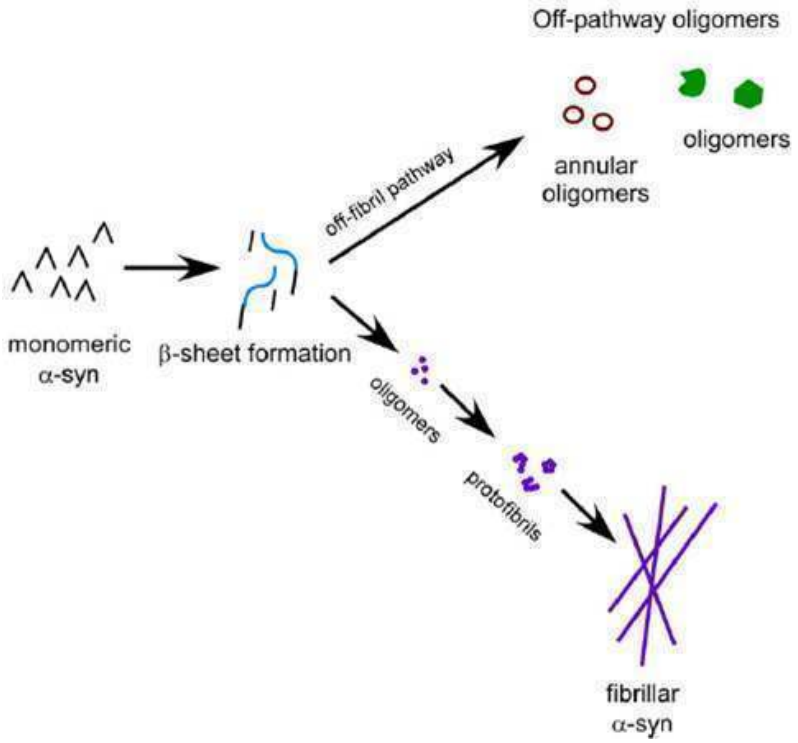

Figure 1-2: Formation of α-synuclein aggregates [61]
Monomeric α-synuclein aggregates into β-sheets and takes either the off-fibril pathway to form annular oligomers or the fibrillar pathway, where oligomers form into protofibrils followed by long fibrillar strands.

α-synuclein is abundant in the adult human brain, with ubiquitous but heterogeneous expression [1]. It is particularly abundant in neurons in the substantia nigra (SN), hypothalamus, olfactory neurons, cerebral neocortex and hippocampus [8]. It is found in the cytosol as well as associated with membranes [62], although mutant forms exhibit increased nuclear targeting [6]. It is also expressed in other tissues.

α-synuclein is a presynaptic nerve terminal protein [38], but its normal function in neurons is not well understood [1]. It has been postulated to participate in the maturation of presynaptic vesicles and the regulation of neurotransmitter release [6], as well as being implicated in learning and neuronal plasticity [1]. It has also been suggested to bind to lipids [6], connecting it with lipid-mediated signalling,

trafficking and metabolism [1]. α-synuclein's natively unfolded structure means it can bind to a broad range of proteins, which makes it difficult to identify targets. Knock-out mouse models of α-synuclein are non-lethal with intact brain morphology, so it is either not required for neuronal development or a compensatory mechanism is in place [63, 64].

The mechanism behind α-synuclein toxicity has yet to be fully elucidated. It is thought that the soluble, oligomeric forms of α-synuclein are the toxic species rather than the aggregated, insoluble fibrils observed in LBs [1], which is a way of sequestering toxic proteins away within the cell if they are unable to be degraded. A simple increase in soluble monomeric α-synuclein may cause cellular toxicity [61]. This occurs with the genetic duplication and triplications of the α-synuclein gene that lead to PD, as well as other non-genetic causes of α-synuclein increase that lead to PD [65]. Enhanced α-synuclein expression is associated with the normal ageing process [65] which is the main risk factor for PD.

Some forms of α-synuclein oligomers and protofibrils have also been proposed to be toxic species, although thus far there is a lack of in *vivo* studies to support this hypothesis [61]. α-synuclein oligomers and fibrils have been proposed to possess cytotoxic properties, such as the ability to permeabilise membranes [65], as pre-fibrillar species are though to have a pore-like activity [59]. Alternatively, the mature α-synuclein fibrils may be toxic by impairing normal cellular function, impairing proteasome function, and acting as a 'sink' by incidentally binding proteins required for normal cellular functions [61].

1.3.2 Leucine Rich Repeat Kinase 2

The leucine rich repeat kinase 2 (LRRK2) gene has an autosomal dominant mode of inheritance with incomplete penetrance [1]. It has no gene-dosage effect, as there is no difference between homozygous and heterozygous carriers [6]. LRRK2 mutations are the most common known cause of familial and sporadic PD [6]. At least 16 pathogenic mutations are known, which cluster in the C-terminal region of the protein [6].

The Gly2019Ser point substitution is the most studied [1, 6], accounting for approximately 5% of familial cases and 1-2% of sporadic cases [1, 4]. Another point

substitution is the Gly2385Arg variant, where the arginine may modify interactions with other proteins that this region would normally bind, and may inhibit kinase activity [4].

LRRK2 is a very large protein of 2,527 amino acids in length, with a molecular weight of 285kDa. It is expressed from 51 exons coding for several functional domains [1, 6]. Its N-terminal contains leucine-rich repeats and its C-terminal has WD40 repeats, which are both likely to mediate protein-protein interactions [1, 66] (see Figure 1.3). The expression of LRRK2 in dopaminergic neurons in the SN is surprisingly low [67] when compared to proteins such as Parkin and DJ-1, but it has high expression rates in striatal neurons that receive dopaminergic input [67].

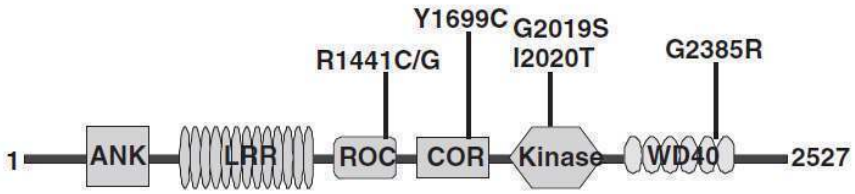

Figure 1-3: Structure of LRRK2 protein [66]
The protein is 2,527 amino acids long and contains leucine-rich repeats (LRR) in the N-terminal region and WD40 repeats in the C-terminal region, both of which mediate protein-protein interactions.

LRRK2 belongs to the ROCO family, which is a novel group of the Ras GTPase superfamily [1]. Its normal and mutant functions are unclear [1], although it does demonstrate kinase activity *in vitro* [1, 6] and mutations appear to enhance this activity [1]. While LRRK2 mutations are unexpectedly common, there is as yet no indication as to how the protein contributes to PD [1].

1.3.3 Mitochondrial-related genes

Parkin, DJ-1 and PTEN-induced putative kinase 1 (PINK1) proteins are all related to mitochondrial function, a deficit in which is hypothesised to play a major role in the development of PD.

The parkin gene is found on chromosome 6q25.2-q27 and has an autosomal recessive mode of inheritance [8]. There have been numerous mutations identified in parkin,

including point mutations, deletions and multiplications [8], which are associated with early onset PD [1].

The parkin protein is 465 amino acids long [8] and has been shown to localise to the mitochondrial matrix [1]. Parkin is an E3 ubiquitin ligase, which is involved in targeting proteins for degradation to the ubiquitin proteasome system (see Section 1.4.1) [6]. It has an ubiquitin homologous domain in the N-terminus and two RING finger domains in C-terminus, which have an ubiquitin ligase function [1, 8]. It has been shown to mediate proteasome-independent monoubiquitylation as well as proteasome-linked polyubiquitylation [6]. The normal localisation and activity of parkin may be regulated by its multiple binding partners [1].

Parkin interacts with α-synuclein [8], so it is possible that mutated forms of parkin cannot bind α-synuclein, resulting in its accumulation and potential cytotoxicity [8]. However, both α-synuclein and ubiquitin positive inclusions are found in patients with compound heterozygous deletions and/or mutations [1]. There is evidence for parkin dysfunction occurring in sporadic PD. Oxidative stress and S-nitrosylation lead to the modification and inactivation of native parkin, and dopamine also covalently modifies and functionally inactivates parkin [1]. There is also a protective role for parkin within mitochondria, but the precise mechanism is unknown [1].

DJ-1 has autosomal recessive inheritance. It is enriched in the brain and ubiquitously expressed, found largely in the cytoplasm except for a pool located in the mitochondria [1, 6]. DJ-1 acts as a redox-dependent chaperone to protect neurons from oxidative stress [1, 6]. Because of this it contains many residues that are readily oxidized, but extensive oxidation inactivates it [1]. In the brains of patients with idiopathic PD, DJ-1 has been found to be oxidatively damaged, suggesting that the aggregation of proteins in PD is mediated by high levels of oxidative stress [1].

PTEN-induced putative kinase 1 (PINK1) has autosomal recessive inheritance. The protein is 581 amino acids long and it is poorly soluble with a propensity to aggregate [1]. It is ubiquitously expressed in the human brain [1], but is mainly located inside the mitochondria [6]. It is targeted to the mitochondrial membrane via a N-terminal targeting motif [1].

PINK1 has a role in aiding mitochondrial function and it may act upstream of parkin to protect mitochondria integrity [1, 6]. It has a catalytic serine-threonine kinase domain [1] and mutations in PINK1 are located near or with this domain, which is though to result in a loss of function effect [6].

1.3.4 Protein degradation-related genes

The ubiquitin C-terminal hydrolase L1 (UCH-L1) and ATP13A2 proteins are both related to protein degradation, with the former involved in the ubiquitin-proteasome system and the latter involved in lysosomes.

The UCH-L1 gene is found on chromosome 4p14-15.1 and has an autosomal dominant mode of inheritance [8]. It is a very rare cause of familial PD, which so far has only been identified in one family [8]. There have been two point mutations identified in this gene, an Ile93Met mis-sense mutation and a Ser18Tyr variant. The latter gives the protein reduced ligase activity but comparable hydrolase activity, which has been shown as a protective mutation in some studies as it facilities the degradation of α-synuclein by the ubiquitin-proteasome system [4].

The UCH-L1 protein has two opposing enzymatic activities that affect the degradation of α-synuclein by the ubiquitin-proteasome system (see section 1.4.1). By hydrolysing polyubiquitin chains to generate re-usable ubiquitin monomers, the ubiquitination and subsequent proteasomal degradation of α-synuclein is promoted [4, 8]. However, it also has a dimerisation-dependent ubiquityl ligase activity, which ligates ubiquitin via a Lys63 linkage to α-synuclein, preventing the degradation of α-synuclein [4].

The ATP13A2 gene is found on chromosome 1p36 and has an autosomal recessive mode of inheritance [6]. The ATP13A2 protein is normally localised in lysosomes. Truncated mutants are retained by the endoplasmic reticulum and degraded by the proteasome system [6]. It functions predominately as a neuronal ATPase, but its contribution to lysosomal integrity in LB-affected neurons is not currently known [6].

1.4 Protein degradation systems

There are two main systems for intracellular protein degradation – the Ubiquitin-Proteasome System (UPS) and the Autophagy-Lysosomal Pathway (ALP). The role of these systems is to prevent the build-up of wrongly synthesised, misfolded and damaged proteins by degrading them and recycling their constituents for future use. This clearance of proteins is of particular importance in neurons, as they are post-mitotic cells and cannot 'dilute out' toxic proteins via cell division [68, 69].

1.4.1 Ubiquitin-Proteasome System

The ubiquitin-proteasome system (UPS) is responsible for the selective degradation of proteins, such as those that are damaged, misfolded, or present at the wrong concentration in the cell [70]. Proteins with short half-lives and rapid turnover are normally degraded by the UPS [68, 71]; long-lived proteins are normally degraded by the ALP instead. For a protein to be degraded by the UPS, it first has to be targeted for degradation by the covalent addition of a polyubiquitin chain, then it has to be translocated into a 26S proteasome for degradation [72].

Ubiquitin is a highly conserved 76 amino acid protein [73]. It has an array of diverse functions, as it can interact with a whole host of ubiquitin-interacting proteins via conjugation to a lysine residue. A single ubiquitin molecule can act as a sorting signal in endosomal and biosynthetic pathways [74], but it can also be conjugated to itself to form polyubiquitin chains on any of its seven lysine residues – 6, 11, 27, 29, 33, 48 and 63 [72]. Polyubiquitination at Lys63 leads to numerous downstream events, such as DNA repair and signal transduction [72, 74]. By contrast, polyubiquitination of four or more residues at Lys48 or Lys 29 marks a protein for degradation by the 26S proteasome [72, 74].

The targeting of proteins for degradation is an enzyme mediated, ATP-dependant process [73]. It involves a set of three types of enzymes – E1 (ubiquitin-activating), E2 (ubiquitin-conjugating), and E3 (ubiquitin-ligating) [73]. These enzymes work together to conjugate ubiquitin to lysine residues on target proteins to form polyubiquitin chains targeting the proteins for degradation, as shown in Figure 1.4. [73, 75].

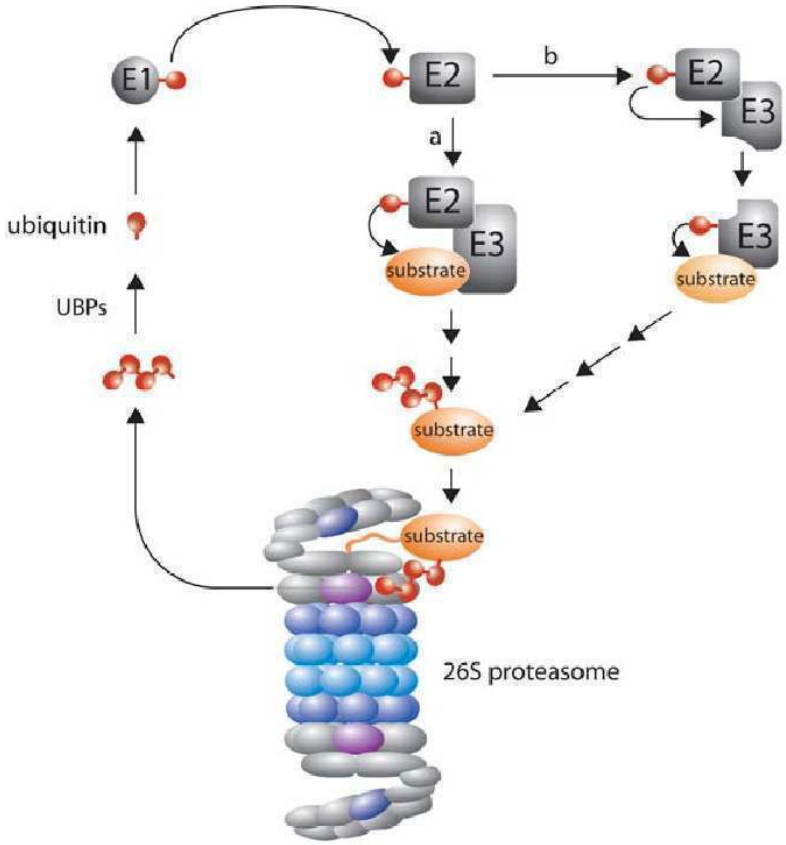

Figure 1-4: UPS pathway [75]
The free ubiquitin monomers are attached to a protein substrate to target it for degradation in the 26S proteasome via a series of enzymes – E1 (ubiquitin-activating), E2 (ubiquitin-conjugating) and E3 (ubiquitin-ligating).

The 26S proteasomes are found in the cytosol, perinuclear and nuclear regions of eukaryotic cells [70]. The structure of a 26S proteasome is shown in Figure 1.5. It consists of a 20S catalytic core unit with 19S (PA700) regulatory caps on each end [72, 76]. The core consists of two heptameric α rings on the outside of two central heptameric β rings [70, 72]. The 20S core and each of the 19S caps are approximately 700 kDa each, forming a 2100 kDa complex [77].

Proteins are targeted to the 19S regulatory caps by ubiquitination. The 19S caps are responsible for the recognition and unfolding of targeted proteins and their translocation into the central core of the complex [72, 76]. The enzymatic activity in the central β rings of the 20S core degrades the proteins back into short peptides and single amino acids for re-use in the cell. Ubiquitin carboxy-terminal hydroxylases convert the polyubiquitin chain back into monomeric ubiquitin for re-use [70].

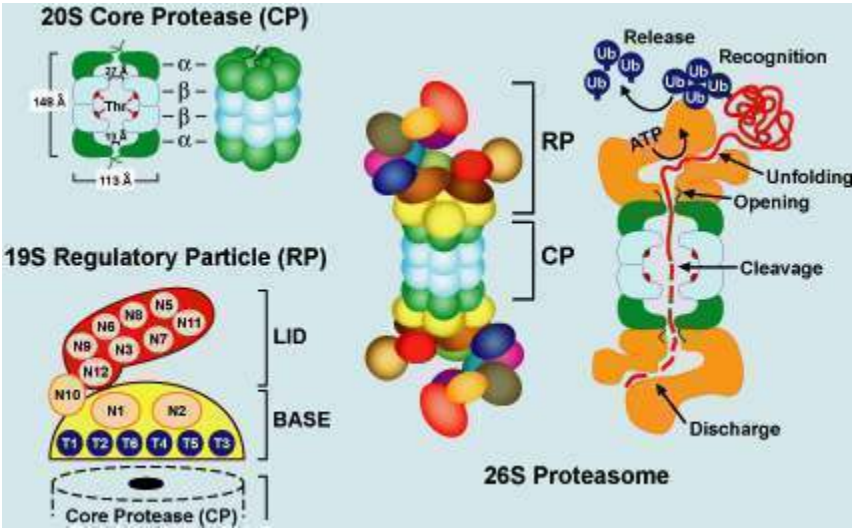

Figure 1-5: The structure of the 26S proteasome
(http://plantsubq.genomics.purdue.edu/plantsubq/html/guide.html)
The 26S proteasome consists of a 20S core protease (CP) with a 19S regulatory particle (RP) at each end. The substrate recognition occurs at the regulatory cap and the substrate cleavage occurs in the core protease region.

1.4.2 Autophagy Lysosomal Pathway

The autophagy-lysosomal pathway (ALP) is a less selective, bulk degradation process compared to the UPS and it is responsible for the turn-over of longer-lived proteins [68]. The ALP serves two purposes in the cell: the removal of aged, altered and potentially damaged components of the cell, including proteins; and the supply of macromolecules and energy during starvation conditions and for the anabolism of new compounds [68, 69].

Autophagy is the process where cytoplasmic compounds such as proteins are delivered to lysosomes for enzymatic degradation [68]. There are three main types of autophagy – microautophagy, chaperone mediated autophagy (CMA) and macroautophagy, depicted in Figure 1.6. All types of autophagy end in lysosomal degradation, but they differ in the substrates targeted, their regulation, and conditions of activation [69].

In microautophagy, small areas of the cytoplasm are sequestered by lysosomal invagination and directly engulfed by the lysosomes for rapid degeneration [68, 69]. This provides a continuous basal turnover of cellular components under normal conditions and this is also the method by which peroxisomes are removed from the

cell [69]. It cannot be easily replicated and manipulated in models, so it is difficult to associate microautophagy with particular disease states [69].

In CMA, proteins with a pentapeptide lysosomal targeting motif are targeted to a LAMP2A receptor on the surface of the lysosomal membrane, which then translocates the protein into the lysosome for degradation [68]. This type of autophagy is particularly useful for damaged proteins, due to its selectivity [69].

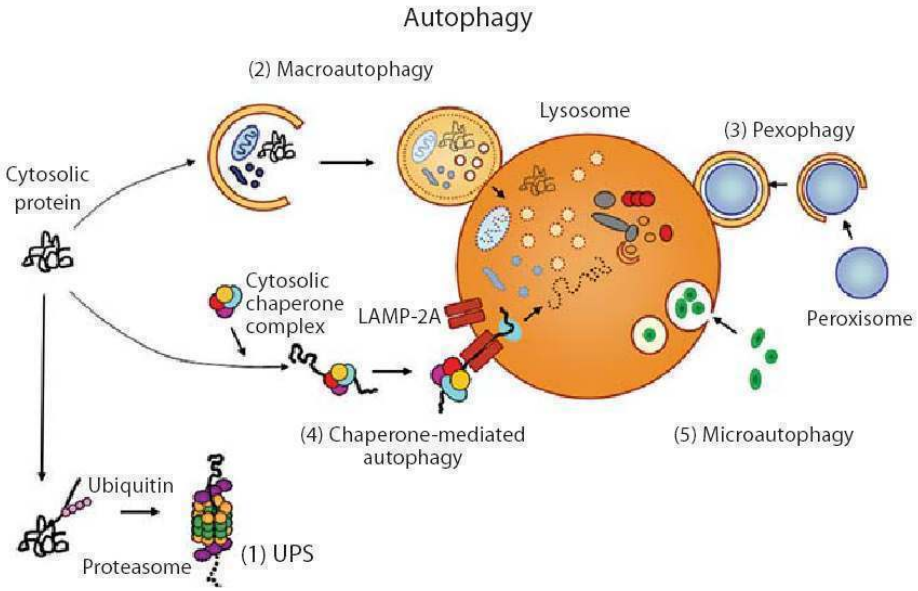

Figure 1-6: Types of autophagy [68]
The three main types of autophagy are macroautophagy (2), chaperone-mediated autophagy (4) and microautophagy (5). Also pictured are pexophagy (3) and the UPS pathway (1).

The term 'autophagy' usually refers to the third type of autophagy, also described as macroautophagy (see Figure 1.7). In macroautophagy, a double-membrane structure known as an isolation membrane or phagosome expands to sequester the portion of the cytoplasm that contains the proteins to be degraded, thus forming a new vacuole termed an 'autophagosome' [68, 69]. This autophagosome then undergoes fusion processes with late endosomes and multivesicular bodies to form an amphisome [68]. This amphisome fuses with a lysosome to generate an autolysosome, in which the hydrolytic enzymes from the lysosome break down the contents of the autosome [68, 69]. The macromolecule components resulting from this degradation are then released from the autolysosome to participate in new anabolic processes [68].

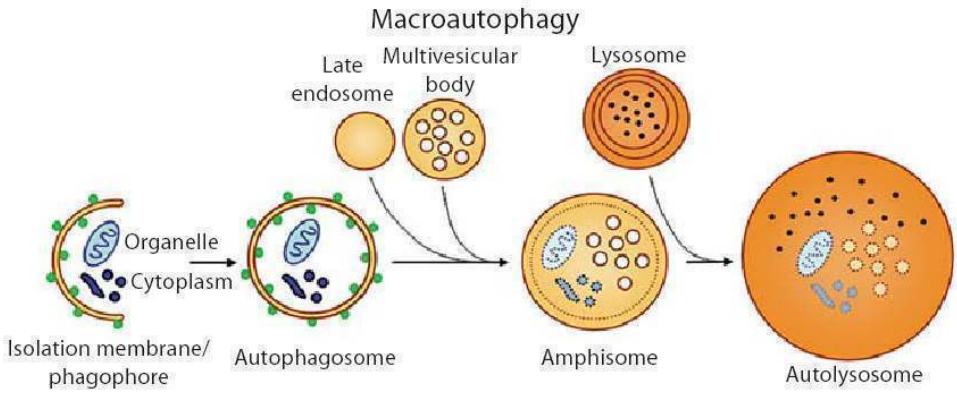

Figure 1-7: Macroautophagy [68]
The process of macrophagy is depicted, where an isolation membrane sequesters the portion of the cytoplasm targeted for degradation and undergoes a series of steps until an autolysosome is formed and the contents are degraded.

This formation of an autolysosome is controlled by a large number of highly conserved Atg genes (autophagy related genes) [68]. These genes code for a family of autophagy related proteins that are involved in the formation process described above, by performing a series of protein-protein and protein-lipid conjugations [69].

1.5 Hypotheses behind inclusion body formation

Hypotheses behind inclusion body formation include impairment of the UPS, impairment of the ALP, mitochondrial dysfunction and oxidative stress [6, 8, 38]. While there is evidence for the involvement of each of these mechanisms in the pathogenesis of PD, it is difficult to determine which defects cause neurodegeneration and which defects are symptomatic of neurodegeneration, as well as how deficiencies in these different systems relate and interact with each other.

1.5.1 UPS impairment

The accumulation of ubiquitinated proteins in inclusions occurs in all chronic neurodegenerative diseases [78]. These proteins may accumulate in preference to degradation due to UPS failure, with the non-degraded proteins accumulated in aggresomes to protect the cell from toxicity [78]. The UPS maintains the levels of a number of important components, including p53 and caspase-3, so a compromised UPS can affect the pathways regulated by these components and cause cell death [79].

Evidence for proteasome dysfunction in PD pathogenesis has been shown in post-mortem tissues and animal models. When post-mortem tissue from the SN region was evaluated using enzymatic assays, PD patients showed significant decreases in chymotrypsin-like, trypsin-like and caspase-like activity compared to age-matched controls [80]. Animal models can mimic features of PD by the administration of proteasome inhibitors [78], although these studies are controversial due to a lack of reproducibility.

The discovery of a loss-of-function mutation in the *parkin* gene in familial PD also provides a key link between the UPS and the development of PD, as parkin functions as an E3 ligase [79, 81]. When its role is compromised, neurodegeneration occurs, as parkin substrates can accumulate and cause neurotoxicity [79]. Age- or stress-induced mutations can also alter the solubility of the parkin protein and promote its aggregation in the cell, thus removing functional soluble parkin [79]. The overexpression of LRRK2, another gene implicated in familial PD, promotes autoubiquitination of parkin, which promotes its degradation by the proteasome [81].

Aggregated α-synuclein has also been shown to interact with the regulatory 19S cap, which inhibits the binding of other substrates to the 26S proteasome [79, 81]. This promotes further aggregation of non-degraded α-synuclein, which further interferes with the proteasome, and so on. A decrease in DJ-1 protein, another of the proteins implicated in familial PD, also contributes to this effect, as it promotes the aggregation of α-synuclein [81].

The function of the UPS may be impaired by free-radical damage [79] and other age- and environmental-related stressors, leading to a build-up of ubiquitinated proteins in the cell which are then sequestered into inclusions. However, it is still unclear whether damage to the UPS causes inclusions to form, or the formation of inclusions causes damage to the UPS.

1.5.2 ALP impairment

Autophagy participates in the clearance of aggresomes and is induced by oxidative stress and proteasome impairment [82, 83]. In early stages of neurodegeneration, autophagy assists in removing cytosolic protein aggregates. In later stages, it can

assist in destroying neurons that are damaged beyond repair by autophagic cell death [84].

When the UPS is overwhelmed or impaired, the autophagy-lysosomal pathway (ALP) provides a line of defense against the accumulation of mis-folded and damaged proteins [82]. While autophagy provides this 'back up' system for the UPS, low-level basal autophagy in itself has an important cytoprotective function in neurons. Mice deficient for basal autophagy have been shown to accumulate ubiquitinated protein inclusions and develop neurodegenerative disease even though the UPS was unaffected [85, 86]. Unlike the UPS, autophagy can also remove damaged mitochondria, which protects the cell from oxidative stress [87].

The efficiency of macroautophagy and chaperone-mediated autophagy (CMA) decreases with age [84, 88], which may explain the late onset of many neurodegenerative diseases. Defects in autophagy have been related to the initiation and progression of neurodegenerative diseases [68], evidenced by the accumulation of autophagosomes in post-mortem brains of PD patients [82, 88, 89]. This increase in autophagosomes can indicate either an increase in autophagosome production or a decrease in the ability of these autophagosomes to fuse with lysosomes to complete the degradation of their contents [84].

While wild-type α-synuclein is degraded by chaperone-mediated autophagy (CMA), the mutant form of α-synuclein inhibits CMA of both α-synuclein and other substrates, leading to the accumulation of mutant α-synuclein in the neuron [90]. Mutant UCH-L1 has also been shown to bind strongly to LAMP2A, the receptor that recognises proteins for degradation by CMA, which blocks other proteins from binding and their subsequent degradation [91]. This inhibition of CMA by mutant α-synuclein and UCH-L1 activates an increase in macroautophagy as a compensatory mechanism [89, 92]. But when this upregulation occurs, the resulting autophagosomes are not completely acidified, suggesting a defect in the fusion of the autophagosomes with lysosomes when macroautophagy is upregulated for this reason [88].

As well as regulating Lys^{48}-linked polyubiquitination of substrates for targeting to the UPS, there is also evidence that parkin regulates Lys^{63}-linked polyubiquitination

which targets substrates to the ALP [82]. Thus, loss of functional parkin may be involved in ALP defects as well as in UPS defects.

The relationship between the loss-of-function mutations in parkin and PINK1 and the development of PD may relate to their proposed role in the removal of defective or excessive mitochondria through autophagy, a process originally observed in neural cultures by Xue *et al.* [93] and later termed 'mitophagy' by Lemasters *et al.* [94]. Mitophagy requires two steps – the induction of general autophagy and the priming of defective mitochondria for selective autophagic recognition [95].

Narendra *et al.* [96] found that parkin is selectively recruited from the cytosol to dysfunctional mitochondria in response to a depolarisation of the mitochondrial membrane. Parkin then mediates the autophagic removal of the targeted mitochondria [96]. PINK1 is normally rapidly degraded under steady-state conditions, but depolarisation of the mitochondrial membrane stabilises the accumulation of PINK1 in the mitochondria [97]. PINK1 then recruits parkin from the cytosol to the mitochondria [97], thus acting upstream of parkin to induce mitophagy.

Thus, the impairment of mitophagy and the subsequent accumulation of defective mitochondria may underlie the development of PD. The link between mitochondrial dysfunction and PD is discussed in the following section.

1.5.3 Mitochondrial dysfunction & oxidative stress

There is evidence for a link between mitochondrial dysfunction and the pathogenesis of PD. Post-mortem studies show a 30-40% decrease in complex 1 activity in the SN region of PD patients [8, 98]. Recently, there has also been evidence for a high burden of mtDNA deletions in the neurons in the SN tissue of PD sufferers [99, 100].

There is both chemical and genetic evidence for mitochondrial involvement in PD. Drugs such as MPTP that inhibit complex I of the electron transport chain cause Parkinson-like symptoms in both humans and animal models [98, 101, 102]. Many of the genes associated with PD also implicate the mitochondria [98], most notably parkin and PINK1. The proteins parkin and PINK1 have both been shown to be important in mitochondrial integrity [103], as discussed in the previous section.

Interpretation of the functions of parkin and PINK1 in relation to mitochondria are complicated by the variation in results between studies using mammalian cell lines and fly and mammalian animal models [101].

Oxidative stress has been demonstrated in PD with increased iron, oxidation of proteins and lipid peroxidation commonly appearing in the SN [98]. Dopamine metabolism may be a source of reactive oxygen species (ROS) in SN neurons in PD [98]. DJ-1 deficiency also increases susceptibility to cell death via oxidative stress [103]. It is not known whether oxidative stress is causative or symptomatic of the death of dopaminergic neurons [1].

1.6 Proteomic investigations into α-synucleopathic disorders

1.6.1 Studies using animal models

Parkinsonism is difficult to reproduce in animals, with single gene-based models in mice failing to replicate clinical and pathological symptoms of human parkinsonism during their 2-year life span [6]. While many animal parkinsonism models can produce substantia nigral degeneration, very few can produce LBs [104]. Two models that can produce LBs are both based on mitochondrial toxicity – rats treated with rotenone, and mice treated with 1-methyl-4-phenyl-1,2,3,6-tetra-hydropyridine (MPTP) and adjuvant probenecid treatment [104].

Jin *et al.* (2005) [104] investigated the changes in mitochondrial proteins associated with parkinsonism. They used a MPTP mouse model of PD and compared the pooled mitochondrial-enriched fraction of the SN from treated animals (n=15) to that of vehicle-only controls (n=20). The protein mixtures were ICAT labelled and the proteins identified by LC-MS/MS. The treated mice showed a 70% loss of SN neurons compared to the controls. From the protein mixture, 318 proteins were identified, of which the majority were mitochondrial and 110 were differentially expressed. DJ-1 was found to be upregulated by greater than 2-fold, which was validated by Western blotting for the mitochondrial-enriched fraction, although its levels in the cytosolic fraction remained unchanged. When evaluated in individual mice, the increase in DJ-1 was found in the majority. Immunohistochemistry (IHC) was also used on human PD brain sections (n=6), and it was found that DJ-1 staining

was apparent in the majority of neurons in the peripheral (halo), but it was not present in all LBs in all patients [104].

1.6.2 Studies using whole substantia nigra tissue

Following on from their animal model study in 2005, Jin *et al.* [105] investigated the changes in mitochondrial proteins in parkinsonism in human tissue in 2006. A mitochondrial-enriched fraction from the SN region was pooled and compared between PD brains (n=5) and control brains (n=5), followed by ICAT labeling and ESI-MS. 653 proteins were identified with 2 or more peptides, of which 119 were differentially expressed. Mortalin (also known as stress-70 protein, mitochondrial precursor mthsp70, PBP74, GRP75) was chosen for further investigation due to its role in cell proliferation and survival. A decrease in expression was confirmed for the mitochondrial-enriched fraction by IHC, Western blot and a cellular PD model, whereas the expression in the cytosolic fraction did not appear to be affected. Unlike the animal model study [104], no upregulation of DJ-1 was found.

Basso *et al.* (2004) [106] compared the soluble fraction from the SN of PD brains (n=4) and control brains (n=4), using 2D-PAGE. Spot matching between Coomassie blue and silver stained gels was performed with ImageMaster 2D Elite software, using a Wilcoxon test to determine differentially expressed spots, which were then picked and identified by MALDI-TOF-MS. 142 spots of interest were picked, of which 44 were identified and of which 9 were differentially expressed. These included two downregulated neurofilament proteins and seven upregulated proteins, including those related to mitochondria. While these differentially expressed proteins may be related to PD, they are unlikely to be related to LBs as the soluble fraction of tissue was used, whereas LBs would have been present in the insoluble fraction.

Werner *et al.* (2008) [107] performed a similar study to Basso's, comparing the soluble fraction from the SN of PD brains (n=5) and control brains (n=5), using 2D-PAGE. Three gels were run for each sample to ensure reproducibility and a representative master gel for each group was used for matching the other gels. The gels were SyproRuby stained, with PDQuest used for spot matching and a Mann-

Whitney Test to determine differentially expressed spots, which were picked and analysed by MALDI-ToF-MS.

An average of 1923 spots (+/- 692) was detected per gel. There were 221 differentially expressed spots between the groups, of which 25 were selected for MS analysis (due to expense) and 16 were successfully identified. There were 312 spots showing a strictly conserved pattern of expression, of which 16 were picked and 12 were identified. Another 9 identifications were made from the remaining group of proteins that were neither differentially expressed nor strongly conserved. Differentially expressed proteins included those involved in iron metabolism (Ferritin H and ferritin L), plus various GST proteins and glial proteins such as GFAP. The conserved group included DJ-1 and UCH-L1. As was the case for the study by Basso *et al.* (2004) [106], the soluble fraction used for analysis would not include LBs.

1.6.3 Studies using purified inclusions

Leverenz *et al.* (2007) [108] used laser capture microdissection (LCM) to collect cortical LBs from DLB brains (n=6), which were pooled and analysed using Multidimensional Protein Identification Technology (MudPIT) and MS/MS. They identified 156 proteins with 2 or more peptides, of which 17 were previously reported to be in LBs, including 14-3-3, α-Crystallin β, α-internexin and α-synuclein. Three proteins, Connexin 43, FSCN1 and HSC70, were chosen for validation, based on multiple peptide hits, commercial availability of an antibody, and involvement in processes potentially important in LB formation. IHC of 7 separate DLB cases was used for target validation, and it was found that only HSC70 was selectively localised to LBs. The others were diffusely present throughout the grey matter, so it cannot be clearly interpreted that they originated from LBs. There is the potential for contamination from the LCM process in this study, with the inclusion of tissue surrounding the LBs. A control could have been used to address this.

Xia *et al.* (2008) [109] enriched LBs using a previously published sucrose gradient method, but without the subsequent FACS sorting in the original method which accounts for the majority of the increase in purity [110]. While a number of samples were purified, only one DLB/normal pair was used for analysis (n=1). The purified

sample was separated by 1-DE as a crude fractionation method, with 10 arbitrary slices cut and digested for analysis on a LCQ MS. Samples were unlabelled and spectral counts were used to quantify the mass spec data between the DLB and normal samples. Using this method, approximately 40 proteins were found to be significantly different between the DLB and normal sample. This study was limited in that only semi-purified samples were used and analysis was performed on only one sample.

1.7 Previously published inclusion purification methods

The comprehensive proteomic analysis of inclusions has been limited by the ability to isolate these inclusions with sufficient purity and yield from the surrounding structures in post-mortem tissue, as there are a limited number of published inclusion purification methods.

Pollanen *et al.* (1993) [111] originally enriched LBs from DLB tissue using basic differential centrifugation. A low-speed (6,000x g) pellet of homogenised, filtered tissue was layered over a sucrose density gradient, with the pellet subjected to urea extraction followed by another sucrose gradient. This crude LB preparation was then sequentially solubilised with 2% SDS and 88% formic acid.

Iwatsubo *et al.* (1996) [110] purified LBs from DLB tissue by using a sucrose density gradient followed by fluorescence-activated cell sorting (FACS) using antibodies against ubiquitin and neurofilament. A high-speed (500,000x g) pellet of homogenised tissue was layered over a sucrose density gradient, with the LB-containing fraction collected and pelleted to give a post-sucrose LB fraction used for FACS. This fraction was probed with an antibody against either neurofilament or ubiquitin and sorted twice sequentially. A purity of 0.1-0.5% LBs was obtained in the post-sucrose LB fraction, which increased to 10-15% after the 1st FACS sort and 60-70% purity after the second FACS sort. A yield of 1.5-3 µg of protein was obtained per 12 g of brain tissue.

Sian *et al.* (1998) [112] purified LBs from PD tissue using immunomagnetic capture. A high-speed (51,000x g) pellet of homogenised tissue was washed and mechanically sheared to reduce viscosity, then probed with a primary antibody

against either neurofilament or ubiquitin, and magnetic Dynabeads R bound to secondary antibody via a DNA spacer. The immunomagnetically captured sample was isolated using a magnetic particle concentrator and the LBs were released from the beads by digesting the DNA spacer with DNAse. This study claims that the antibody against neurofilament that was used was specific against LBs, but no other information on the purity or yield of the immunocaptured sample was provided.

Gai *et al.* (1999) [113] combined and improved features of the previous two methods to purify GCIs from MSA tissue by using a Percoll density gradient followed by immunomagnetic capture with an antibody against α-synuclein, now known to be the main component of GCIs and LBS. A low-speed pellet (1,000x g) of homogenised, filtered tissue was subject to sequential Percoll density gradient centrifugations. The GCI-enriched fraction was then probed with a primary antibody against α-synuclein, a biotinylated secondary antibody, and M-280 streptavidin-coated magnetic Dynabeads. The immunomagnetically captured sample was isolated using a magnetic particle concentrator, to give a yield of 50-70 μg of protein per 12 g of brain tissue. This method was subsequently adapted to the purification of LBs from DLB tissue with minor modifications by Jensen *et al.* (2000) [114], which gave a yield of 60-80 μg of protein per 12 g of brain tissue.

Leverenz *et al.* (2007) [108] purified LBs from DLB tissue by laser capture microdissection (LCM). This involves using laser pressure catapulting to capture selected LBs from 10 μm sections of tissue, with the resulting LB sample subjected to formic acid extraction. While this method allows the direct selection of LBs from the surrounding tissue, the captured sample may still contain other structures as the LBs were captured from 10 μm sections. This is also a time-consuming purification method to generate a very low yield – less than 1 μg of LBs from six pooled cases. Thus, it is only suitable for the downstream application of direct mass spectrometry analysis.

1.8 Project aims and approaches

The presence and location of α-synuclein-containing inclusions is the main diagnostic criteria for neurodegenerative disorders. Yet despite the existence of LBs being known for 100 years, it is still not know why these inclusions form, the

mechanism by which proteins are incorporated into them, and what role they play in disease process. There has been limited proteomic characterisation of inclusions to date, with immunochemistry primarily used to identify single protein components in LBs and GCIs. Inclusions are complex, highly ordered structures and the majority of proteins are yet to be identified. This is due to the scarcity of inclusions in a given volume of brain tissue and limited inclusion purification methods available to date.

LBs and GCIs have very similar structures, despite coming from neurons and oligodendrocytes respectively. α-synuclein is a major protein in both types of inclusions, even though α-synuclein is a neuronal protein that is not expressed in oligodendrocytes. This suggests that there is a potential trafficking mechanism between neurons and oligodendrocytes, which could play a role in inclusion formation. The isolation of a large yield of high-purity inclusions from post-mortem human brain tissue is required, followed by a systematic approach to identifying, quantifying and comparing the proteins present in inclusions. This will provide essential information as to how and why these inclusions form and how their formation relates to the pathophysiology in α-synucleopathic neurodegenerative diseases.

Advances in proteomic technologies now allow the sequencing of low abundance inclusion proteins. The two core technologies currently used for proteomic analysis are two-dimensional gel electrophoresis (2-DE) and mass spectrometry (MS). For 2-DE, a complex mixture of proteins is separated into individual proteins based on their isoelectric point and molecular weight. 2-DE has been revolutionised by the introduction of CyDye™ Difference In-Gel Electrophoresis (DIGE) fluors. DIGE allows for the multiplexing of samples including an internal standard, which controls for gel-to-gel variability associated with traditional 2-DE and leads to highly accurate results. DeCyder™ software is used for spot detection and quantification. DeCyder™ algorithms normalise the spot intensity relative to the pooled internal standard to allow for variation in protein loading and the extinction coefficients of the dyes.

Mass spectrometry allows proteins to be identified from either spots on a 2-D gel or from a complex mixture. The proteins are first digested into peptides using trypsin, then these peptides are ionised using high voltage and the positively charged peptides

are drawn into the negatively charged mass spectrometer. In the case of an Orbitrap mass spectrometer, when operated in the most commonly used FTMS/ITMS mode, a high resolution and high mass accuracy scan is performed on the peptides entering the mass spectrometer to determine the charge state of ions so that singly charged ions (usually background ions) are ignored and that an accurate mass measurement can be made on each peptide. For each Orbitrap m/s scan, the instrument identifies the top n (n is usually around 6) multiply charged ions (peptides) and then fills the ion trap with peptides. All ions except for a 1 Da window around the target precursor ion (peptide) are ejected from the trap by modulation of the RF (radio frequency) and DC (direct current) voltages. The precursor ion is then accelerated into the collision gas helium present in the trap which increases the internal vibrational energy of the peptide. The increased energy causes the peptide backbone to fragment at the peptide bond. The collision energy used is sufficient to cause a single break in the majority of peptides so that a series of ions called b and y ions is produced. B ions retain the charge on the N-terminus of the fragment and y ions on the C-terminus. The stochastic nature of the fragmentation results in all the peptide bonds being broken despite each peptide only having a single break. The b and y ions are scanned out of the ion trap producing a mass chromatogram from which the mass of each ion is determined. The mass difference between each mass from the b and y ion series corresponds to the mass of each amino acid in the sequence. Software is used to compare the sequence with sequence databases to determine the protein from which the peptide was derived.

1.8.1 Aim #1: To optimise the purification of inclusions for improved yield and purity

The published method of Gai *et al.* (1999) [113] for inclusion enrichment involves a combination of density gradient centrifugation and magnetic bead immunoaffinity purification. Using this method, a major enrichment of tubulin occurs, as tubulin is likely to co-purify with inclusions as a result of their tight integration into the cytoskeletal structure. The yield is also too limited to provide enough material for proteomic techniques such as 2D-E. Modifications to the existing protocol, including a limited protease digestion, will be tested to improve the purity and yield of the isolated GCIs. Obtaining a larger yield of highly pure inclusions will allow subsequent analysis of their protein composition.

1.8.2 Aim #2: To elucidate the GCI proteome

GCIs will be purified using the newly optimised purification method and the proteins will be identified using a Thermo LTQ Orbitrap XL mass spectrometer fitted with a nanospray source, using a combination of trypsin-digested complex mixtures and 1-DE and 2-DE separation methods. The biological variation in GCIs between patients will be determined with 2D-DIGE.

1.8.3 Aim #3: To compare LB and GCI proteins

The newly optimised GCI purification method will be adapted for the purification of LBs. 2D-DIGE will be used to compare the protein profiles of LBs and GCIs and the relative abundance of key inclusion proteins in the two inclusion types. LB proteins will be identified by mass spectrometry and compared to those identified in GCIs to develop a proposed mechanism for inclusion formation.

2 Materials and Methods

2.1 Materials

Inclusion purification

Dounce homogeniser (Wheaton, Millville, NJ, USA)

Percoll Plus (GE Healthcare, Buckinghamshire, UK)

Pepstatin A (Sigma, St Louis, MO, USA)

Leupeptin (Sigma)

PMSF (Sigma)

Deoxyribonuclease I (Sigma)

Trypsin, TPCK treated (Sigma)

Dynal® MyOne™ Streptavidin T1 Dynabeads® (Invitrogen, Carlsbad, CA, USA)

Dynal® M-280 Streptavidin Dynabeads® (Invitrogen)

Cy3-conjugated Streptavidin, product no. 016-160-084 (Jackson ImmunoResearch Laboratories, West Grove, PA, USA)

EasySep™ magnet (Stemcell Technologies, Melbourne, VIC, Australia)

Sample preparation and protein quantitation

ReadyPrep™ 2D Cleanup Kit (BioRad, Hercules, CA, USA)

EZQ® Protein Quantitation Kit (Invitrogen)

1-DE and Western blotting

Precision Plus Protein Dual Colour Standards (BioRad)

Precision Plus Protein Unstained Standards (BioRad)

Mini-Protean® TGX™ Any kD™ precast gels (BioRad)

Immobilon™ –P^{SQ} transfer membrane, PVDF 0.2um (Millipore Billerica, MA, USA)

Extra thick blot paper, Protean® XL size (BioRad)

SNAP i.d. single well blot holders (Millipore)

Diploma skim milk power (Fonterra Brands, Mount Waverly, VIC, Australia)

SuperSignal® West Pico chemiluminescent substrate (Thermo Scientific, Rockford, IL, USA)

Immunohistochemistry and immunofluorescence

Superfrost® plus microscope slides (HD Scientific Supplies, Wetherill Park, NSW, Australia)

Normal horse serum (Gibco, division of Invitrogen)

Vectastain® ABC Kit (Vector Laboratories, Burlingame, CA, USA)

DAB tetrahydrochloride tablet (Sigma)

Vectashield® Mounting Medium with DAPI (Vector Laboratories)

2D DIGE

5nmol CyDye DIGE Fluor Minimal labeling kit (GE Healthcare)

IPG Buffer, pH 3-11 NL (GE Healthcare)

Immobiline DryStrip gels (GE Healthcare)

Mineral oil (Sigma)

Strip holder cleaning solution (GE Healthcare)

Whatman No. 1 filter paper (GE Healthcare)

Sypro® Ruby protein gel stain (BioRad)

Urea (Amresco, Solon, OH, USA)

Thiourea (Scharlab, Barcelona, Spain)

CHAPS (Amresco)

DTT (Astral Scientific, Gymea, NSW, Australia)

Iodoacetamide (BioRad)

Mass spectrometry

Vivaspin 500 5 kDa MWCO columns (GE Healthcare)

Trypsin Gold, Mass Spectrometry grade (Promega, Madison, WI, USA)

Flat top full skirt 96-well PCR plates (Scientific Specialties, Lodi, CA, USA)

PDM1.5 OneTouch Plus spot picker (The Gel Company, San Francisco, CA,USA)

Acetonitrile, LiChrosolv® hypergrade for LC-MS grade, 99.9% purity (Merck, Darmstadt, Germany)

Formic acid, puriss. p.a. for mass spectrometry grade, 98% purity (Fluka Analytical, division of Sigma)

2-Propanol, Chromasolv® Plus for HPLC grade, 99.9% purity (Sigma)

All other chemicals and materials were of the highest grade commercially available.

Antibodies

Table 2-1: Primary antibodies

No.	Target	Species	Poly/Mono	Conc. (µg/µL)	Cat. No.	Source
1	α-synuclein	Sheep	Polyclonal	1.0	N/A	Gai *et al.*, Adelaide, Australia
2	α-synuclein	Rabbit	Polyclonal	1.0	N/A	Gai *et al.*, Adelaide, Australia
3	βIII tubulin	Mouse	Monoclonal	0.5	G7121	Promega, Madison, WI, USA
4	α-β-crystallin	Rabbit	Polyclonal	N/A	NCL-ABCRYS	Novocastra Laboratories, Newcastle, UK
5	TPPP	Rabbit	Polyclonal	0.75	N/A	Prof. Paul Henning Jensen, University of Aarhus, Denmark
6	SNAP25	Rabbit	Polyclonal	N/A	OS-219	Osenses, Keswick, SA, Australia
7	VAMP2	Rabbit	Polyclonal	N/A	OS-222	Osenses
8	Synaptotagmin-1	Rabbit	Polyclonal	N/A	OS-213	Osenses
9	Synaptophysin	Rabbit	Polyclonal	N/A	OS-209	Osenses

Table 2-2: Secondary antibodies

No.	Antibody	Conc. (µg/µL)	Cat. No.	Source
10	Biotin-SP-conjugated AffiniPure Donkey Anti-Sheep	0.65	713-065-147	Jackson Laboratories, West Grove, PA, USA
11	Peroxidase-conjugated Rabbit Anti-sheep	0.4	31480	Thermo Fisher Scientific, Waltham, MA, USA
12	Peroxidase-conjugated Goat Anti-rabbit	0.4	31460	Thermo Fisher Scientific
13	Peroxidase-conjugated Goat Anti-Mouse	0.4	31430	Thermo Fisher Scientific
14	HRP-conjugated Donkey Anti-sheep	0.4	713-035-147	Jackson Laboratories
15	HRP-conjugated Donkey Anti-rabbit	0.4	711-035-152	Jackson Laboratories
16	HRP-conjugated Donkey Anti-Mouse	0.4	715-035-150	Jackson Laboratories
17	Cy3-conjugated AffiniPure Donkey Anti-Rabbit	0.75	711-165-152	Jackson Laboratories
18	Cy3-conjugated AffiniPure Donkey Anti-Mouse	0.75	715-165-150	Jackson Laboratories
19	Cy3-conjugated AffiniPure Donkey Anti-Sheep	0.75	713-165-147	Jackson Laboratories
20	Alexa Fluor 488-conjugated Donkey Anti-rabbit	1.0	A-21206	Invitrogen, Carlsbad, CA, USA
21	Alexa Fluor 488-conjugated Donkey Anti-mouse	1.0	A-21202	Invitrogen

2.2 Solutions

2.2.1 Inclusion purification

Sucrose tris buffer (STB)

20 mM tris, 0.32 M sucrose, 0.05% (w/v) sodium azide, pH 7.4

Homogenisation buffer (HB)

20 mM tris, 0.32 M sucrose, 0.05% (w/v) sodium azide, 5 mM EDTA, 1 µg/ml Pepstatin, 1 µg/ml Leupeptin, 0.3 mM PMSF, pH 7.4

TBS-Azide

20 mM tris, 150 mM NaCl, 0.1% (w/v) sodium azide, pH 7.4

TBS-Azide + protease inhibitors (PIs)

20 mM tris, 150 mM NaCl, 0.1% (w/v) sodium azide, 5 mM EDTA, 1 µg/ml Pepstatin, 1 µg/ml Leupeptin, 0.3 mM PMSF, pH 7.4

Washing buffer

20 mM tris, 150 mM NaCl, 0.1% (w/v) sodium azide, 1 mM EDTA, 0.3 mM PMSF, pH 7.4

Protein extraction buffer

7 M urea, 2 M thiourea, 4% (w/v) CHAPS

2.2.2 1-DE and Western Blotting

4x 1D sample buffer

250 mM Tris-HCl, 40% (v/v) glycerol, 8% (w/v) SDS, 400 mM DTT, 0.04% (w/v) bromophenol blue, pH 6.8

Transfer buffer

25 mM tris, 192 mM glycine, 20% (v/v) methanol, 0.05% (w/v) SDS

TBS

20 mM tris, 150 mM NaCl, pH 7.4

TBST

0.1% (v/v) Tween-20 in TBS

Blocking buffer

0.5% (w/v) skim milk powder in TBST, filtered

2.2.3 Immunohistochemistry (IHC) and immunofluorescence (IF)

IHC fixative

2% (v/v) paraformaldehyde, 0.2% (v/v) picric acid, 100 mM PBS

IHC blocking solution

20% (v/v) Normal Horse Serum (NHS) in TBS-Azide

IHC antibody diluent

1% (v/v) Normal Horse Serum (NHS) in TBS-Azide

ABC solution

1 drop each of reagent A and B from Vectastain ABC Kit in 5 mL of TBS

DAB solution

DAB tablet in 5 mL of TBS, 0.021% (v/v) H_2O_2

2.2.4 2D DIGE

DIGE labeling buffer

7 M urea, 2 M thiourea, 4% (w/v) CHAPS, 30 mM tris, pH 8.0

IEF rehydration buffer

7 M urea, 2 M thiourea, 4% (w/v) CHAPS, 0.5% (v/v) IPG Buffer, 0.4% (w/v) DTT

Equilibration buffer

100 mM tris-HCl, 6 M urea, 30% (v/v) glycerol, 2% (w/v) SDS, pH 8.0

Equilibration solution 1 (1% DTT)

1% (w/v) DTT in equilibration buffer

Equilibration solution 2 (4% iodoacetamide)

4% (w/v) iodoacetamide in equilibration buffer, 0.003% (v/v) bromophenol blue solution

Agarose

1% (w/v) low melting point agarose in 1x running buffer

1x running buffer

25 mM tris, 192 mM glycine, 0.06% (w/v) SDS, pH 8.3

Gel fixing solution

20% (v/v) methanol, 7.5% (v/v) acetic acid

Coomassie blue stain

2% (w/v) Coomassie Brilliant Blue R-250, 20% (v/v) methanol, 5% (v/v) acetic acid

Silver staining solution 1 – fixative/stop

30% (v/v) ethanol, 10% (v/v) acetic acid

Silver staining solution 2 – sensitiser

0.006% (w/v) Erichrome Black T, 30% (v/v) ethanol

Silver staining solution 3 – destain

30% (v/v) ethanol

Silver staining solution 4 – silver

0.25% (w/v) silver nitrate, 0.037% (v/v) formaldehyde

Silver staining solution 5 – developer

2% (w/v) potassium carbonate, 0.04% (w/v) sodium hydroxide, 0.002% (w/v) sodium thiosulphate, 0.007% (v/v) formaldehyde

2.2.5 Mass spectrometry

HPLC buffer A

98% (v/v) H_2O, 2% (v/v) ACN, 0.1% (v/v) formic acid

HPLC buffer B

20% (v/v) H_2O, 80% (v/v) ACN, 0.1% (v/v) formic acid

18.2 MΩ water from a Pall Cascada AN system fed by a deionised water source was used for all solutions.

2.3 Methods

2.4 Brain tissue preparation

2.4.1 Brain tissue specimens

Fresh-frozen brain tissue was obtained from the South Australian Brain Bank, Adelaide, with ethics approval received from the Flinders Clinical Research Ethics Committee (Approval 06/067). The brain tissue had been extracted within a 36 hour post-mortem interval and bisected at the midsagittal plane in a dry ice bath, with one half snap-frozen for later use and the other half aldehyde-fixed, blocked and embedded in paraffin for subsequent neuropathological assessment by SA Pathology. MSA, DLB and normal control cases were utilised in this study. See Table 2.3 below for the details of the cases used.

Table 2-3: Case details for post-mortem brain tissue used in this project

Case No.[a]	Pathology	Gender	Age[b]	PMI[c]
SA0162	Normal	M	72	30
SA0230	Normal	M	86	22
SA0113	DLB	F	81	12
SA0133	DLB	M	79	24
SA0166	DLB	M	73	34
SA0058	MSA	F	77	5
SA0061	MSA	F	62	8
SA0071	MSA	F	73	5
SA0101	MSA	M	73	20
SA0132	MSA	F	81	17
SA0190	MSA	M	59	13

[a] SA Brain Bank case number
[b] Age at time of death, in years
[c] Post-mortem interval, in hours

2.4.2 Brain tissue homogenisation

Tissue sections containing glial cytoplasmic inclusions (MSA cases), Lewy bodies (DLB cases), or the matched brain region without inclusions (normal control cases), as determined by the post-mortem report (typically cerebellum, medulla, thalamus, hippocampus, basal ganglia and brainstem), were thawed on ice, dissected at 4°C and divided into 2 g lots. Each lot was mixed with 8 mL of homogenisation buffer and

homogenised in a Dounce homogeniser for approximately 20 strokes with Pestle A (loose) then 20 strokes with Pestle B (tight), until no lumps remained. Homogenised tissue from the same case was pooled and mixed, then divided into 10 mL tubes and snap-frozen in liquid nitrogen. Brain homogenate was then stored at -80°C.

2.5 Inclusion purification

A diagram summarising the entire purification procedure is shown in Figure 2.1. All steps were performed on ice unless otherwise specified.

2.5.1 Inclusion enrichment using a density gradient

All centrifugation was performed using 10 mL open top polypropylene centrifuge tubes in a Beckman J2-MC centrifuge using a JA-21 rotor at 4°C.

Step 1: A 10 mL tube of brain homogenate, containing ~2 g of tissue homogenised in a Dounce homogeniser with 8 mL of homogenisation buffer (HB), was thawed on ice.

Step 2: The brain homogenate was filtered through glass wool in a 20 mL syringe and diluted to a total volume of 24 mL with HB. This filtrate was loaded across three centrifuge tubes (8 mL in each).

Step 3: The filtrate was centrifuged at 1,000x g for 10 minutes. The supernatant (containing soluble α-synuclein) was discarded and each pellet was resuspended to 8 mL in HB and centrifuged as before to wash.

Step 4: Each pellet was resuspended in 0.84 mL of Percoll Plus and diluted to 6 mL in HB to a Percoll concentration of 14% (v/v in HB). A 2.4 mL cushion of 35% Percoll Plus (v/v in HB) was injected underneath the 14% layer using a 10 mL syringe with a long needle. The samples were centrifuged at 35,000x g for 30 minutes to create a density gradient.

Step 5: The waste and myelin fractions, which do not contain inclusions, were discarded. The inclusion-containing Percoll-enriched fractions were collected and pooled and diluted to 32 mL in TBS-Azide and loaded across four centrifuge tubes (8 mL in each). The samples were centrifuged at 1,800x g for 10 minutes. The

supernatant was discarded and the pellets were combined into a single tube, resuspended to 8 mL in TBS-Azide, and centrifuged as before. The supernatant was again discarded, with the pellet resuspended to 2 mL in TBS-Azide and transferred to a 2 mL microfuge tube. A 6 µL aliquot of the sample was solubilised into 60 µL of 1x 1D sample buffer and the protein concentration was determined by an EZQ protein quantitation assay, as described in section 2.6.1, for determining the amount of trypsin enzyme to add in step 7.

2.5.2 DNA digestion and limited tryptic digestion

All washes in Steps 6-10 were performed by centrifugation at 1,800x g for 10 minutes at 4°C using Axygen 2 mL tubes in an Eppendorf 5415 C centrifuge. All incubations in Steps 6-10 were performed in an Eppendorf Thermomixer Comfort at 1,400 RPM.

Step 6: The pH of the sample was set to 8.0 by the addition of 10 µL of 1M NaOH and the tube was warmed to 37°C for 10 minutes (the optimal pH and temperature for trypsin activity). 2 µg of trypsin was added to the sample to lyse the nuclei, with the reaction stopped within 10 seconds by the addition of 0.3 mM PMSF, followed by 1 µg/ml Leupeptin and 1 µg/ml Pepstatin. DNase I and $MgCl_2$ (DNase cofactor) were added to a final concentration of 100 µg/mL and 10 mM respectively, to reduce the oligonucleotides released from the lysed nuclei, and the sample was incubated for 1 hour at 37°C. The sample was washed three times in TBS-Azide.

Step 7: The pH of the sample was set to 8.0 by the addition of 10µL of 1M NaOH and the tube was prewarmed to 37°C for 10 minutes. Trypsin was added at a 1:4000 enzyme to protein ratio and the sample was incubated for 5 minutes at 37°C to perform a limited digestion of the cytoskeletal protein surrounding the inclusions, with the reaction stopped by the addition of 0.3 mM PMSF, followed by 1 µg/ml Leupeptin and 1 µg/ml Pepstatin. The sample was washed three times in TBS-Azide + Protease Inhibitors (PIs).

2.5.3 Immunomagnetic capture of inclusions

Step 8: 60 µg of affinity purified sheep anti-α-synuclein antibody (antibody #1, Table 2.1) was added to the sample to target the inclusions in the protein mixture and

incubated overnight at 4°C. The sample was washed three times (to remove any unbound primary antibody) in TBS-Azide.

Step 9: 30 µg of biotin-conjugated donkey anti-sheep antibody (antibody #10, Table 2.2) was added to the sample to bind to the primary antibody and incubated for 30 minutes at 22°C. The sample was washed three times (to remove any unbound secondary antibody) in TBS-Azide.

Step 10: 20 µL of Dynal MyOne Streptavidin T1 Dynabeads was added to the sample and incubated for 10 minutes at 22°C. 30 µL of Dynal M-280 Streptavidin Dynabeads was added to the sample and incubated for a further 60 minutes at 22°C. The streptavidin coating on the beads binds to the biotin conjugated to the secondary antibody, thus binding the beads to the inclusions through an antibody link.

Step 11: The sample was transferred to an isolation tube and placed in an EasySep magnet for 8 minutes, allowing the magnetic beads with the attached inclusions to bind to the walls of the tube. The supernatant, containing the non-inclusion proteins and any unbound inclusions, was collected with a glass Pasteur pipette (wash fraction). The captured inclusions were washed twice by resuspension of the inclusions in 2 mL of washing buffer, allowing 5 minutes for the beads to reattach to the tube walls in the presence of the magnet before removing the wash fraction as before. The captured inclusions were then washed from the tube walls with 1.5 mL of washing buffer and transferred to a 1.5 mL microfuge tube.

If more than one tube of homogenate from the same case was processed, the second 2 mL sample was pipetted into the isolation tube after the first wash fraction was removed and the tube was returned to the magnet for a further 8 minutes before the supernatant was collected. This process was repeated for any subsequent tubes. After all the tubes had been processed, the total captured inclusions were washed as described above.

2.5.4 Visualising inclusion capture

Avidin-Cy3 conjugate was diluted 1:400 in 1% NHS in TBS-Azide. 10 µL of the wash fraction and 10 µL of the immunomagnetically captured fraction (both from step 11) were each mixed with 2 µL of the diluted avidin Cy-3. Five 1 µL drops of

each fraction were pipetted onto a microscope slide and examined under an Olympus BX50 fluorescence microscope for the presence of inclusions.

2.5.5 Solubilising inclusions

Step 12: The immunomagnetically captured fraction, containing the Dynabeads and their attached inclusions, were centrifuged at 18,000x g for 5 minutes at room temperature in a Sigma I-15 centrifuge. Approximately 1.2 mL of the supernatant was removed without disturbing the beads, then the tube was centrifuged as before and the remaining supernatant was removed from the bead pellet. 200 µL of protein extraction buffer was added to the pellet of beads and inclusions and the pellet was resuspended with pipette mixing. The sample was incubated overnight at room temperature a Thermomixer Comfort (Eppendorf) at 1,400 RPM.

The sample was centrifuged at 18,000x g for 10 minutes to pellet the beads, with the supernatant containing the solubilised inclusions collected into a 3 mL open top polycarbonate ultracentrifuge tube. The sample was then ultracentrifuged at 200,000x g for 30 minutes at 4°C in an Optima^{TM} TLX ultracentrifuge (Beckman Coulter) using a TLA 120.2 rotor, to remove any undissolved protein and remaining beads, then pipetted into a fresh tube for subsequent analysis. The protein concentration of the solubilised inclusions was determined with an EZQ protein quantitation assay, as described in section 2.6.1.

Figure 2-1: Summary of optimised inclusion purification method

Step 1: 2 g of brain tissue was homogenised in a Dounce homogeniser with 8 mL of homogenisation buffer (HB), to give 10 mL of homogenate.

Step 2: The brain homogenate was filtered through glass wool, diluted to a total volume of 24 mL with HB and loaded across three centrifuge tubes (8 mL per tube).

Step 3: The filtrate was centrifuged at 1,000x g for 10 minutes at 4°C. The supernatant (containing soluble α-synuclein) was discarded and the pellets (containing inclusions) were resuspended to 8 mL in HB and centrifuged as before to wash.

Step 4: Each pellet was resuspended in 0.84 mL of Percoll Plus and diluted to 6 mL in HB to a Percoll concentration of 14%. A 2.4 mL cushion of 35% Percoll Plus in HB was injected underneath the 14% layer and the samples were centrifuged at 35,000x g for 30 minutes at 4°C to create a density gradient.

Step 5: The waste and myelin fractions, which do not contain inclusions, were discarded and the inclusion-containing Percoll-enriched fractions were collected and pooled. The Percoll-enriched fraction was diluted to 32 mL in TBS-Azide and washed twice in TBS-Azide by centrifugation at 1,800x g for 10 minutes at 4°C. The washed pellet was resuspended to 2 mL in TBS-Azide and transferred to a 2 mL microfuge tube.

Step 6: 2 µg of trypsin was added to the sample to lyse the nuclei, with the reaction stopped by the addition of protease inhibitors. 100 µg/mL of DNase I and 10 mM $MgCl_2$ (DNase cofactor) were added to remove the DNA released from the lysed nuclei, with the sample incubated for 1 hour at 37°C at 1400 RPM. The sample was washed three times in TBS-Azide by centrifugation at 1,800x g for 10 minutes at 4°C.

Step 7: Trypsin was added at a 1:4000 enzyme:protein ratio. The sample was incubated for 5 minutes at 37°C to perform a limited digestion of the cytoskeletal protein surrounding the inclusions, with the reaction stopped by the addition of protease inhibitors. The sample was washed three times by centrifugation in TBS-Azide + PIs at 1,800x g for 10 minutes at 4°C.

Step 8: 60 µg of affinity purified sheep anti-α-synuclein antibody was added to the sample and incubated overnight at 4°C at 1,400 RPM. The sample was washed three times (to remove any unbound antibody) in TBS-Azide by centrifugation at 1,800x g for 10 minutes at 4°C.

Step 9: 20 µg of biotin-conjugated donkey anti-sheep antibody was added to the sample and incubated for 30 minutes at 22°C at 1,400 RPM. The sample was washed three times in TBS-Azide by centrifugation at 1,800x g for 10 minutes at 4°C.

Step 10: 20 µL of Dynal MyOne Streptavidin T1 Dynabeads was added to the sample and incubated for 10 minutes at 22°C at 1,400RPM. 30 µL of Dynal M-280 Streptavidin Dynabeads was added to the sample and incubated for a further 60 minutes. The streptavidin coating on the beads binds to the biotin conjugated to the secondary antibody, thus binding the beads to the inclusions through an antibody link.

Step 11: The sample was placed in an EasySep magnet to allow the magnetic beads with the attached inclusions to bind to the walls of the tube. The supernatant, containing the non-inclusion proteins and any unbound inclusions, was collected (wash fraction). The captured inclusions were washed twice with 2 mL of washing buffer, and then collected from the tube walls with 1.5 mL of washing buffer.

Step 12: The captured inclusions were centrifuged at 18,000x g for 5 minutes at room temperature. The pellet was resuspended in 200 µL of protein extraction buffer and incubated overnight at room temperature at 1,400RPM to solubilise the inclusion proteins, separating them from the beads. The sample was centrifuged at 18,000x g for 10 minutes to pellet the beads, with the supernatant containing the solubilised inclusions collected.

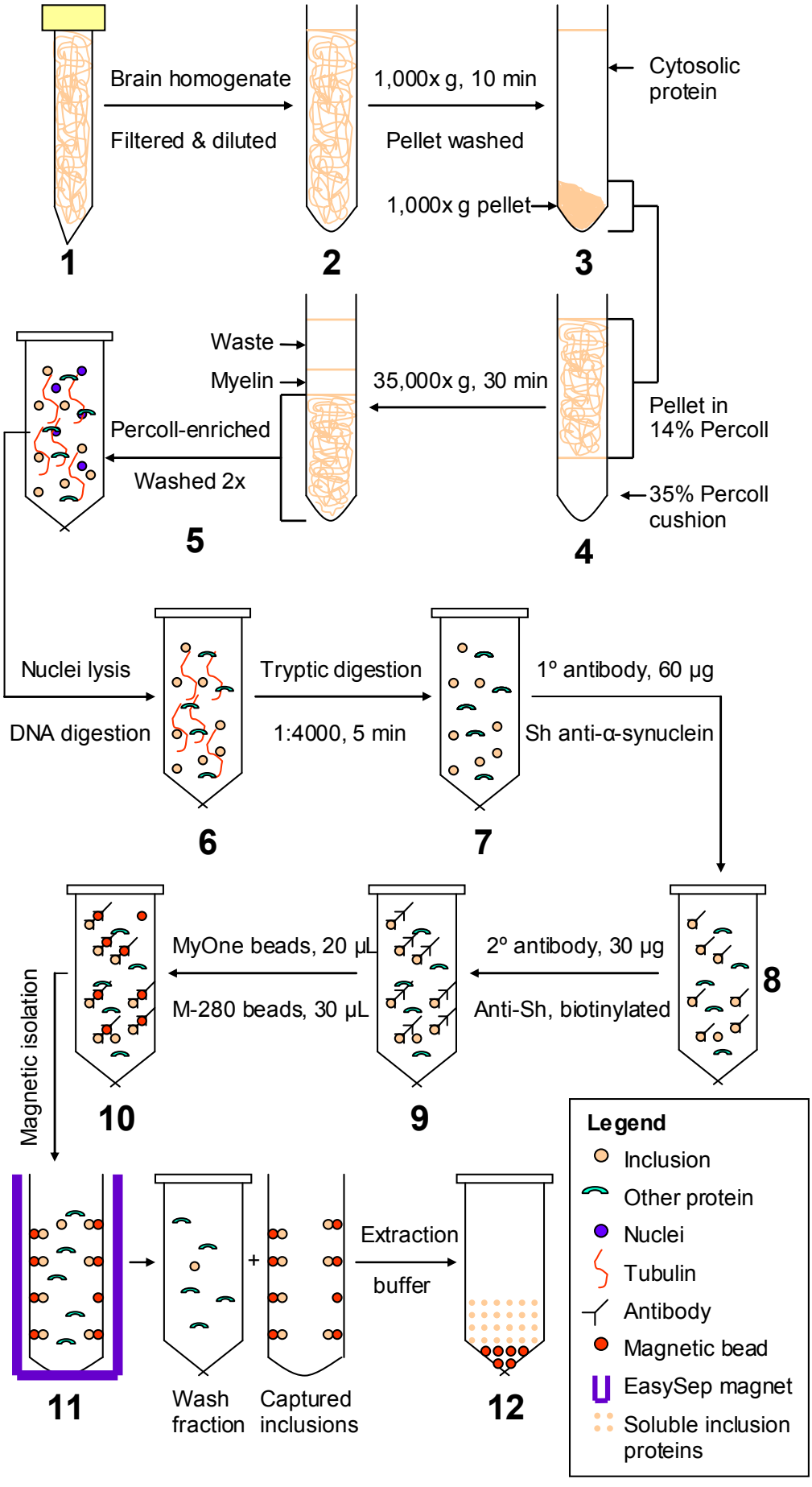
Brain homogenate
Filtered & diluted
1,000x g, 10 min
Pellet washed
Cytosolic protein
1,000x g pellet
1
2
3
Waste
Myelin
35,000x g, 30 min
Pellet in 14% Percoll
Percoll-enriched
Washed 2x
35% Percoll cushion
5
4
Nuclei lysis
DNA digestion
Tryptic digestion
1:4000, 5 min
1° antibody, 60 µg
Sh anti-α-synuclein
6
7
8
MyOne beads, 20 µL
M-280 beads, 30 µL
2° antibody, 30 µg
Anti-Sh, biotinylated
Magnetic isolation
10
9
Extraction buffer
11
Wash fraction
Captured inclusions
12
Legend
Inclusion
Other protein
Nuclei
Tubulin
Antibody
Magnetic bead
EasySep magnet
Soluble inclusion proteins

2.6 Sample preparation and quantitation

2.6.1 EZQ Protein Quantitation Assay

EZQ Protein Quantitation Assays were performed according to the manufacturer's instructions (Invitrogen). A 2 mg vial of ovalbumin was reconstituted with 1 mL of dH_2O to give a 2.0 mg/mL stock solution. Serial dilutions were made from this stock solution to give standards of 1.0, 0.5, 0.2, 0.1, 0.05 and 0.02 mg/mL. Standards were kept for up to 1 month at -20°C.

The assay paper component was fitted into the microplate component and 1 µL of each standard and each sample being assayed was spotted onto the assay paper in triplicate and allowed to dry. The assay paper was removed from the template and incubated in 35 mL of methanol for 5 minutes on an Orbital Shaker (Axyos Technologies, Brendale, QLD, Australia). The methanol was removed and the paper dried on low heat using an Easy Breeze Gel Dryer (Hoefer Scientific Instruments, San Francisco, CA). 35 mL of EZQ Protein Quantification Reagent was added and the assay paper was incubated on an Orbital Shaker for 30 minutes at room temperature. The EZQ reagent was removed and the assay paper washed 3 times with 35 mL of EZQ destain for 3 minutes per wash.

The assay paper was imaged on a Typhoon 9400 variable mode imager at 200 µm using a blue 457 nm laser, 610 BP emission filter and photo-multiplier tube (PMT) value of 580 V. Carestream Molecular Imaging Software Version 5.0.6.20 (Carestream Health Inc., Rochester, NY) was used for analysis of the blot. All protein concentrations were determined using the EZQ Protein Quantitation Assay unless otherwise specified.

2.6.2 ReadyPrep 2-D Clean-Up Kit

ReadyPrep 2-D Protein Clean-Up of samples were performed according to the manufacturer's instructions (BioRad). A sample of up to 100 µL in volume that contained up to 500 µg of protein was pipetted into a 1.5 mL microfuge tube. 300 µL of Precipitating Agent 1 was added; the sample was vortexed for 30 seconds and incubated on ice for 15 minutes. 300 µL of Precipitating Agent 2 was added and the sample was vortexed for 30 seconds. The sample was centrifuged at 18,000x g for 5 minutes and the supernatant removed. The tube was centrifuged again for 30

seconds and any remaining traces of supernatant were removed. 40 µL of Wash Reagent 1 was added on top of the pellet and vortexed for 10 seconds. The tube was centrifuged at 18,000x g for 5 minutes and the wash removed. 25 µL of dH_2O was added on top of the pellet and the sample was vortexed for 10 seconds. 1 mL of Wash Reagent 2 (pre-chilled at -20°C for at least 1 hour) and 5 µL of Wash 2 Additive were added and the sample was vortexed for 1 minute.

The sample was incubated on ice for 30 minutes, with 30 seconds of vortexing every 10 minutes during the incubation. The tube was centrifuged at 18,000x g for 5 minutes and the supernatant was removed. The tube was centrifuged again for 30 seconds and any remaining traces of supernatant were removed. The pellet was left to dry for approximately 1 minute, until translucent, then an appropriate volume of an appropriate resolubilisation buffer was added. The sample was vortexed for 1 minute, incubated at room temperature for 5 minutes, then vortexed for a further minute. The sample was centrifuged at 18,000x g for 5 minutes and the solubilised protein sample was pipetted into a fresh tube for use.

2.7 1-DE and Western Blotting

2.7.1 1-DE

Gels were labcast as 4-20% gradient gels using the Hoefer SE 260 Mighty Small Multiple Gel Caster (GE Healthcare) according to the User Manual. Alternatively, precast BioRad Mini-Protean® TGX™ Any kD™ gels were used. Samples were diluted into 1x 1D sample buffer containing freshly added DTT and heated at 90°C for 5 minutes, then loaded onto the gel. Gels were electrophoresed at 200 V at constant voltage in either a GE Healthcare Hoefer MiniVE vertical electrophoresis system (labcast gels) or a Biorad Mini-Protean Tetra electrophoresis system (precast gels) until the bromophenol blue dye front reached 0.5 cm from the bottom edge of the gel.

2.7.2 Western Blotting

PVDF membrane and two pieces of extra thick filter paper (BioRad) were cut to the same size as the gel. The membrane was wet with 100% methanol for 30 seconds, and then the gel, filter paper and membrane were all separately equilibrated in

transfer buffer for 10 minutes. A plastic mask with a gap 1 mm smaller than the size of the gel was laid in the bottom of a Hoefer TE 77 semi-dry transfer unit (GE Healthcare) and the gap wet with transfer buffer. Filter paper was then layered over the gap, followed by the membrane, the gel, and the second piece of filter paper, to form a sandwich. The proteins were transferred from gel to membrane at 0.8mA per cm^2 for 2 hours.

Western blotting was performed using the SNAP i.d. protein detection system (Millipore) according to the manufacturer's instructions. The SNAP i.d. blot holder was wet with dH_2O and the PVDF membrane was laid onto the blot holder membrane, with the protein side down. A spacer was placed on top of the membrane and the blot holder snapped shut and placed in the unit. 30 mL of blocking solution was applied and suctioned through the membrane immediately, and then primary antibody diluted in 3 mL of TBS at 3x the normal concentration was applied and incubated for 10 minutes at room temperature. Three continuous 30 mL washes of TBST were then suctioned through the membrane, followed by a 10 minute incubation in secondary antibody, diluted as for the primary. Another three continuous 30 mL washes of TBST were applied before imaging. Blots were imaged with a Fujifilm LAS-4000 CCD imager (Tokyo, Japan) following a 5 minute incubation in SuperSignal West Pico ECL substrate.

2.8 2-D DIGE

2.8.1 DIGE minimal labeling

Minimal DIGE labeling was performed according to the Ettan DIGE System User Manual 18-1173-17AB (GE Healthcare). The CyDye vials were allowed to warm at room temperature for 5 minutes. Each new vial was reconstituted with 5 µL of fresh anhydrous DMF, vortexed vigorously for 30 seconds and then briefly centrifuged, to give a 1 mM stock solution. CyDye working solution was prepared by adding one volume of CyDye stock solution to 1.5 volumes of DMF, to give a 400 µM working solution. 400 pmol was needed to label one sample (50 µg of protein), which equates to 1 µL of working solution.

Each 50 µg protein sample, at a 5-10 mg/mL concentration and pH of 8.0 in DIGE labeling buffer, was mixed with 1 µL of working solution and incubated on ice for 30

minutes in the dark to allow covalent labeling of lysine amino acids with the CyDye. The reaction was quenched with 1 µL of 10 mM lysine for a further 10 minutes on ice. The protein samples were then pooled (two 50 µg samples labeled with Cy3 and Cy5 respectively and a 50 µg pooled internal standard labeled with Cy2).

2.8.2 1st dimension isoelectric focusing

Isoelectric focusing was carried out according to the 2D Electrophoresis Principals and Methods Handbook 80-6429-60AC (GE Healthcare). Samples were diluted into 475 µL of IEF rehydration buffer with a trace (0.5 µL) amount of a saturated solution of bromophenol blue added for tracking. Each sample was pipetted evenly between the electrodes of a 24cm IPG strip holder (GE Healthcare). A 24cm Immobiline DryStrip gel pH 3-11 NL (GE Healthcare) was laid acrylamide side down into the sample with the positive end of the strip aligned with the positive end of the strip holder. The strip was covered in mineral oil to prevent sample evaporation and the lid was placed on the strip holder. The samples were then actively rehydrated at 50 V overnight using an Ettan IPGphor 3 IEF unit (GE Healthcare).

The strip was removed from the IPG Strip Holder and drained of excess oil using lint-free wipes. The strip holders were cleaned using Strip Holder Cleaning Solution (GE Healthcare), then small 25mm^2 wicks were cut from filter paper. For each strip, the wicks were wet with deionised water and a single wick was placed over each electrode in the strip holders. The strips were returned to the strip holders and again covered in mineral oil and returned to the Ettan IPGphor 3 IEF unit. The strips were focused overnight according to the following protocol: Step to 200 V for 1 hour, step to 400 V for 1 hour, step to 800 V for 2 hours, linear gradient to 8000 V for 1 hour, hold at 8000 V until 40 000 Vhr, step to 400V and hold until removed from the apparatus.

2.8.3 2nd dimension SDS-PAGE

Second dimension SDS-PAGE was carried out according to the 2D Electrophoresis Principals and Methods Handbook 80-6429-60AC (GE Healthcare). The focusing protocol on the Ettan IPGphor 3 IEF unit was stopped and the strips were immediately equilibrated in 10 mL of equilibration solution 1 for 15 minutes at room

temperature with gentle agitation, followed by 15 minutes in 10 mL of equilibration solution 2.

24cm 12.5% linear gels were labcast using an Ettan DALTsix gel caster (GE Healthcare) and low fluorescence plates according the manufacturer's instructions. Each equilibrated strip was loaded on top of a gel and sealed with 1% low melting point agarose solution, which was set at 4°C for 5 minutes. The gels were run on an Ettan DALTsix electrophoresis unit (GE Healthcare) with a MultiTemp III external thermostatic circulator (GE Healthcare) set to 10°C. The gels were run at constant power at 2 W per gel for 45 minutes, then at 17 W per gel until the bromophenol blue dye front reached 0.5 cm from the bottom edge of the gels.

2.8.4 Staining and imaging

Gels with DIGE-labelled proteins were left in the glass plates and imaged on a Typhoon 9400 variable mode imager at 200 μm. The Cy2-labelled sample was imaged using a blue 488 nm laser, 520 BP emission filter and PMT value of 645 V; the Cy3-labelled sample was imaged using a green 532 nm laser, 580 BP emission filter and PMT value of 600 V; and the Cy5-labelled sample was imaged using a red 633 nm laser, 670 BP emission filter and PMT value of 595 V.

Gels with non-labelled proteins were removed from the glass plates and placed in gel fixing solution, followed by either SyproRuby or silver staining to visualise the proteins. For both SyproRuby and silver staining, 100 mL volumes were used for 1D gels and 250 mL volumes for 2D gels.

SyproRuby staining was performed according to the manufacturer's instructions (BioRad). Gels were fixed for a minimum of 60 minutes, then incubated in SyproRuby stain overnight in the dark. The gel was rinsed in 10% methanol, 7% acetic acid solution for 60 minutes to reduce background fluorescence prior to imaging. Imaging was performed on a Typhoon 9400 variable mode imager at 200 μm using a blue 457 nm laser, 610 BP emission filter and PMT value of 600 V.

Silver staining was performed using an MS-compatible Erichrome black T (EBT)-silver method, as described by Jin *et al.* (2006) [115]. Gels were incubated in silver staining solution 1 (fixative) for 20 minutes, then incubated in solution 2 (sensitiser)

for 2 minutes, solution 3 (destain) for 2 minutes, dH_2O for 2 minutes, dH_2O for a further 2 minutes, solution 4 (silver) for 5 minutes, dH_2O for 20 seconds, dH_2O for a further 20 seconds, then solution 5 (developer). The gel was incubated in developer until no new spots appeared, then the development was stopped by the addition of solution 1 (fixative). The sensitiser, silver and developer solutions were made fresh each time staining was performed and the formaldehyde was added immediately before use.

2.9 Immunohistochemistry

2.9.1 DAB IHC of smears

10 μL of each sample was smeared across a 10 mm x 20 mm area of a microscope slide using a pipette tip and allowed to dry. The following steps were carried out in a humidifying chamber at room temperature. The slides were fixed for 10 minutes with IHC fixative, then washed with a transfer pipette three times for 5 minutes each with TBS-Azide. The slides were blocked for 60 minutes with blocking solution, and then incubated overnight in primary antibody diluted in antibody diluent. The slides were washed with a transfer pipette three times for 5 minutes each with TBS-Azide, then incubated in secondary antibody diluted in antibody diluent for 90 minutes. The slides were washed three times for 5 minutes each with TBS, incubated in ABC solution for 60 minutes, then washed again three times in TBS. The slides were then incubated in DAB solution for 10 minutes and the reaction was stopped by submerging the slides in TBS-Azide.

The slides were counterstained with haematoxylin (haematoxylin for 30 seconds, water for 1 minute, acid alcohol for 2 seconds, water for 1 minute, lithium carbonate for 2 minutes, water for 2 minutes, absolute alcohol three times for 20 seconds each, then xylene twice for 2 minutes each). Slides were coverslipped with depex and viewed with an Olympus BH-2 microscope.

2.9.2 Nanozoomer analysis and inclusion counting

Slides for inclusion analysis were imaged with a NanoZoomer slide imager (Hamamatsu Photonics, Hamamatsu City, Japan), which is a digital microscope that takes a series of 40x magnification images across each slide and digitally stitches

them together into a single large image. Each image was viewed using NDP.view version 1.1.27 (Hamamatsu Photonics) to preview the entire image and measure the size of the total sample area. Four representative fields at 20x magnification were selected from across the image and exported for analysis in ImageJ version 1.44p (National Institutes of Health, Bethesda, MD, USA).

ImageJ was used to count and measure the inclusions in each image. This was performed by converting each image to an RGB stack and selecting the layer that gave the greatest contrast between the inclusions and the surrounding structures (Figure 2.2B), which was green for images that contained magnetic beads and blue for all other images. The threshold for this image was then adjusted to maximise the number of inclusions selected while minimising the amount of surrounding structures visible (Figure 2.2C). This saturation threshold was determined for each experimental group and kept constant for comparing images within that group. This saturated image was then converted to binary and the particles were analysed. Particles of less than 40 pixels were excluded. This value was chosen as the largest magnetic beads present in the samples were 39 pixels when the optimal saturation was chosen, thus allowing for accurate and discriminatory automated counting and measuring. The outlines of the selected particles (inclusions) were then shown for verification (Figure 2.2D) along with the size of each inclusion, the total count, and the average size.

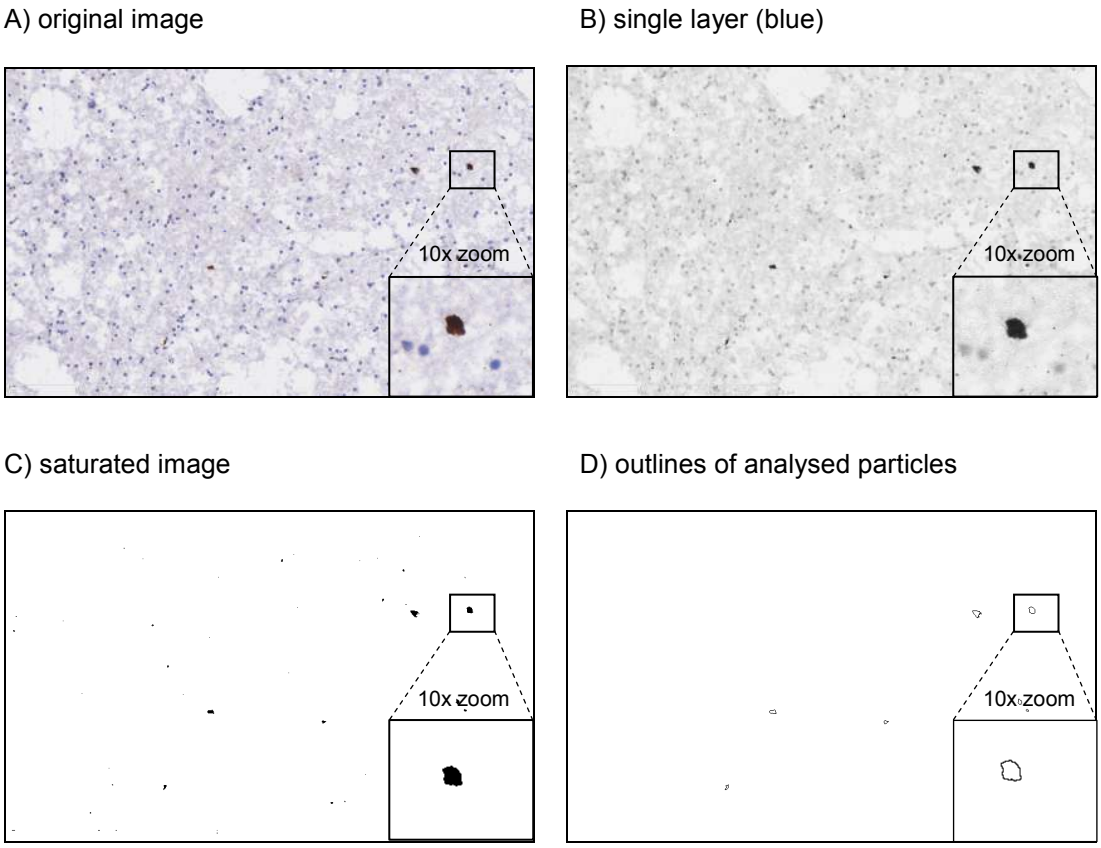

Figure 2-2: ImageJ analysis of Nanozoomer digital images of purification fractions
An example analysis for a single field of one sample. The original image (A) is converted to a single layer for optimised contrast (B), then the saturation threshold is set to discriminate inclusions from surrounding structures (C) and then the structures less than 40 pixels are screened out and the inclusions outlined (D) with the count and sizes reported in separate tables (not shown). A 10x zoomed inset is shown in the bottom right hand corner of each image.

2.10 Immunofluorescence

2.10.1 Immunofluorescence of smears

10 µL of each sample was smeared across a 10 mm x 20 mm area of a microscope slide using a pipette tip and allowed to dry. The following steps were carried out in a humidifying chamber at room temperature. The slides were fixed for 10 minutes with IHC fixative, then washed with a transfer pipette three times for 5 minutes each with TBS-Azide. The slides were blocked for 60 minutes with blocking solution, and then incubated for 2 hours in primary antibody diluted in antibody diluent. Primary antibodies from two different species were mixed together for single staining. Slides were then washed three times for 5 minutes each with TBS-Azide, then incubated in fluorescent-conjugated secondary antibodies diluted in antibody diluent for 60 minutes. The slides were washed three times for 5 minutes each with TBS–Azide and coverslipped with Vectashield Mounting Medium with DAPI.

2.10.2 Immunofluorescence of fixed sections

The slides with the fixed sections were placed into a slide rack and deparrafinised with the following protocol: xylene for 10 minutes x 2, 100% ethanol for 5 minutes x 2, 95% ethanol for 5 minutes, 70% ethanol for 5 minutes, dH_2O for 5 minutes. Antigen retrieval was then performed by immersing the slides in an antigen retrieval tank filled with 1 mM EDTA pH 8.0, which was microwaved on medium power for 10 minutes. The slides were then washed in TBS-Azide for 2 minutes.

The following steps were carried out in a humidifying chamber at room temperature. The slides were incubated in hydrogen peroxide solution (1% H_2O_2 + 50% methanol in dH_2O) for 30 minutes to eliminate endogenous peroxidase activity. The slides were then washed with a transfer pipette three times for 5 minutes each with TBS-Azide. The slides were blocked for 60 minutes with blocking solution and then incubated for 2 hours in primary antibody diluted in antibody diluent. Primary antibodies from two different species were mixed together for single staining. Slides were then washed three times for 5 minutes each with TBS-Azide, then incubated in fluorescent-conjugated secondary antibodies diluted in antibody diluent for 60 minutes. The slides were washed three times for 5 minutes each with TBS–Azide and coverslipped with Vectashield Mounting Medium with DAPI.

2.10.3 Imaging immunofluoresence slides

Images were captured on an Olympus BX-50 fluorescence microscope using the settings in Table 2.4 and a Photometrics CoolSNAP cooled CCD camera. The images from each channel were then colourised and merged in Adobe Photoshop (version CS5) using blue (hue 225) for DAPI, green (hue 105) for Cy3 and red (hue 345) for Alexa488.

Table 2-4: Microscopy fluorescence specifications

Dye	Excitation	Emission
Dapi (UV-excitable blue dye)	360 – 370	420 – 460
Alexa488 (blue-excitable green dye)	465 – 495	515 – 555
Cy3 (green-excitable red dye)	515 – 550	575 – 615

2.11 Tryptic digestion

2.11.1 Buffer-exchange prior to in-solution digestion

Vivaspin 500 5 kDa MWCO columns (GE Healthcare) were used to buffer-exchange samples to 50 mM ammonium bicarbonate prior to in-solution tryptic digestion, as per the manufacturer's instructions. The membrane of the Vivaspin column was rinsed with dH_2O prior to use by filling the column with 500 µL of dH_2O and centrifuging at 15,000x g for 5 minutes. The sample to be buffer-exchanged was then diluted to a total volume of 500 µL in 50mM ammonium bicarbonate. The sample was concentrated to approximately 50 µL by centrifugation at 15,000x g for approximately 10 minutes. The Vivaspin column was refilled to 500 µL with 50 mM ammonium bicarbonate and the sample was concentrated as before. The Vivaspin column was refilled again to 500 µL with 50 mM ammonium bicarbonate and the sample was concentrated as before, to a final volume of approximately 20 µL. The sample was pipetted out of the Vivaspin column into a low protein-binding tube, the protein concentration determined, and an in-solution digestion of the sample performed as described in section 2.11.2.

2.11.2 In-solution tryptic digestion

The complex protein samples were buffer-exchanged into 50 mM ammonium bicarbonate prior to digestion (section 2.11.1). In-solution tryptic digestion was based on the method in Appendix 2 of *Proteomics: A Cold Spring Harbor Laboratory Course Manual* [116]. A 1/10 volume of 50 mM DTT was added and incubated for 5 minutes at 65°C to reduce the disulphide bonds. A 1/10 volume of 100 mM iodoacetamide was added and incubated for 30 minutes at 30°C in the dark to alkylate sulphhydral residues and prevent the reformation of the disulphide bonds. Trypsin was added at a 1:50 trypsin to protein ratio and the sample was incubated at 37°C for a minimum of 4 hours.

2.11.3 Tryptic digestion of 1D SDS-PAGE slices

Tryptic digestion of 1D gel slices was based on the method in Appendix 3 of *Proteomics: A Cold Spring Harbor Laboratory Course Manual* [116]. The gel was washed in dH_2O three times for 30 minutes per wash, to remove traces of acetic acid from the fixative. Bands of interest were excised using a scalpel, diced into 1 mm^2 pieces, and placed into the wells of a 96-well plate.

The gel pieces were washed in 150 µL 50% ACN:dH_2O for 15 minutes. The wash was removed and 150 µL of 100% ACN was added to shrink the gel pieces. The pieces were rehydrated in 75 µL 100mM ammonium bicarbonate for 5 minutes, then 75 µL of ACN was added and the pieces were incubated for 15 minutes. The wash was removed and 150 µL of 100% ACN was added to shrink the gel pieces.

The gel pieces were rehydrated in 150 µL of 10 mM DTT in 100 mM ammonium bicarbonate solution and incubated for 45 minutes at 65°C. The DTT solution was removed and 150 µL of 50 mM iodoacetamide in 100 mM ammonium bicarbonate was added immediately and incubated for 30 minutes at 30°C in the dark. The iodoacetamide solution was removed and the gel pieces were washed in 150 µL of 50% ACN:dH_2O for 15 minutes. The wash was removed and 150 µL of 100% ACN was added to shrink the gel pieces.

Trypsin stock solution (1 µg/µL) was diluted out 100-fold (0.01 µg/µL) in 50mM ammonium bicarbonate. The gel pieces were rehydrated in 28 µL (0.28µg) of trypsin

solution for 30 minutes at room temperature, then incubated at 37°C for a minimum of 4 hours.

2.11.4 Tryptic digestion of 2D SDS-PAGE spots

Tryptic digestion of 2D gel spots was based on the method in Appendix 3 of *Proteomics: A Cold Spring Harbor Laboratory Course Manual* [116]. Gel spots were excised from a 2D gel using a truncated low protein-binding 200 µL pipette tip attached to an OneTouch Plus Spot Picker. The cutting tip was rinsed in 100% ethanol between each spot to minimise cross contamination. Each spot was placed in a separate well of a 96-well plate and any residual liquid was removed. Using a Biomek® 3000 laboratory automation workstation (Beckman Coulter), 150µL of 100 mM ammonium bicarbonate was pipetted into each well and the plugs were washed with shaking at an amplitude of 6 on a DPC Micromix 5 mixing platform for 30 minutes. The ammonium bicarbonate was removed and 150 µL of acetonitrile was pipetted into each well and left overnight to dehydrate the gel plugs.

The plugs were rehydrated with 150 µL of 100 mM ammonium bicarbonate and washed with shaking for 30 minutes. 130 µL of the wash was removed and replaced with 130 µL of fresh 100 mM ammonium bicarbonate and washed for a further 30 minutes. All liquid was removed and the plugs were washed with 150 µL of 50% ACN:dH_2O for 30 minutes. 130 µL of the wash was removed and replaced with 130 µL of fresh 50% ACN:dH_2O and washed for a further 30 minutes. All liquid was removed and 150 µL of acetonitrile was pipetted into each well and left overnight to dehydrate the gel plugs.

Trypsin stock solution (1 µg/µL) was diluted out 100-fold (0.01 µg/µL) in 50 mM ammonium bicarbonate. Each gel plug was rehydrated in 28 µL (0.28µg) of trypsin solution for 30 minutes at room temperature, then incubated at 37°C for a minimum of 4 hours.

2.12 LC MS/MS

2.12.1 HPLC linear ion trap / FTMS mass spectrometry

The digested peptides obtained from either complex mixtures or gel pieces were analysed with a Thermo LTQ Orbitrap XL mass spectrometer (Thermo Fisher Scientific, Waltham, MA, USA) fitted with a nanospray source. 1 to 5 µL of each sample was drawn into a 20 µL loop with buffer on either side using a custom inject program and loaded onto to a Acclaim® PepMap 100 C18 cartridge (Dionex, Sunnyvale, CA, USA) at 5 µL/min for 12 minutes, then separated on a packed nanocapillary column NTCC-360/100-5-153 (Nikkyo Technos, Tokyo, Japan) at 200 nL/min using an Ultimate 3000 HPLC (Dionex) with a gradient from 0% to 40% Buffer B over 52 min, followed by 95% Buffer B for 16 min, followed by 100% Buffer A for 30 min. The mass spectrometer was operated in positive ion mode with one full scan of mass/charge (m/z) 300-2000 in the FTMS analyser, with ions with a charge state of 1 rejected, followed by product ion scans of the six most intense ions in the ion trap analyser, with dynamic exclusion of 15 seconds with a repeat duration of 15 seconds, an exclusion list of 500 proteins, and collision-induced dissociation energy of 35%.

2.12.2 Protein identification

The MS spectra were searched with Thermo Proteome Discoverer (PD) version 1.2.0.208 based on the method by Wilson *et al.* [117] using the Sequest algorithm against the Uniprot human (taxonomy 9606) with isoforms database version August 2011. The search parameters were: trypsin as the protease with up to two missed cleavages; mass tolerance for peptide identification of precursor and product ions of 15 ppm and 0.8 Da respectively; and variable modifications of carbamidomethylation and nitrosylation of carbons, oxidation of methionines, ubiquitination of lysines, and phosphorylation of serines, threonines and tyrosines. The filters were: peptides of a high confidence value, count only rank 1 peptides, count peptide only in top scored proteins, and at least two unique peptides sequenced for each protein. The false discovery rate (FDR) was calculated for each complex mixture analysis using the FDR algorithm in PD. The FDR was less than 0.01 for all samples analysed.

3 Optimisation of a GCI purification method

3.1 Introduction

3.1.1 Optimisation of a published GCI purification method

In order to determine the proteome of glial cytoplasmic inclusions, it was necessary to develop a protocol to purify the inclusions from post-mortem MSA brain tissue with minimum contamination from surrounding structures. We currently have an incomplete understanding of which proteins are present in inclusions, the mechanism for their incorporation into inclusion bodies, and the reason for their incorporation in the first place. Thus, to identify the proteome of GCIs and LBs is a keystone of the research into this area, which provides the vital first step to elucidating the role these inclusions play in neurodegenerative disorders.

Isolating inclusions is extremely difficult, as they must be successfully separated from the surrounding brain tissue within which they are enmeshed. Few attempts have been made in the past to purify inclusions for this reason, with the most successful method thus far being a combination of density gradient centrifugation followed by immunomagnetic capture of inclusions, developed by Gai *et al.* [113], as discussed in Chapter 1.7 However, despite providing a higher yield of inclusions than other published methods, this method still only generates a yield of 50-70 μg of total protein per 12 g of brain tissue [113]. The purity of the final preparation is also questionable, with large amounts of tubulin contamination present (Figure 3.1) [118]. If the inclusions are enmeshed within the cytoskeleton, and then pulled out via immunocapture, the surrounding meshwork and attached proteins will be pulled out with the inclusions and give an impure preparation.

3.1.2 Hypotheses

Glial cytoplasmic inclusions are enmeshed within the cytoskeletal network. When inclusions are pulled out with immunomagnetic beads, the surrounding cytoskeletal structure and attached proteins are also enriched. This leads to increased levels of non-inclusion proteins, particularly tubulin. The addition of a limited protease digestion step during the purification will release the inclusions from the surrounding cytoskeleton and free them for immunocapture, generating higher yield and purity

(Figure 3.2). The brief trypsin exposure may remove some peripheral proteins but it will not remove core inclusion proteins at an appropriate concentration.

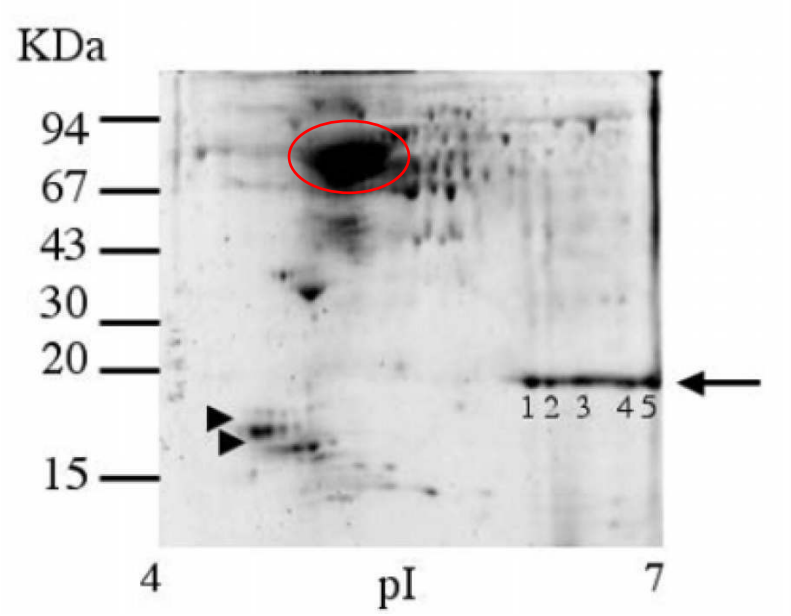

Figure 3-1: 2-D gel electrophoresis of solubilised immunopurified GCIs using Gai *et al.* method [118]
Reproduced from Figure 2B from Pountney et al. 2005 [118]. In the published image, the arrowheads show the α-synuclein isoforms and the arrow shows the α-β-crystallin isoforms. The tubulin has been highlighted in the red circle (my emphasis).

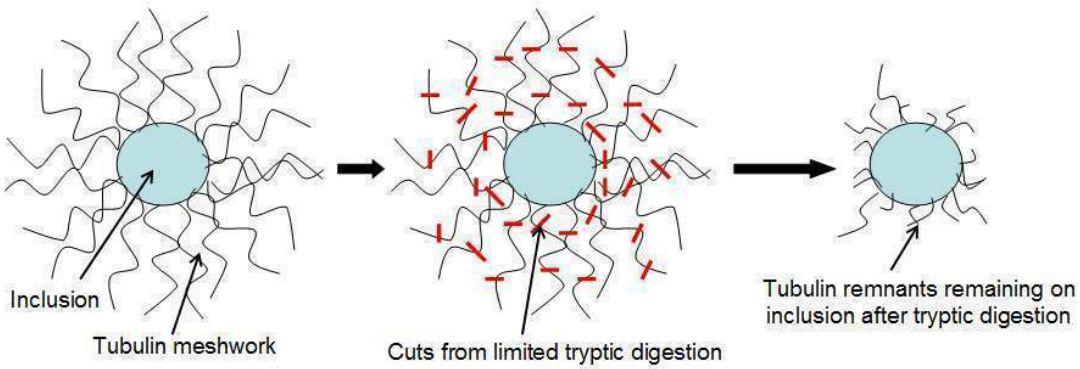

Figure 3-2: Proposed explanation for the presence of tubulin in immunocaptured inclusion preparations
The inclusion is enmeshed in the surrounding tubulin framework, which is cut with a limited tryptic digestion, leaving tubulin remnants on the inclusion surface.

3.1.3 Aim

- To optimise the GCI purification method of Gai *et al.* [113], by making a series of modifications to increase both the yield and the purity. The four principle modifications implemented are summarised in Table 3.1 with the differences between the published and optimised methods shown in Figure 3.3.

3.2 Materials and Methods

3.2.1 Inclusion purifications

Brain tissue homogenisation was performed as described in Chapter 2.4.

3.2.1.1 Inclusion purification for Modification #1

An inclusion purification was performed using 4 tubes of brain homogenate from case SA0101 (Table 2.3) as described in Chapter 2.5. At step 5, prior to collecting the inclusion enriched fractions, eight 1 mL layers were collected from the meniscus of a representative Percoll density gradient tube, using a 1 mL pipette tip blunted by removing the last 5 mm of the tip with a scalpel. The part of the gradient contained in each fraction was noted. The P1 and lower fractions from the other tubes (Figure 3.4A) were collected separately. At the end of step 5, the P1 fraction was transferred to 2x 2 mL microfuge tubes and the lower fraction to a single 2 mL microfuge tube. Step 6 was omitted. 45 µg of primary antibody (step 8), 20 µg of secondary antibody (step 9), 19.2 µL of MyOne beads and 29.6 µL of M-280 beads (step 10) were added per tube. At step 12, the inclusions from each fraction were solubilised in 475 µL of protein extraction buffer. As step 6 (nuclei lysis and DNA digestion, modification #3) was omitted, data from this experiment was presented in section 3.3.1.3 as a comparison for the data after the development of modification #3.

A second inclusion purification with P1 and lower fractions collected and processed separately, from which data was used, is described in section 3.2.1.4.

3.2.1.2 Inclusion purification for Modification #2

Steps 1-5 of an inclusion purification were performed using 2 tubes of brain homogenate from case SA0133 (Table 2.3) as described in Chapter 2.5. At the end of step 5, the sample was transferred to a single 2 mL microfuge tube. The pH of the sample was set to 8.0 by the addition of 10 µL of 1M NaOH and the tube was prewarmed to 37°C for 10 minutes (the optimal pH and temperature for the trypsin enzyme to be active). Trypsin was added at a 1:4000 enzyme to protein ratio, as determined by an EZQ protein quantification assay of the fraction at the end of step 5. The sample was incubated at 37°C at 1400 RPM in a Thermomixer Comfort, with 25 µL aliquots taken at 1, 5 and 10 minutes and added immediately to 25 µL of 2x

protease inhibitor mix (0.6 mM PMSF, 2 µg/mL Pepstatin and 2 µg/mL Leupeptin in TBS Azide). At 15 minutes, the entire reaction was stopped by the addition of 0.3 mM PMSF, followed by 1 µg/ml Leupeptin and 1 µg/ml Pepstatin. The 0, 1, 5, 10 and 15 minute digest fractions were then analysed by Western blotting and immunohistochemistry.

3.2.1.3 Inclusion purification for Modification #3

An inclusion purification was performed using 3 tubes of brain homogenate from case SA0101 (Table 2.3) as described in Chapter 2.5. At the end of step 5, the sample was transferred to two 2 mL microfuge tubes. Step 6 (modification #3), as described in Chapter 2.5.2, was introduced prior to the tryptic digestion (step 7) for the first time. 70 µg of primary antibody (step 8), 30 µg of secondary antibody (step 9), 28.8 µL of MyOne beads and 44.4 µL of M-280 beads (step 10) were added per tube. At step 12, the inclusions were solubilised in 500 µL of protein extraction buffer.

An inclusion purification performed without modification #3 (nuclei lysis and DNA digestion), used as a comparison for the data after modification #3 was developed, is described in section 3.2.1.1.

3.2.1.4 Inclusion purification for Modification #4

An inclusion purification was performed using 4 tubes of brain homogenate from case SA0058 (Table 2.3) as described in Chapter 2.5. The P1 and lower fractions were collected separately from each other in step 5, with the lower fraction stored at 4°C for a subsequent experiment. At the end of step 5, the P1 fraction was transferred to 2x 2 mL microfuge tubes. Step 6 was omitted. After step 7, one 2 mL tube was stored at 4°C for a subsequent experiment and one 2 mL tube was processed through steps 8-12. 22.5 µg of primary antibody (step 8), 10 µg of secondary antibody (step 9), 9.6 µL of MyOne beads and 14.8 µL of M-280 beads (step 10) were added. The wash fraction from step 11 was processed again through steps 10-11, due to a high number of uncaptured inclusions present in the wash fraction, with 19.2 µL of MyOne beads and 29.6 µL of M-280 beads added at step 10. As no additional inclusions were captured with the addition of beads only, the new wash fraction from step 11 was processed again through steps 8-11. 45 µg of

primary antibody (step 8), 20 µg of secondary antibody (step 9), 19.2 µL of MyOne beads and 29.6 µL of M-280 beads (step 10) were added. At step 12, the total inclusions captured from the experiment were combined and solubilised in 100 µL of 1x sample buffer.

From the experiment above, the lower fraction was processed through steps 5-12 of the inclusion purification protocol and the remaining half of the P1 fraction through steps 8-12. At the end of step 5, the lower fraction was transferred to a single 2 mL microfuge tube. Step 6 was omitted. 67.5 µg of primary antibody (step 8), 30 µg of secondary antibody (step 9), 28.8 µL of MyOne beads and 44.4 µL of M-280 beads (step 10) were added per tube. At step 12, the inclusions from each sample were solubilised in 50 µL of 6 M urea and 1x sample buffer.

3.2.2 DAB immunohistochemistry

DAB immunohistochemistry was performed on selected fractions from the purification procedure as described in Chapter 2.9.1. All staining was performed using a sheep anti-α-synuclein primary antibody (antibody no. 1, Table 2.1) used at 1:1000 (1 µg/mL) and an anti-sheep biotinylated secondary (antibody no. 10, Table 2.2) used at 1:500 (2.6 µg/mL).

Nanozoomer analysis and inclusion counting was performed as described in Chapter 2.9.2. A saturation threshold of 139 was used.

3.2.3 1-DE and Western blotting

1-DE and Western blotting was performed on fractions from the partial tryptic digestion time-course experiment (section 3.2.1.2) as described in Chapter 2.7. Prior to 1-DE, each fraction was solubilised in 1x 1D sample buffer without bromophenol blue, vortexed and heated at 95°C for 5 minutes. The samples were vortexed again, spun at 18,000x g and the supernatants collected. The protein concentration of each fraction was determined using the EZQ Protein Quantification Kit (Invitrogen) as described in Chapter 2.6.1. Samples were diluted to 1 µg/µL in 1x 1D sample buffer with bromophenol blue and subjected to 1-DE using 4-20% SDS-PAGE as described in Chapter 2.7.1.

The gels were transferred to PVDF membrane and Western blotting was performed using the SNAP ID system as described in Chapter 2.7.2. The primary antibodies used were mouse anti-BIII tubulin (antibody no. 3, Table 2.1) at 1:300 (1.67 μg/mL) and rabbit anti-α-synuclein (antibody no. 2, Table 2.1) at 1:450 (2.22 μg/mL). HRP-conjugated secondary antibodies against mouse and rabbit (antibodies no. 12 and no. 11 respectively, Table 2.2) were used at 1:1500 (0.27 μg/mL).

The blots were imaged on a Fujifilm LAS-4000 CCD imager and analysed using Carestream Molecular Imaging Software Version 5.0.6.20. For quantitation, rectangular boxes of uniform size were draw around the band or region of interest (ROI) in each lane for comparison. Background subtraction was performed using the median of each ROIs perimeter.

3.2.4 2-DE – Ettan large format

2D gel electrophoresis was performed as described in Chapter 2.8. 75 μg of solubilised inclusions purified prior to the development of modification #3 (section 3.2.1.1) were subjected to isoelectric focusing using a 24cm pH 3-11NL Immobiline DryStrip (GE Healthcare), as described in section 2.8.2. The strip was focused for 80,000 volt hours according to the following protocol: Step to 500 V for 30 min, step to 1 000 V for 30 min, gradient to 10 000 V for 30 min, hold at 10 000 V until 65 000 Vhr, step to 1 000 V and held until removed. The 2nd dimension was performed as described in section 2.8.3 with an 8-19% gradient gel, run at constant voltage at 350 V. The gel was stained with SyproRuby and imaged on a Typhoon 9400 variable mode imager, as described in Chapter 2.8.4, with a photomultiplier tube value of 900 V.

3.2.5 2-DE – medium format

2D gel electrophoresis was performed as described in Chapter 2.8. 170 μg of solubilised inclusions purified after the development of modification #3 (section 3.2.1.3) were subjected to isoelectric focusing using a 13cm pH 3-11NL Immobiline DryStrip (GE Healthcare), as described in section 2.8.2. The strip was focused for 63,000 volt hours according to the following protocol: Step to 500 V for 30 min, step to 1 000 V for 30 min, gradient to 10 000 V for 30 min, hold at 10 000 V until 30 000 Vhr, step to 1 000 V and held until removed. The 2nd dimension was performed

as described in section 2.8.3 with a 12.5% linear gel, run at constant voltage at 300 V. The gel was placed in fixative overnight, then stained with Coomassie Blue for 60 minutes. After destaining, the gel was imaged on a Typhoon 9400 variable mode imager using a green (532 nm) laser and a photo-multiplier tube value of 600 V. The gel was scanned at 200 μm.

3.2.6 Tryptic digestion and mass spectrometry

Selected 2D gel spots were excised and digested with trypsin, as described in Chapter 2.11.4. The digested peptides were analysed with a Thermo LTQ XL linear ion trap mass spectrometer fitted with a nanospray source (Thermo Fisher Scientific, Waltham, MA, USA). The samples were loaded onto a 300 μm i.d. 5 mm C18 PepMap 100 precolumn (Dionex Corp, Sunnyvale, CA, USA) at 20 μL/min for 3 minutes, then separated on a 75 μm 150 mm C18 PepMap 100 column (Dionex) at 200 nL/min using an Dionex Ultimate 3000 HPLC with a gradient from 0% to 55% Buffer B over 55 min, followed by a step to 100% Buffer B for 9 min. The mass spectrometer was operated in positive ion mode with one full scan of mass/charge (m/z) 300-2000, followed by product ion scans of the six most intense ions, with dynamic exclusion of 30 seconds with a repeat duration of 30 seconds, an exclusion list of 500 proteins, and collision-induced dissociation energy of 35%.

3.2.7 Protein identification

The MS spectra were searched with Bioworks 3.3 (Thermo Electron Corp, San Jose, CA, USA) using the Sequest algorithm against the IPI Human database v3.39 using Trypsin digestion as the protease, allowing for two missed cleavages, with homoserine and homo-serine lactone as variable methionine modifications and using the following filters: 1) the cross-correlation scores of matches were greater than 1.5, 2.0 and 2.5 for charge state 1, 2 and 3 peptide ions respectively, 2) peptide probability was less than 0.001, and 3) each protein identified had at least two different peptides sequenced. The mass tolerance for peptide identification of precursor ions was 1 Da and 0.5 Da for product ions.

3.3 Results

3.3.1 Optimisation of inclusion purification method

The Gai *et al.* [113] inclusion purification method was optimised to deliver a greater yield and purity. Four principle modifications were developed (Table 3.1). The differences between the published method and the optimised method are summarised in Figure 3.3.

Table 3-1: Major modifications made in the optimisation of the published inclusion purification method of Gai *et al.* [113]

No.	Steps	Modification
1	5	Collection of a greater part of the Percoll gradient
2	7	Limited tryptic digestion to release inclusions
3	6	Lysis of nuclei prior to DNase digestion
4	8, 9 & 10	Increase in antibody and magnetic bead amounts

Figure 3-3: Summary of differences between published and optimised inclusion purification methods

Steps 1-4: No major modifications.

Step 5: In the published method, the P1 fraction was collected, with the waste and myelin fractions (above P1) and the lower fraction (below P1) discarded. In the optimised method, the Percoll-enriched fraction (which encompasses the P1 and lower fractions) was collected, with the waste and myelin fractions (above the Percoll-enriched fraction) discarded. See Figure 3.4 for illustration of fractions.

Step 6: In the published method, 1 µg/mL of DNase I and 5 mM $MgCl_2$ (DNase cofactor) were added (however, the nuclei were still intact) and the suspension was shaken and incubated for 3 hours at 37°C, then filtered through 20 µm nylon mesh. In the optimised method, 2 µg of trypsin was added to the sample for 10 seconds to lyse the nuclei, with the reaction stopped by the addition of protease inhibitors. 100 µg/mL of DNase I and 10 mM $MgCl_2$ (DNase cofactor) were added and the sample was incubated for 1 hour at 37°C at 1400RPM.

Step 7: In the published method, the sample underwent a second Percoll density gradient. As in step 4, the sample was diluted to 6 mL in 14% (v/v) Percoll Plus in HB, overlaid on a 2.4mL cushion of 35% Percoll Plus (v/v) in HB, and centrifuged at 35,000x g for 30 mins at 4°C to create a density gradient. The material banding near the sample/35% interface (P2 fraction) was collected. In the optimised method, a limited tryptic digestion was performed, with trypsin added at a 1:4000 enzyme:protein ratio, as determined by an EZQ protein quantification assay. The sample was incubated for 5 mins at 37°C, with the reaction stopped by the addition of protease inhibitors.

Steps 8-10: Larger quantities of antibodies and magnetic beads were used to capture the larger amount of inclusions available from the introduction of the other modifications. In the published method, 1.3 µg/mL of primary antibody, 1.3 µg/mL of secondary antibody and 30 µL of M-280 beads per 10^6 inclusions were added. In the optimised method, 30 µg/mL of primary antibody, 15 µg/mL of secondary antibody, 20 µL of MyOne beads and 30 µL of M-280 beads were added.

Step 11: No major modifications.

Step 12: A minor modification was made to the solubilisation buffer. In the published method, the solubilisation buffer was 2% SDS, 8 M urea, 0.1 mM PMSF, 5 mM EDTA in 50 mM Tris-HCl pH 7.0. 15 µL of buffer was added per 10^6 inclusions and incubated from 2 hours to overnight at 37°C. In the optimised method, the solubilisation buffer was 7M urea, 2M thiourea, 4% CHAPS. 200 µL was added and the inclusions were incubated overnight at room temperature. This change was made for compatibility with downstream 2-DE application.

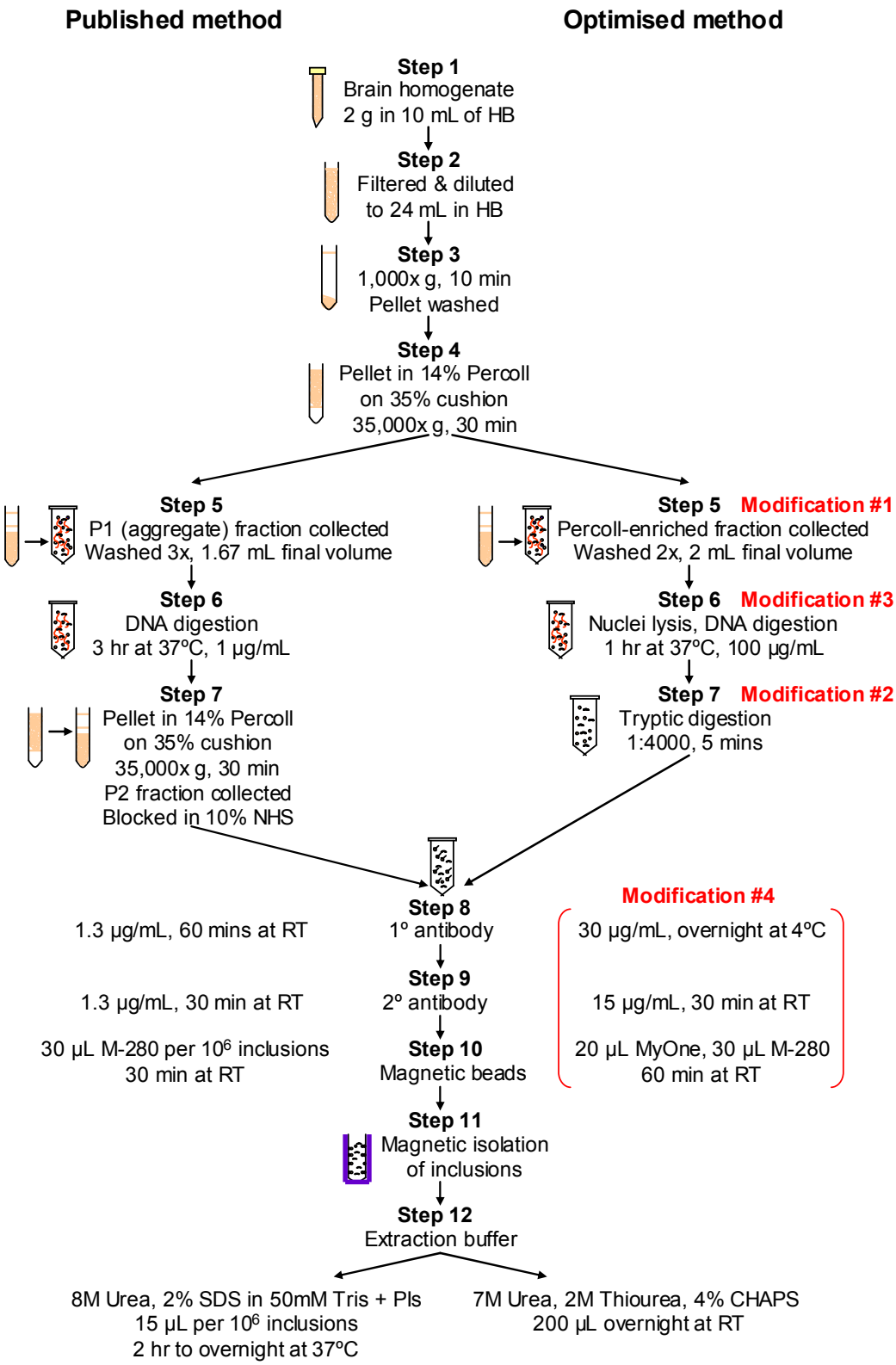
Published method
Optimised method
Step 1
Brain homogenate
2 g in 10 mL of HB
Step 2
Filtered & diluted
to 24 mL in HB
Step 3
1,000x g, 10 min
Pellet washed
Step 4
Pellet in 14% Percoll
on 35% cushion
35,000x g, 30 min
Step 5
P1 (aggregate) fraction collected
Washed 3x, 1.67 mL final volume
Step 6
DNA digestion
3 hr at 37ºC, 1 µg/mL
Step 7
Pellet in 14% Percoll
on 35% cushion
35,000x g, 30 min
P2 fraction collected
Blocked in 10% NHS
Step 5 Modification #1
Percoll-enriched fraction collected
Washed 2x, 2 mL final volume
Step 6 Modification #3
Nuclei lysis, DNA digestion
1 hr at 37ºC, 100 µg/mL
Step 7 Modification #2
Tryptic digestion
1:4000, 5 mins
Step 8
1º antibody
1.3 µg/mL, 60 mins at RT
Modification #4
30 µg/mL, overnight at 4ºC
Step 9
2º antibody
1.3 µg/mL, 30 min at RT
15 µg/mL, 30 min at RT
Step 10
Magnetic beads
30 µL M-280 per 10^6 inclusions
30 min at RT
20 µL MyOne, 30 µL M-280
60 min at RT
Step 11
Magnetic isolation
of inclusions
Step 12
Extraction buffer
8M Urea, 2% SDS in 50mM Tris + PIs
15 µL per 10^6 inclusions
2 hr to overnight at 37ºC
7M Urea, 2M Thiourea, 4% CHAPS
200 µL overnight at RT

3.3.2 Modification #1

The published method of Gai *et al.* [113] describes using only the 'P1' fraction from the Percoll gradient (Figure 3.4A). From an 8 mL Percoll density gradient tube (step 4 of inclusion purification method), 1 mL fractions were taken from the top down using a 1 mL pipette tip with a blunted end. IHC was performed on a 10 µL smear from each fraction to check for the presence of inclusions (Figure 3.5). GCIs were present in the P1 fraction, bound up in clumps with nuclei, but they also appear singularly throughout the 'lower' fraction, below the P1 fraction.

The P1 fraction and the lower fraction from the Percoll density gradient were processed separately in two different purification experiments, with the GCIs from each fraction solubilised and the protein content determined by EZQ assay. The lower fraction yielded a very similar amount of purified protein compared to the P1 fraction (Table 3.2). Thus, by collecting the entire section below the myelin layer (the "Percoll enriched" fraction, Figure 3.4B), a 2.0-fold greater yield of GCIs was available for immunomagnetic capture.

Table 3-2: Inclusion protein yield from different fractions of the Percoll gradient

Replicate	Yield (µg)[a]			Increase[b]
	P1	Lower	Total	(-fold)
1	76	77	153	2.0
2	82	84	166	2.0
Mean	79	80.5	159.5	2.0

[a] yield per 4 tubes of brain homogenate
[b] increase in total yield compared to the yield from the P1 fraction only

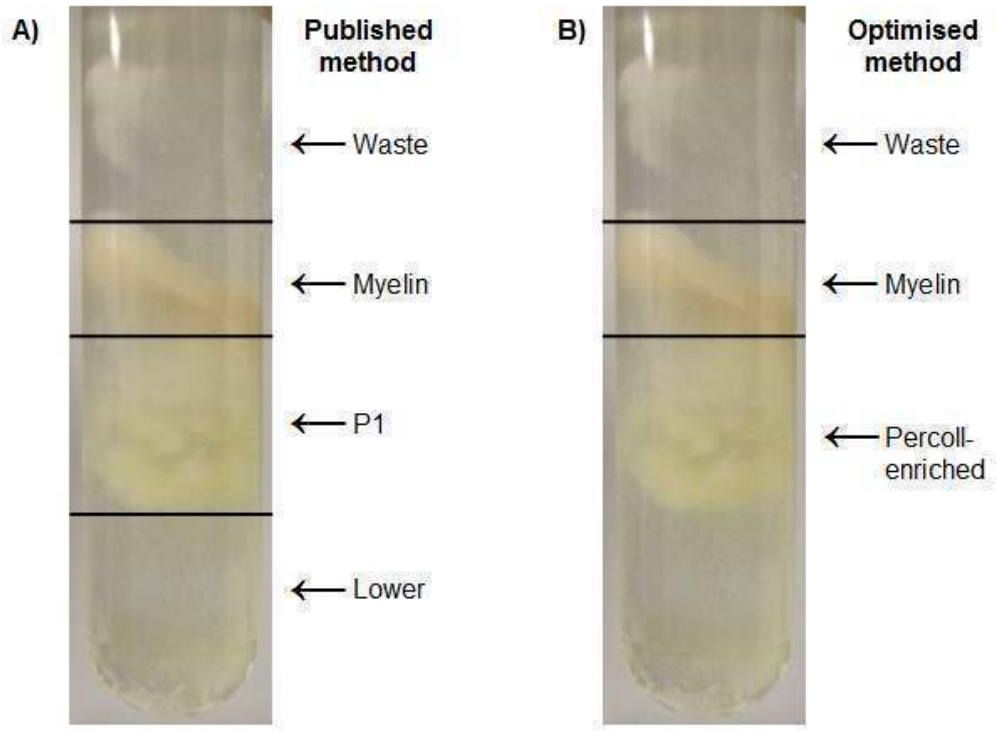

Figure 3-4: Percoll density gradient centrifugation (step 4) from inclusion purification protocol

A representative tube from the Percoll density gradient centrifugation (step 4) of the inclusion purification protocol is shown (image duplicated). A) In the published method, only the P1 fraction was collected and processed for immunomagnetic capture of inclusions. B) In the optimised method, the entire Percoll-enriched fraction was found to contain inclusions (Figure 3.5) and was processed further, increasing the yield of inclusions available for immunomagnetic capture.

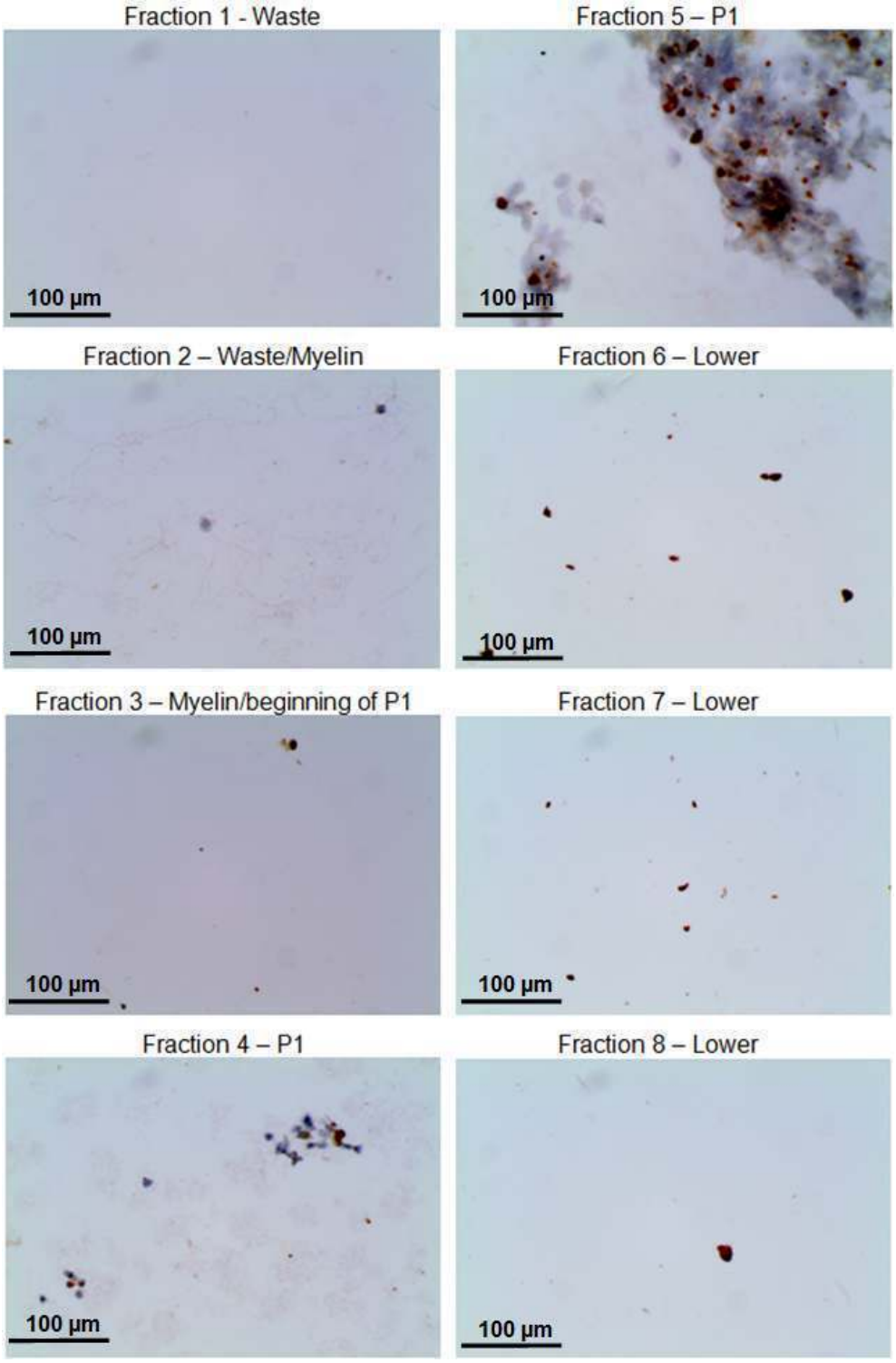

Figure 3-5: Immunohistochemistry of Percoll gradient fractions
An 8 mL Percoll gradient tube from step 4 of the inclusion purification was collected into 1 mL sections from the top down using a 1 mL pipette tip with a blunted end. A 10 µL smear of each fraction was DAB stained against α-synuclein (antibody no. 1, Table 2.1) and counterstained with haematoxylin. All images were taken at 20x magnification. The waste and myelin sections of the gradient do not contain inclusions (Fractions 1 and 2), with inclusions beginning to appear where the myelin fraction meets the P1 fraction (Fraction 3). The inclusions become denser, enmeshed with nuclei, throughout the P1 fraction (Fractions 4-5) and then singular inclusions appear scattered throughout the 'lower' fraction (Fractions 6-8).

3.3.3 Modification #2

A limited protease digestion (step 7) was introduced into the purification procedure after the collection of the Percoll-enriched fraction (step 5). This modification was made to release the inclusions from the cytoskeleton, allowing individual inclusions to be isolated and not the surrounding meshwork of tubulin and attached proteins. The existing step 7, a 2nd Percoll density gradient, was eliminated from the new method because inclusions were found to settle across a range of densities (as shown by the immunohistochemistry of the Percoll gradient layers in Figure 3.5) as opposed to banding tightly at one interface, which limits the effectiveness of a density gradient as an enrichment technique.

Proteinase K (at 1 mg/mL) and trypsin (at a 1:20 enzyme:protein ratio) were both trialled for a limited digestion, with the effect on both tubulin and the inclusions assessed using immunofluoresence. Trypsin was chosen for further investigation, as proteinase K digested the inclusions completely within 1 minute, whereas trypsin reduced the size of the inclusions, but they still remained after 60 minutes (data not shown). The optimum trypsin concentration was then determined by trialling a range of enzyme:protein ratios (1:100, 1:400 and 1:4000). At the 1:400 ratio, inclusion size was still visibly reduced after 15 minutes of digestion, but no effect was discernable for the 1:4000 ratio upon visual examination after 15 minutes (data not shown).

To optimise the digestion conditions, an incubation time-course with the 1:4000 ratio was performed, with aliquots taken and quenched with protease inhibitors at 1, 5, 10, and 15 minute timepoints. These timepoints were assessed with Western blotting and immunohistochemistry to determine which duration gave a reduction in the surrounding tubulin while having a minimal impact on the inclusions themselves. β-tubulin was used as a marker for cytoskeletal contamination, to show the effect of the digestion, and α-synuclein was used as a marker of inclusion integrity.

The increase in lower molecular weight fragments of β-tubulin occurred within 1 minute of digestion (Lane 2, Figure 3.6A), increasing by 5 minutes (Lane 3, Figure 3.6A) with no further increase of lower molecular weight fragments observable with

further digestion (Lanes 4-5, Figure 3.6A). See also quantitation of β-tubulin fragments in Figure 3.7.

A slight decrease in abundance of dimeric α-synuclein was apparent beyond 5 minutes of digestion (Lanes 4-5, Figure 3.6B) with no observable change in monomeric α-synuclein at any of the digestion timepoints assessed. See also the quantitation of monomeric α-synuclein in Figure 3.8.

The pre-digestion fraction and the 5 minute and 15 minute digestion fractions were also assessed by immunohistochemistry (Figure 3.9). The impact of the partial tryptic digestion on the structures surrounding the inclusions was visible by 5 minutes of digestion (Figure 3.9B). The slides were imaged with a Nanozoomer Digital Imager and the inclusions from four representative 20x fields from each sample were analysed, as described in Chapter 2.9.2. There appears to be no reduction in inclusion size as a result of the tryptic digestion after either 5 or 15 minutes of digestion (Table 3.3).

Thus, 5 minutes was chosen as the optimal digestion timepoint, as no further benefit to tubulin degradation was observed beyond this time and impact on the α-synuclein structure of inclusions may occur beyond this time.

Table 3-3: Inclusion size after partial tryptic digestion

Digestion time (minutes)	Number of inclusions measured[a]	Average size (pixels)
0	94	92
5	70	104
15	137	95

[a] Total number of inclusions counted and analysed across four representative 20x fields using ImageJ, as described in Chapter 2.9.2.

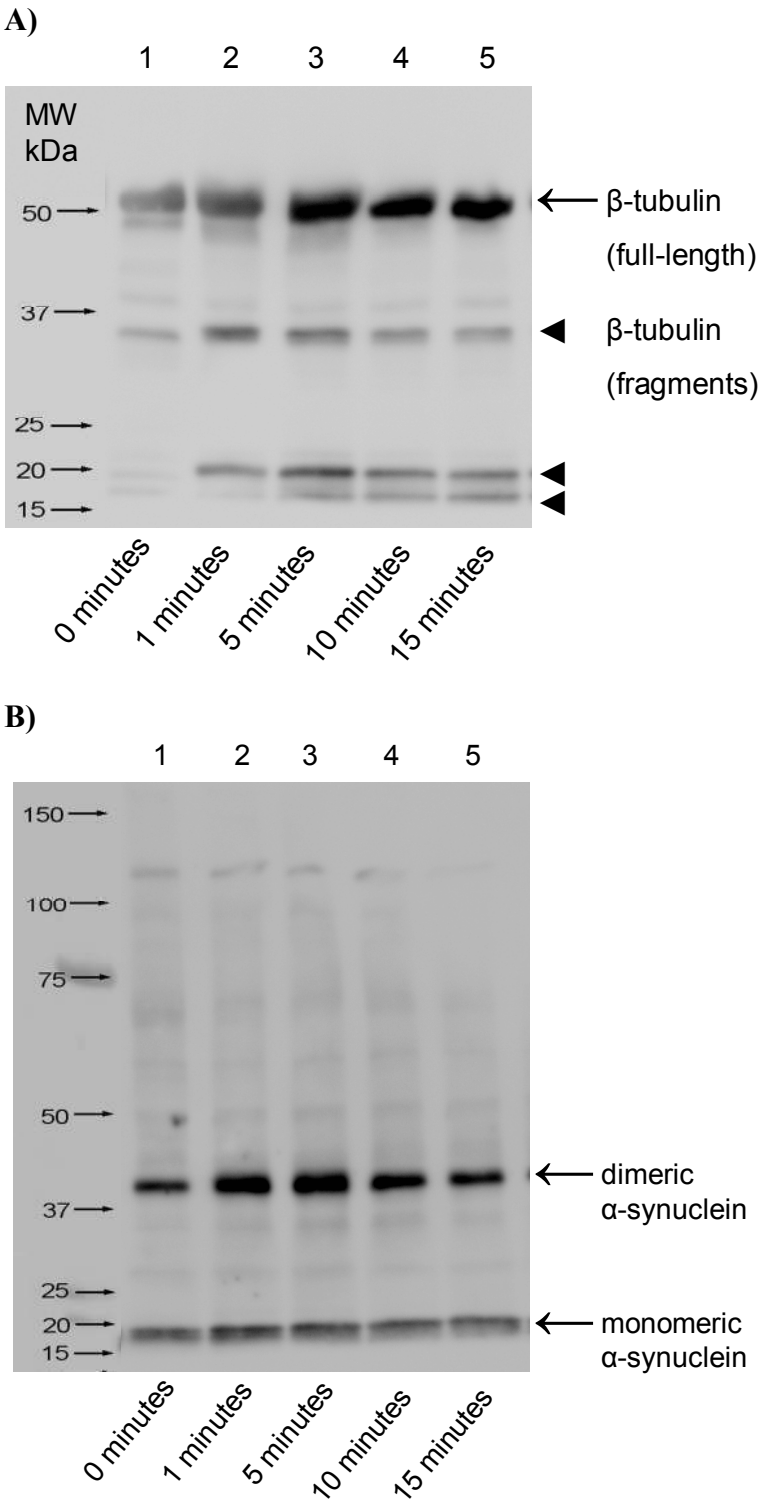

Figure 3-6: Antibody detection of β-tubulin and α-synuclein in the optimisation of partial tryptic digestion of the Percoll enriched fraction (n=1).
2 tubes of brain homogenate were processed according to steps 1 to 5 of the inclusion purification protocol (as described in section 3.2.1.2). The Percoll-enriched fraction (step 5) was incubated with trypsin for 0 minutes (Lane 1), 1 minute (Lane 2), 5 minutes (Lane 3), 10 minutes (Lane 4) or 15 minutes (Lane 5) at a ratio of 1 µg trypsin/4,000 µg protein at 37°C. The samples were solubilised in 1x sample buffer and 20 µg of each sample was separated by 4-20% SDS-PAGE, transferred to PVDF and probed with antibodies against either A) β-tubulin (antibody no. 3, Table 2.1) or B) α-synuclein (antibody no. 2, Table 2.1).

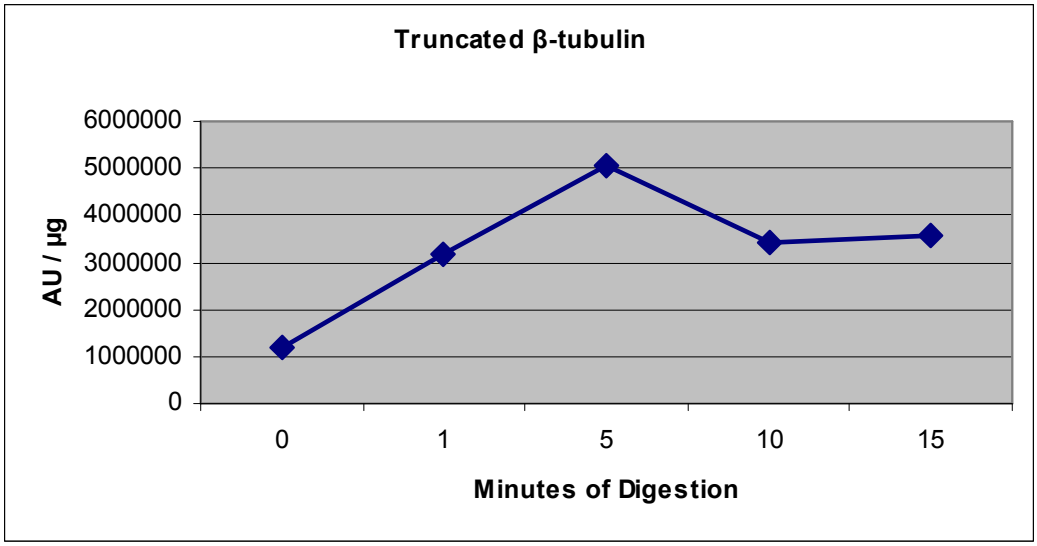

Figure 3-7: Quantitation of truncated β-tubulin from Western blotting of trypsin time-course digestion.
The Western blot in Figure 3.6A was analysed using Carestream Molecular Imaging Software Version 5.0.6.20 as described in section 3.2.3. The truncated forms from 15 to 37 kDa were selected as a single region in each lane for quantitation. Values have been normalised to the number of total µg of protein loaded in each lane.

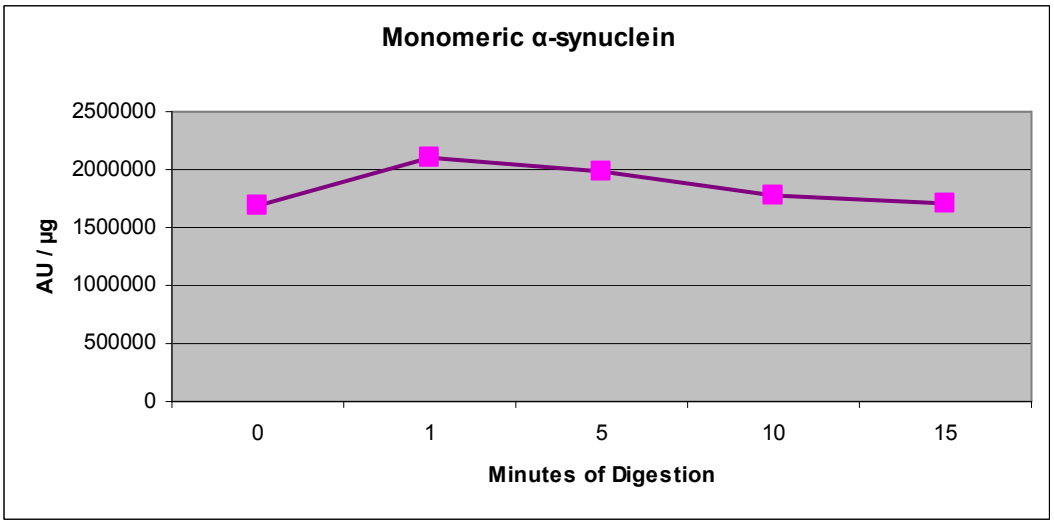

Figure 3-8: Quantitation of monomeric α-synuclein from Western blotting of trypsin time-course digestion.
The Western blot in Figure 3.6B was analysed using Carestream Molecular Imaging Software Version 5.0.6.20 as described in section 3.2.3. The monomeric band between 15 and 20 kDa was selected for quantitation in each lane. Values have been normalised to the number of total µg of protein loaded in each lane.

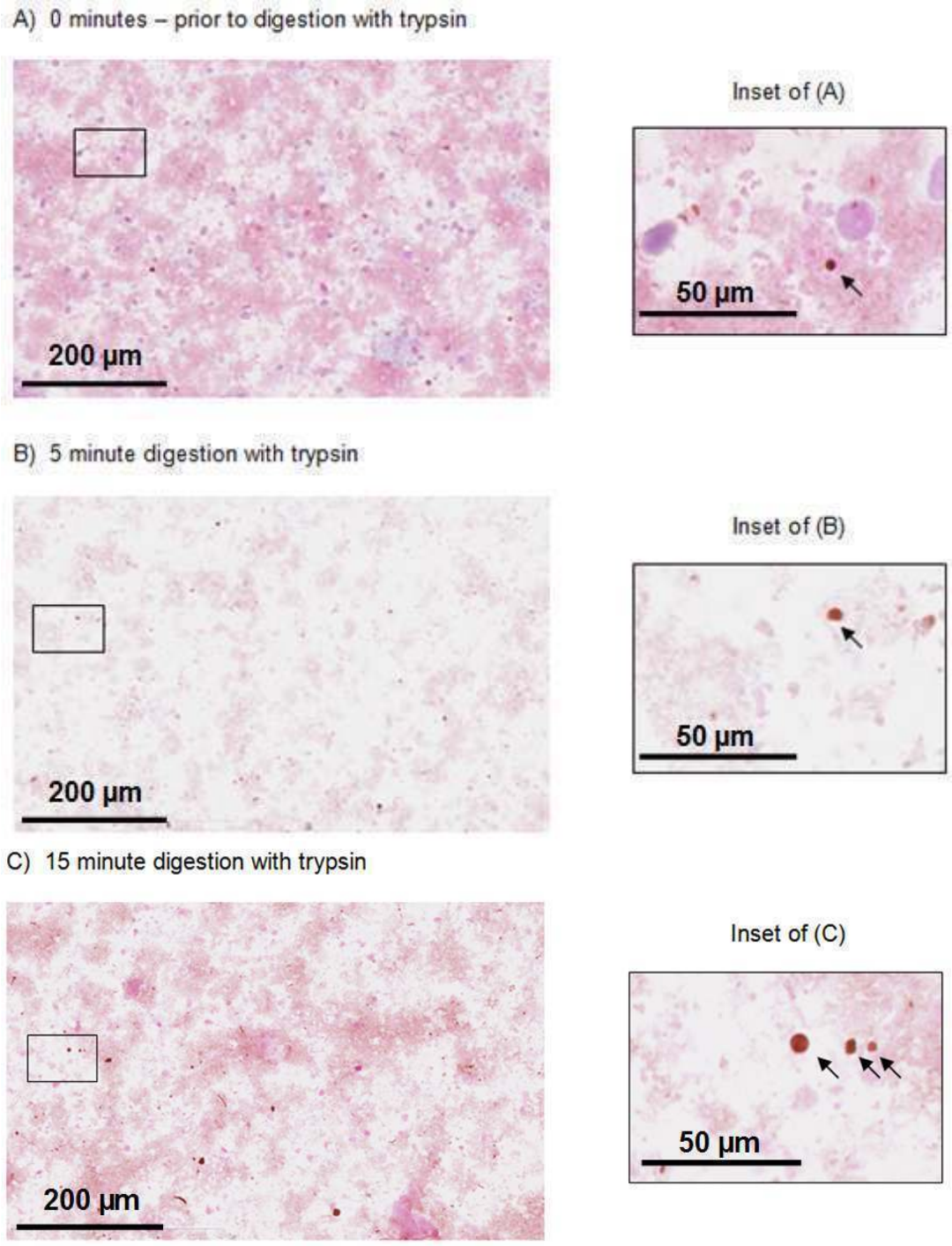

Figure 3-9: Immunohistochemistry of tryptic digestion time-course experiment
A Percoll-enriched fraction from the end of step 5 of the inclusion purification (A) was used for a partial tryptic digestion series. Trypsin was added to this fraction at a 1:4000 enzyme:protein ratio. At 5 minutes, a 25 µL aliquot of the trypsin-containing fraction was added to 25 µL of 2x protease inhibitor mix to stop the action of trypsin (B). At 15 minutes the entire digest reaction was stopped by the addition of protease inhibitors to the trypsin-containing sample (C). A 10 µL smear of each fraction was DAB stained against α-synuclein (antibody no. 1, Table 2.1) and counterstained with haematoxylin and eosin. All images were taken at 20x magnification, the boxed area on each image has been enlarged to 400x total magnification and the inclusions indicated with arrows.

3.3.4 Modification #3

In the published purification method, a DNase digest is performed on the Percoll-enriched fraction collected from the Percoll density gradient (step 5). However, the nuclei are still intact at this point (Figure 3.9A), thus the DNase has little effect, hence this step was excluded from the new method. However, with the addition of trypsin, rapid nuclei lysis occurs and DNA spills into the sample in a viscous mass.

It was hypothesised that this released DNA bound up some of the inclusions and surrounding structures, limiting the effect of the limited tryptic digestion step, as the trypsin did not have equal access to all of the inclusions. Thus, modification #3 was developed at step 6, which was to re-introduce a DNase digest *with* prior nuclei lysis. 2 µg of trypsin (per one tube of brain homogenate) was used to lyse the nuclei and the action of the trypsin was stopped within 10 seconds by the addition of the protease inhibitors PMSF and leupeptin. DNA digestion was then performed with 100 µg/mL DNase I for 1 hour at 37°C before proceeding with the limited tryptic digestion (step 7).

The introduction of this modification greatly improved the efficiency of the limited tryptic digestion (step 7), with a 2.5-fold increase in yield (Table 3.4) and a dramatic reduction in tubulin, as shown by 2D electrophoresis of inclusions purified with modification #3 (Figure 3.10B) compared to before the development of modification #3 (Figure 3.10A).

Table 3-4: Improvement in yield of inclusion protein from modification #3

Purification	Yield (µg)[a]	Increase[b] (-fold)
Without Modification #3	125	
With Modification #3	308	2.5

[a] yield per 3 tubes of brain homogenate from the same case
[b] increase in yield as a result of introducing modification #3

Figure 3-10: 2-DE of purified inclusions before (A) and after (B) the development of modification #3

A) 75 µg of inclusions purified using the optimised method *without* modification #3 (section 3.2.1.1) were subjected to 2-DE using a 24cm pH 3-11NL strip and 8-19% gradient SDS-PAGE as described in Chapter 2.8. The gel was stained with SyproRuby and imaged on a Typhoon 9400 variable mode imager.

B) 170 µg of inclusions purified using the optimised method *with* modification #3 (section 3.2.1.3) were subjected to 2-DE using a 13cm pH 3-11NL strip and 12.5% linear SDS-PAGE as described in chapter 2.8. The gel was stained with Coomassie blue and imaged on a Typhoon 9400 variable mode imager.

The indicated proteins were identified on both gels with a Thermo LTQ XL linear ion trap mass spectrometer. Tubulin is dramatically reduced on gel (B) compared to gel (A), whereas the inclusion protein α-synuclein appears enriched.

A)

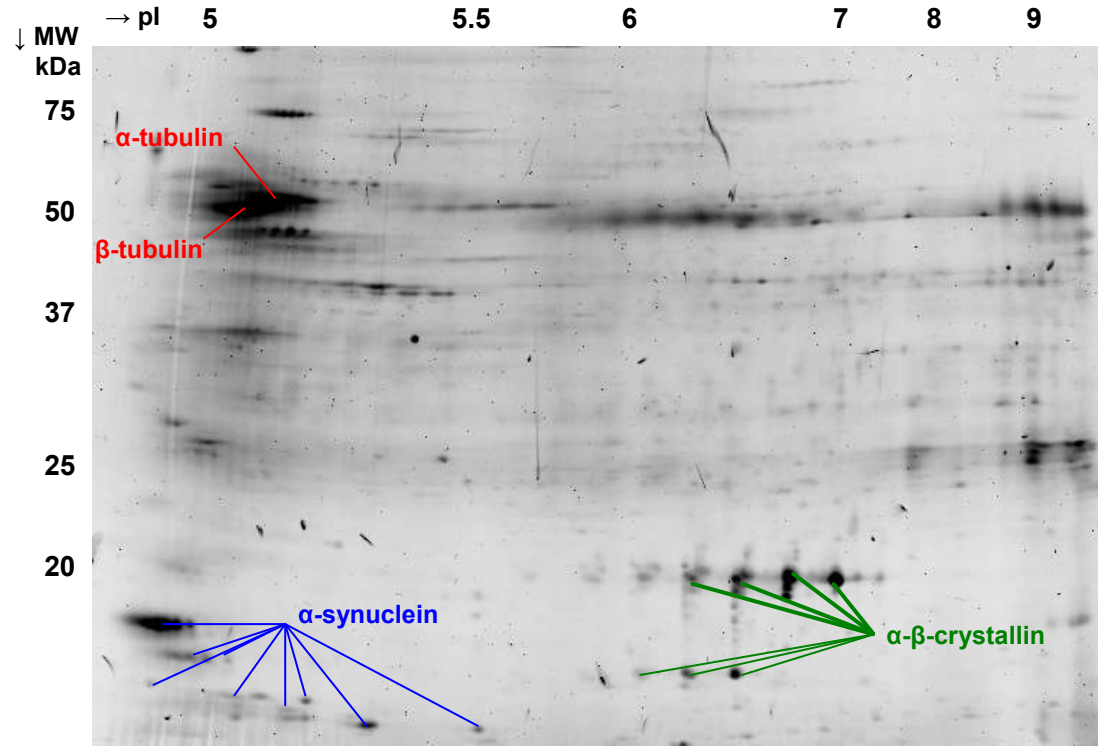
→ pI
5
5.5
6
7
8
9
↓ MW kDa
75
50
37
25
20
α-tubulin
β-tubulin
α-synuclein
α-β-crystallin

B)

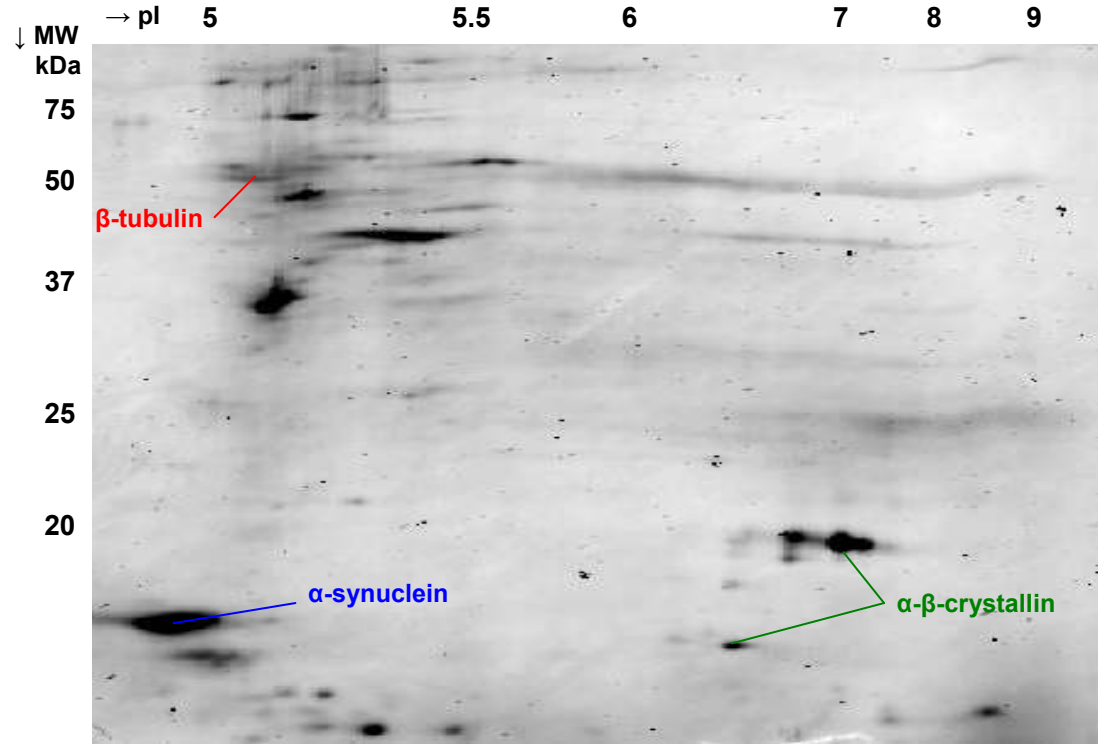
→ pI
5
5.5
6
7
8
9
↓ MW kDa
75
50
37
25
20
β-tubulin
α-synuclein
α-β-crystallin

3.3.5 Modification #4

A greater number of inclusions were available for immunocapture as a result of including the entire inclusion-containing part of the Percoll gradient (modification #1), performing a limited tryptic digestion (modification #2), and lysing the nuclei and removing the DNA from the preparation prior to the tryptic digest (modification #3). Therefore a larger quantity of primary and secondary antibodies and magnetic beads were required to capture the available inclusions.

The need for additional antibody and magnetic beads is demonstrated in Figure 3.11. After immunomagnetic capture (step 11) was performed, approximately one-third of the inclusions were captured (Figure 3.11B) with two-thirds remaining uncaptured in the wash fraction (Figure 3.11C). These inclusions may have remained in the wash fraction due to a limiting amount of magnetic beads and/or antibody. The wash fraction was reprocessed through only steps 10-11, with the addition of 2x the initial quantities of magnetic beads in step 10 (as a 1x amount captured 1/3 of the inclusions, a 2x amount was predicted to capture the remaining 2/3). No additional inclusion capture occurred (data not shown), suggesting that the antibody quantity was a limiting factor. The wash fraction was reprocessed through steps 8-11, with the addition of 2x the initial quantities of primary antibody (step 8), secondary antibody (step 9) and magnetic beads (step 10). As a result, greater than 95% of the inclusions were captured (Figure 3.11D) with few remaining in the wash fraction (Figure 3.11E).

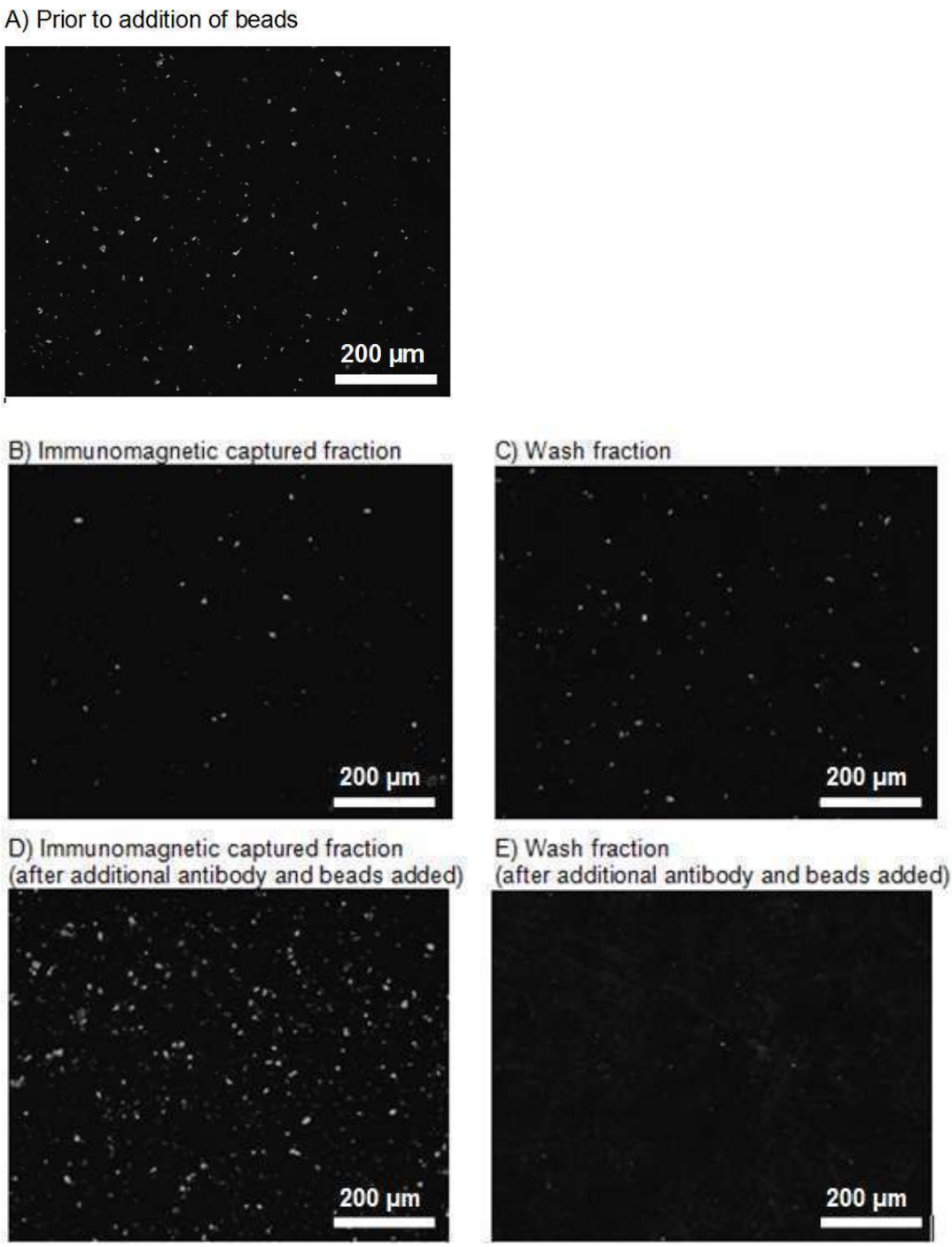

Figure 3-11: Immunofluorescence staining of GCIs during purification protocol demonstrating the effect of additional antibody and magnetic beads
In an inclusion purification, 22.5 µg of primary antibody was added at step 8 and 10 µg of secondary antibody was added at step 9 (A) (1:2400). 9.6 µL of MyOne beads and 14.8 µL of M-280 beads were added in step 10 and the immunomagnetically captured fraction (B) (1:1800) from step 11 contained approximately one-third of the inclusions, with two thirds remaining uncaptured in the wash fraction (C) (1:2400). The wash fraction was re-processed through steps 8-11 of the purification protocol, with an additional 45 µg of primary antibody (step 8), 20 µg of secondary antibody (step 9), 19.2 µL of MyOne beads and 29.6 µL of M-280 beads (step 10). Over 95% of the GCIs were immunomagnetically captured at step 11 (D) (1:1800), with few remaining in the wash fraction (E) (1:2400). All quantities specified were relative to one tube of brain homogenate. α-synuclein was visualised with avidin-Cy3 conjugate and all images were taken at 10x magnification.

3.4 Discussion

In this study, the GCI purification method of Gai *et al.* [113] was optimised. Four main modifications were introduced to the method to increase the number of GCIs captured while reducing the contamination from surrounding structures.

3.4.1 Modification #1

GCIs appeared across a wide range of densities rather than banding tightly at a single interface when fractions across a Percoll density gradient were assessed using immunohistochemistry. The GCIs that appeared higher in the gradient (lower density) were present in clusters with nuclei and other structures, whereas the GCIs that appeared lower in the gradient (higher density) were present singularly, away from surrounding structures. The appearance of these GCIs clusters with nuclei and other structures in the gradient provides evidence for the hypothesis that GCIs are variably enmeshed within the cytoskeletal network.

One explanation for the appearance of GCI clusters at top of the gradient is that they have a greater degree of enmeshment with surrounding lower-density structures, which gives the entire cluster a lower average density compared to singular GCIs. Another explanation is that GCIs themselves have variable densities. While the latter explanation may account for a degree of spread across the density gradient, it is unlikely to account for such a diffuse range especially considering the change in characteristic appearance (i.e. the clustering with nuclei and other structures) across the gradient. Thus, the former explanation of GCI enmeshment is more likely to account for the differing densities.

By collecting the entire inclusion-containing fraction of the Percoll density gradient (Modification #1), the yield was increased 2.0-fold compared to when only the 'P1' fraction of the gradient was collected. However, these results were obtained prior to the development of modification #3 (nuclei lysis). Given the large numbers of nuclei clustered with GCIs in the 'P1' fraction but not in the 'lower' fraction, it is likely that a greater number of GCIs are still present in the 'P1' fraction, but these were being discarded along with the viscous DNA during the immunocapture process,

subsequently lowering the apparent yield of inclusions from this fraction (see discussion of the effects of modification #3 on yield in section 3.4.3),

Given the large fraction over which inclusions were present, the Percoll density gradient provides only a limited enrichment of inclusions. Therefore the 2nd Percoll density gradient in the published method was eliminated from the optimised method due to negligible benefit. The initial Percoll density gradient was still maintained, as it provides a means of removing the myelin from the sample.

3.4.2 Modification #2

Because of the enmeshment of GCIs within the cytoskeleton, it is hypothesised that GCIs bring the surrounding cytoskeletal proteins with them when they are immunocaptured. This is why high levels of tubulin have been seen in previous preparations. The introduction of a limited digestion with trypsin into the procedure (Modification #2) cuts away the surrounding cytoskeleton to release the GCIs for immunocapture. Trypsin cuts at arginine and lysine residues (unless followed by a proline), and by performing a limited digestion rather than allowing the enzyme to digest until completion, cuts will only occur at some of these residues. Thus, rather than aggressively digesting the proteins surrounding the inclusions and compromising the integrity of the inclusions themselves, it is proposed that the limited digestion with trypsin instead puts a series of cuts into the meshwork surrounding the inclusions. This leaves the inclusions themselves unaffected with truncated fragments of tubulin still attached to the surface, while removing the bulk of the tubulin contamination and associated proteins from the final immunocaptured inclusion preparation (Figure 3.2).

The other possible effect from the partial tryptic digestion is the loss or truncation of some of the surface proteins on the GCIs, due to partial digestion by trypsin. However, core proteins will remain unaffected, as the size of the inclusions before and after partial tryptic digestion was analysed and no diminishment in size could be ascertained at the 1:4000 enzyme:protein ratio. The optimisation of the trypsin-to-protein ratio and the optimisation of the digestion duration aimed for a balance between tubulin fragments remaining and the loss of surface proteins. This was determined by assessing the impact of digestion on both β-tubulin (contaminant) and

α-synuclein (GCI protein) via Western blotting – no further truncation of full-length tubulin into fragments was observed beyond 5 minutes of digestion, but a slight reduction in dimeric α-synuclein was observed by 10 minutes, thus a 5 minute digestion at 1:4000 enzyme:protein ratio was determined to be optimal.

The increase in truncated forms of tubulin after digestion without impact on monomeric α-synuclein was shown via Western blotting in Figure 3.6 and the significant reduction of full length tubulin when Modification #2 and #3 were combined is shown with 2-DE in Figure 3.10B. The reduction in tubulin will be quantified in the next chapter.

While LBs were used in the optimisation of this modification rather than GCIs due to a temporary issue with tissue availability, it was expected that the two inclusion types would be able to be purified using the same optimised protocol, given the original published protocol had been successfully applied to both GCIs [113] and LBs [114]. The subsequent use of modification #2 with GCIs was successful and the entire optimised protocol was successfully applied to LBs in Chapter 6.

3.4.3 Modification #3

The immunohistochemistry from modification #2 revealed that before the tryptic digestion, the nuclei were still intact, with the addition of trypsin causing the nuclei to lyse. Thus, prior to the partial tryptic digestion step (step 7), a modification was made whereby trypsin was used to lyse the nuclei, then the released DNA was digested with DNase.

This has three subsequent effects. Firstly, it increases the effectiveness of the digestion step against tubulin, as trypsin now has equal access to all of the GCIs present in the preparation, rather than having GCIs bound up in a surrounding mass of viscous DNA. Secondly, there may be a further increase in purity, as when the DNA remains the increased viscosity of the sample interferes with the wash steps and could also affect immunocapture by binding other proteins to the inclusions with the DNA. Thirdly, the yield is increased, because previously GCIs bound up with the DNA were discarded along with the DNA during the immunocapture process, and now these GCIs are available for immunocapture.

When GCIs were purified with the inclusion of modification #3 compared to without it, the yield of solubilised protein increased 2.5-fold. The purity of the immunocaptured GCIs was also improved, as evidenced by the significant reduction in tubulin present on 2D gels (shown in Figure 3.10) from GCI samples purified with and without modification #3. An enrichment of α-synuclein can also be seen, as further evidence of improved purity.

3.4.4 Modification #4

In the published method, the amount of antibody was added relative to sample volume. After the addition of secondary antibody, the number of inclusions was counted and the amount of beads added was relative to the number of inclusions. However, manual inclusion counting has a poor accuracy due to the highly subjective nature of the counting process. The counting also takes place after the addition of the secondary antibody. The secondary antibody appears to be a more limiting factor than the amount of magnetic beads, as additional beads alone resulting in no improvement in inclusion capture, compared to additional antibody and beads together, which led to the capture of additional inclusions.

For the optimised method, reagent quantities were based on the average inclusions expected to be present in the sample, given the quantity of brain homogenate used for purification. For the immunocapture steps (steps 8-11), if the number of inclusions present was lower than expected, the excess unbound antibody would be removed during the washes after both step 8 (primary antibody addition) and step 9 (secondary antibody addition). Any additional magnetic beads in step 10 would remain unbound, to be pelleted and discarded with the remainder of the beads after GCI solubilisation in step 12. If the number of inclusions present was higher than expected, the antibody and bead binding capacities would be saturated and the additional uncaptured inclusions would remain in the first 'wash' fraction from step 11. This fraction can then be reprocessed through steps 8-11 to capture additional inclusions if required.

Therefore, with the exception of the tryptic digestion, based on EZQ assay of total protein quantity, all reagent quantities were developed in a ratio to the number of tubes of brain homogenate used for purification (based on 2g of tissue homogenized

into a 10 mL total volume per tube). The use of the MyOne magnetic beads (1 µm diameter) in addition to the M-280 magnetic beads (2.8 µm diameter) for the immunomagnetic capture step was an innovation of Gai *et al.* after the publication of their inclusion purification method. Thus the use of both bead types is included in the optimised method although it was not developed as a part of this project.

3.5 Conclusion

An existing GCI purification method published by Gai *et al.* [113] has been optimised to deliver a superior yield and purity. A 2-12 g quantity of brain tissue is processed over four days through a series of enrichment steps including a density gradient, nuclei lysis and DNA digestion, limited tryptic digestion, and immunomagnetic capture, to isolate and capture GCIs using an antibody-magnetic bead linkage. The improvements in yield and purity from the optimised method over the previously published method will be quantified in the next chapter, along with the characterisation of the newly optimised method.

4 Characterisation of optimised GCI purification method

4.1 Introduction

4.1.1 Characterisation of the newly optimised GCI purification method

A method for GCI purification was optimised in the previous chapter, with each modification delivering either a higher purity or greater yield of inclusions. The total quantitative improvement in purity and yield over the previously published method [113] will be determined in this chapter, as will the profile and quantity of the most abundant proteins present in GCIs compared to crude brain homogenate.

4.1.2 Hypotheses

- The optimised method of inclusion purification, which utilises a limited tryptic digestion, will yield a higher purity of inclusions than the published method [113], as determined by an increase in the major GCI protein α-synuclein and a reduction of the contaminating cytoskeletal protein tubulin.

- The optimised method will deliver a greater yield of purified inclusions than the previously published method [113].

- Proteins in GCIs are present as a result of selective incorporation rather than as a random aggregation of proteins in a stoichiometric ratio to the protein complement in the surrounding cell.

4.1.3 Aims

- To compare the newly optimised method for inclusion purification to the previously published method [113] to determine the improvement in purity and yield.

- To compare the profile of GCI proteins to crude brain homogenate using 2D-DIGE.

- To validate the presence of known GCI proteins α-β-crystallin and TPPP in the purified inclusions.

4.2 Materials and Methods

4.2.1 Inclusion purification using published and optimised methods in parallel

Brain tissue homogenisation was performed as described in Chapter 2.4. An inclusion purification was performed using 6 tubes of brain homogenate from case SA0058 (Table 2.3) as described in Chapter 2.5. After step 3, the material was split into two equal fractions, with one fraction processed according to the newly optimised inclusion purification method and the other processed according to the previously published method of Gai *et al.* [113]. For the optimised method, the purification was performed as described in Chapter 2.5.

For the published method of Gai *et al.* [113], the purification was performed as follows. Steps 1-4 of the purification were performed as described in Chapter 2.5, with one additional wash of the pellet fraction performed at step 3. At step 5, only the P1 fraction was collected and processed further. This P1 fraction was washed three times in TBS-Azide at 4,000x g for 10 min at 4°C. The pellets were combined and resuspended to 5 mL in TBS-Azide + PIs + 2 mM EDTA. 1 µg/mL DNase I and 5 mM $MgCl_2$ were added to the sample, which was vortexed thoroughly and incubated for 3 hours at 37°C. The fraction was brought to 8 mL with HB and filtered through 20 µm nylon mesh using vacuum filtration. The filtered fraction was washed three times in HB at 4,000x g for 10 min at 4°C. The pellets were combined and resuspended in 6 mL of 14% (v/v) Percoll Plus in HB, with a 2.4 mL cushion of 35% (v/v) Percoll plus in HB injected underneath the 14% layer. The tube was centrifuged at 35,000x g for 30 minutes at 4°C to create a density gradient.

The P2 fraction (near the interface of the two Percoll layers) was collected. 400 µL of NHS was added to the P2 fraction and the volume was brought to 4 mL with HB, to block the sample with 10% NHS. 5.2 µg of primary antibody was added (1.3 µg/mL) and incubated at 60 minutes at room temperature. The sample was washed three times in TBS-Azide at 4,000x g for 10 min at 4°C. 5.2 µg of secondary antibody was added (1.3 µg/mL) and incubated for 30 minutes at room temperature. The sample was washed three times in TBS-Azide at 4,000x g for 10 min at 4°C. After the final wash, the sample was brought to 1.5 mL with TBS-Azide. Inclusions were visualised as described in Chapter 2.5.4. Inclusions were counted from four 1

µL drops and the dilution factor allowed for to calculate the total number of inclusions present in the 1.5 mL sample (estimated at 1.11 x 10^6 inclusions). 33.3 µL of M-280 beads were added (30 µL per 10^6 inclusions) and incubated for 30 minutes at room temperature. The inclusions were captured as described in step 11 in Chapter 2.5.3, with two additional washes performed. Inclusions were solubilised as described in step 12 in Chapter 2.5.4, with 100 µL of protein extraction buffer used.

4.2.2 DAB immunohistochemistry

DAB immunohistochemistry was performed on selected fractions from the purification procedure as described in Chapter 2.9.1. All staining was performed using a sheep anti-α-synuclein primary antibody (antibody no. 1, Table 2.1) used at 1:1000 (1 µg/mL) and an anti-sheep biotinylated secondary (antibody no. 10, Table 2.2) used at 1:500 (2.6 µg/mL). Nanozoomer analysis and inclusion counting was performed as described in Chapter 2.9.2. A saturation threshold of 102 was used.

4.2.3 1-DE and Western blotting

1-DE and Western blotting was performed on fractions from the GCI purifications (Chapter 2.5). Prior to 1-DE, each fraction was solubilised in 1x 1D sample buffer without bromophenol blue, vortexed and heated at 95°C for 5 minutes. The samples were vortexed again, spun at 18,000x g and the supernatants collected. The protein concentration of each fraction was determined using the EZQ Protein Quantification Kit (Invitrogen) as described in Chapter 2.6.1. Samples were diluted to 1 µg/µL in 1x 1D sample buffer with bromophenol blue and separated by SDS-PAGE using a BioRad Mini-Protean TGX Any kD gel as described in Chapter 2.7.1.

The gels were transferred to PVDF membrane and Western blotting was performed using the SNAP ID system as described in Chapter 2.7.2. The primary antibodies used were rabbit anti-α-synuclein (antibody no. 2, Table 2.1) at 1:450 (2.22 µg/mL), mouse anti-BIII tubulin (antibody no. 3, Table 2.1) at 1:300 (1.67 µg/mL), rabbit anti-α-β-crystallin (antibody no. 4, Table 2.1) at 1:100, and rabbit anti-TPPP (antibody no. 5, Table 2.1) at 1:1000 (0.75 µg/mL). HRP-conjugated secondary antibodies against mouse and rabbit (antibodies no. 12 and no. 11 respectively, Table 2.2) were used at 1:1500 (0.27 µg/mL).

The blots were imaged on a Fujifilm LAS-4000 CCD imager and analysed using Carestream Molecular Imaging Software Version 5.0.6.20. For quantitation, rectangular boxes of uniform size were draw around the band or region of interest (ROI) in each lane for comparison. Background subtraction was performed using the median of each ROIs perimeter.

4.2.4 2D DIGE

DIGE labeling and 2D gel electrophoresis was performed as described in Chapter 2.8. The solubilised inclusions purified using both the published and optimised methods and an aliquot of the crude homogenate used were purified with a ReadyPrep 2D Clean-Up Kit (BioRad) as described in Chapter 2.6.2 and resolubilised in DIGE labeling buffer at pH 8.5. The samples were labelled as described in Chapter 2.8.1, according to the experimental design outlined in Table 4.1.

Table 4-1: DIGE experimental design for purification method comparison

Gel	Cy3	Cy5	Protein quantity (µg)	Dye quantity (pmol)
1	Published method	Optimised method	19	200
2	Crude homogenate	Optimised method	50	400

The labelled protein extracts were combined for their respective gels and subjected to isoelectric focusing using 24cm pH3-11NL Immobiline DryStrips (GE Healthcare), as described in Chapter 2.8.2. The strips were focused for 86,000 volt hours according to the following protocol: Step to 500 V for 30 min, step to 1 000 V for 30 min, gradient to 10 000 V for 30 min, hold at 10 000 V until 65 000 Vhr, step to 1 000 V until end. The 2nd dimension was performed as described in Chapter 2.8.3 but with 12.5% linear gels, run at constant voltage at 350 V.

Gel imaging was performed on a Typhoon 9400 variable mode imager as described in Chapter 2.8.4. The photo-multiplier tube values for the green (532 nm) and red (633 nm) channels were set at 540 V and 630 V respectively for gel # 1 and 510 V and 530 V respectively for gel # 2. The gels were analysed in DeCyder version 7.0 (GE Healthcare).

4.2.5 2D-DIGE analysis of multiple protein isoforms

The workflow for this analysis is outlined in Figure 4.1. The Cy3 and Cy5 channels of each gel were analysed in the DIA (Differential In-gel Analysis) module of DeCyder version 7.0 (GE Healthcare). Each spot was reviewed manually and non-protein spots were excluded as artefacts. The spots corresponding to different isoforms of the proteins of interest were then selected based on spot-matching to preparative gels where protein identifications had been made (Figures 3.10 and 5.6).

The spot volumes for each isoform of a protein were summed together to give a total integrated spot volume for that protein (performed separately for each channel). The spot volumes of every spot on the gel (excluding artifacts) were summed to give the total protein volume on the gel (performed separately for each channel). The integrated spot volume for the protein of interest was then compared to the total protein volume on the gel to determine the relative abundance of the protein of interest. The relative abundance of each protein was compared between samples to obtain a fold-change ratio.

To obtain the spot volume for each spot in both channels, the protein table from DeCyder was exported into Microsoft Excel. The spot volume for a particular spot in each channel was extrapolated from the maximum spot volume and volume ratio columns, allowing for the difference in dye intensity. The difference in dye intensity was calculated for each gel by comparing the actual ratio between the spot volumes in each channel for a particular spot to the spot volume ratio calculated by the DIA module, to obtain the coefficient of intensity.

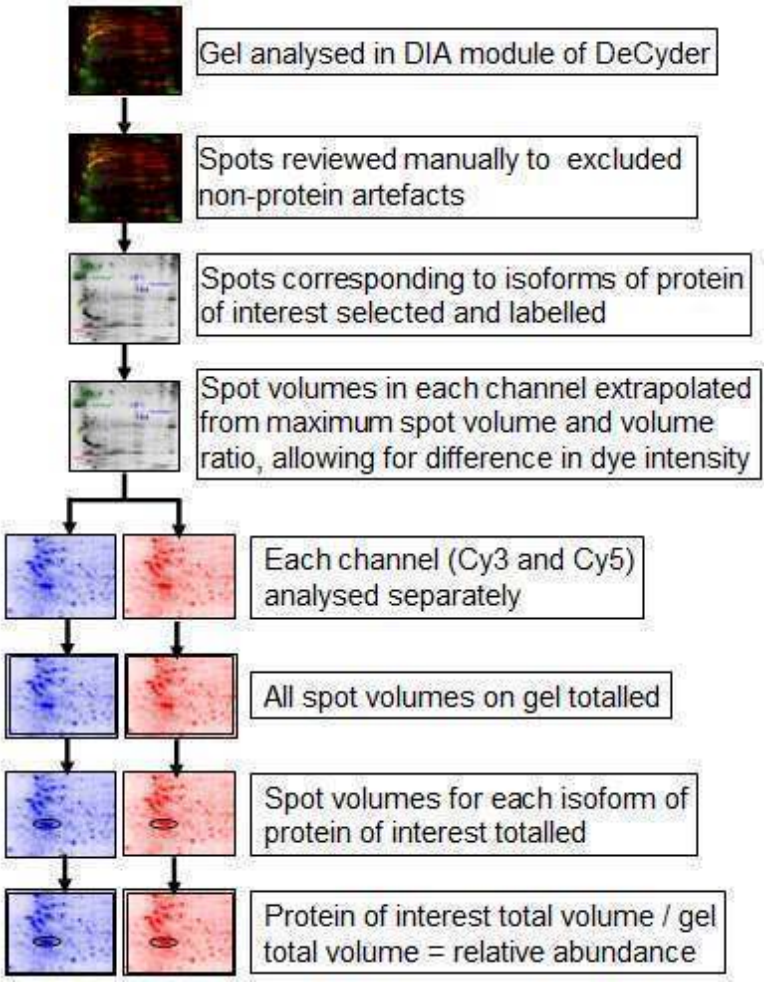

Figure 4-1: Workflow for 2D-DIGE analysis of multiple isoforms
Analysis method developed for comparison of integrated spots in DIA module of DeCyder (GE Healthcare).

4.3 Results

4.3.1 Comparison of published and optimised methods

After the optimisation of the inclusion purification method was completed, an inclusion purification was performed using the newly optimised method and the previously published method in parallel to verify the effects of the modifications. Six tubes of brain homogenate (12 g of tissue) were pooled and processed together for steps 1-3 of the purification protocol, after which it was split into two equal fractions (equivalent to 6 g of brain tissue each). One fraction was then processed according to the published method and the other according to the optimised method (section 4.2.1).

The yield from 6 g of brain tissue using the published method was 22 µg, as determined by an EZQ protein assay of the solubilised inclusion proteins. This is comparable to the published yield of 25-35 µg per 6 g of tissue [113]. The yield from 6 g of brain tissue using the optimised method was 615 µg, which represents a 28-fold increase in protein yield compared to the 22 µg obtained from the same amount of tissue using the published method.

4.3.1.1 Immunohistochemistry comparison

Immunohistochemistry was performed on selected fractions from the purification procedure (Figure 4.2), with the slides imaged using a Nanozoomer Digital Imager and the inclusions analysed as described in Chapter 2.9.2 (Table 4.2). There is a 31-fold increase in the number of inclusions counted in the immunocaptured fraction from the optimised method compared to the published method.

Table 4-2: Comparison of inclusion yields for published and optimised purification methods

Purification fraction	No. of inclusions measured[a]	Average size (pixels)	Total no. of inclusions[b]	Recovery from homogenate (%)[c]
Published method				
Step 1 (Homogenate)	26	199	1.27×10^7	100.0
Step 3 (Pellet)	79	172	1.20×10^7	94.2
Step 6 (P1)	34	239	1.58×10^6	12.5
Step 7 (P2)	26	153	7.69×10^5	6.1
Step 11 (Captured)	21	138	1.19×10^5	0.9
Optimised method				
Step 1 (Homogenate)[d]	26	199	1.27×10^7	100.0
Step 3 (Pellet)[d]	79	172	1.20×10^7	94.2
Step 6 (Post-DNA digest)	153	139	5.11×10^6	40.2
Step 7 (Post-tryptic digest)	105	147	3.80×10^6	29.9
Step 11 (Captured)	1116	177	3.70×10^6	29.1

[a] Total number of inclusions counted and analysed across four representative 20x fields using ImageJ, as described in Chapter 2.9.2.

[b] Total inclusions were estimated by multiplying the average number of inclusions per 20x field by the estimated number of 20x fields per slide by the dilution factor of the original sample volume.

[c] The percentage of inclusions remaining in the sample compared to the homogenate fraction (step 1), based on the estimated total number of inclusions for each fraction.

[d] These fractions were taken before the purification was split into the two methods, but the data is presented twice for the sake of clarity.

Figure 4-2: Immunohistochemistry from parallel GCI purifications using the published and optimised purification methods

A GCI purification was performed using the published and optimised methods in parallel. Brain homogenate from the same case (MSA case SA0058) was processed together for steps 1-3, then split into two equal parts for steps 4-12, with one part processed according to each method (section 4.2.1). A 10 µL smear of each fraction was DAB stained against α-synuclein (antibody no. 1, Table 2.1) and counterstained with haematoxylin. All images were taken at 20x magnification (C).

A zoom image from the Step 11 (Immunocaptured Fraction) from (C) is shown for the published method (A) and the optimised method (B), demonstrating the process of immunomagnetic capture.

A) Published method

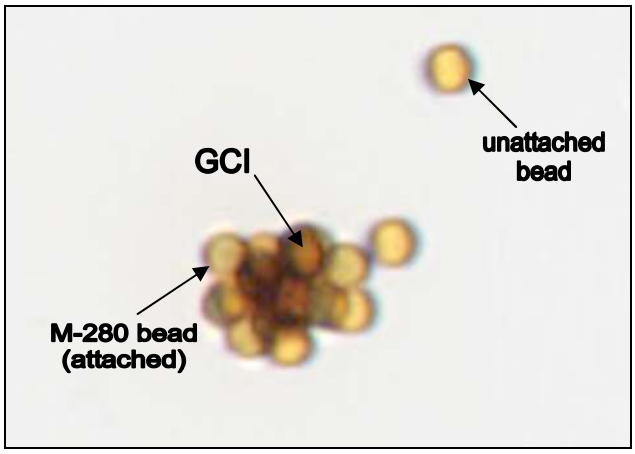

B) Optimised method

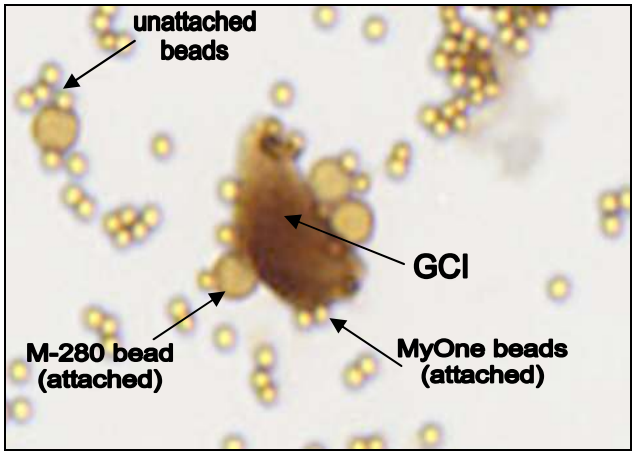

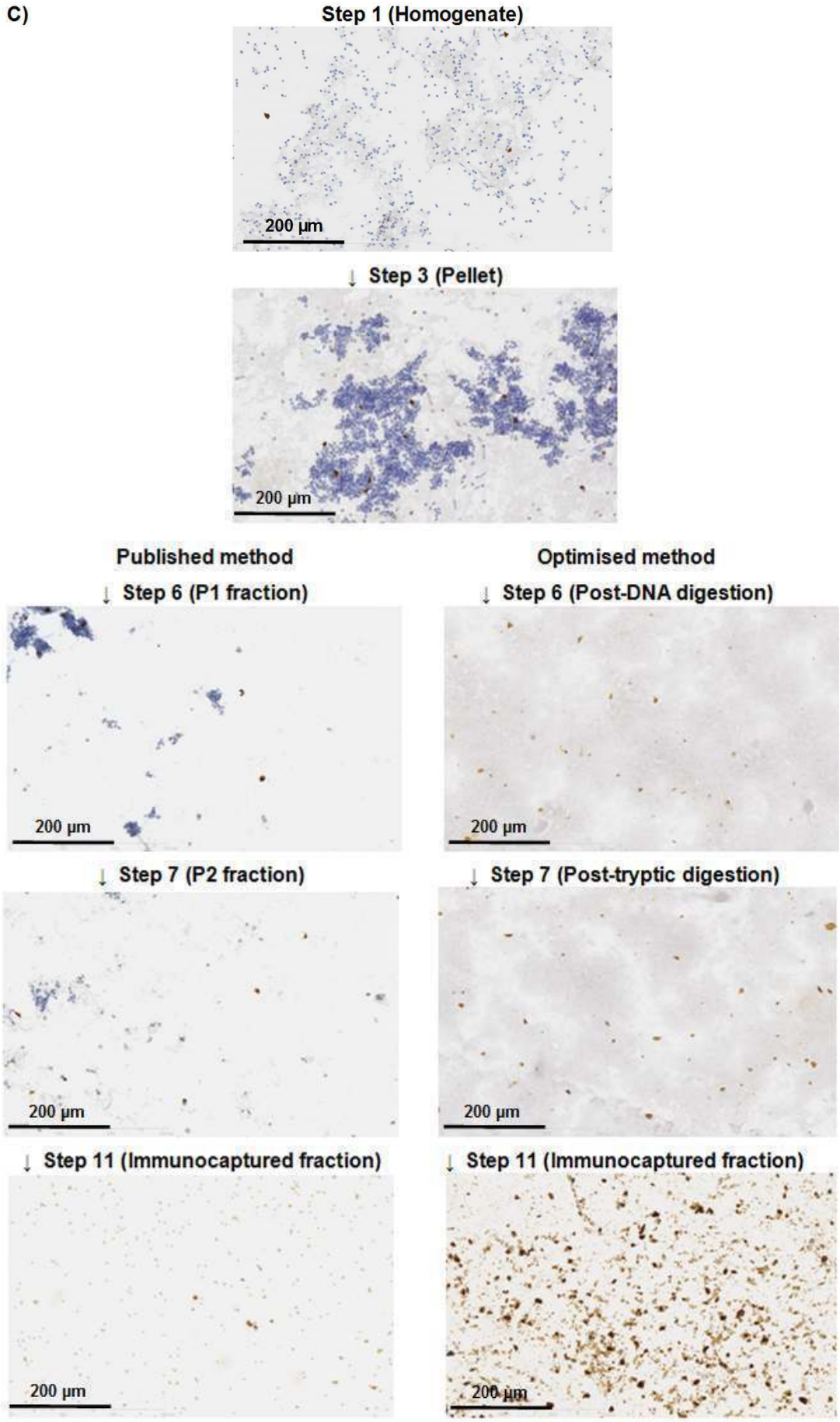
C)
Step 1 (Homogenate)
200 µm
↓ Step 3 (Pellet)
200 µm
Published method
Optimised method
↓ Step 6 (P1 fraction)
200 µm
↓ Step 6 (Post-DNA digestion)
200 µm
↓ Step 7 (P2 fraction)
200 µm
↓ Step 7 (Post-tryptic digestion)
200 µm
↓ Step 11 (Immunocaptured fraction)
200 µm
↓ Step 11 (Immunocaptured fraction)
200 µm

4.3.1.2 2D-DIGE comparison

From each purification method, 19 μg of inclusion proteins were purified using a BioRad ReadyPrep 2D Clean-Up kit and labelled with 200 pmol of Cy3 (published. method) or Cy5 dye (optimised method). The samples were combined and run on a single 2D gel (Figure 4.3), using a 24cm pH 3-11NL strip and 12.5% linear SDS-PAGE. The gel was imaged on a Typhoon imager and analysed in the DIA (Differential In-gel Analysis) module of DeCyder version 7.0 (GE Healthcare). The search algorithm was processed with an estimation setting of 2,500 spots.

The proteins α-synuclein, tubulin, α-β-crystallin and 14-3-3 were chosen for analysis based on two criteria. Firstly, they have all been previously reported to be present in GCIs [31]. Secondly, the 2-DE spots corresponding to these proteins could be reliably matched from an analytical DIGE gel to a preparative gel from which protein identifications had been made using mass spectrometry

The labelled protein spots in Figure 4.3 were based on spot-matching to preparative gels where protein identifications had been made (Figures 3.10 and 5.6). The relative abundance of each protein of interest was determined as described in section 4.2.5. The integrated spot volumes for each isoform of a protein were summed together and compared to the total protein volume on the gel to determine the relative abundance of the protein of interest (Table 4.3). The relative abundance of each protein was then compared between the two samples to obtain a fold-change ratio. The GCI proteins α-synuclein and α-β-crystallin were enriched with the optimised method versus the published method, while the tubulin contamination was reduced by more than 5-fold.

Table 4-3: Abundance of proteins of interest in optimised and published GCI purification methods

		% of total protein	
	Fold change[a]	Published	Optimised
α-synuclein	3.8	2.5	9.6
Tubulin	-5.2	4.7	0.9
α-β-crystallin	2.0	1.1	2.2
14-3-3 proteins	-1.2	2.2	1.9

[a] Fold-change in abundance between the optimised and published methods of GCI purification

Figure 4-3: 2-D DIGE image of GCIs purified using the A) published method and B) optimised method

19 µg of inclusions purified from MSA case SA0058 using the published method and the optimised method were separately labelled with 200 pmol of Cy3 and Cy5 dye, respectively. The labelled proteins were combined and subjected to 2-DE using a 24cm pH 3-11NL strip and 12.5% linear SDS-PAGE as described in Chapter 2.8. The gel was imaged on a Typhoon 9400 variable mode imager with scans performed using both the green (532 nm) and red (633 nm) lasers, set at photo-multiplier tube values of 540 V and 630 V respectively. The gel was analysed in DeCyder version 7.0. The protein spots labeled as α-synuclein, α-β-crystallin, tubulin or 14-3-3 were based on spot-matching to preparative gels where protein identifications had been made using mass spectrometry (Figures 3.10 and 5.6).

A)

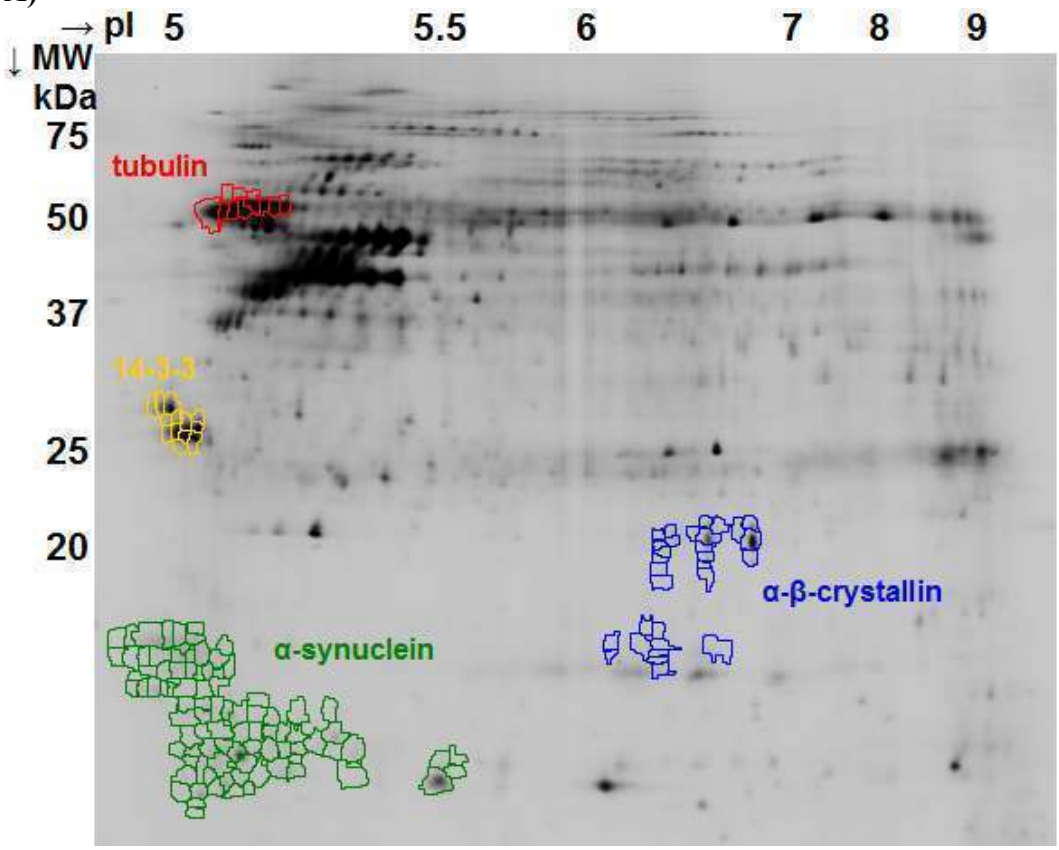
→ pI 5
5.5
6
7
8
9
↓ MW kDa
75
50
37
25
20
tubulin
14-3-3
α-β-crystallin
α-synuclein

B)

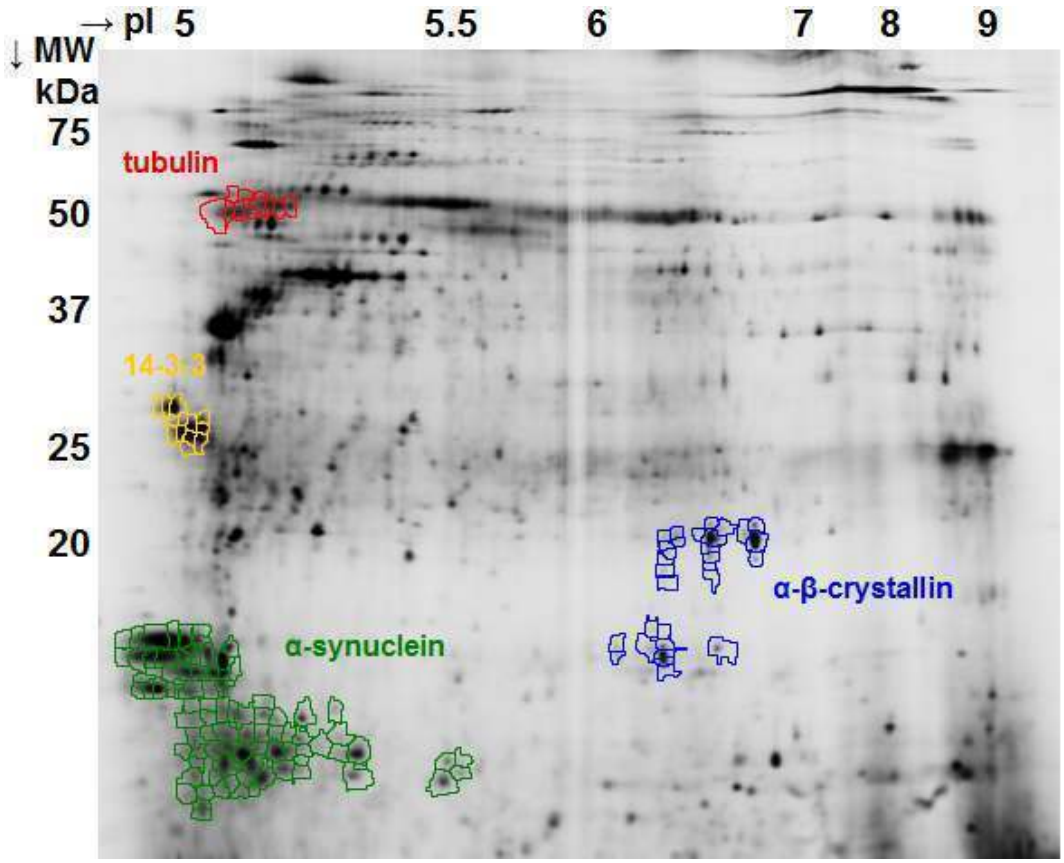
→ pI 5
5.5
6
7
8
9
↓ MW kDa
75
50
37
25
20
tubulin
14-3-3
α-β-crystallin
α-synuclein

4.3.2 Characterisation of optimised method for GCI purification

4.3.2.1 2D-DIGE characterisation

GCIs purified using the optimised method were compared to crude brain homogenate from the same case used for the purification using 2D-DIGE. The samples were purified using a BioRad ReadyPrep 2D Clean-Up kit and 50 µg of each was labeled with 400 pmol of Cy3 dye (homogenate) or Cy5 dye (purified GCIs). The samples were then combined and run on a single 2D gel (Figure 4.4), using a 24cm pH 3-11NL strip and 12.5% linear SDS-PAGE. The gel was imaged on a Typhoon 9400 variable mode imager and analysed in DeCyder version 7.0 using the DIA (Differential In-gel Analysis) module and a spot estimation setting of 2 500 spots.

The protein spots labeled as α-synuclein, tubulin, α-β-crystallin or 14-3-3 were based on spot-matching to preparative gels where protein identifications had been made using mass spectrometry (Figures 3.10 and 5.6) and the protein quantification performed as described in section 4.3.1.2. While crude homogenate contains approximately 2% α-synuclein and 2.5% tubulin, GCIs consist of over 10% α-synuclein with less than 1% tubulin (Table 4.4). The highly dissimilar 2-DE profiles of purified inclusions compared to homogenate are shown in Figure 4.4.

Table 4-4: Abundance of proteins of interest in purified GCIs compared to crude homogenate

		% of total protein			
	Fold change[a]	Homogenate	GCIs[b]	GCIs[c]	Average[d]
α-synuclein	5.4	2.0	11.8	9.6	10.7
Tubulin	-2.8	2.5	0.9	0.9	0.9
α-β-crystallin	2.4	0.8	1.6	2.2	1.9
14-3-3 proteins	1.2	1.9	2.7	1.9	2.3

[a] Fold-change in abundance between purified GCIs (average) and the crude homogenate from which they were purified (MSA case SA0058)
[b] Purified GCIs from this experiment
[c] Purified GCIs from previous experiment (Table 4.3), data repeated for comparison
[d] Average of GCI data from both replicates

A)

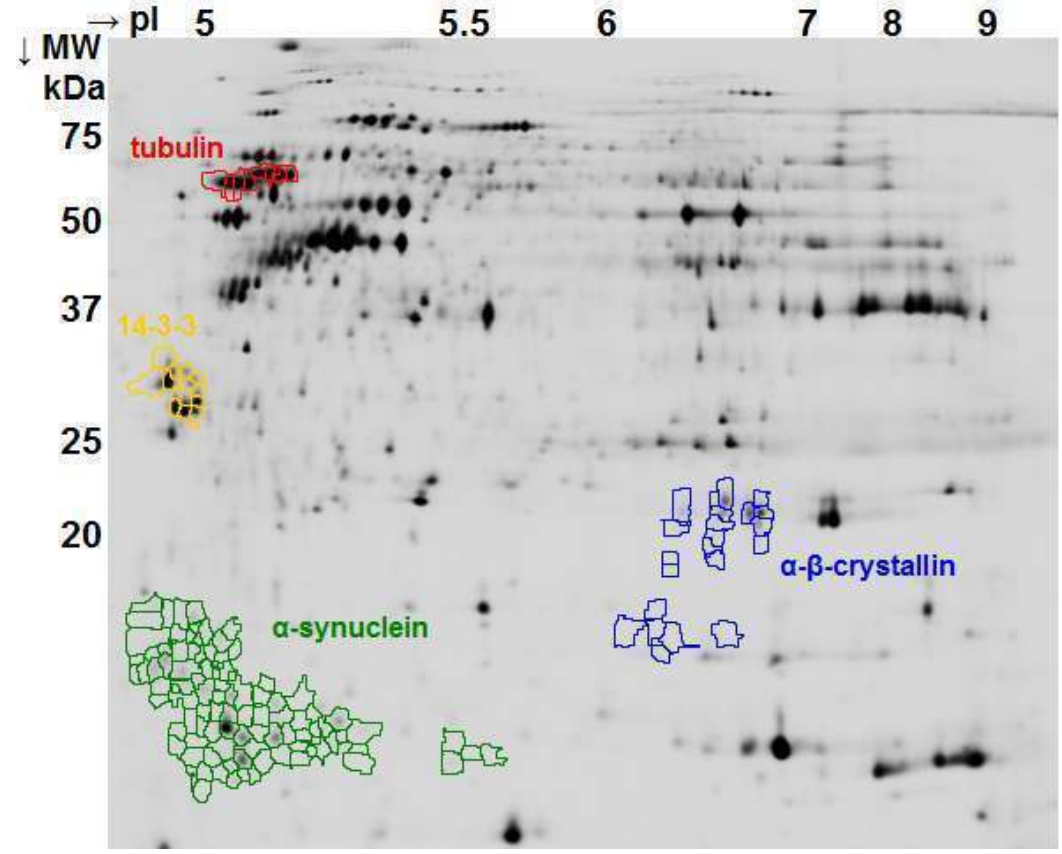
→ pI 5 5.5 6 7 8 9
↓ MW kDa
75
50
37
25
20
tubulin
14-3-3
α-β-crystallin
α-synuclein

B)

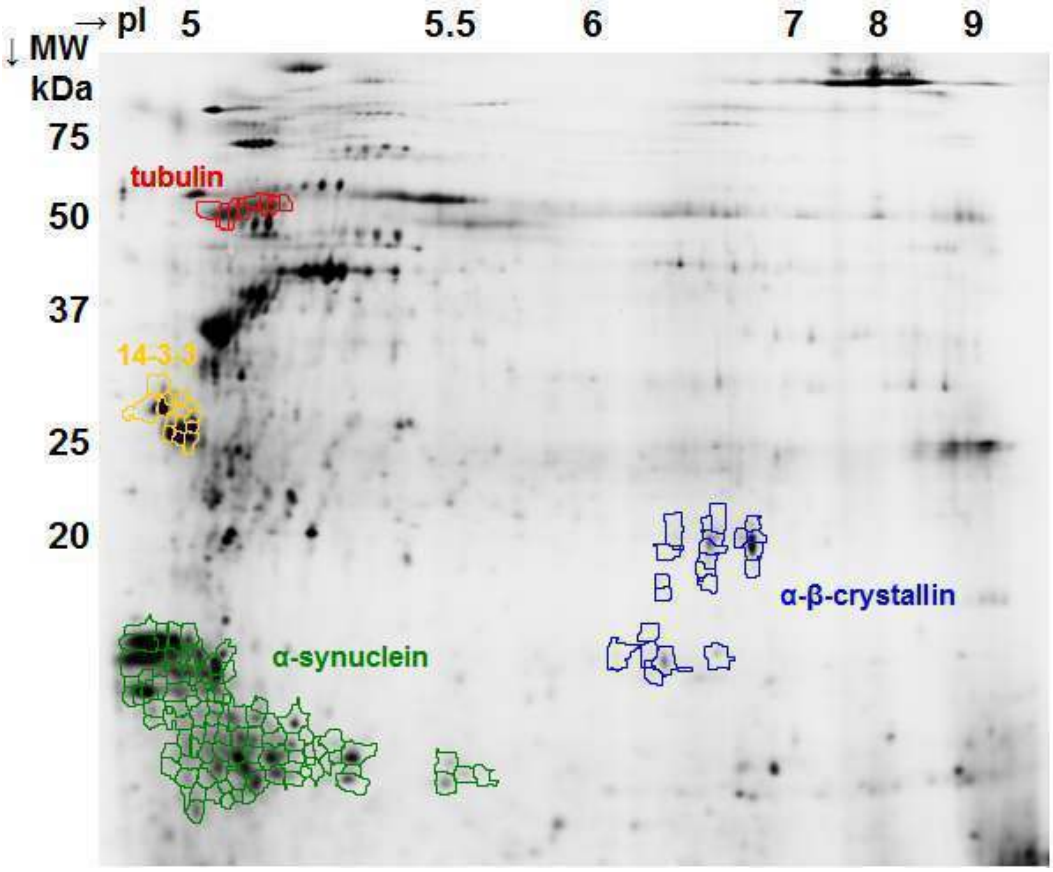
→ pI 5 5.5 6 7 8 9
↓ MW kDa
75
50
37
25
20
tubulin
14-3-3
α-β-crystallin
α-synuclein

C)

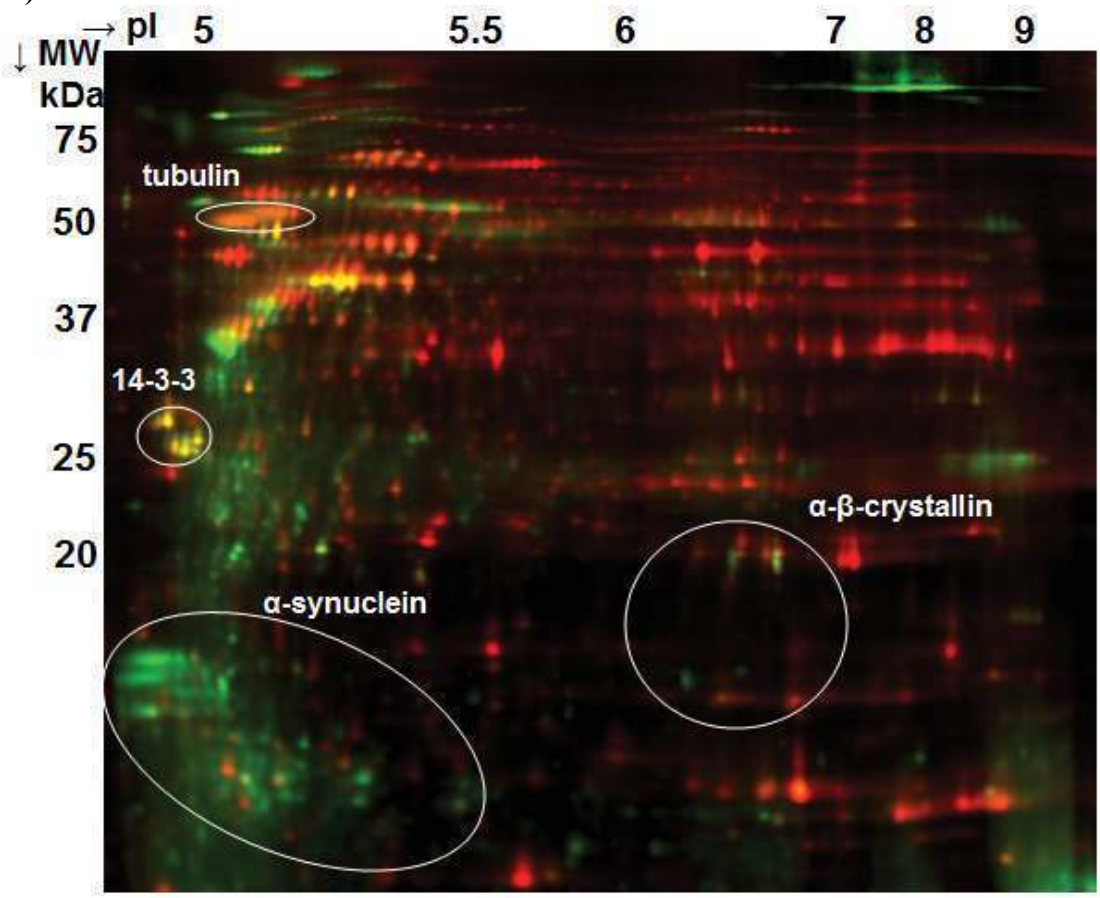

Figure 4-4: 2D-DIGE spot maps of inclusions purified using the optimised method compared to brain homogenate

50 µg of inclusions purified using the optimised method and 50 µg of crude brain homogenate (from which the inclusions were purified, MSA case SA0058) were separately labeled with 400 pmol of Cy5 and Cy3 dye, respectively. The labelled proteins were combined and subjected to 2-DE using a 24cm pH 3-11NL strip and 12.5% linear SDS-PAGE as described in Chapter 2.8. The gel was imaged on a Typhoon 9400 variable mode imager with scans performed using both the green (532 nm) and red (633 nm) lasers, set at photo-multiplier tube values of 540 V and 630 V respectively.

The spot map for the crude homogenate is shown in (A) and the spot map for GCIs purified using the optimised method is shown in (B), with a colour overlay of the Cy3-labelled GCIs (green) and the Cy5-labelled homogenate (red) shown in (C), so proteins that are increased in abundance in inclusions compared to homogenate appear green, whereas proteins that are decreased in abundance in inclusions compared to homogenate appear red, with proteins showing similar levels in both appearing yellow. The protein spots indicated as α-synuclein, tubulin, α-β-crystallin, or 14-3-3 were based on spot-matching to preparative gels where protein identifications had been made using mass spectrometry (Figures 3.10 and 5.6).

4.3.2.2 Western blot characterisation

Western blotting was performed using the fractions from a GCI purification using the optimised method. The dominant protein in GCIs is α-synuclein [119], which is greatly enriched in the immunocaptured fraction (Step 12, Lane 7, Figure 4.5A). β-tubulin, a cytoskeletal contaminant, is greatly reduced in abundance in the immunocaptured fraction (Step 12, Lane 7, Figure 4.5B), with the majority of tubulin separated from the inclusions in the wash fraction (Step 11, Lane 6, Figure 4.5B). A graph comparing the amounts of monomeric, polymeric and total α-synuclein in each fraction is shown in Figure 4.6A and a comparison of the amounts of full-length, truncated and total β-tubulin in each fraction is shown in Figure 4.6B.

These quantifications were performed on the representative Western blots shown in Figure 4.5. The duplicate α-synuclein blot, which showed a highly similar pattern of enrichment, was not suitable for quantitation due to a technical issue with background spotting. While previous blots against both α-synuclein and β-tubulin displayed similar protein profiles, they were not directly comparable for quantitation as the samples that were applied to these gels were generated during the optimisation process. The samples applied were similar but not identical and so could not be combined to provide more comprehensive quantitation.

Co-enrichment of known GCI protein α-β-crystallin is also demonstrated (Step 12, Lane 7, Figure 4.7A), and the presence of known GCI protein TPPP (or p25) in the GCI fraction is also shown (Step 12, Lane 7, Figure 4.7B). While these blots are not of sufficient quality for quantitation, they confirm the presence of these inclusion proteins in the immunocaptured preparation.

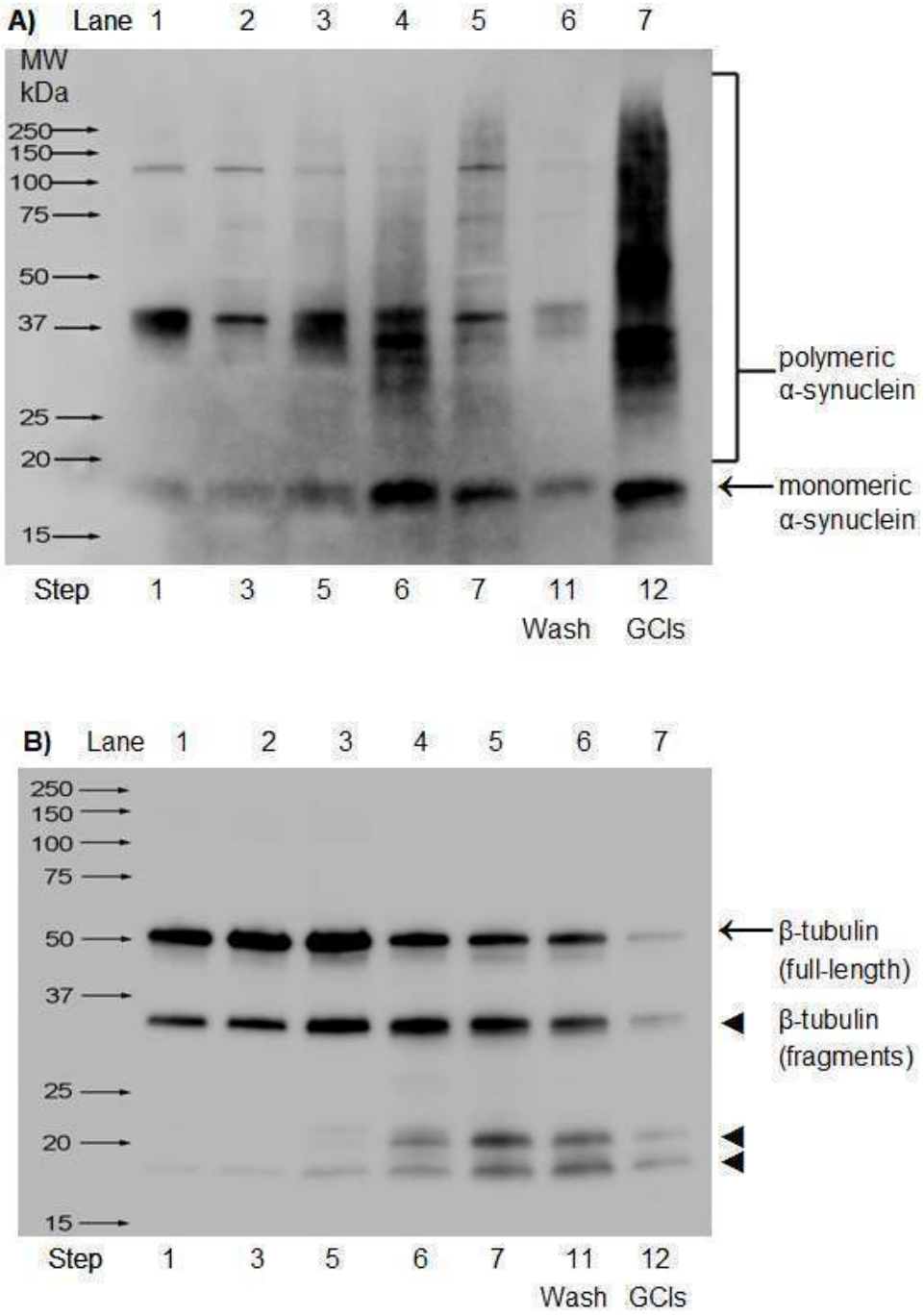

Figure 4-5: Antibody detection of A) α-synuclein and B) β-tubulin in fractions from GCI purification using the optimised method

Representative Western blots from a GCI purification using the optimised method, as described in Chapter 2.5. The MSA homogenate (Lane 1, Step 1) was pelleted at 1,000x g (Lane 2, Step 3), from which a Percoll-enriched fraction (Lane 3, Step 5) was obtained and subjected to nuclei lysis and DNA digestion (Lane 4, Step 6), a limited tryptic digestion (Lane 5, Step 7) and immunomagnetic capture, with the wash fraction (Lane 6, Step 11) removed and the captured GCIs solubilised (Lane 7, Step 12). The samples were solubilised in 1x sample buffer and 20 µg of each sample was separated by SDS-PAGE using a BioRad Mini-Protean TGX Any kD gel, transferred to PVDF and probed with antibodies against either A) α-synuclein (n=2) (antibody no. 2, Table 2.1) or B) β-tubulin (n=1) (antibody no. 3, Table 2.1). On gel A), only 2 µg was loaded in lane 7 to avoid overloading the immunocaptured fraction for α-synuclein detection. The blots were imaged on a Fujifilm LAS-4000 CCD imager and analysed using Carestream Molecular Imaging Software Version 5.0.6.20.

A)

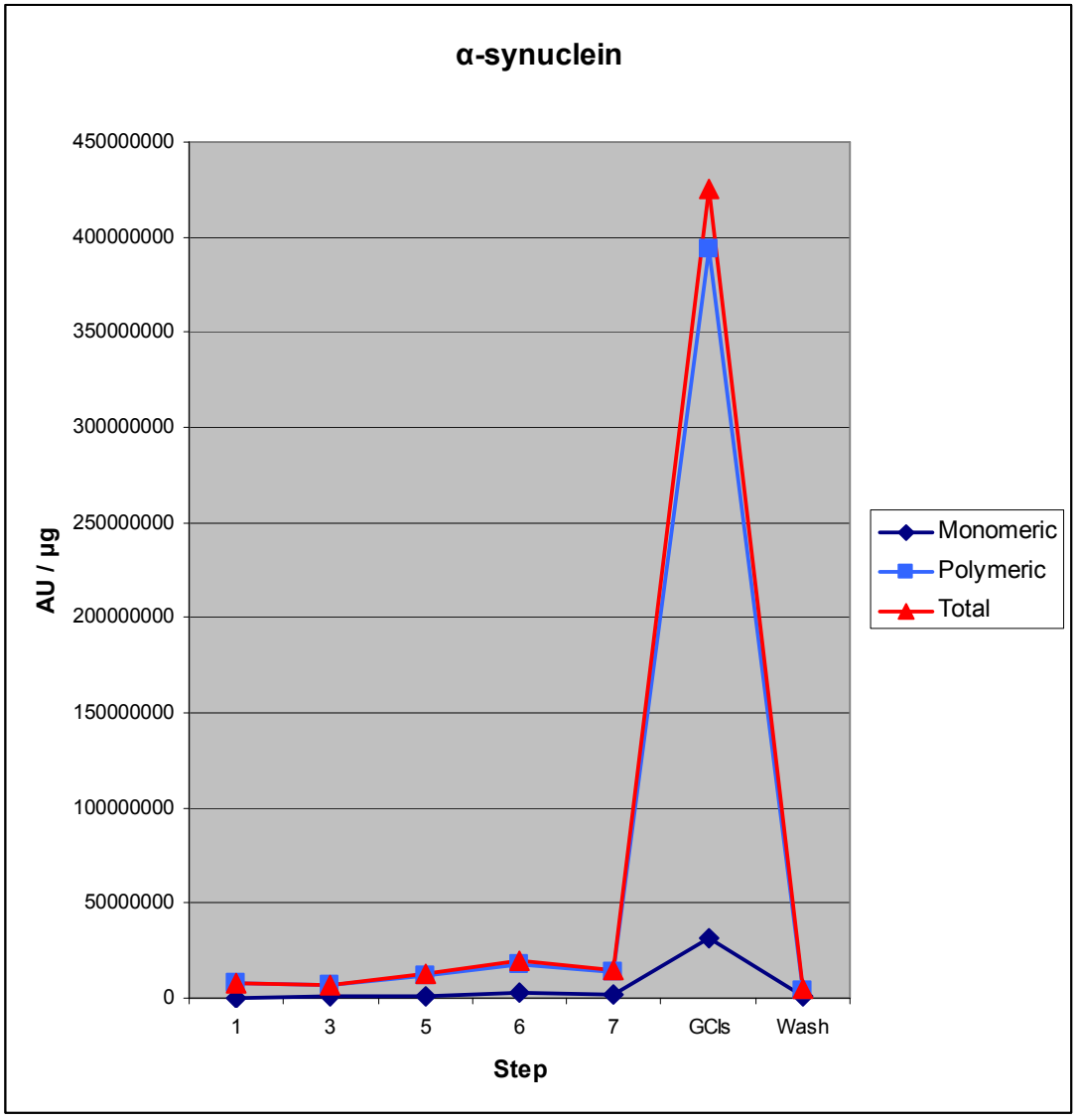
α-synuclein
450000000
400000000
350000000
300000000
250000000
200000000
150000000
100000000
50000000
0
AU / µg
1
3
5
6
7
GCls
Wash
Step
Monomeric
Polymeric
Total

B)

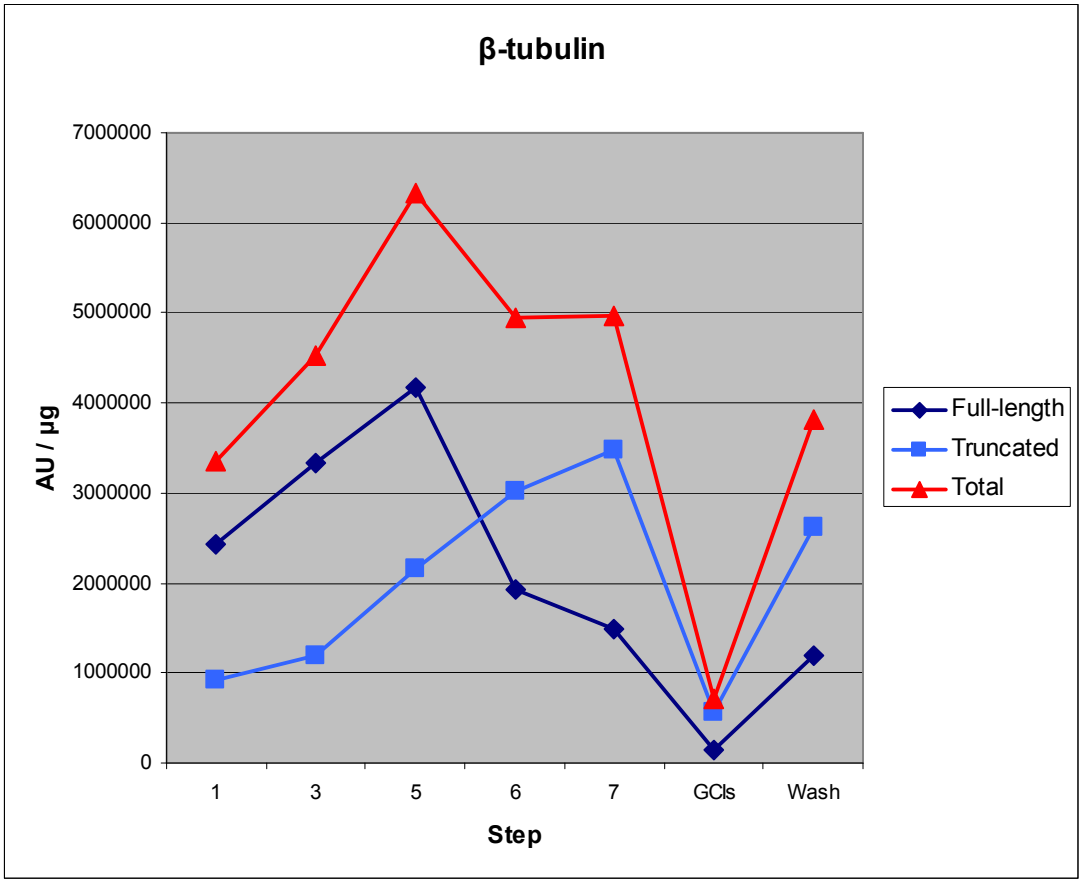

Figure 4-6: Quantitation from Western blotting of GCI purification fractions of A) monomeric, polymeric and total α-synuclein, and B) full-length, truncated and total β-tubulin

The Western blots in Figure 4.5A (A) and Figure 4.5B (B) were analysed using Carestream Molecular Imaging Software Version 5.0.6.20 as described in section 4.2.3. All values have been normalised to the number of total µg of protein loaded in each lane.

In A), the monomeric band between 15 and 20 kDa was selected for quantitation in each lane and the polymeric forms from 20 kDa upwards were selected as a single region in each lane for quantitation. The total was obtained from the sum of these two measurements in each lane. In B), the full-length band at ~50 kDa was selected for quantitation in each lane and the truncated forms from 15 to 37 kDa were selected as a single region in each lane for quantitation. The total was obtained from the sum of these two measurements in each lane.

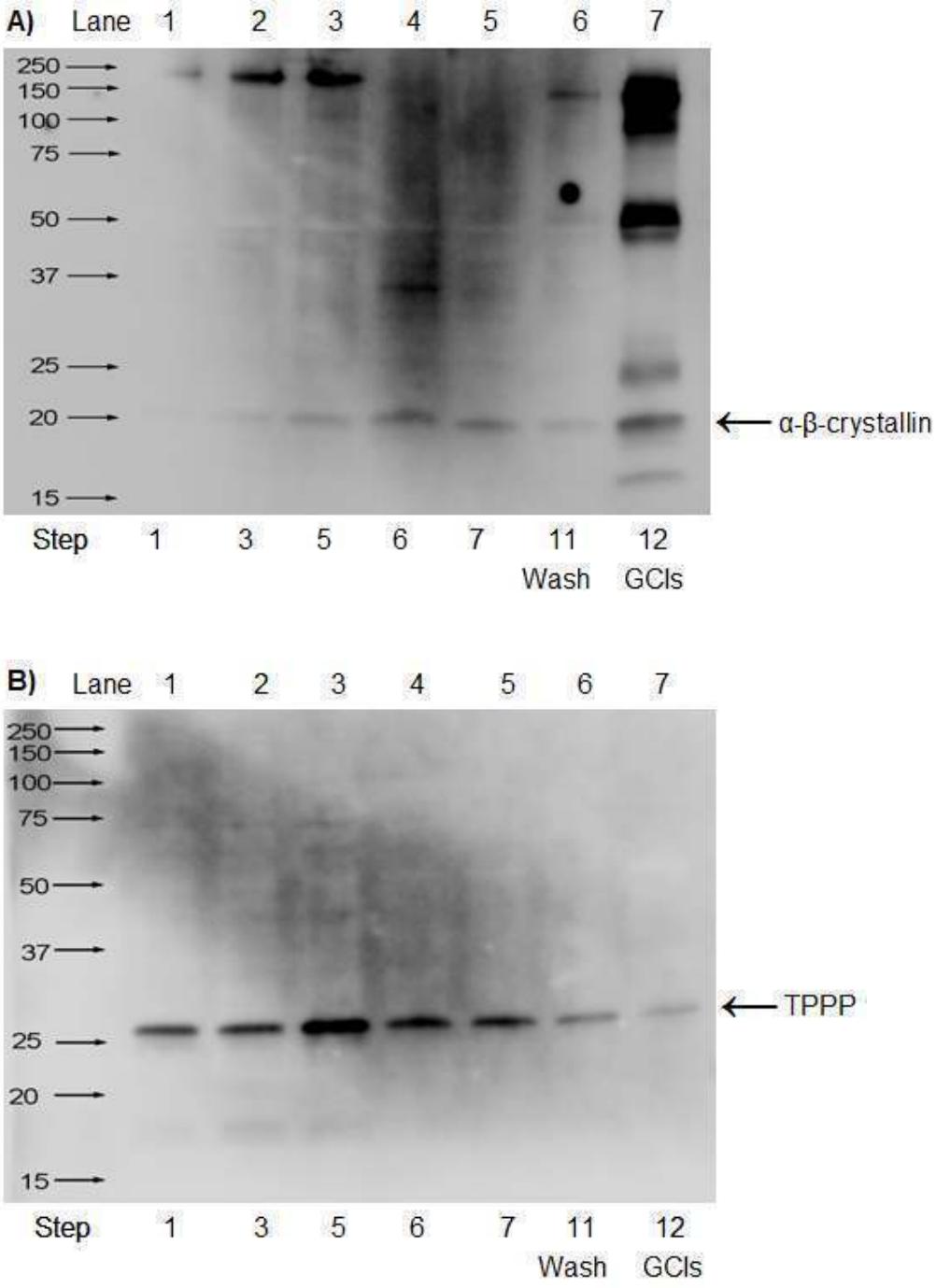

Figure 4-7: Antibody detection of A) α-β-crystallin and B) TPPP in fractions from a GCI purification using the optimised method

A GCI purification using the optimised method was performed as described in Chapter 2.5. The MSA homogenate (Lane 1, Step 1) was pelleted at 1,000x g (Lane 2, Step 3), from which a Percoll-enriched fraction (Lane 3, Step 5) was obtained and subjected to nuclei lysis and DNA digestion (Lane 4, Step 6), a limited tryptic digestion (Lane 5, Step 7) and immunomagnetic capture, with the wash fraction (Lane 6, Step 11) removed and the captured GCIs solubilised (Lane 7, Step 12). The samples were solubilised in 1x sample buffer and 20 µg of each sample was separated by SDS-PAGE using a BioRad Mini-Protean TGX Any kD gel, transferred to PVDF and probed with antibodies against either A) α-β-crystallin (n=1) (antibody no. 4, Table 2.1) or B) TPPP (n=1) (antibody no. 5, Table 2.1). The blots were imaged on a Fujifilm LAS-4000 CCD imager.

4.4 Discussion

In this study, the newly optimised method for purifying glial cytoplasmic inclusions (developed in Chapter 3) was compared to the previously published method [113] and characterised.

4.4.1 Improvements in purity and yield using the optimised method

The improvements in purity and yield in the optimised purification method compared to the published purification method was determined by using the two methods in parallel to purify GCIs from crude brain homogenate. As a result of developing the key modifications shown in the previous chapter, the yield of GCI proteins was dramatically increased (28-fold) alongside successful reduction of tubulin contamination (5.2-fold).

The yield of the two purification methods was assessed by looking at the yield of solubilised protein, as determined by EZQ assay, and the number of inclusions in the final immunocaptured fraction, as determined by immunohistochemistry and automated counting. The 28-fold increase in solubilised GCI protein agrees closely with the 31-fold increase in the number of inclusions counted.

The purity of the two methods was assessed by comparing the solubilised immunocaptured fractions from each method via 2D-DIGE, to show the comparative enrichment and diminishment of specific proteins. The individual spot volumes corresponding to the proteins α-synuclein, α-β-crystallin, 14-3-3 and tubulin were integrated and the total volume for each protein compared between the experiments. The 3.8-fold and 2.0-fold enrichments of the known GCI proteins α-synuclein and α-β-crystallin, respectively, show an improved purity in the optimised method, as does the 5.2-fold reduction in tubulin contamination. There is a 1.2-fold reduction in 14-3-3 proteins in GCIs purified using the optimised method. 14-3-3 is an adaptor protein that has been reported to have over 300 binding partners, including α-synuclein and tubulin [120]. Using the published method, 14-3-3 may have been co-enriched through binding to the contaminant tubulin in addition to being present as an inclusion protein, which would account for the slight reduction in 14-3-3 proteins when using the optimised method, which reduces the co-purification of tubulin.

While comparative analysis of α-synuclein and tubulin in the purification fractions from the two methods using Western blotting was desirable, the low yield of inclusions from the published method was insufficient for both 2D-DIGE and Western blot analysis, so the 2D-DIGE analysis was chosen as it presented information on a wider range of proteins and provided greater quantitative data.

4.4.2 Characterisation of the optimised method

The comparison of the solubilised GCI proteins purified using the optimised method to crude brain homogenate suggests a selective formation process, not just a stoichiometric incorporation of homogenate proteins into inclusions. If inclusions were a stoichiometric incorporation of homogenate proteins into insoluble forms due to lack of degradative ability of the cell, a similar protein profile to homogenate would be expected. Instead, α-synuclein and other proteins were shown to be incorporated in a higher proportion then their presence in crude homogenate would indicate, suggesting a selective incorporation process for inclusion formation.

Another explanation for the dissimilarity of the GCI proteome from the surrounding homogenate is that GCI proteins are only incorporated from the surrounding cytosol of the oligodendroglial cell, whereas homogenate consists of proteins from the cytosol, membrane, nucleus, mitochondria and other organelles, from various cell types. Also, proteins with a high turn-over rate would be expected to be present in a higher proportion in GCIs, where they are unable to be degraded, compared to the homogenate from which they are subsequently removed by degradation pathways. However, neither of these alternative explanations can account for the presence of α-synuclein, a neuronal protein not expressed in oligodendrocytes, in GCIs, which still suggests the specific targeting of proteins to inclusions.

The 2D-DIGE experiments reveal that GCIs contain 10.7% α-synuclein, 1.9% α-β-crystallin and 2.3% 14-3-3 proteins. By comparison, crude MSA brain homogenate contains approximately 2.0% α-synuclein, 0.8% α-β-crystallin and 1.9% 14-3-3 proteins. Previous studies have shown up to 1% of soluble brain protein to be α-synuclein [121] and 1.3% of soluble protein in the brain to be 14-3-3 [122], which agrees closely with the results obtained from the 2D-DIGE analysis. The relative abundance of the proteins of interest in both samples may be overestimated due to

the loss of very hydrophobic (membrane), very acidic and basic, and high molecular weight proteins from the sample during the isoelectric focusing, which increases the relative abundance of the proteins that have focused successfully. However, the quantitation may also be understated due to a conservative selection of known protein spots, which does not include any higher molecular weight complexes of the proteins of interest.

Western blot analysis of the fractions obtained from the optimised purification method revealed greatly enriched α-synuclein in the immunocaptured fraction compared to the crude homogenate and greatly reduced β-tubulin. The co-enrichment of known GCI protein α-β-crystallin in the immunocaptured fraction demonstrates the enrichment of α-synuclein-containing inclusions as opposed to simply the capture of soluble α-synuclein or α-synuclein oligomers. IHC was also used to verify the presence of GCIs in the immunocaptured fraction. The known GCI protein TPPP (or p25) was also shown with Western blotting to be present in the immunocaptured fraction, but it was diminished relative to the homogenate. This may due to a higher presence in the cell outside of inclusions than its ratio of incorporation into inclusions. The previous reporting of this protein may also have been over-reported due to its association with tubulin, which is reduced in this preparation.

The quantitation of α-synuclein and β-tubulin from the Western blots suggests a much greater enrichment and reduction of these proteins respectively, from the crude homogenate, than revealed by the 2D-DIGE analysis. Without the incorporation of internal standards or determining the linearity of the reactivity of α-synuclein antibodies with monomeric and polymeric α-synuclein, the Western blot quantitation is likely to be an approximate measure but will not have the accuracy of the DIGE quantitation, which has a linear dynamic range of more than 4 orders of magnitude. Because of the normalisation of the total intensity of each CyDye, DIGE is also robust for differences in protein load between samples.

4.4.3 Critical review of the purification method

The optimised method produces highly enriched GCI preparations, although the presence of some residual tubulin suggests that the inclusion preparations are not totally pure.

The introduction of each development was both time- and cost-intensive. The purification process takes one week for the purification of GCIs from 6 tubes of brain homogenate plus an additional week for follow-up analysis with Western blotting and IHC. Many of the purification reagents are expensive, especially the primary antibody and magnetic beads. The availability of brain tissue is also a limiting factor, with approximately 50% of the GCI-rich sections and up to 20% of the total available MSA tissue depleted from the SA brain bank from the experiments in this project. However, now that the purification method has been optimised to deliver a higher yield of inclusions for a given volume of tissue, more efficient use of brain sections will be made in the future.

Washing and filtration may give a small increase in purity with a trade-off of a large decrease in yield. The optimised method gives a significant yield of inclusions from the amount of brain tissue consumed, making downstream experiments possible. The enrichment of α-synuclein may also make analysis of α-synuclein modifications possible. The developed method is extremely robust. Since its development, the laboratory of Gai *et al.* has adopted the optimised method for their inclusion purifications and have obtained a similar degree of success with a different operator based in a different laboratory.

The high yield delivered by the newly optimised method allows sufficient protein for downstream proteomic analysis using 2-DE and Western blotting, compared to the laser capture microdissection method of Leverenz *et al.* [108] and the sucrose gradient/FACS method of Iwatsubo *et al.* [110], where the yields of approximately 1 µg and 1.5-3 µg respectively are only suitable for direct mass spectrometry analysis. By using an antibody against α-synuclein for immunomagnetic capture, compared to the antibodies against ubiquitin and neurofilament utilised by of Iwatsubo *et al.* [110] and Sian *et al.* [112], a greater specificity against inclusions is likely to be obtained. The original published method of Gai *et al.* [113] had already addressed many of

these pitfalls, which is why it was chosen as the best available method for optimisation, and why it was used as the basis of comparison in this chapter. It is difficult to compare the purity of the optimised method directly to other previously published methods due to differences in how purity is determined and reported.

4.5 Conclusion

A robust, high-yield, high-purity method for GCI purification has now been developed and characterised. The next step is to identify the proteins present in GCIs via mass spectrometry.

5 Identification of Glial Cytoplasmic Inclusion proteins

5.1 Introduction

When the newly optimised method for GCI purification was applied to MSA brain tissue, approximately 200 μg of GCIs could be highly enriched from 10 mL of crude brain homogenate (2 g of tissue). This improved method now allows for the identification of the GCI proteome.

5.1.1 Identification of GCI proteins

Identification of GCI proteins can be performed by mass spectrometry, either by injection of a trypsin-digested soluble GCI fraction (a complex mixture), or by injection of trypsin-digested 1D gel bands or 2D gel spots following 1D or 2D electrophoresis fractionation of the soluble GCI fraction. Proteins can also be identified by immunohistochemistry.

For this study, the analysis of whole solubilised inclusions, digested with trypsin, was performed because this allowed for repeat analysis of multiple MSA cases, with the sensitivity of the instrument still making identification of over 150 proteins per sample possible. Comprehensive protein identifications from complex samples are possible because of three capabilities of the hybrid Orbitrap MS which contains both an Orbitrap mass analyser and an ion trap.

Firstly, the high resolution capability of the Orbitrap analyser allows for the charge state of the precursor ion to be determined prior to MS/MS, thereby permitting rejection of all singly charged ions (which are mostly background ions) and analysing only multiply charged ions (which are generated by trypsin digestion). This increases the number of peptides that the instrument can analyse, which is of particular value for complex mixtures of proteins.

Secondly, the Orbitrap operates in tandem with a lower resolution/mass accuracy ion trap which fragments the peptide to generate b and y ions from which the amino acid sequence is calculated. The ion trap can accumulate peptides in the trap for up to 100 milliseconds, which increases sensitivity for very low abundance peptides. The ion trap trades mass accuracy and resolution for a higher scan rate, which allows the ion trap to fragment and sequence approximately five peptides per seconds compared

to the single scan per second of the Orbitrap. As the ion trap is used for MS/MS, there are numerous product ions generated by the fragmentation of the peptide from which the sequence is calculated, so the mass accuracy and resolution are less important because the peptide sequence is calculated from multiple data points instead of a single data point, as is the case for MS.

Thirdly, the very high mass accuracy of the Orbitrap enables the mass measurement of the precursor ion (peptide) with an error of that approaching the mass of an electron (< 5ppm, 1000 Da peptide). This very accurate mass measurement of the peptide substantially increases the confidence of the peptide sequence determined in the ion trap. Proteomic studies demonstrate the ability of the Orbitrap to elucidate the composition of complex samples with peptides distributed over a wide m/z and concentration ranges [123], including bacterial [124, 125], plant [126, 127], animal [128] and human [129-131] studies.

While 1D and 2D fractionation have the advantage of reducing the complexity of the sample and making a larger number of protein IDs theoretically possibly, the large number of gel slices or spots these fractionation methods produce for mass spectrometry analysis is prohibitively time consuming and expensive, with two hours of instrument time required per sample, when mapping the entire proteome of protein spots rather than identifying a small set of proteins of interest. 1D and 2D fractionation were performed in single experiments in this study, to corroborate the results from the trypsin-digested complex mixtures, to generate a spot map of the GCI proteome, and to identify small molecular weight proteins that may be missed in a complex sample due to the low number of peptides generated.

As immunohistochemistry (IHC) is useful for confirming the presence of single proteins in inclusions, rather than proteome mapping, IHC was used to provide an independent verification of the presence of some of the key identifications made by mass spectrometry (Chapter 7.3.3).

5.1.2 Identification of core and adherent GCI proteins

To elucidate which GCI proteins are present at the core of the inclusions and which are adherent at the periphery, a stripping protocol utilising sodium carbonate [132], which is commonly used for separating membrane-adherent proteins from core

membrane proteins, was used. This method used ice-cold sodium carbonate applied to purified, intact GCIs to remove non-covalently bound proteins from the periphery of the inclusions. The remaining GCI structure was then solubilised to reveal the core GCI proteins.

5.1.3 Controls for purification process

While the optimised inclusion purification method highly enriches GCIs from crude brain homogenate, a 100% pure preparation is not possible. To identify if any of the enriched proteins are artifacts of the purification process as a result of non-specific binding, a secondary-antibody only control was performed, where the primary antibody is omitted from the purification procedure. Thus, any proteins captured with this experiment were not captured as a result of binding to the anti-α-synuclein primary antibody, but by direct interaction with either the secondary antibody or the magnetic beads.

To investigate what structures from 'normal' control brain tissue are purified via immunocapture, brain tissue from normal control cases was processed using the optimised method for GCI purification. This was to demonstrate if any non-inclusion proteins bound to the primary anti-α-synuclein antibody and also provide an insight into what α-synuclein aggregates are present in a 'normal' aged brain.

5.1.4 Biological variation in the GCI proteome

To investigate the degree of biological variation in the GCI proteome between different MSA cases, GCIs were purified separately from multiple MSA cases and the protein profile obtained from each case compared using 2D-DIGE. The use of an internal standard with 2D-DIGE eliminates the need for technical gel replicates by providing improved spot match and adjustment for variations in protein load, so that the abundance of each protein spot can be compared across the entire cohort to assess variability between cases. Any technical variation in the purification procedure was determined by purifying GCIs from the same MSA case on two separate occasions, and comparing the two samples using 2D-DIGE.

5.1.5 Aims

The aims of these experiments were:

- To identify GCI proteins by mass spectrometry, utilising 1D fractionation, 2D fractionation, and trypsin-digested complex mixtures.
- To identify core and adherent GCI proteins by mass spectrometry by using carbonate stripping to separate the GCI-adherent proteins from the core GCI proteins.
- To identify proteins purified in a secondary antibody-only control and in normal case controls by mass spectrometry, to identify proteins that are artifacts of the purification process rather than genuine GCI proteins.
- To compare GCI proteins from multiple MSA cases to assess the degree of biological variation in GCI proteins.
- To determine the reproducibility of the optimised GCI purification method by purifying GCIs from the same case on two separate occasions and comparing the samples by 2D-DIGE.

5.2 Materials and Methods

5.2.1 Inclusion purifications

Brain tissue homogenisation was performed as described in Chapter 2.4.

5.2.1.1 GCI purification from multiple MSA cases

GCI purifications were performed on MSA tissue as described in Chapter 2.5, with each case processed separately. The cases used and the number of tubes of homogenate processed for each case are listed in Table 5.1. Sample MSA 2 was processed on two separate occasions, to assess the technical variation in the purification technique, with 1.5 tubes of homogenate processed for purification replicate 1 (p1) and 1.0 tubes of homogenate processed for purification replicate 2 (p2).

Table 5-1: Post-mortem brain tissue used for GCI purifications for biological variation analysis by 2D-DIGE and complex mixture analysis by mass spectrometry

Case No.[a]	Brain region	Name[b]	No. of tubes[c]
SA0101	Basal ganglia	MSA 1	2
SA0061	Basal ganglia	MSA 2	2.5
SA0132	Basal ganglia	MSA 3	1.5
SA0071	Basal ganglia	MSA 4	2.5
SA0190	Basal ganglia	MSA 5	2

[a] SA Brain Bank case number
[b] Sample name used in this thesis to avoid confusion between different pathologies when quoting case numbers.
[c] Number of 10 mL tubes of homogenate (each containing ~2 g tissue) used for inclusion purification

5.2.1.2 GCI purification – 2-DE and 1-DE maps

A GCI purification was performed using 3 tubes of brain homogenate pooled from cases SA0058 and SA0101 (Table 2.3) as described in Chapter 2.5. These purified GCIs were used for 2-DE, as described in section 5.2.2. A separate GCI purification was performed using 3 tubes of brain homogenate from case SA0101 as described in Chapter 2.5. These purified GCIs were used for 1-DE, as described in section 5.2.4.

5.2.1.3 Purification of core and adherent GCI proteins

An inclusion purification was performed on two tubes of MSA homogenate from case SA0132 (Table 2.3) as described in Chapter 2.5. In step 12, prior to centrifugation of the 1.5 mL suspension of beads and attached inclusions, the suspension was split into two 750 µL fractions. One fraction was processed through the remainder of Step 12 as described in Chapter 2.5, as a total GCI protein preparation. The other fraction was processed with a carbonate stripping protocol, to remove the GCI-adherent proteins from the core GCI proteins. This protocol is based on the method described by Molloy (2008) [132] and adapted to a starting quantity of approximately 100 µg of GCIs (the expected minimum yield from one tube of MSA homogenate).

The 750 µL fraction was centrifuged and the supernatant removed as described in Step 12 in Chapter 2.5.5 until a pellet of beads and attached inclusions remained. Instead of adding protein solubilisation buffer, 250 µL of cold 100 mM sodium carbonate was added to strip away the adherent proteins. The tube was incubated for 30 minutes at 4°C at 1,400 RPM in a Thermomixer (Eppendorf). The sample was centrifuged at 18,000x g for 10 minutes at 4°C. The supernatant containing the adherent GCI proteins was collected. The pellet was then washed in 250 µL of TBS-Azide by pipette mixing and centrifuged again at 18,000x g for 10 minutes at 4°C. 200 µL of protein solubilisation buffer was added to the remaining pellet of beads and core GCI proteins and the fraction was processed alongside the total GCI proteins as described in Chapter 2.5.5.

5.2.1.4 Secondary antibody-only control for GCI purification

An inclusion purification was performed on two tubes of MSA homogenate pooled from cases SA0101 and SA0132 (Table 2.3) as described in Chapter 2.5. After Step 7, the sample was split into two equal fractions. One half was processed without the addition of primary antibody in Step 8 (as a secondary-only control) and the other half was processed with the addition of primary antibody. The samples were processed in parallel through steps 9-12 according to the standard protocol described in Chapter 2.5.

5.2.1.5 Control purification on 'normal' brain tissue

Normal control cases SA0162 and SA0230 were used (Table 2.3), hereafter referred to as normal cases 1 and 2, respectively. An inclusion purification was performed on one tube of homogenate from each normal control case as described in Chapter 2.5, with each case processed separately. The same reagent amounts and volumes as for a GCI purification were used.

5.2.2 2-DE

2D gel electrophoresis was performed as described in Chapter 2.8, except that cup loading isoelectric focusing was used instead of rehydration loading isoelectric focusing. A 24 cm Immobiline DryStrip gel pH 3-11 NL was rehydrated as described in Chapter 2.8.2, but with IEF rehydration buffer only (no sample). The strip was passively rehydrated overnight. The strip was then placed gel side up in an IPGphor Manifold (GE Healthcare) and the manifold set up for cathodic cup loading, as described in Chapter 2.3.4 of the 2D Electrophoresis Principals and Methods Handbook 80-6429-60AC (GE Healthcare). 250 µg of solubilised inclusions, purified using a 2D Clean-up Kit (BioRad), were applied to the strip. Isoelectric focusing was performed using the IEF protocol outlined in Chapter 2.8.2, with the strip focused for 52,000 Vhr. The 2nd dimension was performed as described in Chapter 2.8.3 with a 12.5% linear gel. The gel was stained with SyproRuby and imaged on a Typhoon 9400 variable mode imager, as described in Chapter 2.8.4. The gel was scanned at 200 µm with a photomultiplier tube value of 700 V. Subsequent silver staining was performed as described in Chapter 2.8.4 to visualise spots to excise for tryptic digestion.

5.2.3 2D DIGE

DIGE labeling and 2D gel electrophoresis was performed as described in Chapter 2.8. The solubilised inclusions (section 5.2.1.1) were purified with a ReadyPrep 2D Clean-Up Kit (Biorad) as described in Chapter 2.6.2 and resolubilised in DIGE labeling buffer at pH 8.5. 50 µg of each inclusion preparation was labeled with 400 pmoles of CyDye as described in Chapter 2.8.1. The experimental design is outlined in Table 5.2. The pooled internal standard was 50 µg of a protein pool consisting of 25 µg of each of the samples used in this experiment.

Table 5-2: DIGE experimental design for GCI biological variation comparison

Gel	Cy2 Standard	Cy3	Cy5
1	Pooled Internal Standard	MSA 2 p1*#	MSA 2 p2*
2	Pooled Internal Standard	MSA 1	MSA 4#
3	Pooled Internal Standard	MSA 3	MSA 2 p1#
4	Pooled Internal Standard	MSA 4#	MSA 5

* p1 = purification replicate 1, p2 = purification replicate 2
# replicates of sample MSA 2 p1 and MSA 4 were run

The labeled protein extracts were combined for their respective gels and subjected to isoelectric focusing using 24 cm pH 3-11NL Immobiline DryStrips (GE Healthcare), as described in Chapter 2.8.2. The strips were focused for approximately 80,000 Vhr according to the following protocol: Step to 500 V for 30 min, step to 1,000 V for 30 min, linear gradient to 10,000 V for 30 min, hold at 10,000 V until 65,000 Vhr, step to 1,000 V until end. The 2nd dimension was performed as described in Chapter 2.8.3, but with 12.5% linear gels. Gel imaging was performed on a Typhoon 9400 variable mode imager as described in Chapter 2.8.4. The photo-multiplier tube values for the green (532 nm), red (633 nm) and blue (488 nm) channels were set at 540 V, 520 V and 650 V respectively for gels 1 and 2, and 540 V, 510 V and 640 V respectively for gels 3 and 4. The gels were analysed in DeCyder version 7.0 (GE Healthcare).

5.2.4 1-DE

Immunocaptured fractions from the carbonate stripping, secondary only control, and normal control experiments (sections 4.2.1.3, 4.2.1.4 and 4.2.1.5), and selected fractions from a GCI purification (section 4.2.1.2) were subjected to 1-DE, which was performed as described in Chapter 2.7. Prior to 1-DE, each fraction was solubilised in 1x 1D sample buffer without bromophenol blue, vortexed and heated at 95°C for 5 minutes. Solubilised immunocaptured fractions were purified with a BioRad ReadyPrep 2D Clean-Up kit prior to solubilisation in 1x sample buffer. The samples were vortexed again, spun at 18,000x g and the supernatants collected for 1-DE. SyproRuby staining and imaging was performed as described in Chapter 2.8.4. Subsequent silver staining was performed as described in Chapter 2.8.4 to visualise bands to excise for tryptic digestion.

5.2.5 DAB immunohistochemistry

DAB immunohistochemistry was performed on selected fractions from the normal control and secondary only control purification procedures as described in Chapter 2.9.1. All staining was performed using a sheep anti-α-synuclein primary antibody (antibody no. 1, Table 2.1) used at 1:1000 (1 μg/mL) and an anti-sheep biotinylated secondary (antibody no. 10, Table 2.2) used at 1:500 (2.6 μg/mL). Nanozoomer analysis and inclusion counting was performed for the secondary-only control experiment as described in Chapter 2.9.2. A saturation threshold of 102 was used.

5.2.6 Tryptic digestion

20 μg of purified GCIs from each of the five MSA cases in Table 5.1, one-third of the solubilised immunocaptured samples from the secondary only control experiment, and one-third of the total, core and peripheral GCI protein preparations from the carbonate stripping experiment, were buffer-exchanged into 50 mM ammonium bicarbonate using Vivaspin columns, as described in Chapter 2.11.1. An in-solution tryptic digestion of the samples was performed as described in Chapter 2.11.2.

1D gel slices were excised and trypsin digested as described in Chapter 2.11.3. 2D gel spots were excised and trypsin digested as described in Chapter 2.11.4.

5.2.7 Mass spectrometry

The digested peptides were analysed with a Thermo LTQ Orbitrap XL mass spectrometer as described in Chapter 2.12.1 and spectra interrogated with Protein Discoverer 1.2 as described in Chapter 2.12.2.

5.3 Results

5.3.1 Identification of GCI proteins

5.3.1.1 Identification of GCI proteins from complex mixtures

GCI purifications were performed on tissue from the same brain region of five separate MSA cases, as described in section 5.2.1.1. 20 µg from each of these samples was digested with trypsin and the digested peptides analysed by LTQ Orbitrap XL mass spectrometry (sections 5.2.6 and 5.2.7), with two replicates for each of the five samples. The False Discovery Rate (FDR) was <0.01 for each of the samples analysed.

From the ten injections, a total of 502 proteins were identified. 164 of these proteins were present in a minimum of 4 out of the 5 cases (Appendix A). 24 protein isoforms of 10 proteins previously established to be in GCIs, as summarised in a review by Wenning *et al.* (2008) [31] were identified and these are listed in Table 5.3. In Appendix A, the proteins that were also identified in the secondary-only control (section 5.3.4) have been marked with an *.

Table 5-3: Established GCI proteins identified by MS

Protein	No. of cases[a]
α-synuclein	5
α-β-crystallin	5
14-3-3 proteins (7 isoforms)	5
Tubulin (9 isoforms)	5
Microtubule-associated protein 1A (MAP1A)	2
Microtubule-associated protein 1B (MAP1B)	5
Microtubule-associated protein 2 (MAP2)	3
Heat shock 70 kDa protein 12A	5
Tubulin polymerization-promoting protein (TPPP)	3
Carbonic anhydrase 2	1

[a] number of MSA cases in which the protein was identified

In this experiment, a broad range of synaptic vesicle-related proteins were identified, including 15 established synaptic vesicle proteins (Table 5.4), 56 proteins transiently associated with the synaptic vesicle membrane (Appendix B), and 19 putative novel synaptic vesicle proteins (Appendix C). The classification of these proteins was based on a review of the synaptic vesicle proteome by Burre and Volknandt (2007) [133]. Of the proteins identified in 4+ MSA cases, 21% were synaptic vesicle-related. The relationships between the protein identifications in this experiment are shown in Figure 5.1.

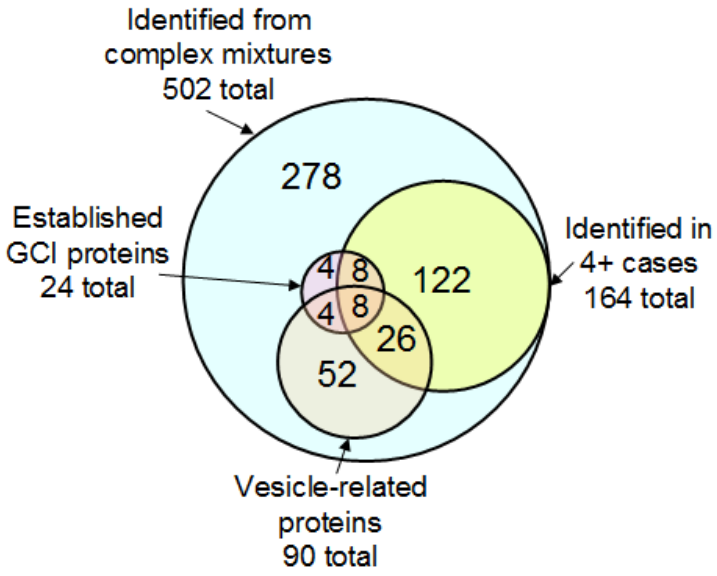

Figure 5-1: Venn diagram of GCI protein identifications from trypsin-digested complex mixtures (n=5)
Solubilised Inclusions isolated from 5 MSA cases were trypsin-digested and the digested peptides were analysed by LTQ Orbitrap XL mass spectrometry. 502 proteins were identified in total, with 164 identified in 4 or more cases. The overlap between the identification of established GCI proteins and vesicle-related proteins with the total protein identifications is shown.

Table 5-4: MS Identification of 15 GCI proteins that are established synaptic vesicle proteins

Acc. No.[a]	Name	Calc. pI	Calc. MW (Da)	No. of cases[b]	Avg. Xcorr[b]	Avg. No. of Peptides[c]	Avg. % Sequence Coverage[d]
P60880	*Synaptosomal-associated protein 25	4.77	23300	5	20.2	3.9	25.5
P38606	V-type proton ATPase catalytic subunit A	5.52	68300	4	35.6	4.8	12.3
P61421	V-type proton ATPase subunit d 1	5.00	40300	4	24.5	3.7	20.1
P21281	V-type proton ATPase subunit B, brain isoform	5.81	56465	4	21.0	3.6	11.6
P36543	V-type proton ATPase subunit E 1	8.00	26129	1	10.5	2.0	11.1
Q9UI12	V-type proton ATPase subunit H	6.48	55800	1	6.7	2.0	6.6
Q16864	V-type proton ATPase subunit F	5.52	13362	1	6.4	2.0	26.1
P20336	Ras-related protein Rab-3A	5.03	25000	3	18.8	3.8	23.6
P21579	*Synaptotagmin-1	8.12	47543	2	27.7	4.5	13.8
P61266	Syntaxin-1B	5.38	33200	2	16.3	2.3	11.7
Q16623	Syntaxin-1A	5.24	33000	1	7.2	2.0	7.6
P08247	*Synaptophysin	4.81	33823	2	16.2	2.0	8.0
P63027	*Vesicle-associated membrane protein 2	8.13	12655	2	14.6	2.0	28.5
Q7L0J3	Synaptic vesicle glycoprotein 2A	5.57	82600	2	10.8	2.3	3.3
O43759	Synaptogyrin-1	4.68	25400	1	5.9	2.0	10.3

[a] SwissProt accession number
[b] Number of MSA cases in which the protein was identified
[c] Average Xcorr significance score
[d] Average number of unique peptides sequenced
[e] Average % of the full-length amino acid sequence covered by identified peptides
* Presence in GCIs validated with immunofluorescence (Chapter 7.3.3)

5.3.1.2 Identification of GCI proteins by 1-DE fractionation

Purified GCIs were subjected to 1-DE fractionation (Lane 8, Figure 5.2). The lane was cut into 10 fractions, from the top to the bottom of the gel (high molecular weight to low molecular weight). Each of the ten fractions was digested with trypsin and the digested peptides analysed by LTQ Orbitrap XL mass spectrometry (as described in sections 5.2.6 and 5.2.7).

From the ten fractions, 201 identifications of 117 unique proteins were made (excluding cytokeratins, likely to arise from epidermal contamination of the gel). Of the 117 proteins, 81 were exclusive to only one fraction (Appendix D) and 36 were present in two or more fractions (Appendix E) and thus identified multiple times. The number of proteins identified in each fraction is listed in Table 5.5. Three proteins previously established to be in GCIs were identified – α-synuclein, 14-3-3 proteins (6 isoforms), and tubulin (8 isoforms forms). α-β-crystallin was not identified. The established synaptic vesicle proteins synaptotagmin 1, vesicle-associated membrane protein 2, and v-type proton ATPase subunit a were also identified.

Of the 117 proteins identified, 92 were also identified from trypsin-digested complex mixtures in the previous experiment (section 5.3.1.1), and 25 were only identified through 1-D fractionation. The overlap in protein identifications between the two experiments is shown in Figure 5.3. The 25 proteins identified only through 1-D fractionation included two vesicle-related proteins, elongation factor 1-alpha fragment and tubulin beta-2B chain, of which the tubulin beta-2B chain has also been reported to be an established GCI protein. These classifications were omitted from Figure 5.3 for the sake of clarity.

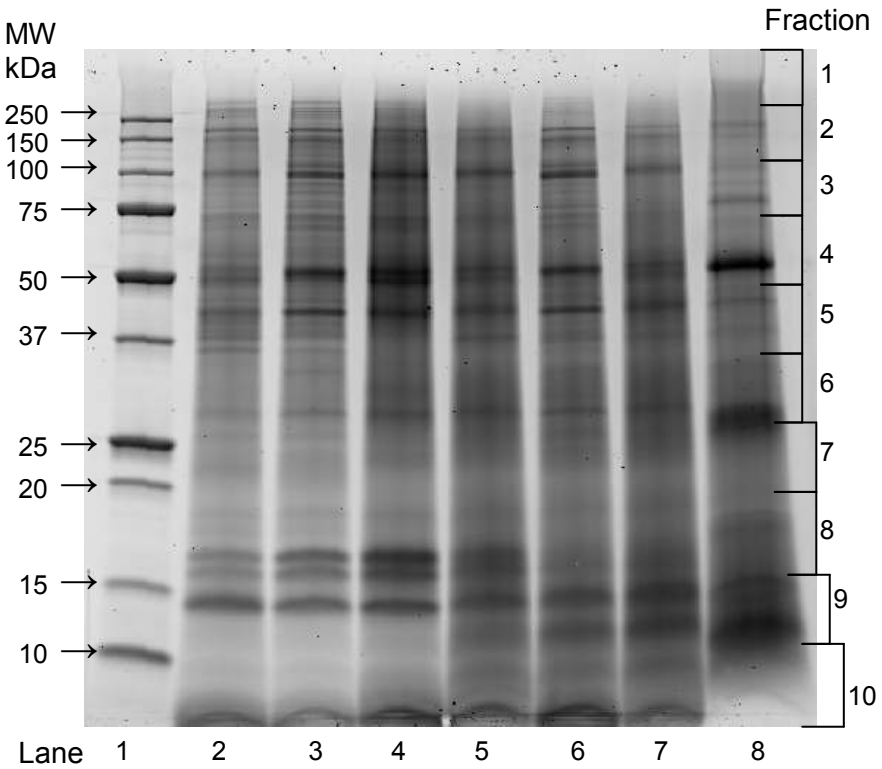

Figure 5-2: 1-DE of GCI purification fractions
The MSA homogenate (Lane 2, Step 1) was pelleted at 1,000x g (Lane 3, Step 3), from which a Percoll-enriched fraction (Lane 4, Step 5) was obtained and subjected to nuclei lysis and DNA digestion (Lane 5, Step 6), a limited tryptic digestion (Lane 6, Step 7) and immunomagnetic capture, with the wash fraction (Lane 7, Step 11) removed and the captured GCIs solubilised (Lane 8, Step 12). The samples were solubilised in 1x sample buffer and 18 µg of each sample was separated by SDS-PAGE using a BioRad Mini-Protean TGX Any kD gel, with 5 µL of unstained molecular weight markers (Lane 1). The gel was stained with SyproRuby, and imaged on a Typhoon 9400 variable mode imager. The gel was subsequently silver stained, and the purified GCI proteins (Lane 8) were cut into 10 fractions as shown. Each fraction was digested with trypsin and analysed by LTQ Orbitrap XL mass spectrometry.

Table 5-5: Number of proteins identified in each 1D fraction of purified GCIs

Fraction[a]	Estimated MW (kDa)[b]	No. of proteins identified	No. of exclusive proteins[c]
1	>300	2	0
2	110-300	22	11
3	70-110	45	28
4	48-70	25	9
5	35-48	28	10
6	26-35	19	5
7	19-26	17	3
8	16-19	23	9
9	10-16	17	5
10	<10	3	1
Total		201	81

[a] from top (1) to bottom (10) of gel (Figure 5.2)
[b] the estimate molecular weight range of proteins contained in the gel fraction
[c] the number of proteins identified only in that fraction

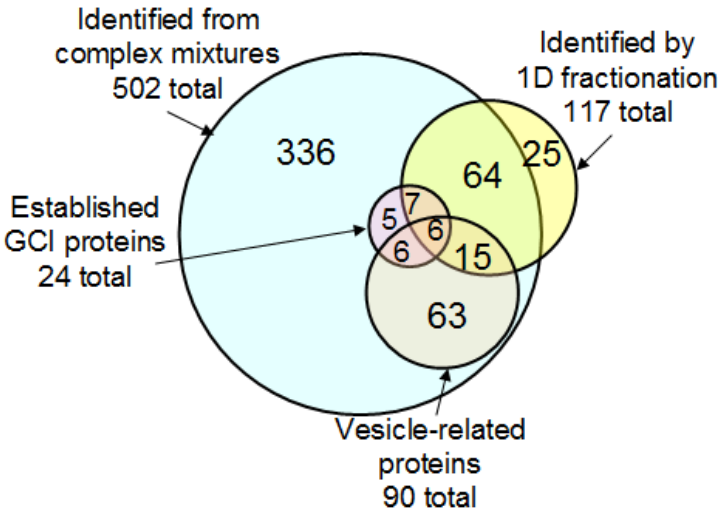

Figure 5-3: Venn diagram of GCI protein identifications by 1D fractionation (n=1) compared to complex mixtures (n=5)
Solubilised Inclusions isolated from 5 MSA cases were trypsin-digested and the digested peptides were analysed by LTQ Orbitrap XL mass spectrometry. 502 proteins were identified in total from these complex mixtures compared to 117 identifications from one sample subjected to 1D fractionation prior to tryotic digestion and MS analysis. The overlap between the identification of established GCI proteins and vesicle-related proteins with the protein identifications made from complex mixtures and 1D fractionation is shown.

5.3.1.3 Identification of GCI proteins from a 2-DE spot map

Purified GCIs were subjected to 2-DE (Figure 5.6), and the selected spots were digested with trypsin and the digested peptides analysed by LTQ Orbitrap XL mass spectrometry (as described in sections 5.2.6 and 5.2.7). 135 variants of 99 different proteins were identified (Table 5.6) from a total of 209 spots (refer to Appendix F for details).

The overlap in identifications made from trypsin-digested complex mixtures, 1D fractionation and 2D fractionation is shown in Figure 5.4 and the overlap in synaptic vesicle-related protein identifications is shown in Figure 5.5.

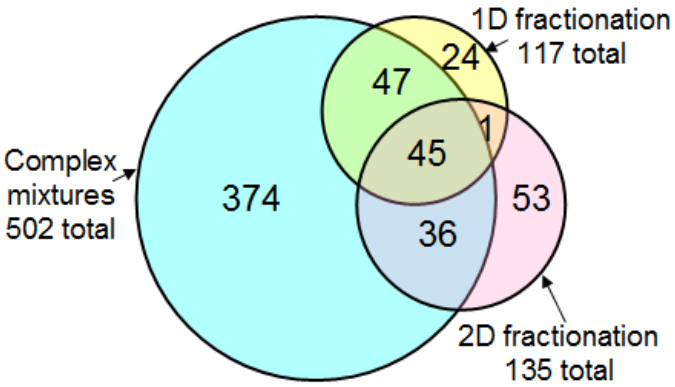

Figure 5-4: Venn diagram of GCI protein identifications from complex mixtures (n=5), 1D fractionation (n=1) and 2D fractionation (n=1)
Solubilised Inclusions isolated from 5 MSA cases were trypsin-digested and the digested peptides were analysed by LTQ Orbitrap XL mass spectrometry. 502 proteins were identified in total from these complex mixtures compared to 117 identifications from a sample subjected to prior 1D fractionation 135 identifications from a sample subjected to prior 2D fractionation. The overlap between the identifications is shown.

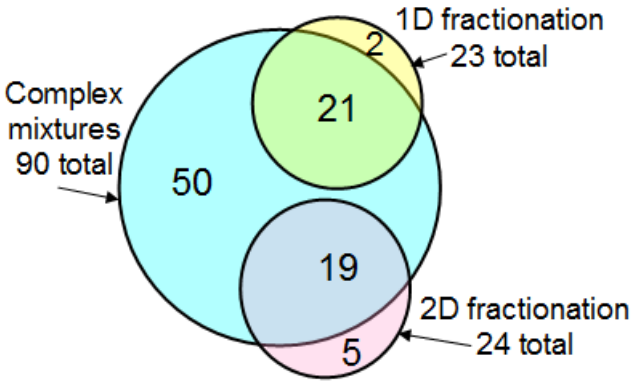

Figure 5-5: Venn diagram of vesicle-related protein identifications from complex mixtures (n=5), 1D fractionation (n=1) and 2D fractionation (n=1)
The overlap between the vesicle-related protein identifications from Fig 5.4 is shown.

A)

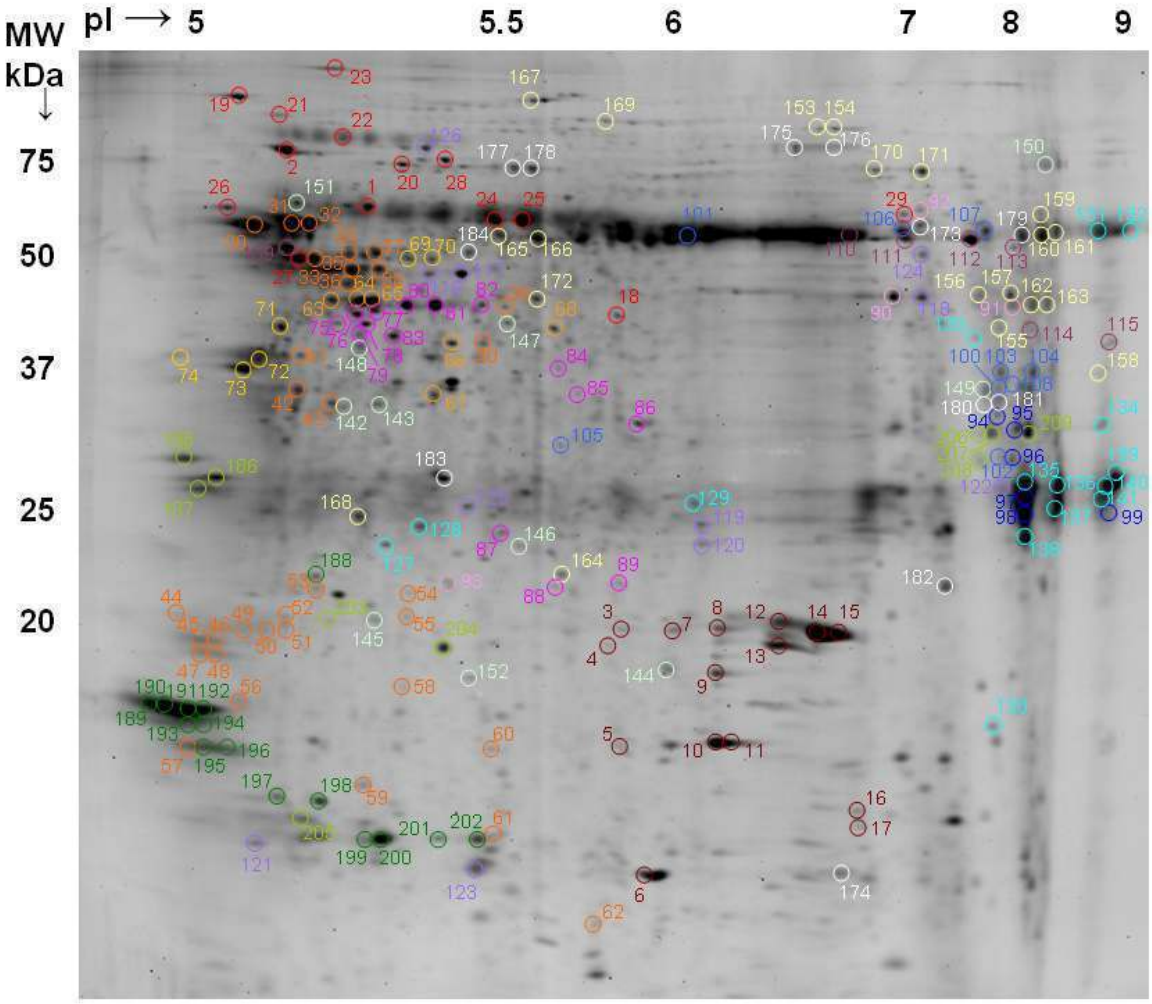

	Chaperones – Alpha-β-crystallin
	Chaperones – all others
	Cytoskeletal component – Tubulin
	Cytoskeletal component – Actin
	Cytoskeletal component – GFAP
	Kinases – Creatine kinase B
	Kinases – all others
	Oxidative stress – Carbonyl reductase [NADPH] 1
	Oxidative stress – all others
	Electron transport chain – ATP synthase
	Electron transport chain – all others
	Immunoglobulins
	Protein trafficking, ubiquitination, G-protein signaling and calcium binding
	TCA cycle, hydrolases, transferases and ligases
	Serum proteins, protein biosynthesis, ribonucleoproteins, DNA-related and mRNA processing proteins
	Others – Alpha-synuclein
	Others – all others

B)

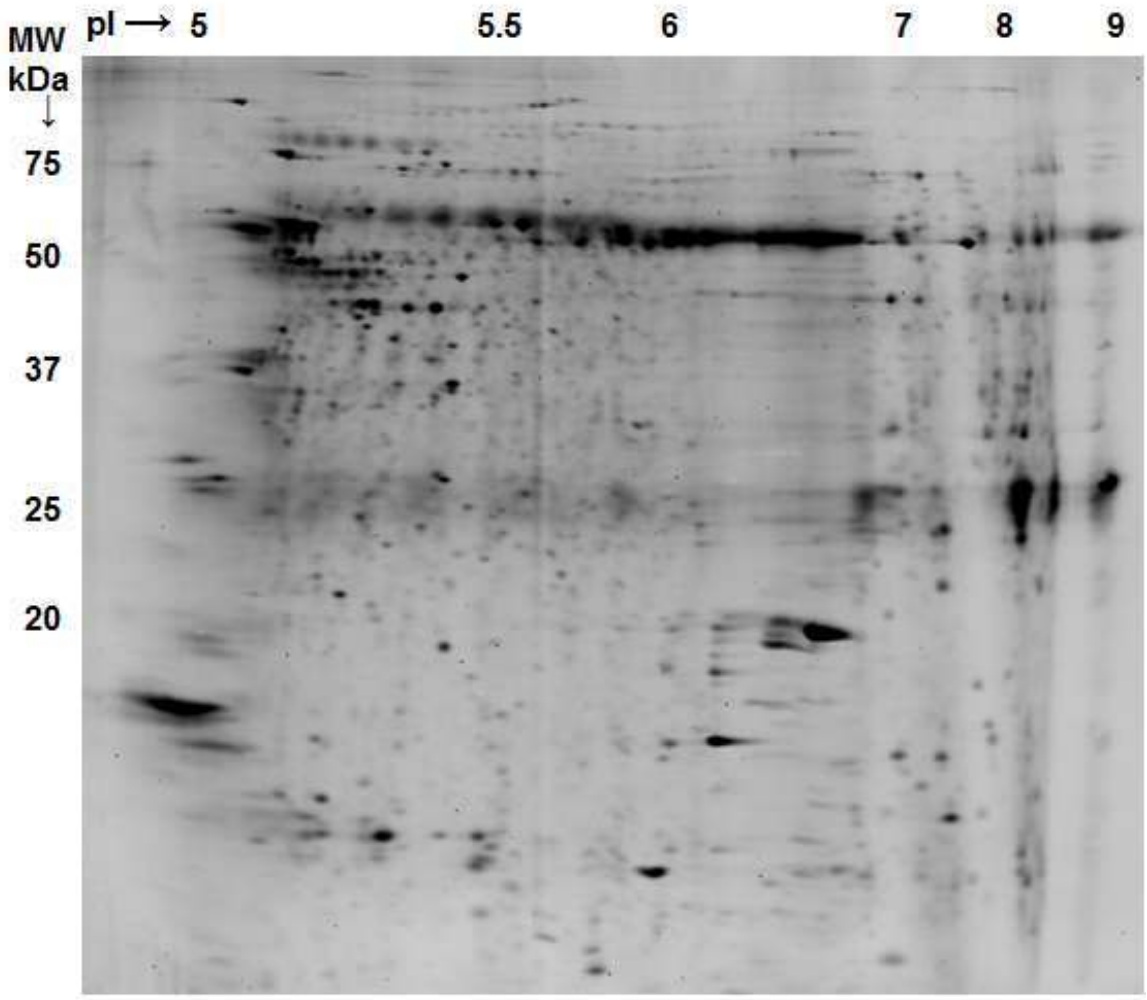

Figure 5-6: 2-DE spot map of solubilised proteins from immunocaptured GCIs
250 µg of inclusions purified using the optimised GCI purification method (section 5.2.1.5) were subjected to 2-DE using a 24cm pH 3-11NL strip and 12.5% linear SDS-PAGE (as described in section 5.2.5). The gel was stained with SyproRuby and imaged on a Typhoon 9400 variable mode imager. The labelled spots in (A) were identified by Thermo LTQ Orbitrap XL mass spectrometry as described in section 5.2.8, and the protein identifications are listed in Table 5.6. The unlabelled gel is shown in (B) for visual clarity.

Table 5-6: MS protein identifications from 2-D spot map of purified GCIs

Protein	Main constituent of spot no.	Also identified in spot no.
Chaperones		
60 kDa heat shock protein	1	151
78 kDa glucose-regulated protein	2	
Alpha-β-crystallin	3-17	
DnaJ homolog subfamily B member 11	18	
Endoplasmin	19	
Heat shock cognate 71 kDa protein	20	
Heat shock protein HSP 90, alpha and beta chains	21-22	
Hypoxia up-regulated protein 1	23	
Peptidyl-prolyl cis-trans isomerase FKBP4		36, 116, 184
Protein disulfide-isomerases, standard, A3 and A6	24-27	33
Stress-70 protein	28	
T-complex protein 1, subunit eta	29	
Cytoskeletal components		
Tubulin, alpha and beta chains	30-62	27,69-70,72,74, 84,109,116,172, 184,193-196
Actin	63-68	172
Glial fibrillary acidic protein (GFAP)	69-74	36,41,116
Kinases		
6-phosphofructokinase		176
cAMP-dependent protein kinase type I-alpha regulatory subunit		34
Creatine kinase B-type	75-89	
Creatine kinase U-type	90	
Phosphoglycerate kinase 1	91	
Pyruvate kinase isozymes M1/M2, isoform M1	92	
UMP-CMP kinase	93	
Oxidative stress		
Carbonyl reductase [NADPH] 1	94-99	102,134-136,138, 140,206-208
Corticosteroid 11-beta-dehydrogenase isozyme 1	100	103
D-3-phosphoglycerate dehydrogenase	101	
D-beta-hydroxybutyrate dehydrogenase	102	
Glyceraldehyde-3-phosphate dehydrogenase	103-104	
Glycerol-3-phosphate dehydrogenase [NAD+]		84
HMOX2 protein	105	
Methylmalonate-semialdehyde dehydrogenase [acylating]	106-107	110
Mitochondrial lon protease-like protein		167
Peroxiredoxin-2		93
Peroxisomal multifunctional enzyme type 2	108	

Protein	Main constituent of spot no.	Also identified in spot no.
Electron transport chain		
ATP synthase, alpha, beta and gamma subunits	109-115	117,134
Cytochrome b-c1 complex subunits 1, 2 and Rieske	116-120	
Cytochrome c oxidase subunit 5A	121	
Electron transfer flavoprotein subunit beta	122	
Iron-sulfur protein NUBPL		96
NADH dehydrogenase [ubiquinone] 1 alpha subcomplex subunit 5	123	
NADH dehydrogenase [ubiquinone] flavoprotein 1	124	
NADH dehydrogenase [ubiquinone] iron-sulfur protein 3	125	
NADH-ubiquinone oxidoreductase 75 kDa subunit	126	
Immunoglobulins		
Immunoglobulins - IGK, gamma, kappa and light chains	127-141	97-98,158
Protein trafficking		
NSF attachment proteins, alpha- and beta-soluble	142-143	
Sorting nexin-30		36
Transmembrane emp24 domain-containing proteins 2 and 10	144-145	
Vesicle-fusing ATPase		175-176
Protein ubiquitination		
26S proteasome non-ATPase regulatory subunits 5, 10 and 13	146-147	37
Cullin-1		176
Proteasome subunit alpha type-7		122
Ubiquitin carboxyl-terminal hydrolase 14		36
G protein signalling		
Guanine nucleotide-binding protein G(o), alpha and alpha isoform subunits	148	40
Rap1 GTPase-GDP dissociation stimulator 1		37
Calcium binding proteins		
Annexin A2	149	
Calcium-binding mitochondrial carrier protein Aralar2	150	
Nucleobindin-1	151	
Translocon-associated protein subunit delta	152	
Tricarboxylic acid cycle		
Aconitate hydratase	153-154	
Isocitrate dehydrogenase [NAD] subunit gamma	155	
Isocitrate dehydrogenase [NADP]	156-157	
Malate dehydrogenase	158	108
Hydrolases		
2',3'-cyclic-nucleotide 3'-phosphodiesterase	159-163	91,133,155,157
Abhydrolase domain-containing protein 14B	164	
Cytosolic non-specific dipeptidase	165-166	
GDH/6PGL endoplasmic bifunctional protein		153-154
Neutral alpha-glucosidase AB (Highly similar to)	167	
Serine/threonine-protein phosphatase PP1-beta catalytic subunit		84

Protein	Main constituent of spot no.	Also identified in spot no.
Transferases		
Glutathione S-transferase Mu 3	168	
Nicotinamide phosphoribosyltransferase		110
Protein-glutamine gamma-glutamyltransferase, subunits E and K	169	
Transketolase	170-171	
Ligases		
Methylcrotonoyl-CoA carboxylase subunit alpha		175
Propionyl-CoA carboxylase beta chain		101
Succinate-CoA ligase, ADP-forming, beta subunit, isoform CRA_d	172	
Serum proteins		
Fibrinogen, beta and gamma chains	173	184
Hemoglobin subunit beta	174	
Serotransferrin and transferrin variant	175-176	
Serum albumin	177-178	
Protein biosynthesis		
Aspartyl-tRNA synthetase		101
Elongation factor 1-alpha and 1-alpha 1		91,156-157,159, 162
Probable glutamyl-tRNA synthetase	179	
Ribonucleoproteins		
60S acidic ribosomal protein P0		96
Heterogeneous nuclear ribonucleoproteins A1, A3 and A2/B1	180-182	100
Poly(RC) binding protein 2		108
DNA-related proteins		
Prohibitin	183	
RuvB-like 2		116
mRNA processing proteins		
Putative pre-mRNA-splicing factor ATP-dependent RNA helicase DHX15		175-176
Spliceosome RNA helicase DDX39B	184	
Others		
14-3-3 proteins, beta/alpha, epislon, eta, gamma, theta and zeta/delta	185-187	54
Alpha-synuclein	188-202	57,61,121,123,205
Arfaptin-2		84
COMM domain-containing protein 3		93
Endoplasmic reticulum aminopeptidase 1		167
Erlin-2		82
Ferritin, heavy and light chains	203-204	
Fructose-bisphosphate aldolase A		114,155
Retinol-binding protein 1	205	
UNC84B protein		184
Voltage-dependent anion-selective channel protein 1	206-209	

5.3.2 Elucidation of core and adherent GCI proteins

To investigate which GCI proteins are present at the core of the inclusions and which are adherent to the surface of GCIs, a carbonate stripping experiment was performed on intact immunomagnetically captured inclusions (from step 11 of the purification procedure). The carbonate extraction solution removed non-covalently bound proteins from the surface of GCIs (adherent protein fraction), with the remaining core of the inclusions washed and then solubilised in protein extraction buffer (core protein fraction). This was performed in parallel with the solubilisation of the entire immunomagnetically capture inclusions, according to the standard purification protocol (control fraction). The yield for each fraction is shown in Table 5.7.

Table 5-7: Protein yields from carbonate stripping experiment

Sample	Yield (µg)[a]	Yield (%)[b]
Total GCI protein (control) [c]	183.0	
Total GCI protein (carbonate stripping) [d]	125.1	100
Core GCI proteins	107.8	86
Adherent GCI proteins	17.3	14

[a] per single tube of brain homogenate
[b] core and adherent protein fractions are compared to the calculated total GCI protein
[c] total GCI protein from the parallel standard purification
[d] the calculated total of the core and adherent protein fractions from the carbonate stripping experiment

As revealed by carbonate stripping, purified GCIs are made up of approximately 86% core proteins and 14% adherent proteins (Table 5.7). However, the stripping process also appears to have caused a loss of approximately 30% of the total protein compared to when the entire GCIs are solubilised.

One-third of the protein in each fraction was reserved for trypsin digestion and mass spectrometry analysis of the digested peptides. There were 158 proteins identified in the core fraction and 115 proteins identified in the adherent fraction. Of these, there were 51 proteins identified in the adherent fraction that were not present in the core fraction (Appendix G), including SNAP25, V-ATPase, TPPP and albumin. 94 proteins were identified in the core fraction that were not present in the adherent fraction (Appendix H), including dynein, calnexin and fascin. 64 proteins were

identified in both fractions (Appendix I), including α-synuclein, α-β-crystallin, 14-3-3 and HSP90, indicating their presence at both the core and periphery of GCIs.

The remaining two-thirds of the protein in each fraction was analysed by 1D SDS-PAGE (Figure 5.7). The lane containing the core protein fraction (Lane 2, Figure 5.7) was cut into 10 equal sized slices, from the top to the bottom of the gel (high molecular weight to low molecular weight). Each of the ten slices were digested with trypsin and the digested peptides analysed by LTQ Orbitrap XL mass spectrometry (as described in sections 5.2.6 and 5.2.7), with two replicate injections of each fraction performed.

A) B)

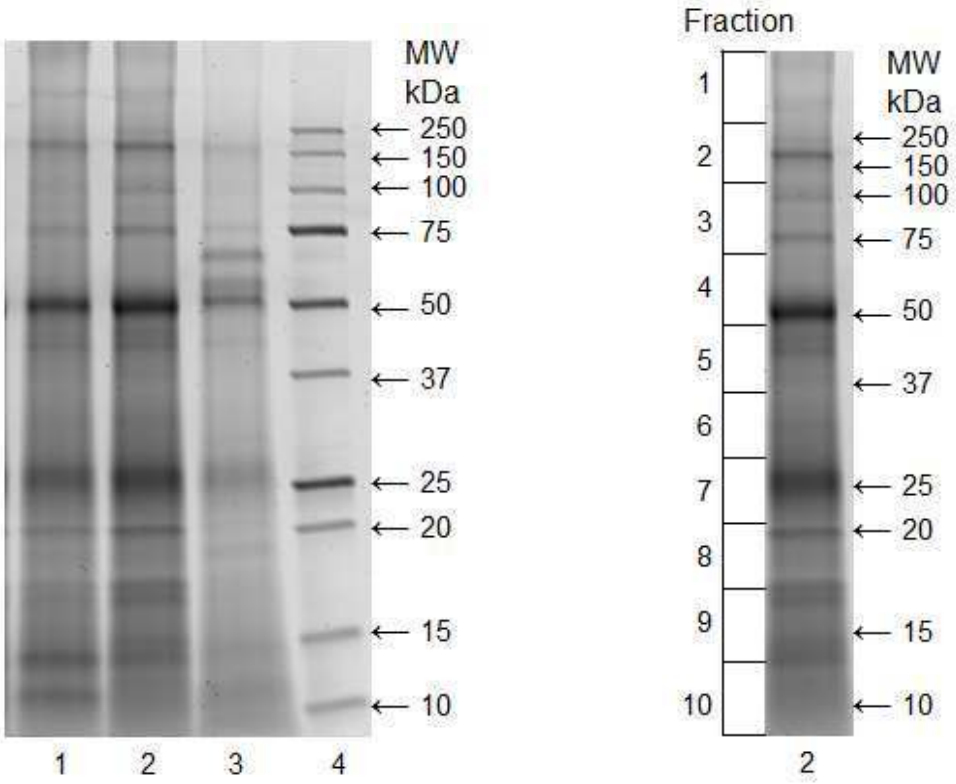

Figure 5-7: 1-DE of total, core and adherent GCI proteins
In (A), the total (Lane 1), core (Lane 2) and adherent (Lane 3) GCI proteins revealed by carbonate stripping (section 5.2.1.3) were separated by SDS-PAGE using a BioRad Mini-Protean TGX Any kD gel, with 5 µL of unstained molecular weight markers (Lane 4). 100% of the adherent fraction (12 µg) was loaded in Lane 3, with 50% of the core fraction (36 µg) loaded in Lane 2 and 25% of the total fraction (31 µg) loaded in Lane 1, to avoid overloading. The gel was stained with SyproRuby, and imaged on a Typhoon 9400 variable mode imager. The gel was subsequently silver stained, and the core GCI proteins (Lane 2) were cut into 10 fractions, as shown in (B). Each fraction was digested with trypsin and analysed by LTQ Orbitrap XL mass spectrometry.

From the ten fractions, 377 identifications of 173 unique proteins were made (excluding cytokeratins, arising from epidermal contamination of the gel). Of the 173 proteins, 97 were exclusive to only one fraction (Appendix J) and 76 were present in two or more fractions (Appendix K) and thus identified multiple times. The number of proteins identified in each fraction is listed in Table 5.8. Four proteins previously established to be in GCIs were identified – α-synuclein, α-β-crystallin, 14-3-3 proteins (6 isoforms), and tubulin (6 isoforms forms). The established synaptic vesicle proteins synaptosomal-associated protein 25 (SNAP25) and vesicle-associated membrane protein 2 (VAMP2) were also identified.

Table 5-8: Number of proteins identified in each 1D fraction of core proteins from purified GCIs

Fraction[a]	Estimated MW (kDa)[b]	No. of proteins identified	No. of exclusive proteins[c]
1	>300	14	1
2	110-300	27	7
3	70-110	38	14
4	48-70	24	6
5	37-48	62	22
6	28-37	53	11
7	12-28	38	8
8	17-22	35	6
9	13-17	26	3
10	<13	60	19
Total		377	97

[a] from top (1) to bottom (10) of gel
[b] the estimated molecular weight range of proteins contained in the gel fraction
[c] the number of proteins identified only in that fraction

Of the 173 proteins identified, 76 were identified from a complex mixture of the same core GCI protein fraction that was subjected to 1-DE. The overlap in identifications between the complex mixtures of the core and adherent fractions and the 1D fractionation of the core fraction is shown in Figure 5.8. 134 of the 173 proteins had previously been identified from either complex mixtures, 1D fractionation or 2D fractionation (section 5.3.1). Thus, 39 new protein identifications were revealed through 1-D fractionation of a carbonate-stripped (core protein) fraction.

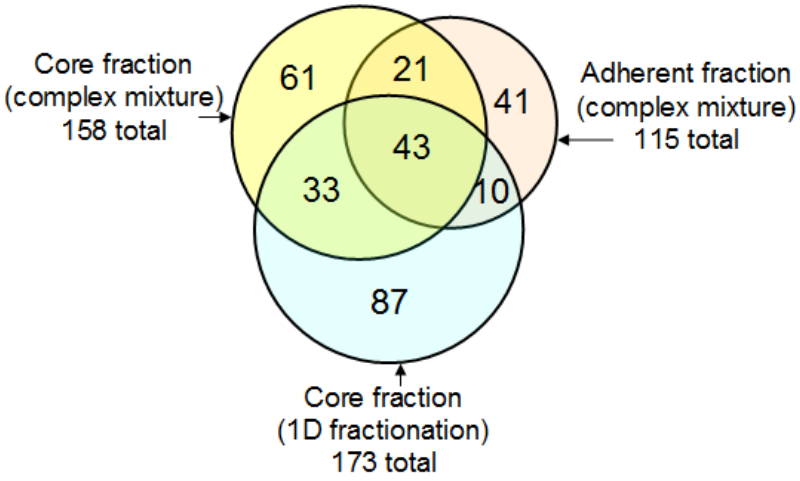

Figure 5-8: Venn diagram of core and adherent GCI protein identifications from complex mixtures and 1D fractionation
The overlap between the protein identifications by LTQ Orbitrap XL mass spectrometry of trypsin digested peptides from a complex mixture of a GCI-adherent fraction, a complex mixture of a core GCI fraction and a 1D fractionated sample of a core GCI fraction.

5.3.3 Control experiments for the GCI purification method

A GCI purification from MSA tissue was split into two equal fractions at the end of step 7. One fraction was processed with primary antibody, to bind inclusions, and the other fraction was processed without primary antibody (secondary-only control), to determine if any non-specific binding to either the secondary antibody or the magnetic beads was occurring. A separate experiment was performed where tissue from two 'normal' cases was processed using the same procedure for purifying GCIs from MSA tissue, to determine what other brain components may bind to the primary anti-α-synuclein antibody. The yields for each of these purifications are shown in Table 5.9 and Figure 5.9.

Table 5-9: Protein yields from purification control experiments

Tissue	1° Ab	2° Ab	Yield (µg)[a]	Yield (%)[b]
MSA – same tissue	+	+	107.4	100
in parallel	-	+	15.5	14
Normal – Case 1	+	+	51.1	48
– Case 2	+	+	34.7	32

[a] per single tube of brain homogenate
[b] secondary only and normal brain controls are compared to the standard GCI purification

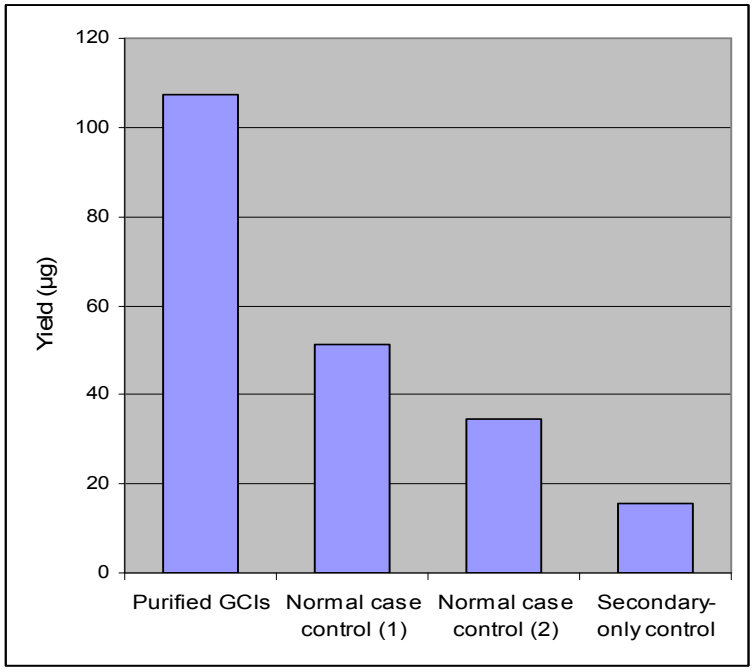

Figure 5-9: Comparison of control experiment yields to GCI purification
Comparison of protein yield (µg) isolated per tube (2 g) of brain homogenate from a standard GCI purification, two normal case controls and a secondary-only control.

Immunohistochemistry was performed on selected fractions from the secondary-only control experiment (Figure 5.10), with the slides imaged using a Nanozoomer Digital Imager and the inclusions analysed as described in Chapter 2.9.2. An average of 6.5 inclusions per field were counted in the immunocaptured fraction from the parallel standard purification versus zero inclusions per field in the immunocaptured fraction from the secondary-only purification.

The normal case controls gave a higher-than-expected yield of approximately 30-50% of the protein obtained from a comparable amount of MSA tissue (Table 5.9). Immunohistochemistry was performed on selected fractions from the normal control experiment (Figure 5.11), revealing α-synuclein positive inclusions in the immunocaptured fractions from both control cases.

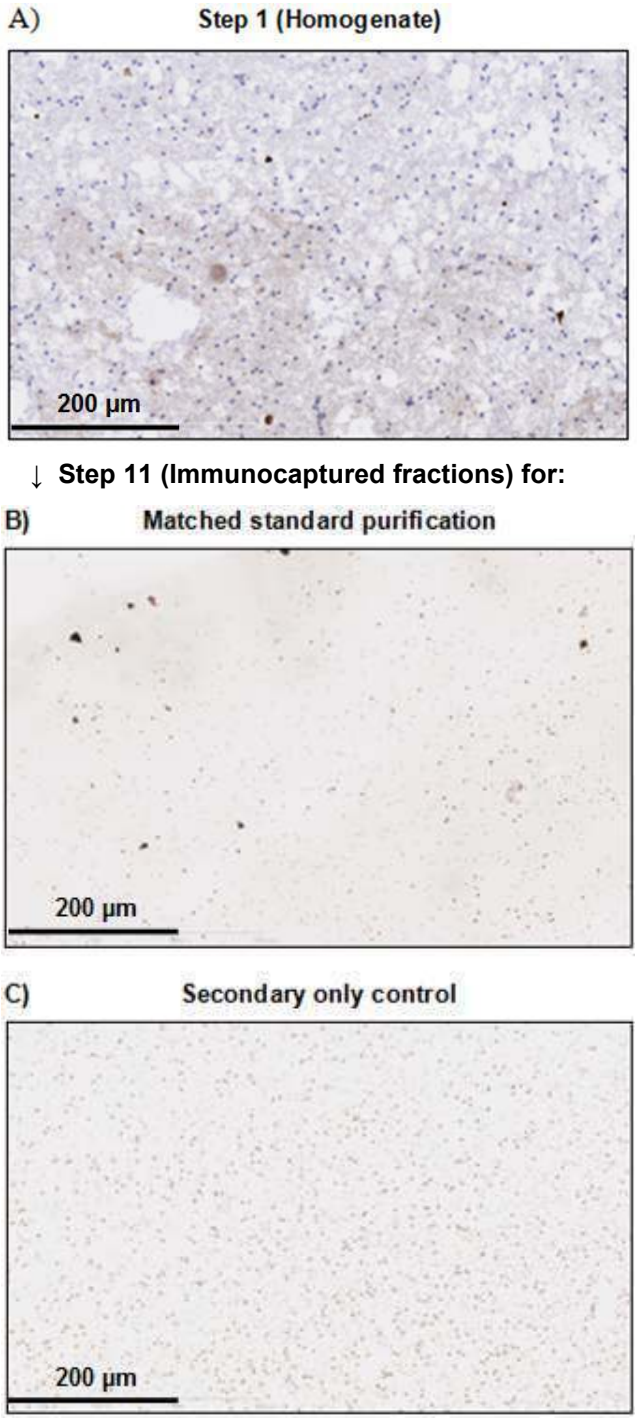

Figure 5-10: Immunohistochemistry from secondary antibody only control purification revealed no inclusions in immunocaptured control fraction
A secondary-only control for the optimised GCI purification method was performed (section 5.2.1.4). Brain homogenate was processed through steps 1-7, then split into two equal fractions for steps 8-12, with one half processed with 60 µg of primary antibody in Step 8 and the other half processed with the primary antibody omitted. A 10 µL smear of the final fractions (B) and (C) and the starting homogenate (A) were DAB stained against α-synuclein (antibody no. 1, Table 2.1) and counterstained with haematoxylin. All images were taken at 20x magnification.

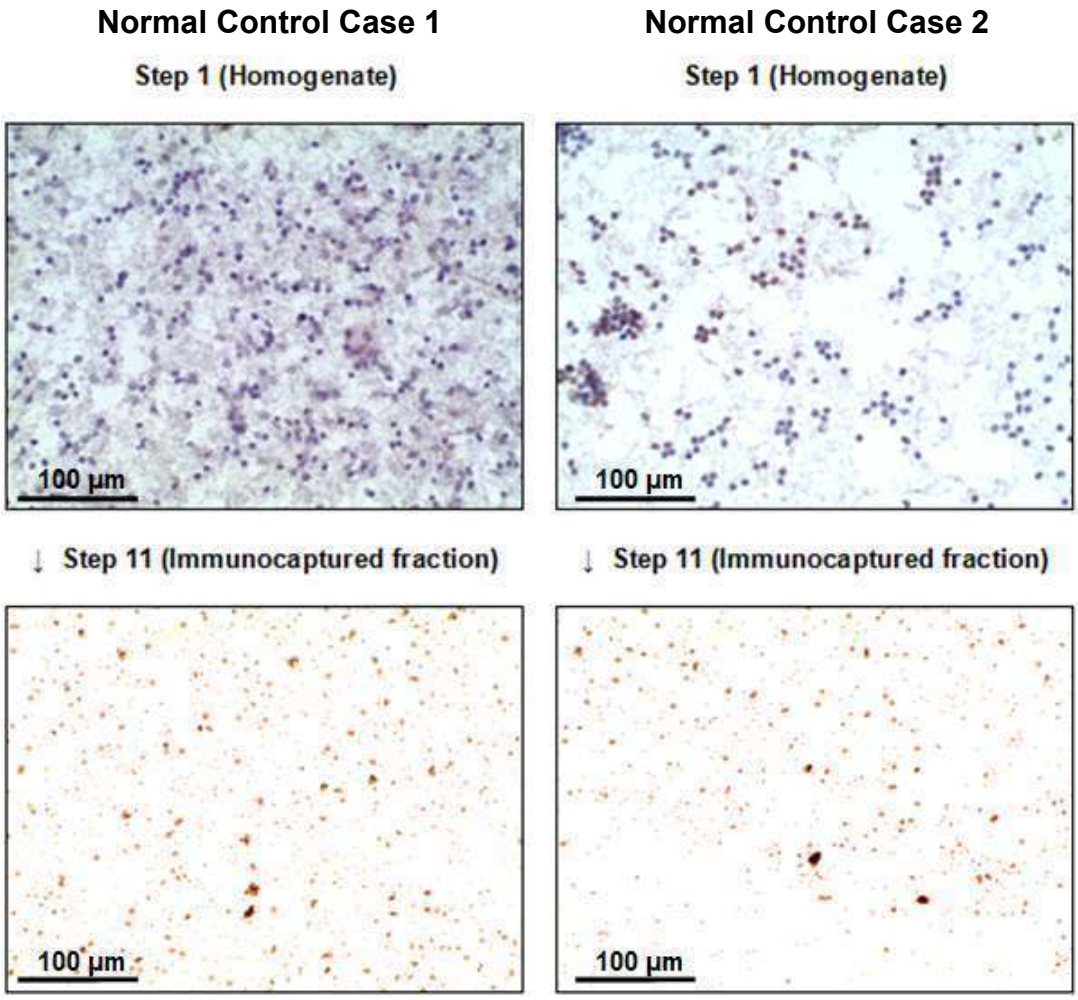

Figure 5-11: Immunohistochemistry from normal control purification revealed the presence of α-synuclein-positive inclusions in the immunocaptured fractions
A normal control purification was performed using the optimised GCI purification method (section 5.2.1.5), from normal control homogenate from cases 1 and 2 (SA0162 and SA0230 respectively, Table 2.3). A 10 µL smear of each fraction was DAB stained against α-synuclein (antibody no. 1, Table 2.1) and counterstained with haematoxylin. All images were taken at 20x magnification.

Two-thirds of the protein obtained for each of the control purifications was subject to 1D SDS-PAGE (Figure 5.12). The 1D protein profile from the inclusions purified from the normal case controls (Lanes 2-3, Figure 5.12) is similar to that of GCIs purified from MSA tissue (Lane 5, Figure 5.12). The secondary only control contains three main bands apparent at 50 kDa, 25 kDa, and 13 kDa (Lane 4, Figure 5.12).

One-third of the protein from both the secondary-only control and the matched immunocaptured fraction was digested with trypsin and analysed by mass spectrometry. There were 113 proteins identified in the secondary-only control fraction and 138 proteins identified in the matched immunocaptured GCI fraction. 74 proteins were identified in both fractions (Appendix L), thus 64 proteins were identified in only the matched immunocaptured GCI fraction (Appendix M) and 39 proteins were identified in only the secondary-only control fraction (Appendix N). In Appendix A, the proteins that were also identified in the secondary-only control have been marked with an *.

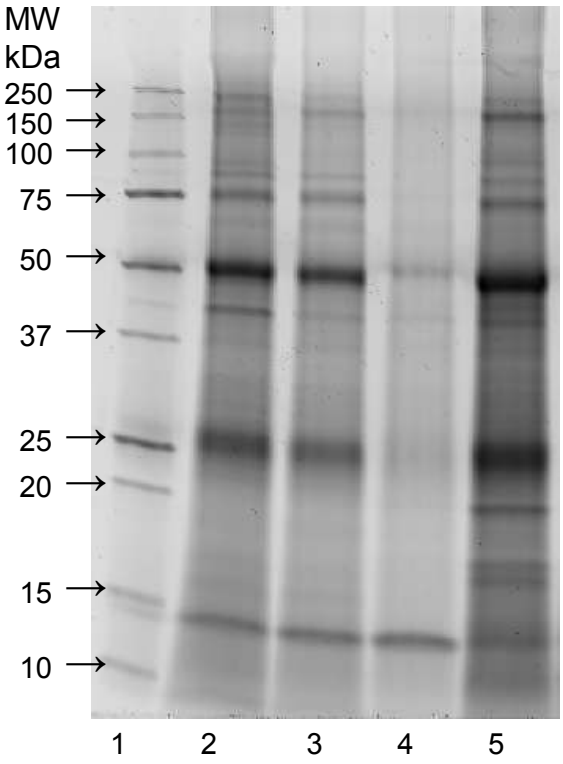

Figure 5-12: 1-DE of normal control cases and secondary antibody only control
The immunomagnetically captured fractions from an inclusion purification of normal case control 1 (Lane 2) and 2 (Lane 3), and the secondary-only control (Lane 4) and matched standard GCI purification (Lane 5), were separated by SDS-PAGE using a BioRad Mini-Protean TGX Any kD gel, with 5 µL of unstained molecular weight markers (Lane 1). Two-thirds of the purified protein was loaded in Lane 2 (34 µg), Lane 3 (23 µg) and Lane 4 (10 µg), with only one-third loaded in Lane 5 (36 µg) to avoid overloading. The gel was stained with SyproRuby, and imaged on a Typhoon 9400 variable mode imager.

5.3.4 2D-DIGE comparison of MSA cases

GCI purifications were performed on tissue from the same brain region of five separate MSA cases, as described in section 5.2.1.1. GCIs were also purified from the second MSA case (MSA 2) on two separate occasions, to demonstrate the reproducible and robust nature of the purification method. The yield of solubilised GCI protein (from Step 12) from each purification is shown in Table 5.10 below.

Table 5-10: Protein yields from multiple MSA case purifications

Sample	Yield (µg)[a]
MSA 1	135
MSA 2 p1[b]	246
MSA 2 p2[b]	185
MSA 3	281
MSA 4	165
MSA 5	138
Average	230

[a] per single tube of brain homogenate
[b] p1 = purification replicate 1, p2 = purification replicate 2

A 2D-DIGE experiment was performed using the purified GCIs from these five cases as described in section 5.2.3, to determine the degree of biological variation between MSA cases and the technical variation in the purification procedure. Quantitative analysis was also performed to assess what proportion of the immunocaptured GCIs consisted of α-synuclein, α-β-crystallin, 14-3-3 proteins and tubulin.

5.3.4.1 Technical variability of purification process

The two purification replicates from the same case were run on a single gel and the gel was analysed in the Direct In-gel Analysis (DIA) module of DeCyder 7.0 (GE Healthcare). The search algorithm was processed with an estimation setting of 1,000 spots, which resulted in the actual detection of 898 spots on the gel. Each gel spot was reviewed manually and 66 spots were excluded as artifacts. The distribution of the 832 genuine protein spots is shown in the histogram generated by the DeCyder software (Figure 5.13).

Of the 832 protein spots, only 5.2% displayed a difference in expression ≥ 1.5-fold, with only 0.6% displaying a difference in expression ≥ 2.0-fold and no differences at 3-fold or above (Table 5.11).

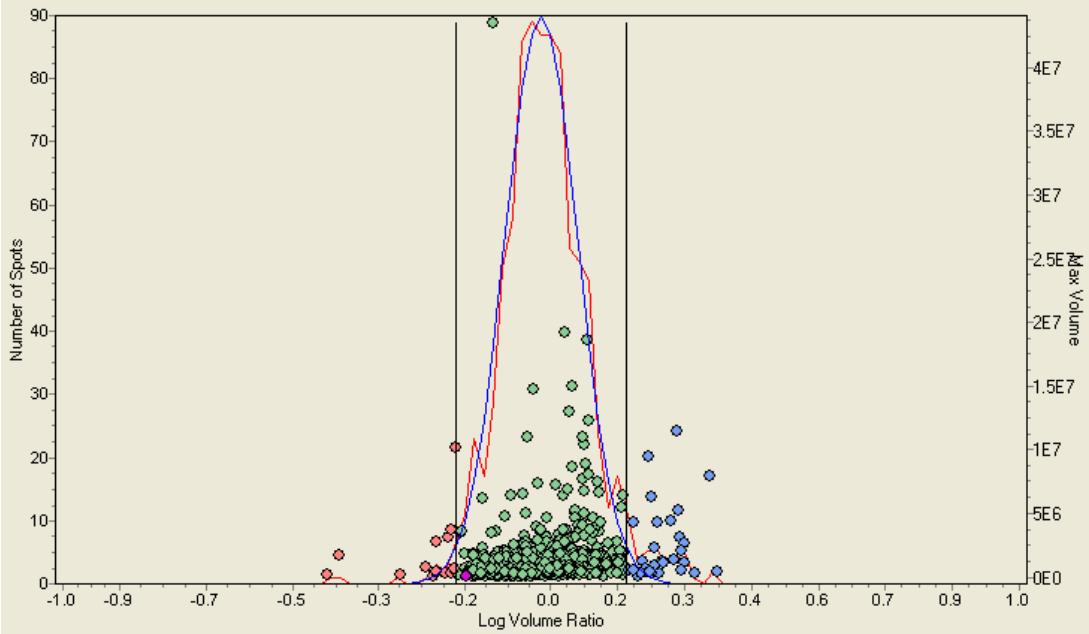

Figure 5-13: Histogram from DIA analysis of GCI purification replicates
The two purification replicates for case MSA 2 were DIGE labelled, separated on a 12.5% gel and analysed in the DIA module of DeCyder 7.0 (GE Healthcare). This histogram shows the distribution of spot volume changes of the 832 protein spots detected. Spots with <1.5-fold difference in volume are shown in green and those with a >1.5-fold increase or decrease in replicate 2 are shown in blue or red, respectively.

Table 5-11: Technical variation in GCI purification as determined by 2D-DIGE

Fold-change	No. of spots			% of spots		
Threshold	Similar	Inc.	Dec.	Similar	Inc.	Dec.
>1.5	789	30	13	94.8	3.6	1.6
>2.0	827	3	2	99.4	0.4	0.2
>3.0	832	0	0	100.0	0.0	0.0

5.3.4.2 Biological variability between MSA cases

The four 2D-DIGE gels, containing the 6 GCI preparations and duplicates of 2 samples which were applied to separate gels (Table 5.2), were analysed in the Biological Variation Analysis (BVA) module of DeCyder 7.0 (GE Healthcare). 938 spots were detected in total, with 409 spots matched across all four gels.

Two samples (MSA2p1 and MSA4) were run in duplicate, on separate gels. While the similarity between technical replicates using the DIGE system is theoretically 100%, due to the normalisation to the internal standard, this can be affected by inaccurate spot matching due to poor gel resolution. To verify that the degree of matching was sufficient, the replicates were compared to each other and gave a similarity of >97% at the 1.5-fold level and >99% at the 2-fold level, with no differences of 3-fold or greater (Table 5.12).

Table 5-12: Technical variation when comparing gel replicates in 2D-DIGE

Comparison	Fold-change threshold	No. of spots			% of spots		
		Similar	Inc.[a]	Dec.[b]	Similar	Inc.[a]	Dec.[b]
MSA2 v MSA2 (502 spots)	>1.5	487	6	9	97.0	1.2	1.8
	>2.0	499	1	2	99.4	0.2	0.4
	>3.0	502	0	0	100.0	0.0	0.0
MSA4 v MSA4 (633 spots)	>1.5	619	4	10	97.8	0.6	1.6
	>2.0	633	0	0	100.0	0.0	0.0
	>3.0	633	0	0	100.0	0.0	0.0

[a] increased
[b] decreased

Each MSA case was compared to the other four cases as a group and the results of these comparisons are presented in Table 5.13. Overall, more than 77% of spots displayed variations in abundance <1.5-fold and greater than 94% with variations <2-fold and more than 99% with variations <3-fold.

Based on spot-matching to a preparative 2D gel used for protein identifications by mass spectrometry (Figure 5.6), the majority of protein spots with a difference in expression >3-fold in MSA1 appear to be a cluster of nine GFAP and tubulin isoforms at ~40 kDa, pI of ~5. Differences in two α-synuclein isoforms and three unidentified high molecular weight proteins were also seen in MSA1. In MSA2, the protein spots with an expression difference >3-fold were a single GFAP isoform in

the same location as the cluster present in MSA1, and three unidentified higher molecular weight proteins. In MSA4, there was a cluster of six GFAP and tubulin isoforms similar to that seen in MSA1 (but with increased expression >3-fold compared to the other cases, whereas in MSA1 the expression was decreased >3-fold) along with five unidentified higher molecular weight proteins. MSA3 and MSA5 had no spots with expression differences greater than 3-fold (data not shown).

Table 5-13: Differences between GCIs purified from multiple MSA cases as determined by 2D-DIGE

Fold-change threshold	Comparison	No. of spots				% of spots		
		Total	Similar	Inc. [a]	Dec. [b]	Similar	Inc. [a]	Dec. [b]
>1.5	Average	789.2	616.2	77.8	95.2	78.1	9.9	12.1
	MSA1 v all	938	654	155	129	69.7	16.5	13.8
	MSA2 v all	777	598	70	109	77.0	9.0	14.0
	MSA3 v all	660	539	38	83	81.7	5.8	12.6
	MSA4 v all	938	709	103	126	75.6	11.0	13.4
	MSA5 v all	633	581	23	29	91.8	3.6	4.6
>2.0	Average	789.2	747.0	21.0	21.2	94.7	2.7	2.7
	MSA1 v all	938	859	48	31	91.6	5.1	3.3
	MSA2 v all	777	734	17	26	94.5	2.2	3.3
	MSA3 v all	660	643	6	11	97.4	0.9	1.7
	MSA4 v all	938	868	32	38	92.5	3.4	4.1
	MSA5 v all	633	631	2	0	99.7	0.3	0.0
>3.0	Average	789.2	783.4	2.2	3.6	99.3	0.3	0.5
	MSA1 v all	938	924	2	12	98.5	0.2	1.3
	MSA2 v all	777	773	0	4	99.5	0.0	0.5
	MSA3 v all	660	660	0	0	100.0	0.0	0.0
	MSA4 v all	938	927	9	2	98.8	1.0	0.2
	MSA5 v all	633	633	0	0	100.0	0.0	0.0

[a] increased
[b] decreased

5.3.4.3 Quantification of proteins of interest

Each gel was analysed in the DIA (Differential In-gel Analysis) module of DeCyder version 7.0 (GE Healthcare). The search algorithm was processed with an estimation setting of 1,000 spots. Protein spots on each gel corresponding to isoforms of α-synuclein, α-β-crystallin, 14-3-3 proteins and tubulin were selected based on spot-matching to preparative 2D gels where protein identifications had been made using mass spectrometry (Figures 3.10 and 5.6). The relative abundance of each protein of interest was determined as described in Chapter 4.2.5. The integrated spot volumes for each isoform of a protein were summed together, then the total volume for each

protein was compared to the total protein volume on the gel to determine what percentage of total protein the protein of interest occupied.

The results for the technical replicates (performed for MSA cases 2 and 4) are shown in Table 5.14 and the results for the biological replicates (MSA cases 1-5) are shown in Table 5.15. GCIs were shown to consist of approximately 12% α-synuclein, 3% α-β-crystallin and 2% 14-3-3 proteins, with less than 2% tubulin. There were minimal variations between the technical replicates, with a wider range of variance between the different MSA cases. The data from this experiment agreed closely with the quantitative analysis performed on a single GCI case in Chapter 4 (Table 4.4), and this data will be compared as a part of a larger analysis in Chapter 6.

Table 5-14: Abundance of proteins of interest in technical replicates of purified GCIs

		% of total protein			
Case	**Rep.[b]**	**α-synuclein**	**α-β-crystallin**	**14-3-3s**	**Tubulin**
MSA 2	1	16.4	4.5	2.3	1.5
	2	17.9	5.2	2.0	1.0
	3	17.4	4.6	2.4	1.7
Mean ± S.D.[a]		**17.2 ± 0.8%**	**4.8 ± 0.4%**	**2.2 ± 0.2%**	**1.4 ± 0.4%**
MSA 4	1	7.0	2.3	1.5	1.2
	2	9.6	2.4	1.7	1.7
Mean ± S.D.[a]		**8.3 ± 1.8%**	**2.4 ± 0.0%**	**1.6 ± 0.1%**	**1.5 ± 0.4%**

[a] S.D. = standard deviation
[b] Replicate number

Table 5-15: Abundance of proteins of interest in biological replicates of purified GCIs

		% of total protein			
Case	**Reps[b]**	**α-synuclein**	**α-β-crystallin**	**14-3-3s**	**Tubulin**
MSA 1	1	14.5	2.9	1.0	1.2
MSA 2	3	17.2	4.8	2.2	1.4
MSA 3	1	9.7	3.1	2.9	1.7
MSA 4	2	8.3	2.4	1.6	1.5
MSA 5	1	9.4	2.5	1.0	1.2
Range		8.3 - 17.2	2.4 - 4.8	1.0 - 2.9	1.2 - 1.7
Mean ± S.D.[a]		**11.8 ± 3.8%**	**3.1 ± 1.0%**	**1.7 ± 0.8%**	**1.4 ± 0.2%**

[a] S.D. = standard deviation
[b] Number of technical replicates analysed, the mean data is shown when n>1

5.4 Discussion

5.4.1 Identification of GCI proteins from complex mixtures

A total of 502 proteins were identified by mass spectrometry from trypsin-digested complex mixtures of solubilised immunocaptured GCIs obtained from five different MSA cases. 164 of these proteins were present in a minimum of 4 out of the 5 MSA cases, which supports the presence of these proteins being common to all GCIs, and thus related to their formation and function. However, the proteins identified in fewer cases may still be common to all GCIs, but at a lower abundance, thus eluding detection in a complex mixture in some of the cases. For each injection, approximately 180 to 220 proteins were identified, but when solubilised GCIs were separated via 2D gel electrophoresis, a well-resolved gel displayed approximately 2,000 spots. While these spots include multiple isoforms of the same proteins (including up to 50-100 isoforms of α-synuclein), it still indicates that there could be up to 1,000 proteins present in GCIs, so the identifications made from complex mixtures represent the most abundant and easily identifiable proteins present in the sample.

Ten previously established GCI proteins, as summarised in a review by Wenning *et al.* (2008) [31] were identified – α-synuclein, α-β-crystallin, 14-3-3 proteins, tubulin, MAP1A, MAP1B, MAP2, TPPP, heat shock 70 kDa protein 12A and carbonic anhydrase 2.

α-synuclein is a 14.5 kDa presynaptic nerve terminal protein [38] that is natively unfolded in solution Its normal function is not well understood, but it is thought to be the most abundant protein present in GCIs [28, 30, 31]. α-β-crystallin belongs to the class of abundant, ubiquitous proteins known as small heat shock proteins [134]. These proteins prevent the aggregation and precipitation of proteins under stressful conditions and they also have anti-apoptotic features and protect and stabilise the cytoskeleton [134]. While α-β-crystallin is commonly known as an eye lens protein, it is also found in the brain [134]. Pountney *et al.* [118] used both immunohistochemistry and proteomics approaches to show that α-β-crystallin is a major component of GCIs. 14-3-3 proteins are a family of ubiquitous adaptor proteins with over 300 reported binding partners [120]. There are seven 14-3-3 isoforms in humans [120].

Tubulin is the cytoskeletal protein that forms microtubules in neurons and oligodendrocytes. Each microtubule is a heterodimer of a form of α-tubulin and β-tubulin [135]. These microtubules are used for intracellular protein trafficking as well as playing other roles in cell growth and function [135]. Microtubule-associated proteins (MAPs) stabilise microtubules in neurons and have a role in the development of neural polarity and outgrowth [136, 137]. The functional role of MAPs in oligodendrocytes has yet to be established, but they are speculated to be involved in the regulation and stabilisation of the dynamic microtubule network in the myelin-containing cellular processes [136, 137]. Tubulin polymerisation promoting protein (TPPP), as its name suggests, has a basic function of promoting the polymerisation of tubulin [138]. It is an unstructured and unfolded protein (as is α-synuclein) [138].

Heat shock 70 kDa protein 12A is from the heat shock protein 70 family, which responds to a variety of cellular stressors, including heat shock, oxidants, hypoxia, heavy metals and glucose deprivation [139]. HSP70s are molecular chaperones that maintain or assist cellular protein folding [139]. Carbonic anhydrase 2 catalyses the conversion of carbon dioxide and water into carbonic acid, which then dissociates into protons and bicarbonate ions [140]. Bicarbonate ions are exchanged for chloride ions in an acidification process [140].

Proteins previously reported to be in GCIs including midkine, DARPP32, dorfin, DJ-1, MAPK, and septin -2, -3, -5, -6 and -9, were not identified in this experiment. Midkine (MK) is a 13 kDa carbohydrate-binding growth factor [141]. It promotes growth, survival, migration and gene expression of its target cells [141]. The dopamine and cAMP-regulated phosphoprotein of 32 kDa (DARP-32) is a neuronal protein that acts as a protein phosphatase inhibitor [142]. Dorfin is an E3 ubiquitin ligase that ubiquitinates superoxide dismutase-1 and synphilin-1 [143]. DJ-1 is a mitochondrial protein of ~20 kDa that acts as a redox-dependent chaperone to protect neurons from oxidative stress [1, 6]. Mitogen-activated protein kinases (MAPKs) are protein Ser/Thr protein kinases that participate in a range of signal transduction pathways that regulate multiple cellular functions [144]. Septin proteins are a family of GTP-binding proteins [145]. They associate with the actin and microtubule cytoskeletal network [145].

5.4.2 Vesicular proteins present in GCIs

A comprehensive set of synaptic vesicle-associated proteins were identified by mass spectrometry. These may be related to how the inclusion proteins are targeted to the GCIs or LBs. Further, many vesicle proteins such as VAMP-2 are low molecular weight, which means they generate few peptides and are easily missed when performing MS analysis of complex mixtures. In the future this could be addressed by using targeted MS to identify specific proteins. The established synaptic vesicle-related proteins that were identified in this study, including synaptosomal-associated protein 25, syntaxin I (two subunits), vesicle-associated membrane protein 2, synaptotagmin I, synaptophysin, rab-3A, v-type proton ATPase (6 subunits), synaptic vesicle glycoprotein 2A and synaptogyrin, are reviewed briefly here.

Synaptosomal-associated protein 25 (SNAP25) is a 25 kDa membrane protein that participates in the regulation of synaptic vesicle exocytosis. It is located on the cytosolic face of the neuronal membrane, attached in the central region of the protein via palmitoylated cysteines, with both the N- and C-terminal ends interacting with syntaxin I to form a three-helix t-SNARE complex [146, 147]. SNAP25 also influences calcium dynamics by negatively modulating neuronal voltage-gated calcium channels [148]. See Figure 5.14 for the primary structures of SNAP25, syntaxin I and VAMP2.

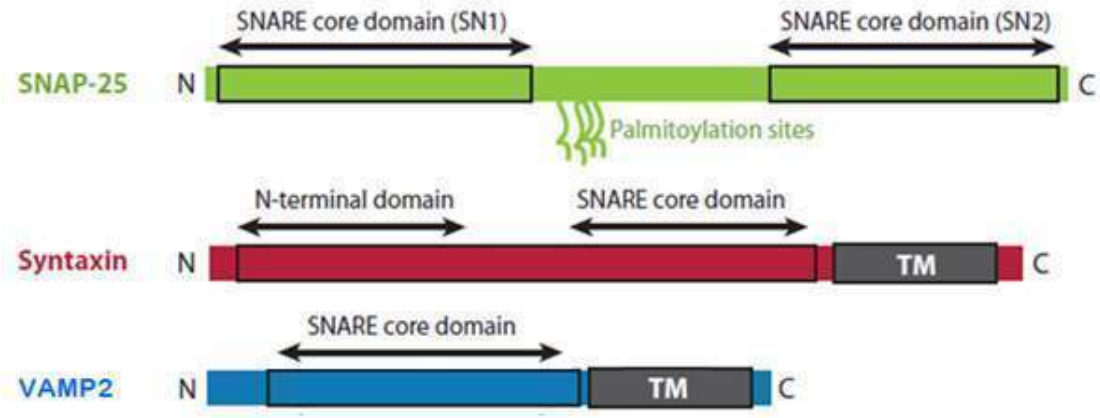

Figure 5-14: Primary structures of SNAP25, syntaxin I and VAMP2
Figure adapted from Brunger *et al.* (2009) [149]. The location of the palmitoylation sites and the two SNARE core domains (SN1 and SN2) of SNAP25 are shown along with the transmembrane (TM) regions and SNARE core domains of syntaxin I and VAMP2.

Syntaxin I is a transmembrane protein bound to the presynaptic membrane of neurons (t-SNARE) [146]. Vesicle-associated membrane protein 2 (VAMP2) is a 13 kDa transmembrane protein in synaptic vesicles (v-SNARE) [146]. SNAP25, syntaxin 1 and VAMP2 (previous known as synaptobrevin 2), assemble together into a SNARE complex [147, 148, 150, 151], which is required for fusing the synaptic vesicle membrane with the presynaptic membrane during exocytosis (see Figure 5.15 for SNARE-complex formation). The formation of the SNARE complex must be tightly regulated during the synaptic vesicle cycle prior to fusion, which is usually achieved through association with other proteins that make them temporarily unavailable for the assembly of the fusion complex [152].

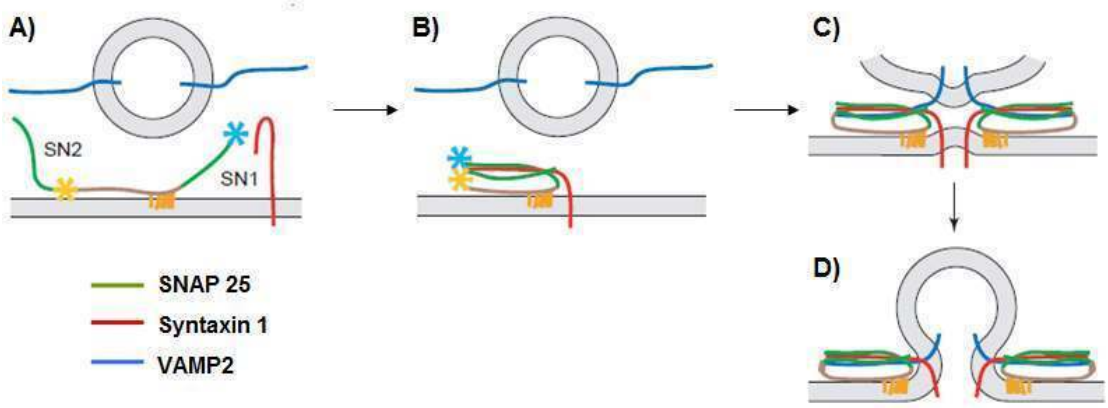

Figure 5-15: Formation of a SNARE complex for membrane fusion
Figure adapted from Sorenson *et al.* (2005) [147]. (A) SNAP25 is attached to the neuronal membrane in the central region via palmitoylated cysteines, leaving the SN1 and SN2 ends of the protein available to interact with syntaxin I (B) to form a three-helix t-SNARE complex. This t-SNARE complex then binds VAMP2 on the vesicle membrane (C), with this four-residue SNARE complex leading to membrane fusion and exocytosis (D).

Synaptotagmin I (syt) is a transmembrane calcium sensor [150] with two Ca^{2+} sensing C2 domains [153]. Syt synchronises and accelerates Ca^{2+} triggered membrane fusion and regulates fusion pore dynamics for the final stages of membrane fusion [153]. Syt interacts with syntaxin I, and it has been proposed that it acts as a "fusion clamp", where an influx of Ca^{2+} causes syt to release syntaxin I to participate in vesicle fusion and exocytosis [153, 154].

Synaptophysin is a transmembrane protein which is required for the calcium-induced exocytotic release of neurotransmitter [152]. Synaptophysin may be a component of

the fusion pore, the structure that joins the two opposing membranes before complete merging [152]. It binds reversibly to VAMP2, preventing the assembly of VAMP2 into a SNARE complex [152]. Thus, the availability and/or stability of VAMP2 may depend on synaptophysin [152].

Rab-3A is from the large family of Rab GTPases that participate with SNAREs in vesicle targeting and membrane fusion [150, 155]. Rab proteins may regulate the interaction of vesicles with the cytoskeleton, and thus their targeting to appropriate destinations, and they may also regulate membrane trafficking at the vesicle docking step [155]. Rab3A is the most abundant rab protein located on synaptic vesicles [155]. Rab3A regulates calcium-induced exocytosis [150, 154]. It associates with Rabphillin-3A and is involved in the pre-docking or docking stages of synaptic vesicle fusion [154], compared to synaptotagmin which is involved in fusion after docking [154].

V-type proton ATPase (V-ATPase) is a multi-molecular nanomotor, which consists of two major ring structures – a peripheral V_1 complex that interacts with ATP and ADP and an integral membrane V_0 complex that mediates the transport of protons [156, 157]. The V_1 complex consists of eight different subunits (A-H) and the V_0 complex has six different subunits (a,c,c',c"d,e) [156, 158]. V-ATPases are ubiquitously present on all intracellular membranes where they have a major role in luminal acidification [157]. The V_1 and V_0 sectors dissociate in the absence of glucose, but re-associate in its presence, thus regulating organelle acidification [157]. V-ATPases acidify the vesicle lumen of synaptic vesicles and this proton gradient is used by specific transporters to fill the vesicles with neurotransmitters [157]. Independent of its role in vesicle acidification, the V-type proton ATPase may also have a direct role in budding and fusion events in vesicle trafficking [158]. It may do this by scaffolding and recruiting small GTPases [158] or by the integral membrane V_0 complex interacting with VAMP2 as a part of forming the fusion pore [157].

Synaptic vesicle glycoprotein 2A (SV2A) is one of a family of three membrane proteoglycans found on the membrane of secretory vesicles in neural cells [159]. While a variety of functions for SV2A have been postulated, its exact function in secretory vesicles and its role in synaptic transmission remains unknown [159]. SV2A binds synaptotagmin I and the binding is calcium-dependent [159].

Synaptogyrin-1 is an integral membrane protein located on synaptic vesicles [160]. It has four membrane-spanning domains and is tyrosine phosphorylated [160]. Its function is not well understood, but it has been suggested to play a role in the regulation of synaptic vesicle exocytosis or membrane trafficking [160].

The presence of these vesicle-related proteins in GCIs may relate to how α-synuclein, a neuronal protein, is trafficked into oligodendrocytes and targeted to GCIs.

5.4.3 Identification of GCI proteins with prior 1-DE fractionation

To address the potential bias of the analysis of trypsin-digested complex mixtures towards both higher abundance and higher molecular weight proteins, a purified GCI sample was fractionated by 1D gel electrophoresis, with ten fractions of descending molecular weight cut from the gel and digested and analysed separately.

The total number of identifications did not increase compared to the complex mixture analysis, with a total of 117 proteins identified from across the ten fractions (excluding cytokeratins, likely to arise from epidermal contamination of the gel). Three proteins previously established to be in GCIs were identified – α-synuclein, 14-3-3 proteins, and tubulin – but the established GCI protein α-β-crystallin was not identified. A single injection of digested peptides from each fraction was analysed, so if there was a technical issue with the one fraction expected to contain α-β-crystallin, such as an incomplete trypsin digestion, this could account for the missed identification. If the trypsin digestion of the fractions in this experiment was sub-optimal, it may also explain the lower-than-expected number of total identifications.

The established synaptic vesicle proteins synaptotagmin 1, VAMP2 and V-ATPase were also identified from the 1-DE fractions. Of the 117 proteins identified, 92 had already been identified from complex mixtures, so 25 new protein identifications were revealed by 1D fractionation. One new protein revealed by the 1D fractionation is vesicle-trafficking protein SEC22b, which is a 24 kDa SNARE protein involved in targeting and fusion in the ER-Golgi complex [161]. Other proteins related to the ER-Golgi complex, including inositol 1,4,5-trisphosphate receptor type 1, coatomer subunit beta and golgi apparatus protein 1, were also revealed.

Cytokeratin proteins were excluded from analysis in this experiment, and from the subsequent 1D and 2D fractionation experiments, as they are likely to arise from epidermal contamination of the gel. A gel is subject to a number of handling steps during the process of fixing, staining and imaging, and the subsequent excision of gel bands or spots for tryptic digestion. Despite precautions, cytokeratins from skin and hair can contaminate the surface of the gel and their presence on the surface enables them to digest more readily than target proteins enmeshed within the gel. Studies of keratin contamination of gels have been published as early as the 1980s [162] and the sensitivity of mass spectrometry analysis now makes the detection of cytokeratins in gel samples more likely. The identification of a particular cytokeratin across multiple samples within an experiment makes it more likely that the cytokeratin is a contaminant [163].

The trypsin-digested complex mixtures, which have reduced handling compared to gel slices or spots, displayed significantly lower keratin levels. Six keratin isoforms were identified across the ten complex mixture samples, with keratin appearing as the 22nd-highest scoring protein identification on average. By contrast, 16 keratin isoforms were identified across the ten 1D gel fractions, with keratin appearing as the 2nd-highest scoring protein identification on average.

5.4.4 Identification of GCI proteins with prior 2-DE fractionation

A wide range of proteins across a variety of functional groups were identified with 2-DE separation and mass spectrometry. While no established synaptic vesicle proteins were identified from the analysed spots, several proteins with a protein trafficking function were identified, including: alpha- and beta-soluble NSF attachment proteins; sorting nexin-30; transmembrane emp24 domain-containing proteins 2 and 10; and vesicle-fusing ATPase. Low molecular weight synaptic vesicle proteins are easily missed with 2-DE, as there are fewer peptides present in low molecular weight proteins and greater losses during washing and handling steps. Also, many vesicle proteins have transmembrane regions, thus their hydrophobic nature may cause them to separate poorly via 2D-E and thus for their identification to be missed on a 2D gel.

Soluble N-ethylmaleimide sensitive factor (NSF) attachment proteins (SNAPs) are required for vesicle transport between ER and Golgi complexes [164]. SNAPs are peripheral membrane protein adaptors that bind NSF to the Golgi membranes [164]. There are three SNAPs in humans – α, β and γ [164], of which α and β were identified in this experiment. α -SNAP binds weakly to the syntaxin/SNAP-25 heterodimer and when this complex binds to VAMP2 a third binding site for α -SNAP is made available, which dramatically enhances its binding [164].

Sorting nexin-30 is from a family of sorting nexin proteins that all contain a phox-homology (PX) domain [165]. It is predominantly localised in the endosomal system and is thought to be important in endocytic and endosomal membrane sorting processes [165]. Transmembrane emp24 domain-containing proteins, also known as p24 proteins, act as cargo receptors for the specific incorporation of secretory cargo molecules into vesicles for transport [166]. They are localised to the ER-Golgi complex and are involved in COPI vesicle formation [166]. Vesicle-fusing ATPase is involved in the fusion of membrane vesicles with target membranes in the ER-Golgi system [167].

The presence of serum proteins, such as albumin and serotransferrin, may be explained by the presence of the primary antibody used in the affinity purification in the solubilised preparation. Despite the antibody being affinity purified prior to use, it is still likely to have a small amount of high abundance serum proteins present.

There were a variety of truncated forms of tubulin identified on the 2D gel in addition to the two spots of full-length α-tubulin and β-tubulin. As previously discussed, the limited tryptic digestion step in the inclusion purification is likely to leave fragments of tubulin attached to the surface of the inclusions while removing the majority of the attached cytoskeletal contamination. The myriad of truncated forms of tubulin present on the 2D gel are likely to be the result of this digestion. To remove a greater amount of tubulin fragments with more aggressive digestion conditions would have compromised the integrity of the peripheral inclusion proteins.

While large amounts of aggregated higher molecular weight forms of α-synuclein were previously revealed by Western Blotting, nearly all the α-synuclein on the 2D

gel was identified in monomeric and truncated isoforms. This may be explained by the different sample buffers used in the sample preparation. The combined presence of urea, thiourea and CHAPS in the 2D gel sample could denature and disaggregate α-synuclein more than the SDS present in the 1D gel sample, thus the aggregates that are unable to be separated in 1-DE are able to be returned to their monomeric state when using 2-DE. This makes the visualisation of individual isoforms of α-synuclein possible using 2D separation, and the analysis of the post-translational modifications present on each of these isoforms is possible in the future.

5.4.5 Elucidation of core and adherent GCI proteins

During the tryptic digestion step in the purification process, designed to remove cytoskeletal contamination, there is the possibility that trypsin may remove or truncate some of the proteins present on the surface of GCIs. Conversely, there is the possibility that there may be proteins adherent to the surface of the GCIs that are not an integral part of the GCI structure. The carbonate stripping experiment was designed to remove any non-covalently bound peripheral proteins from the GCIs, so that these could be identified separately from the core proteins.

The stripping experiment was performed in parallel with a total GCI solubilisation, but the total protein yield of the core and adherent fractions together from the carbonate stripping experiment together was approximately 30% less than the total solubilised GCI protein obtained in the parallel experiment. This difference may be explained by a technical error in splitting the fraction evenly prior to beginning the carbonate stripping, or more likely, the stripping and subsequent wash step caused a loss of protein through residual protein losses with each additional handling step.

When the trypsin-digested soluble core and adherent fractions were analysed by mass spectrometry, the established GCI proteins α-synuclein, α-β-crystallin, 14-3-3 and MAP1B were identified in both the adherent and core fractions. The established GCI protein TPPP was found in only the adherent fraction, as were the established synaptic vesicle proteins SNAP25 and V-ATPase. When the core fraction was separated by 1-D gel electrophoresis prior to analysis by mass spectrometry, the established GCI proteins α-synuclein, α-β-crystallin, 14-3-3 were again identified, as were the established synaptic vesicle proteins SNAP25 and VAMP2.

When peptides in a complex mixture are identified by mass spectrometry, the most abundant and easily ionisable peptides are favoured, which makes it difficult to determine which proteins are definitively present at the core or periphery of GCIs, as the absence of an identification does not necessarily denote the absence of the protein. For example, SNAP25 was only detected in the adherent sample and not the core sample when the complex mixtures were analysed, but when the core sample was fractionated by 1-DE prior to analysis, SNAP25 was detected in one of the fractions. 1D gel fractionation reduces the number of peptides that the instrument has to sequence in a single sample, so it is more able to sequence lower abundance peptides which do not ionise as efficiently.

5.4.6 Normal case controls

The immunohistochemistry of the immunocaptured fractions from the normal case controls revealed α-synuclein positive inclusions. The presence of these inclusions in 'normal' aged brains explains the reason behind the higher-than-expected protein yield from the normal case controls. Instead of revealing what non-inclusion proteins are pulled out by the primary antibody, the normal cases have also revealed α-synuclein-positive inclusions. This leads to the question of whether an aged brain, even when not diagnosed with a particular pathology, is really "normal".

There is evidence in the literature that brains from individuals without clinical evidence of neurodegenerative disease can contain α-synuclein-positive inclusions. Fujishiro *et al.* [168] screened the brains of 241 individuals with no clinical evidence of neurological disease and found LBs in 36 cases (15%) and GCIs in one case (0.4%). In a separate series of 125 individuals without neurological disease, GCIs were found in one case (0.8%) (LBs were not assessed) [168]. In another study of 290 cases of progressive supranuclear palsy (PSP), LBs were detected in 31 cases (11%) and GCIs in one case (0.3%) [169]. Another study, looking for the presence of GCIs, detected five cases out of 1,800 brains (0.3%) [170]. Gibb *et al.* [171] examined 273 brains from patients without Parkinson's Disease and found that the presence of LBs increased with age, with LBs present in 3.8% of cases aged 50-59, 4.7% of cases aged 60-69, 9.3% of cases aged 70-79 and 12.8% of cases aged 80-89. Parkkinen *et al.* [172] discovered LBs in 14% of elderly subjects and Adler *et al.* [173] discovered LBs in 20%. Together, these studies suggest an incidence of 0.3-

0.8% and 10-20% for GCIs and LBs respectively in neuropathologically 'normal' cases.

Where LB pathology is present in individuals without symptoms of Parkinsonism, it is known as Incidental Lewy Body Disease (ILBD) [174]. ILBD has typically been regarded as a 'pre-disease' stage in the lead up to PD onset [174], but some evidence such as the typically later age of onset [175] points to ILBD being a related but distinct phenomena [174]. Thus, it is likely that the 'normal' controls in this study suffered from ILBD.

If the protein obtained from the normal cases in this experiment was simply non-specific binding, the quantity of protein obtained should be directly proportionate to the amount of antibody added. However, one normal case gave a higher yield of protein than the other, despite both being purified from the same amount of crude homogenate with the same quantity of antibody. Thus the unequal amounts of protein obtained from each 'normal' case lends support to the conclusion that α-synuclein positive inclusions are being captured from the 'normal' cases, with the number of inclusions in each case being proportional to the yield of protein.

5.4.7 Secondary antibody-only control

The immunohistochemistry did not reveal any captured inclusions in the secondary-only control, so it was expected that any proteins obtained from this preparation would be artifacts of the purification process rather than genuine inclusion proteins. However, a surprisingly large number of proteins, including known GCI proteins such as α-synuclein, were revealed by mass spectrometry. For this reason, the list of proteins identified cannot be used in a direct subtractive manner from GCI protein identifications without quantification – i.e. it cannot be concluded that α-synuclein is not a genuine inclusion protein because it was identified in the secondary-only control.

There are numerous explanations for the comprehensive list of protein identifications in the secondary-only control. The magnetic Dynal beads used in the immunocapture process are streptavidin-coated, to allow them to bind with high affinity to the biotinylated secondary antibody. Therefore, it is possible that the magnetic beads bound directly to biotinylated proteins in the sample. In this

instance, the majority of proteins identified would be expected to have a biotin modification. This hypothesis was tested by searching the identified peptides specifically for biotinylation modifications, of which very few were revealed (data not shown), making this hypothesis unlikely.

However, it is still possible that an inclusion containing a single biotinylated protein on the surface could bind directly to a streptavidin-coated magnetic bead. While no inclusions were observed in the fields examined from the small sample used for immunohistochemistry, it is still possible that a very small number of inclusions were present throughout the entire sample. If a directly-bound inclusion was digested in the sample used for mass spectrometry, the sensitivity of the instrument makes the detection of GCI proteins possible.

Another explanation is the non-specific binding of proteins to the beads due to incomplete bead blocking, or more likely, the binding of proteins to the BSA (blocking buffer) coating on the beads. Due to continuing improvements in the sensitivity and resolution of mass spectrometers, increasing amounts of contaminant proteins are identified in experiments such as these due to non-specific binding [176]. The term 'bead proteome' has been coined to describe the set of proteins that bind non-specifically to a particular affinity matrix, such as magnetic beads [176].

The amount of protein obtained in this control, 15 μg, is a small fraction of the 100-200 μg of protein obtained from comparable preparations with the primary antibody included. When this fraction was separated by 1D electrophoresis, three main bands were apparent at 50 kDa, 25 kDa and 13 kDa (Lane 4, Figure 5.12). These are likely to represent heavy chain IgG, light chain IgG and streptavidin monomer, respectively, arising from the streptavidin coating on the magnetic beads and the attached biotinylated secondary antibody.

To eliminate this small background of potentially non-inclusion proteins, a future modification to the inclusion purification method could be trialled, to include a pH 2.5 step to elute the inclusions from the magnetic beads by disrupting the antibody-antigen binding, followed by removal of the beads (and any proteins directly attached to them) with a magnet. The remaining inclusions could then be pelleted and solubilised after the beads are removed, compared to the current protocol where the

beads are still present at the time of protein solubilisation. Direct solubilisation was used to minimise protein loss, so a low pH elution would be less efficient but may give a higher purity. Quantitative mass spectrometry techniques can also be developed to create a 'bead proteome' list that can then be used to filter out non-specific proteins from the list of identified proteins in a sample [176].

5.4.8 2D-DIGE comparison of multiple MSA cases

GCIs were purified from five separate MSA cases to compare the biological variation in GCI protein profiles. To determine that the variation seen was due to biological variability rather than variability in the purification technique, an experiment was performed where GCIs were purified from the same MSA case on two separate occasions. When the two samples were compared, the protein expression levels displayed 95% similarity at the 1.5-fold level, demonstrating the reproducible and robust nature of the technique. The majority of the protein spots that did display expression differences appeared to α-synuclein isoforms.

Two of the samples to be compared were run in duplicate on different gels as a part of the experimental design. The spot matching between these duplicates was assessed, and as there was >97% similarity between the duplicates for both samples, the spot matching of the gel set was deemed to be sufficient for analysis.

On average, 78% of spots displayed variations in abundance less than 1.5-fold, with nearly 95% of spots displaying variations less than 2.0-fold, and over 99% less than 3.0-fold. So while approximately 22% of various proteins and isoforms display smaller differences (between 1.5-fold and 3-fold), less than 1% of protein spots on average reveal major differences between cases (>3-fold), and the majority of these spots appear to be truncated forms of GFAP and tubulin, which are both cytoskeletal components. The limited tryptic digestion step in the purification was implemented to reduce the amount of cytoskeletal contamination surrounding the purified GCIs. The variable amount of truncated cytoskeletal protein isoforms between cases may not be a biological difference in the protein content of GCIs themselves, but may instead reflect a difference between cases in the efficiency of reducing the surrounding cytoskeletal contamination.

While this pilot study provides an indication as to the biological variation in GCIs between MSA cases, a larger number of replicates are needed so that statistical analysis can be performed. This was outside the scope of this study due to limitations in available MSA brain tissue and time and cost restraints.

5.5 Conclusion

580 protein identifications were made by mass spectrometry through a combination of complex mixtures, 1D fractionation and 2D fractionation of solubilised purified GCIs. These identifications included 97 synaptic vesicle-related proteins, indicating that proteins may be targeted to GCIs via a vesicle trafficking mechanism. SNAP25 and VATPase were both identified in at least four of the MSA cases analysed. A carbonate stripping experiment was performed to determine which proteins are located at the core of GCIs or adherent to the periphery. The SNARE complex proteins SNAP25 and VAMP2 were both identified in the core protein fraction when 1D fractionation was used prior to mass spectrometry analysis.

The normal case controls revealed the presence of α-synuclein positive inclusions, which restricted the ability to assess any non-specific binding to the anti-α-synuclein antibody. The secondary antibody-only control revealed a comprehensive list of protein identifications, including known GCI proteins such as α-synuclein. This is likely to arise from either the non-specific binding of an inclusion directly to the magnetic beads or the direct binding of proteins to the BSA coating on the magnetic beads. The amount of 'background' protein obtained in this manner is only 8-15% of the protein obtained from equivalent GCI purification preparations.

There was minimal technical variation between GCI purifications, with 95% of protein spots displaying less than 1.5-fold variation between repeat purifications from the same MSA case. There were also minimum biological differences between GCI protein profiles from different MSA cases, with an average of 95% of protein spots displaying less than 2.0-fold variation between cases. The GCIs from the five different MSA cases analysed consisted of an average of 12% α-synuclein, 3% α-β-crystallin and 2% 14-3-3 proteins, with less than 2% tubulin.

The next step is to adapt the optimised GCI purification method to the purification of Lewy Bodies from DLB tissue. By comparing LB proteins to GCI proteins, a set of common inclusion proteins can be identified. The identification of these proteins may elucidate their role in the inclusion formation process.

6 Identification of Lewy Body proteins

6.1 Introduction

In Chapter 3, a published protocol [113] for the purification of Glial Cytoplasmic Inclusions from MSA brain tissue was optimised to dramatically increase yield and purity. This purification method utilises affinity capture with an α-synuclein-specific antibody, the most abundant protein in GCIs [177, 178]. As α-synuclein has also been shown to be a major component of Lewy Bodies [179], the newly optimised protocol can be adapted to purify Lewy Bodies from DLB brain tissue. The published method for GCI purification [113] was previously adapted by Jensen *et al.* [114] for the purification of LBs, with a resulting yield of 10-13 µg of protein per tube of homogenate (2g brain tissue) [114].

Lewy bodies are approximately $1/5^{th}$ to $1/3^{rd}$ as abundant as GCIs, as determined by IHC examination of fixed tissue sections, depending on the brain region involved and the severity of the disease (Wei-Ping Gai, personal communication, April 29, 2011). By adapting the immunocapture steps of the optimised method with a 1:3 ratio (relative to the amount of brain homogenate), Lewy Body purification and characterisation can be performed. The LB proteome can then be determined by mass spectrometry analysis of solubilised inclusions via direction injection as performed for GCIs in Chapter 5.3.1.1. The protein profiles of purified LBs and purified GCIs can be compared to determine the similarity between the inclusion types and to quantify and compare the relative abundance of major inclusion proteins between GCIs and LBs.

6.1.1 Aims

The aims of these experiments were:

- To apply the optimised GCI purification protocol to DLB tissue to purify Lewy Bodies and to characterise the purity by Western blotting and immunohistochemistry.
- To identify LB proteins by mass spectrometry of trypsin-digested complex mixtures of solubilised immunocaptured LBs.

- To compare the protein composition of immunocaptured LBs to GCIs and a normal control using 2D-DIGE and to compare the relative quantities of proteins of interest, including α-synuclein.

6.2 Materials and Methods

6.2.1 Adaptation of optimised GCI purification method to the purification of Lewy Bodies from DLB brain tissue

Brain tissue homogenisation of two DLB cases was performed as described in Chapter 2.4. Cases SA0113 and SA0166 were used, hereafter referred to as DLB cases 1 and 2, respectively (see Table 2.3 for case details). A Lewy Body inclusion purification was performed on two tubes of homogenate from each DLB case as described for Glial Cytoplasmic Inclusions (Chapter 2.5), with each case processed separately. The steps 1 to 7 were the same as for Glial Cytoplasmic Inclusion purification, as the amounts of reagents were optimised relative to the amount of starting homogenate. The steps 8 to 12, for which the key reagents are relative to the approximate number of inclusions, were modified with a 1:3 ratio of primary antibody, secondary antibody, MyOne beads, M-280 beads, and protein extraction buffer, as outlined in Table 6.1 below.

Table 6-1: Adaptation of optimised GCI purification procedure to LBs

Step	Reagent	GCI purification[a]	LB purification[a]
8	Primary antibody	60 µg	20 µg
9	Secondary antibody	30 µg	10 µg
10	Dynal MyOne beads	20 µL	6.67 µL
10	Dynal M-280 beads	30 µL	10 µL
12	Protein extraction buffer	200 µL	67 µL

[a] amount used per tube of homogenate

6.2.2 Inclusion purification for mass spectrometry and 2D-DIGE

Brain tissue homogenisation of the DLB and normal control cases outlined in Table 6.2 was performed as described in Chapter 2.4 (see Table 2.3 for case details). LB purifications were performed on DLB tissue using a yield-adapted method of the GCI purification protocol, as described in section 6.2.1. A control purification was performed on 'normal' tissue using the same yield-adapted method, as the number of inclusions contained in a normal case is expected to be equivalent to or less than the

number of LBs in a DLB case. The number of tubes of homogenate processed for each case is listed in Table 6.2. Each case was processed separately.

Table 6-2: Post-mortem brain tissue used for inclusion purifications for 2D-DIGE

Case No.[a]	Pathology	Brain Region	Sample Name[b]	No. of tubes[c]
SA0113	DLB	Brainstem	DLB 1	3
SA0166	DLB	Brainstem	DLB 2	3
SA0230	Normal	Cerebellum	Normal 2	6

[a] SA Brain Bank case number
[b] Sample name used in this thesis to avoid confusion between different pathologies when quoting case numbers
[c] Number of tubes of homogenate used for inclusion purification

6.2.3 Immunofluorescence

Immunofluorescence was performed on selected fractions from the LB purification procedure as described in Chapter 2.10.1. Dual staining was performed using a sheep anti-α-synuclein primary antibody (antibody no. 1, Table 2.1) used at 1:1000 (1 µg/mL) and mouse anti-β-tubulin primary antibody (antibody no. 3, Table 2.1) used at 1:1000 (0.5 µg/mL). Anti-sheep Cy-3 conjugated secondary (antibody no. 19, Table 2.2) and anti-mouse Alexa488 conjugated secondary (antibody no. 21, Table 2.2) were both used at 1:200 (3.75 µg/mL and 5 µg/mL, respectively). Nuclei were stained with DAPI in the mounting media. Samples were viewed and photographed on an Olympus BX50 Fluorescence microscope and channels were merged in Adobe Photoshop v. CS5, as described in Chapter 2.10.3

6.2.4 DAB immunohistochemistry

DAB immunohistochemistry was performed on selected fractions from the LB purification procedure as described in Chapter 2.9.1. All staining was performed using a sheep anti-α-synuclein primary antibody (antibody no. 1, Table 2.1) used at 1:1000 (1 µg/mL) and an anti-sheep biotinylated secondary (antibody no. 10, Table 2.2) used at 1:500 (2.6 µg/mL).

6.2.5 1-DE and Western blotting

1-DE and Western blotting was performed on selected fractions from the LB purification procedure, as described in Chapter 2.7. Prior to 1-DE, each fraction was solubilised in 1x 1D sample buffer without bromophenol blue, vortexed and heated at

95°C for 5 minutes. The immunocaptured fraction was purified with a BioRad ReadyPrep 2D Clean-Up kit prior to solubilisation in 1x sample buffer. The samples were vortexed again, spun at 18,000x g and the supernatants collected. The protein concentration of each fraction was determined and samples were diluted to 1 µg/µL in 1x 1D sample buffer with bromophenol blue and subjected to 1-DE using BioRad Mini-Protean TGX Any kD gels as described in Chapter 2.7.1.

The gels were transferred to PVDF membrane and Western blotting was performed using the SNAP ID system as described in Chapter 2.7.2. The primary antibodies were rabbit anti-α-synuclein (antibody no. 2, Table 2.1) at 1:450 (2.2 µg/mL) and mouse anti-BIII tubulin (antibody no. 3, Table 2.1) at 1:300 (1.67 µg/mL). HRP-conjugated secondary antibodies against rabbit and mouse (antibodies no. 11 and no. 12 respectively, Table 2.2) were used at 1:1500 (0.27 µg/mL).

1-DE and Western blotting was also performed on homogenate from an MSA case (SA0101), DLB case (SA0113) and a normal case (SA0230) alongside the immunocaptured fractions from each of these cases as described in Chapter 5.2.1.1 (MSA) and section 6.2.2 (DLB and normal). The 1-DE and Western blotting was performed as described above for the DLB purification samples. The blots were imaged on a Fujifilm LAS-4000 CCD imager (Tokyo, Japan) and analysed using Carestream Molecular Imaging Software Version 5.0.6.20. For quantitation, rectangular boxes of uniform size were draw around the band or region of interest (ROI) in each lane for comparison. Background subtraction was performed using the median of each ROIs perimeter for Figure 6.3, and from the median of a ROI selected from a blank region of the blot for Figure 6.10.

6.2.6 2D DIGE

DIGE labelling and 2D gel electrophoresis was performed as described in Chapter 2.8. The purification of the DLB and normal samples used in this experiment are described in section 6.2.2 and the purification of the MSA samples are described in Chapter 5.2.1.1. The solubilised inclusions from these cases were purified with a ReadyPrep 2D Clean-Up Kit (Biorad) as described in Chapter 2.6.2 and resolubilised in DIGE labeling buffer at pH 8.5. 34 µg of each inclusion preparation was labeled with 400 pmoles of CyDye as described in Chapter 2.8.1. The experimental design is

outlined in Table 6.3. The pooled internal standard was 34 µg of a protein pool consisting of 17 µg of each of the samples used in this experiment. The pooled internal standard contained protein from other cases, as this experiment was designed as a six-gel experiment but the 2nd dimension focusing was unsuccessful on 3 gels.

Table 6-3: DIGE experimental design for LB and GCI comparison

Gel	Cy2 Standard	Cy3	Cy5
1	Pooled Internal Standard	MSA 1	DLB 1
2	Pooled Internal Standard	DLB 2	MSA 5
3	Pooled Internal Standard	Normal 2	MSA 2

The labelled protein extracts were combined for their respective gels and subjected to isoelectric focusing for 52 000 Vhr using 24 cm pH 3-11NL Immobiline DryStrips (GE Healthcare), as described in Chapter 2.8.2. The 2nd dimension was performed as described in Chapter 2.8.3, but with 12.5% linear gels. Gel imaging was performed on a Typhoon 9400 variable mode imager as described in Chapter 2.8.4. The photo-multiplier tube values for the green (532 nm), red (633 nm) and blue (488 nm) channels were set at 550 V, 550 V and 630 V respectively for gels 1 and 2, and 550 V, 520 V and 630 V respectively for gel 3. The gels were analysed in DeCyder version 7.0 (GE Healthcare).

6.2.7 Correlation analysis of relative protein abundance

From the 2D-DIGE quantification, the relative abundance values of each pair of proteins analysed were plotted against each other and a linear regression analysis performed using Microsoft Office Excel 2003 (Microsoft, Redmond, WA, USA). The Pearson correlation coefficient (*r* value) and R^2 value were also calculated using Excel 2003 to determine the strength of the relationship for each protein pair. The statistical significance of each correlation was determined using the correlation value (*r*) and the sample size with the p-value calculator for correlation coefficients from Statistics Calculators version 3 (Dr Daniel Soper, Fullerton, CA, USA, http://www.danielsoper.com/statcalc3/calc.aspx?id=44).

6.2.8 Tryptic digestion and mass spectrometry

20 µg of solubilised purified LBs from DLB cases 1 and 2 (section 6.2.2) were buffer-exchanged into 50 mM ammonium bicarbonate as described in Chapter 2.11.1

and an in-solution tryptic digestion was performed as described in Chapter 2.11.2. The digested peptides were analysed with a Thermo LTQ Orbitrap XL mass spectrometer as described in Chapter 2.12.1 and spectra interrogated with Protein Discoverer 1.2 as described in Chapter 2.12.2.

6.3 Results

6.3.1 Application of optimised GCI purification method to Lewy Body purification

Lewy Bodies were highly enriched from DLB tissue using a yield-adapted version of the optimised purification method for GCIs (section 6.2.1.1). Immunofluorescent staining of the purification fractions showed the presence of inclusions, tubulin and nuclei together in the homogenate and pellet fractions in Steps 1 and 3, with increased clumping of nuclei in the Percoll-enriched fraction in Step 5. The elimination of nuclei is shown in step 6, the diminishment of tubulin in step 7, and the presence of abundant Lewy Bodies in the immunomagnetically captured fraction with minimal inclusions remaining in the wash fraction from Step 11 (Figure 6.1).

The average yield of solubilised inclusions for DLB cases 1 and 2 was 33 μg and 46 μg respectively, per tube of homogenate (40 μg average). A comparison of the homogenate (Step 1), post-tryptic digestion fraction (Step 7), and immunocaptured fraction (Step 11) for each case using immunohistochemistry is shown in Figure 6.2.

The dominant protein in LBs is α-synuclein, which is enriched in the immunocaptured fraction (Lane 7, Figure 6.3A), given the 10-fold reduced protein load in this lane compared with the others. β-tubulin, a cytoskeletal contaminant, is greatly reduced in abundance in the immunocaptured fraction (Lane 7, Figure 6.3B), with the majority of tubulin separated from the inclusions in the wash fraction (Lane 6, Figure 6.3B).

A graph comparing the amounts of monomeric, polymeric and total α-synuclein in each fraction is shown in Figure 6.4 and a comparison of the amounts of full-length, truncated and total β-tubulin in each fraction is shown in Figure 6.5. These quantifications were performed on the representative Western blots shown in Figure 6.3. The duplicate α-synuclein blot, which showed a highly similar pattern of enrichment, was not suitable for quantitation due to background spotting.

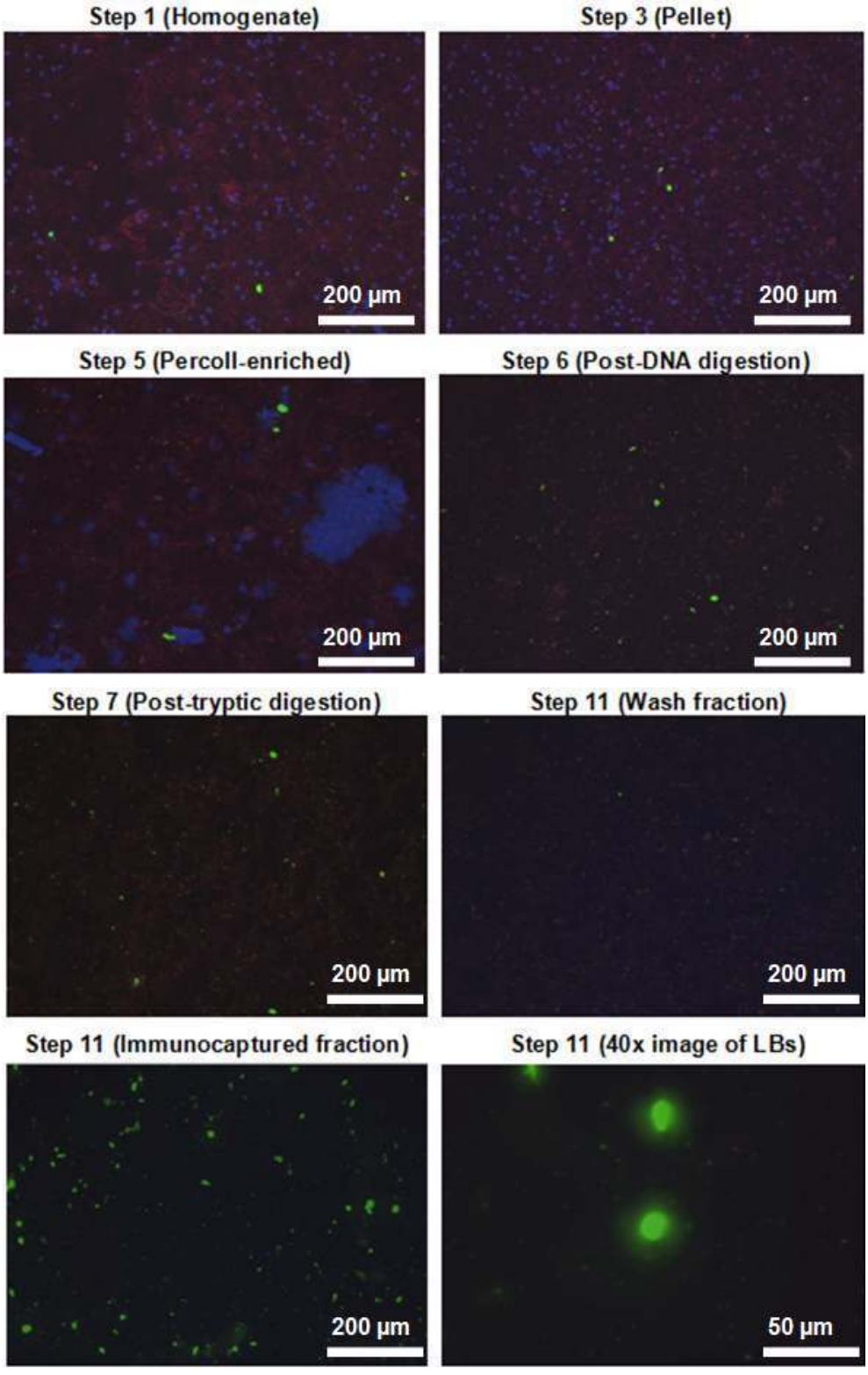

Figure 6-1: Successful purification of LBs shown with immunofluorescence
A Lewy Body purification was performed using a modified version of the optimised GCI purification method (section 6.2.1). A 10 µL smear of each fraction was dual stained against α-synuclein and β-tubulin. A Cy3-conjugated secondary antibody was used for α-synuclein, appearing green, and an Alexa488-conjugated secondary antibody was used for β-tubulin, appearing red. Nuclei were stained with DAPI and appear blue. All images were taken at 10x magnification unless otherwise specified.

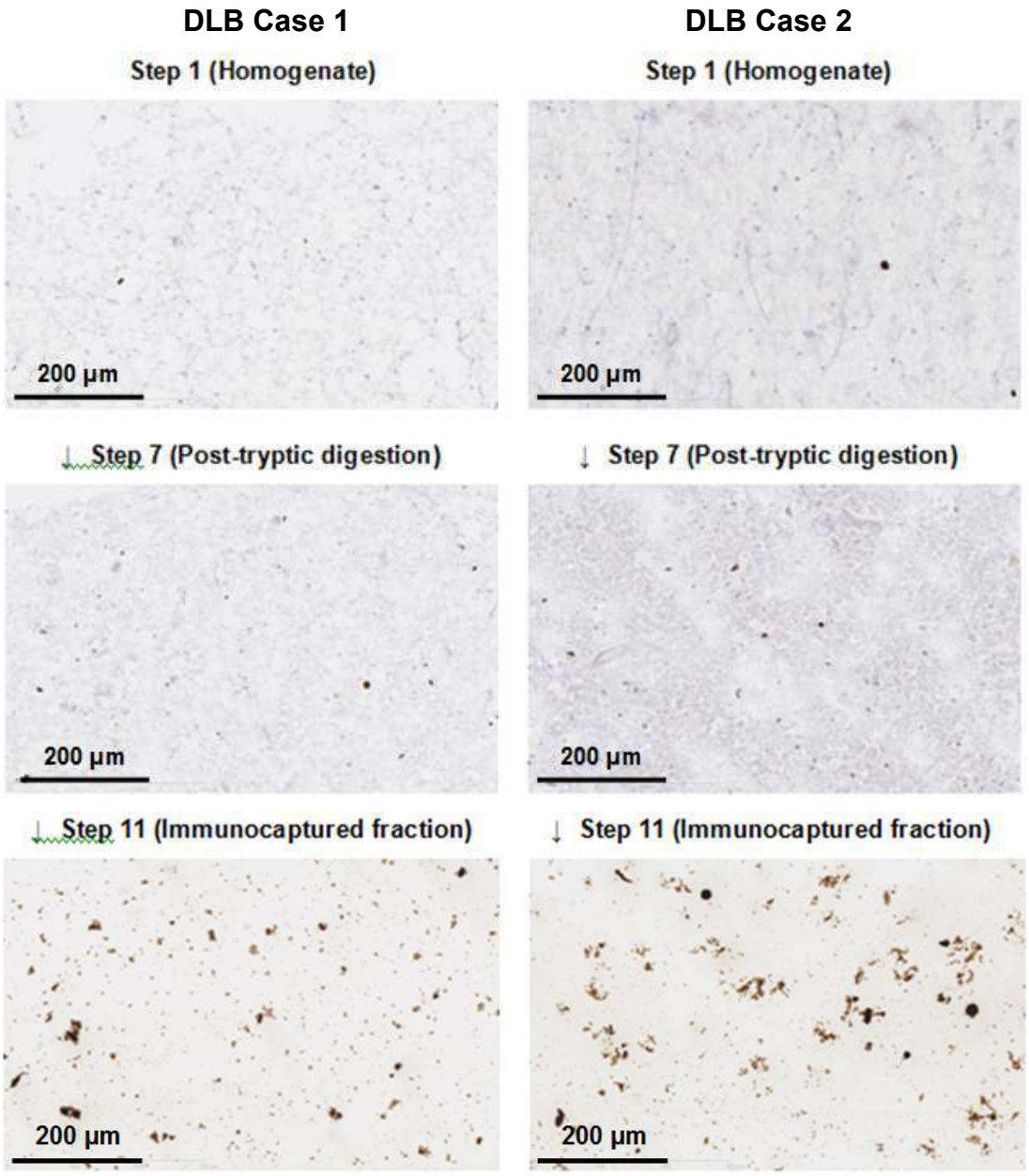

Figure 6-2: Successful purification of LBs shown with immunohistochemistry
A Lewy Body purification was performed using a modified version of the optimised GCI purification method (section 6.2.1), from DLB homogenate from cases 1 and 2 (SA0113 and SA0133 respectively, Table 2.3). A 10 µL smear of each fraction was DAB stained against α-synuclein (antibody no. 1, Table 2.1) and counterstained with haematoxylin. All images were taken at 20x magnification.

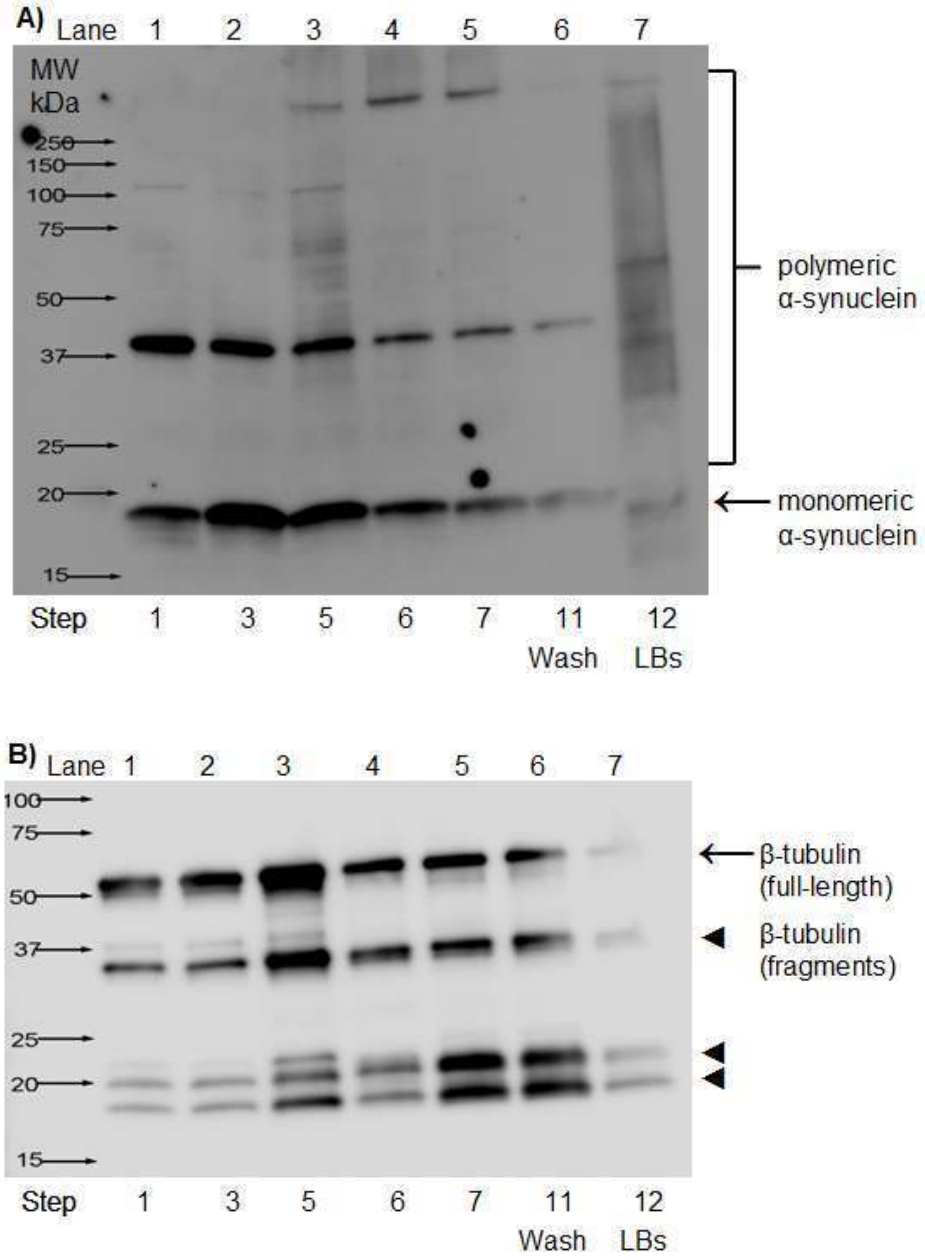

Figure 6-3: Enrichment of A) α-synuclein and reduction of B) β-tubulin associated with LB purification from DLB homogenate using the optimised purification method
Representative Western blots from a LB purification using the optimised GCI purification method adapted for Lewy Bodies, as described in section 5.2.1. The DLB homogenate (Lane 1, Step 1) was pelleted at 1,000x g (Lane 2, Step 3), from which a Percoll-enriched fraction (Lane 3, Step 5) was obtained and subjected to nuclei lysis and DNA digestion (Lane 4, Step 6), a limited tryptic digestion (Lane 5, Step 7) and immunomagnetic capture, with the wash fraction (Lane 6, Step 11) removed and the captured LBs solubilised (Lane 7, Step 12). The samples were solubilised in 1x sample buffer and 20 µg of each sample was separated by SDS-PAGE using a BioRad Mini-Protean TGX Any kD gel, transferred to PVDF and probed with antibodies against either A) α-synuclein (n=2) or B) β-tubulin (n=1). For gel A, only 2 µg was loaded in lane 7 to avoid overloading of the immunocaptured fraction for α-synuclein detection. The blots were imaged on a Fujifilm LAS-4000 CCD imager and analysed using Carestream Molecular Imaging Software Version 5.0.6.20.

A)

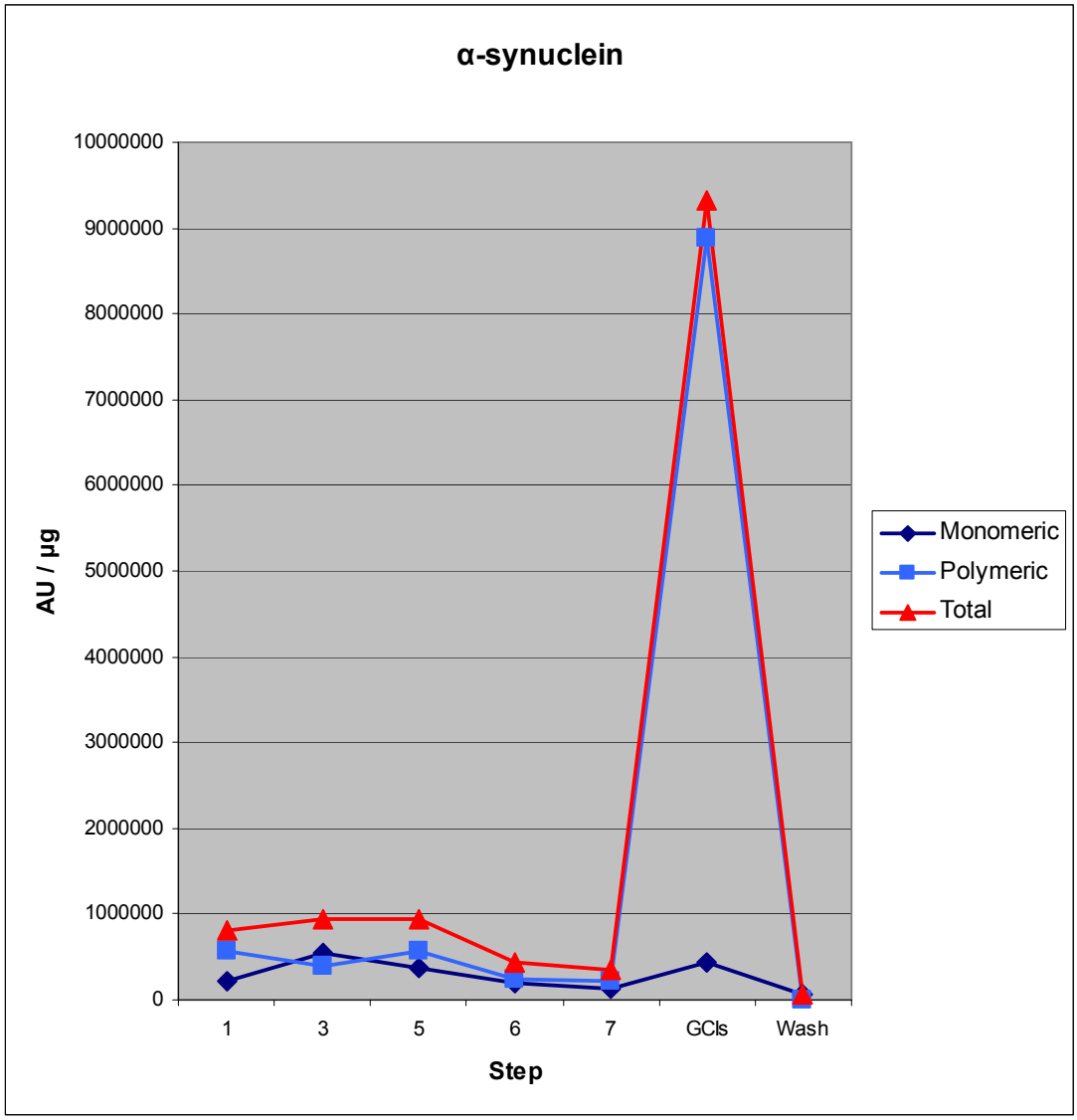
α-synuclein
10000000
9000000
8000000
7000000
6000000
5000000
4000000
3000000
2000000
1000000
0
AU / µg
1
3
5
6
7
GCls
Wash
Step
Monomeric
Polymeric
Total

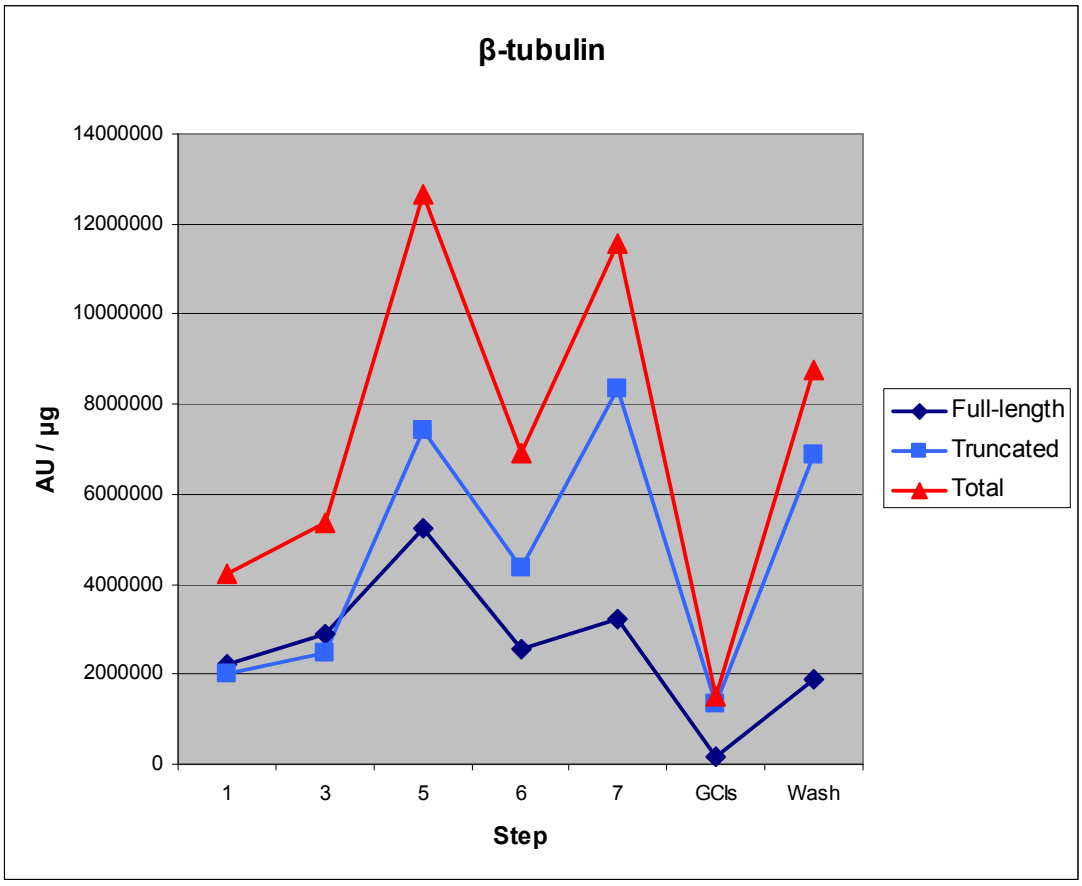

Figure 6-4: Quantitation from Western blotting of LB purification fractions of A) monomeric, polymeric and total α-synuclein, and B) full-length, truncated and total β-tubulin

The Western blots in Figure 6.3A (A) and Figure 6.3B (B) were analysed using Carestream Molecular Imaging Software Version 5.0.6.20 as described in section 6.2.5. All values have been normalised to the number of total µg of protein loaded in each lane. In A), the monomeric band between 15 and 20 kDa was selected for quantitation in each lane and the polymeric forms from 20 kDa upwards were selected as a single region in each lane for quantitation. The total was obtained from the sum of these two measurements in each lane. In B), the full-length band at ~50 kDa was selected for quantitation in each lane and the truncated forms from 15 to 37 kDa were selected as a single region in each lane for quantitation. The total was obtained from the sum of these two measurements in each lane.

6.3.2 Identification of Lewy Body proteins

LB purifications were performed on tissue from two DLB cases, as described in section 6.2.2. 20 µg of each sample was digested with trypsin and the digested peptides were analysed by LTQ Orbitrap XL mass spectrometry (section 6.2.8), with two replicates for each of the two samples. The False Discovery Rate (FDR) was <0.01 for each of the samples analysed.

From the four injections, a total of 348 proteins were identified. 174 of these proteins (50%) were present in both cases (Appendix O). 34 protein isoforms of 19 proteins previously established to be in LBs, as summarised in Licker *et al.* [180] and Leverenz *et al.* [108], were identified and these are listed in Table 6.4.

Table 6-4: Established Lewy Body proteins identified by MS

Protein Name	No. of cases[a]
α-synuclein	2
α-β-crystallin	2
14-3-3 protein (6 isoforms)	2
Tubulin (8 isoforms)	2
Neurofilament (3 isoforms)	2
Alpha-internexin	2
Heat shock protein HSP 90 (2 isoforms)	2
Heat shock 70 kDa protein (3 isoforms)	1
Microtubule-associated protein 1A	1
Microtubule-associated protein 1B	2
Microtubule-associated protein 2	2
Agrin	2
Gelsolin	1
Ubiquitin carboxyl-terminal hydrolase isozyme L1 (UCH-L1)	2
Calcium/calmodulin-dependent protein kinase type II (4 isoforms)	2
Tropomyosin	1
Synaptotagmin	1
Glyceraldehyde-3-phosphate dehydrogenase (GAPDH)	1
Superoxide dismutase [Cu-Zn]	1

[a] number of DLB cases in which the protein was identified

In this experiment, a broad range of synaptic vesicle-related proteins were identified, including 9 established synaptic vesicle proteins (Table 6.5), 37 proteins transiently associated with the synaptic vesicle membrane, and 9 putative novel synaptic vesicle proteins. The classification of these proteins was based on a review of the synaptic vesicle proteome by Burre and Volknandt (2007) [133]. Of the proteins identified in both cases, 21% were vesicle-related. These relationships between the protein identifications in this experiment are shown in Figure 6.5.

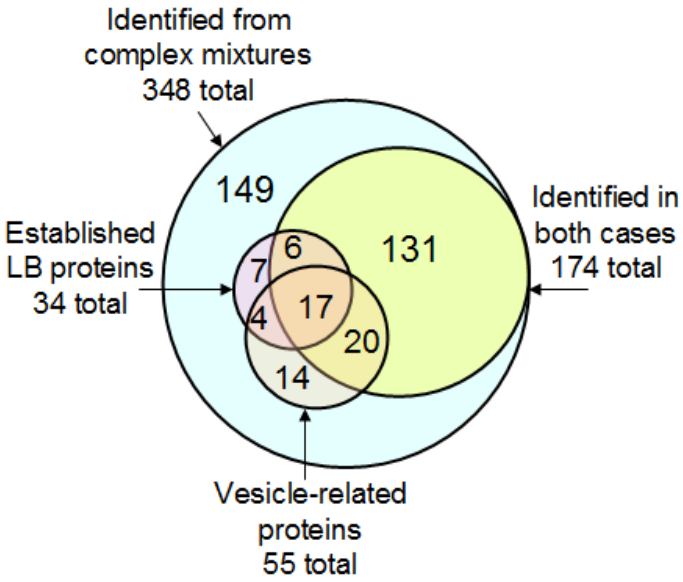

Figure 6-5: LB protein identifications from complex mixtures (n=2)
Solubilised Inclusions isolated from 2 DLB cases were trypsin-digested and the digested peptides were analysed by LTQ Orbitrap XL mass spectrometry. 348 proteins were identified in total, with 174 identified in both cases. The overlap between the identification of established LB proteins and vesicle-related proteins with the total protein identifications is shown.

Table 6-5: MS Identification of 9 LB proteins that are established synaptic vesicle proteins

Acc. No.[a]	Name	Calc. pI	Calc. MW (Da)	No. of cases[b]	Avg. Xcorr[b]	Avg. No. of Peptides[c]	Avg. % Sequence Coverage[d]
P60880	*Synaptosomal-associated protein 25	4.77	23300	2	19.4	3.8	24.6
P38606	V-type proton ATPase catalytic subunit A	5.52	68300	2	42.6	5.5	15.6
P61421	V-type proton ATPase subunit d 1	5.00	40300	2	30.5	3.8	21.6
P21281	V-type proton ATPase subunit B, brain isoform	5.81	56465	2	21.1	3.3	10.2
P36543	V-type proton ATPase subunit E 1	8.00	26129	1	11.8	3.0	15.9
Q9UI12	V-type proton ATPase subunit H	6.48	55800	1	7.9	2.0	6.6
P21579	*Synaptotagmin-1	8.12	47543	1	6.4	2.0	6.6
P63027	*Vesicle-associated membrane protein 2	8.13	12655	2	9.8	2.0	28.5
Q7L0J3	Synaptic vesicle glycoprotein 2A	5.57	82600	2	8.8	2.0	3.1

[a] SwissProt accession number
[b] Number of DLB cases in which the protein was identified
[c] Average Xcorr significance score
[d] Average number of unique peptides sequenced
[e] Average % of the full-length amino acid sequence covered by identified peptides
* Presence in LBs validated with immunofluorescence (Chapter 7.3.3)

6.3.3 2D DIGE comparison of MSA, DLB and normal cases

Inclusion purifications were performed on brain tissue from two DLB cases and one normal case, as described in section 6.2.2. The yield of solubilised protein (Step 12) from each purification is shown in Table 6.6 below.

Table 6-6: Protein yields from multiple DLB and normal case purifications

Sample	Yield (µg)[a]
DLB 1	34
DLB 2	44
Normal 2	38

[a] per single tube of brain homogenate

A 2D-DIGE experiment was performed as described in section 6.2.6 using the purified inclusions from the two DLB cases and normal case 2, as well as GCIs purified from three MSA cases (Chapter 5.2.2.1). The three gels were analysed in the Biological Variation Analysis (BVA) module of DeCyder 7.0 (GE Healthcare). 1686 spots were detected in total, with 1108 spots matched across all three gels. A separate analysis of each gel was also performed in the Difference In-gel Analysis (DIA) module for the quantification of proteins of interest from each gel.

There were 1315 spots matched in both DLB cases and a minimum of two MSA cases. Of these, 84.3% showed variations in abundance less than 1.5-fold (Table 6.7), revealing a high degree of similarity between LBs and GCIs. The spots with a difference in abundance >1.5-fold are shown on the spot map in Figure 6.6A and the spots with a difference in abundance >2-fold are shown in Figure 6.6B. The majority of the spots with a difference in abundance >2-fold appear to be α-synuclein isoforms, based on previous mass spectrometry identification, indicating that α-synuclein is less abundant in LBs than in GCIs.

When the two DLB cases were compared to each other, 85.8% of the 1315 spots showed variations in abundance less than 1.5-fold (Table 6.7). Thus, the case-to-case variation between DLB cases is very similar to the variation between DLB and GCI cases, making it difficult to ascertain which differences relate to the inclusion

type as opposed to biological variation between cases. A much larger number of samples are needed to determine this.

When GCIs and LBs were compared to inclusions purified from 'normal' brain tissue, there was a greater degree of dissimilarity (Table 6.7). The spots with a variation in abundance >3-fold are shown in Figure 6.7. The majority of the spots with an abundance >3-fold lower in the normal sample compared to both GCIs and LBs appear to α-synuclein and α-β-crystallin isoforms, based on previous mass spectrometry identification. This indicates that α-synuclein is less abundant in the normal control cases than in LBs, which in turn is less abundant than in GCIs.

Table 6-7: Differences between LBs, GCIs and inclusions present in normal cases as determined by 2D-DIGE

Comparison	Fold-change threshold	No. of spots			% of spots		
		Similar	Inc.[a]	Dec.[b]	Similar	Inc.[a]	Dec.[b]
LB to GCI (1315 spots)	>1.5	1109	72	134	84.3	5.5	10.2
	>2.0	1272	7	36	96.7	0.5	2.7
	>3.0	1310	1	4	99.6	0.1	0.3
LB to LB (1315 spots)	>1.5	1128	92	95	85.8	7.0	7.2
	>2.0	1268	30	17	96.4	2.3	1.3
	>3.0	1313	2	0	99.8	0.2	0.0
Normal to GCI (1337 spots)	>1.5	803	227	307	60.1	17.0	23.0
	>2.0	1076	95	166	80.5	7.1	12.4
	>3.0	1237	29	71	92.5	2.2	5.3
Normal to LB (1108 spots)	>1.5	751	139	218	67.8	12.5	19.7
	>2.0	965	55	88	87.1	5.0	7.9
	>3.0	1066	14	28	96.2	1.3	2.5

[a] increased
[b] decreased

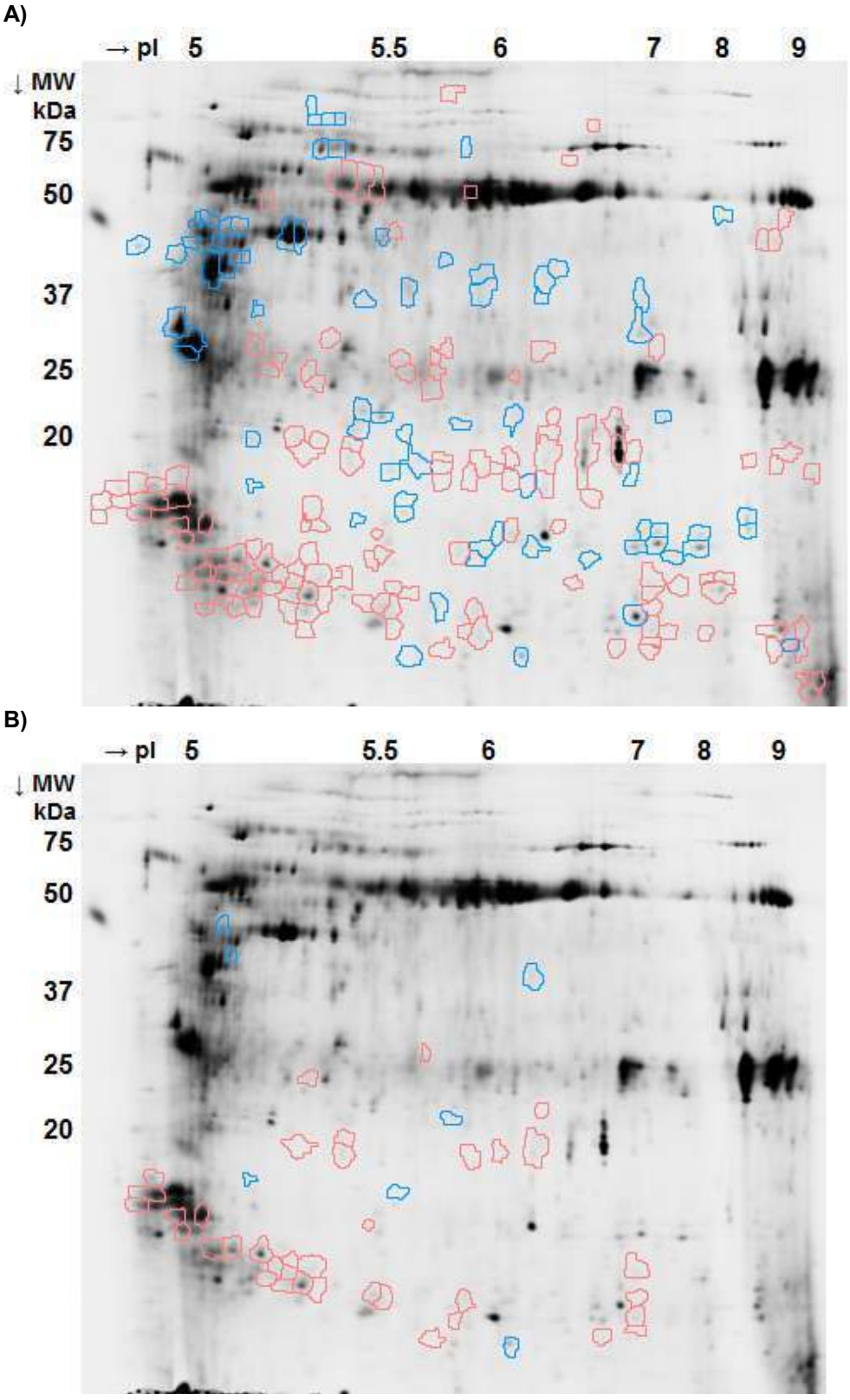

Figure 6-6: Comparison of LB proteins to GCI proteins by 2D-DIGE
Spot map of LB proteins exhibiting changes in protein abundance between LBs and GCIs. Spots exhibiting an average ratio change in abundance of >1.5 or <-1.5 (A) and >2.0 or <-2.0 (B) in two LB samples compared to a minimum of 2 GCI samples are shown. Blue spot boundaries indicate an increase in protein abundance in LBs relative to GCIs. Red spot boundaries indicate a decrease in protein abundance in LBs relative to GCIs.

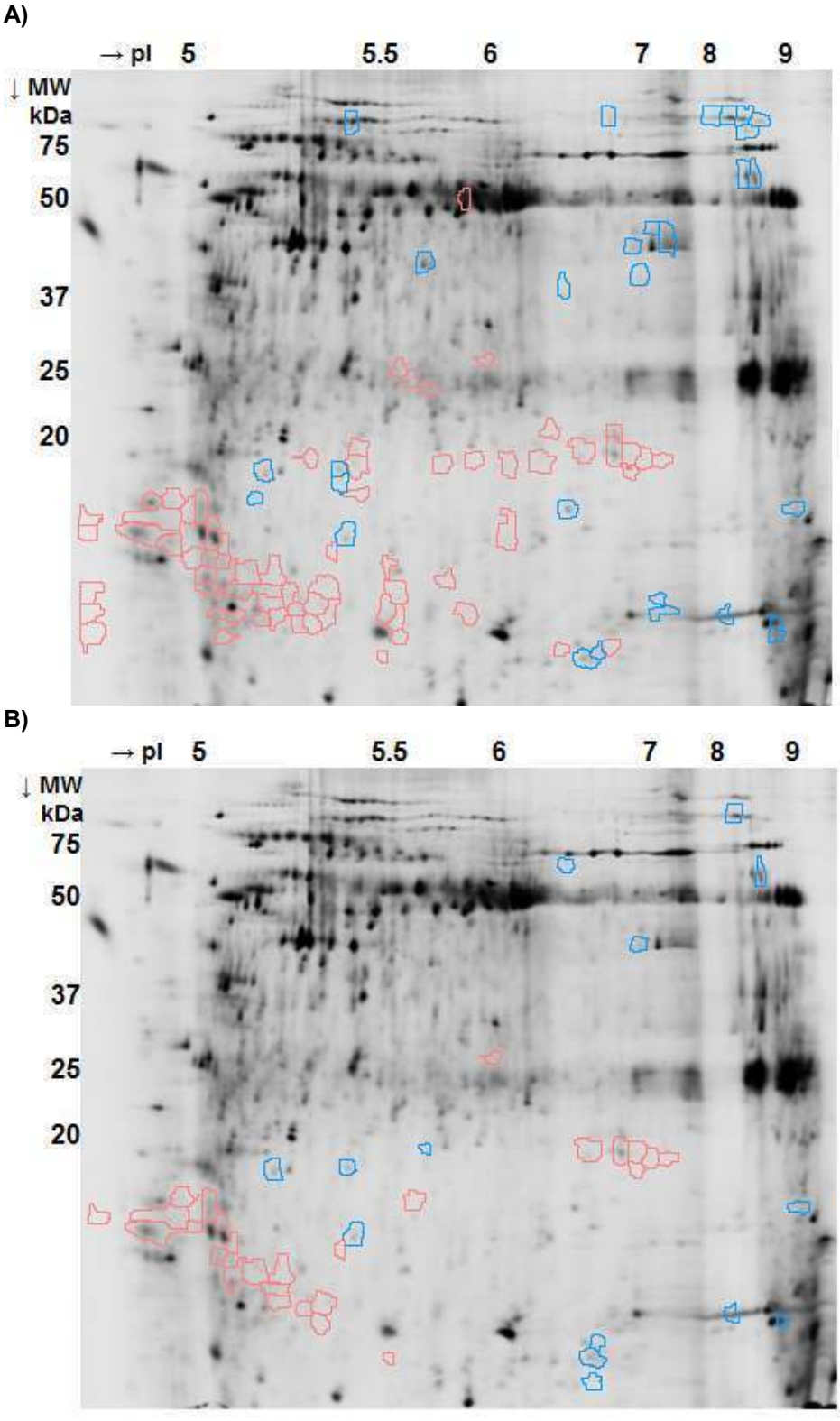

Figure 6-7: 2D-DIGE comparison of immunocaptured normal control proteins to (A) GCI proteins and (B) LB proteins with changes in protein abundance >3-fold or <-3-fold

Spots exhibiting an average ratio change in abundance of >3 or <-3 in a normal sample compared to a minimum of two GCI samples (A) or two LB samples (B). Spots with an increase or decrease in protein abundance, in normal control inclusions relative to GCIs or LBs, are shown in blue or red, respectively.

6.3.4 Quantitation of proteins of interest by 2D-DIGE

Each gel was analysed in the DIA (Differential In-gel Analysis) module of DeCyder version 7.0 (GE Healthcare). The search algorithm was processed with an estimation setting of 1,800 spots. Protein spots on each gel corresponding to isoforms of α-synuclein, α-β-crystallin, 14-3-3 proteins or tubulin were selected based on spot-matching to preparative 2D gels where protein identifications had been made using mass spectrometry (Figures 3.10 and 5.6). The relative abundance of each protein of interest was determined as described in Chapter 4.2.5. The integrated spot volumes for all protein isoforms were summed together, with the total volume for each protein compared to the summed volumes of all the protein spots on the gel to determine the percentage of total protein the protein of interest occupied. The same analysis had been performed on 2D-DIGE gels from three previous experiments, in Chapters 4.3.1.2, 4.3.2.1 and 5.3.4.3. The data from all four experiments are aggregated here for analysis.

The variability between technical replicates, where a sample from the same case was run and analysed on different gels, was assessed for MSA cases 0, 1, 2, 4 and 5 to determine what degree of variance was due to technical variation rather than biological differences (Table 6.8). The coefficient of variation between the quantification results of proteins of interest from technical replicates of the same case is approximately 10-20%. Variability between technical replicates is lower for α-synuclein and α-β-crystallin (~10%) than for 14-3-3 proteins and tubulin (~20%).

Table 6-8: Quantification results from technical replicates of immunocaptured GCIs to determine technical variability.

		% of total protein			
Case	**Rep.[d]**	**α-synuclein**	**α-β-crystallin**	**14-3-3s**	**Tubulin**
MSA 0 [a]	1	11.8	1.6	2.7	0.9
	2	9.6	2.2	1.9	0.9
Mean ± S.D.[b]		**10.7 ± 1.6%**	**1.9 ± 0.4%**	**2.3 ± 0.6%**	**0.9 ± 0.0%**
MSA 1	1	14.5	2.9	1.0	1.2
	2	15.5	2.6	0.5	0.8
Mean ± S.D.		**15.0 ± 0.7%**	**2.7 ± 0.2%**	**0.7 ± 0.4%**	**1.0 ± 0.3%**
MSA 2	1	16.4	4.5	2.3	1.5
	2	17.9	5.2	2.0	1.0
	3	17.4	4.6	2.4	1.7
	4	21.0	2.8	1.1	0.9
Mean ± S.D.		**18.2 ± 2.0%**	**4.3 ± 1.0%**	**1.9 ± 0.6%**	**1.3 ± 0.4%**
MSA 4	1	7.0	2.3	1.5	1.2
	2	9.6	2.4	1.7	1.7
Mean ± S.D.		**8.3 ± 1.8%**	**2.4 ± 0.0%**	**1.6 ± 0.1%**	**1.5 ± 0.4%**
MSA 5	1	9.4	2.5	1.0	1.2
	2	10.2	2.4	0.9	1.0
Mean ± S.D.		**9.8 ± 0.6%**	**2.5 ± 0.1%**	**1.0 ± 0.0%**	**1.1 ± 0.2%**
Mean		**12.4**	**2.7**	**1.5**	**1.1**
S.D.		**1.3**	**0.4**	**0.3**	**0.2**
C.O.V.[c]		**11%**	**13%**	**22%**	**21%**

[a] Case SA0058, from analyses in Chapter 4
[b] S.D. = standard deviation
[c] C.O.V. = coefficient of variation, the S.D. expressed as a % of the mean
[d] Replicate number

The quantification results for the biological replicates of GCIs immunocaptured from MSA cases, LBs immunocaptured from DLB cases and inclusions immunocaptured from a normal control case, as analysed by 2D-DIGE, are shown in Table 6.9. The variation between biological replicates was approximately 30% for α-synuclein and tubulin in both GCIs and LBs. The variation for α-β-crystallin was also approximately 30% in GCIs, but only 12% in LBs. 14-3-3 proteins displayed a higher amount of variance, with approximately 50-60% variance in GCIs and LBs. When the data for the immunocaptured inclusions from MSA, DLB and normal cases (from Table 6.9) was aggregated and analysed (section 6.2.7), a positive linear relationship was found between the relative quantities of α-synuclein and α-β-crystallin in each case (Figure 6.8). A very strong correlation is indicated with an R^2 value of 0.683 and the relationship is highly statistically significant ($p = 0.006$). No significant relationships were found between the other protein pairs analysed (Table 6.10).

Table 6-9: Abundance of proteins of interest in biological replicates of immunocaptured samples

		% of total protein			
	Reps[c]	α-synuclein	α-β-crystallin	14-3-3s	Tubulin
MSA cases					
MSA 0	2	10.7	1.9	2.3	0.9
MSA 1	2	15.0	2.7	0.7	1.0
MSA 2	4	18.2	4.3	1.9	1.3
MSA 3	1	9.7	3.1	2.9	1.7
MSA 4	2	8.3	2.4	1.6	1.5
MSA 5	2	9.8	2.5	1.0	1.1
Range		8.3 - 18.2	1.9 - 4.3	0.7 - 2.9	0.9 - 1.7
Mean ± S.D. [a]		**11.9 ± 3.8%**	**2.8 ± 0.8%**	**1.7 ± 0.8%**	**1.2 ± 0.3%**
C.O.V.[b]		**32%**	**30%**	**47%**	**25%**
DLB cases					
DLB 1	1	10.3	1.8	0.9	1.6
DLB 2	1	6.7	2.1	2.2	1.1
Mean ± S.D.		**8.5 ± 2.5%**	**2.0 ± 0.2%**	**1.5 ± 0.9%**	**1.3 ± 0.4%**
C.O.V.		**29%**	**12%**	**62%**	**30%**
Normal cases					
Normal control	1	4.2	0.8	1.0	1.1
Mean		**4.2%**	**0.8%**	**1.0%**	**1.1%**

[a] S.D. = standard deviation
[b] C.O.V. = coefficient of variation, the S.D. expressed as a % of the mean
[c] Number of technical replicates analysed, the mean data is shown when n>1

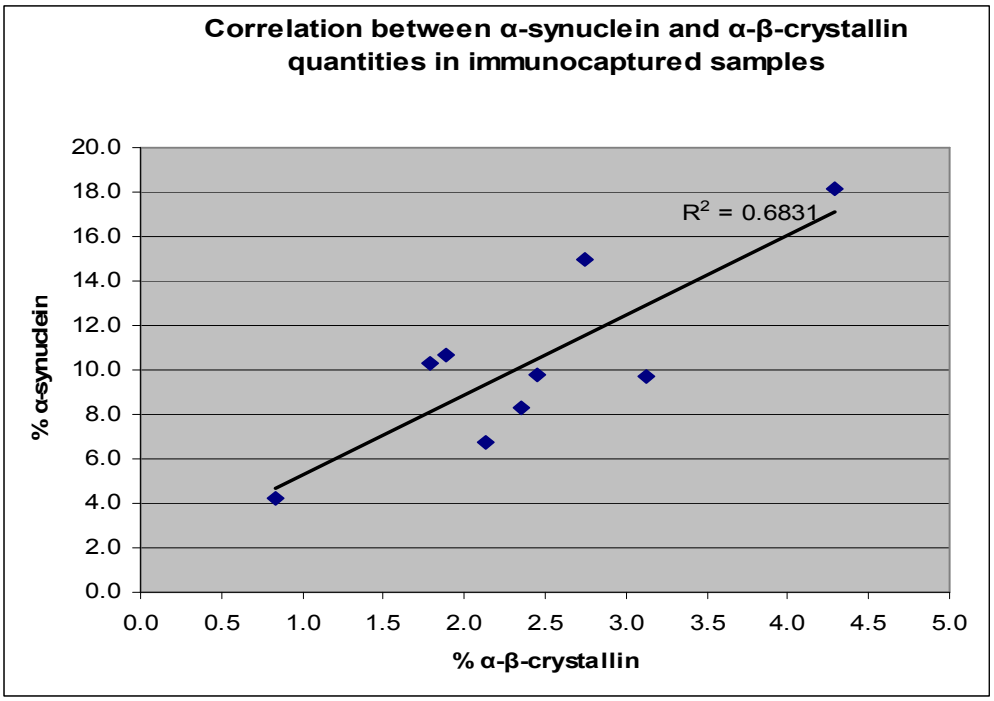

Figure 6-8: Very strong correlation between relative abundance of α-synuclein and α-β-crystallin in immunocaptured inclusions (n=9) as determined by 2D-DIGE
The relative quantities of α-synuclein and α-β-crystallin were quantified in a 2D-DIGE analysis of inclusions isolated from MSA cases (n=6), DLB cases (n=2) and a 'normal' control case where inclusions were discovered (n=1).

Table 6-10: Analysis of correlation in protein abundance in nine immunocaptured samples

Protein pair analysed	α-synuclein α-β-crystallin	α-synuclein 14-3-3s	α-synuclein tubulin	α-β-crystallin 14-3-3s	α-β-crystallin tubulin	14-3-3s tubulin
Pearson's correlation coefficient (R value)	0.82650	-0.00131	-0.02583	0.36313	0.22736	0.25536
Relationship strength[a]	Very strong	Negligible	Negligible	Moderate	Weak	Weak
Relationship direction	Positive	Negative	Negative	Positive	Positive	Positive
R^2 value	0.6831	0.0013	0.0258	0.1319	0.0517	0.0652
p-value (two-tailed)	0.0060	0.9973	0.9474	0.3368	0.5563	0.5072
Significance[b]	Highly significant	Not significant	Not significant	Not significant	Not significant	Not significant

[a] R>0.70 = very strong, 0.40-0..69 = strong, 0.30-0.39 = moderate, 0.20-0.29 = weak, 0.01-0.19 = negligible
[b] p>0.05 = not significant, p<0.05 = significant, p<0.01 = highly significant

A comparative analysis of the proteins of interest in GCIs, LBs, a normal control and a MSA homogenate is presented in Table 6.11. GCIs were shown to consist of approximately 12% α-synuclein, compared to 8.5% in LBs and 4% in the normal control. α-β-crystallin and 14-3-3 protein concentrations were also highest in GCIs, with less in LBs and less still in the normal control. The amount of tubulin appears to remain similar between inclusion types, with just over 1% tubulin present in each sample type. The MSA homogenate contains approximately double the quantity of tubulin as that found in the immunocaptured inclusions, and a slightly higher level of 14-3-3 proteins. However, both α-synuclein and α-β-crystallin were greatly enriched (up to 6-fold) in GCIs and LBs compared to MSA homogenate. These relationships are portrayed graphically with a comparison of the protein composition of each sample relative to total protein (Figure 6.9).

Table 6-11: Abundance of proteins of interest in GCIs compared to LBs, immunocaptured normal control and MSA homogenate

Sample	α-synuclein	α-β-crystallin	14-3-3s	Tubulin
	% of total protein			
*GCIs	11.9	2.8	1.7	1.2
*LBs	8.5	2.0	1.5	1.3
*Normal control	4.2	0.8	1.0	1.1
Homog. (MSA)	2.0	0.8	1.9	2.5
	% of protein relative to GCIs			
GCIs	100	100	100	100
LBs	71	70	88	108
Normal control	35	30	57	90
Homog. (MSA)	17	30	108	199
	Fold change relative to GCIs			
GCIs	1.0	1.0	1.0	1.0
LBs	-1.4	-1.4	-1.1	1.1
Normal control	-2.8	-3.4	-1.7	-1.1
Homog. (MSA)	-6.0	-3.3	1.1	2.0

* Immunocaptured preparations from MSA, DLB and normal control tissue, respectively

Note: mean data is presented from biological replicates of GCIs (n=6), LBs (n=2), normal control (n=1) and MSA homogenate (n=1).

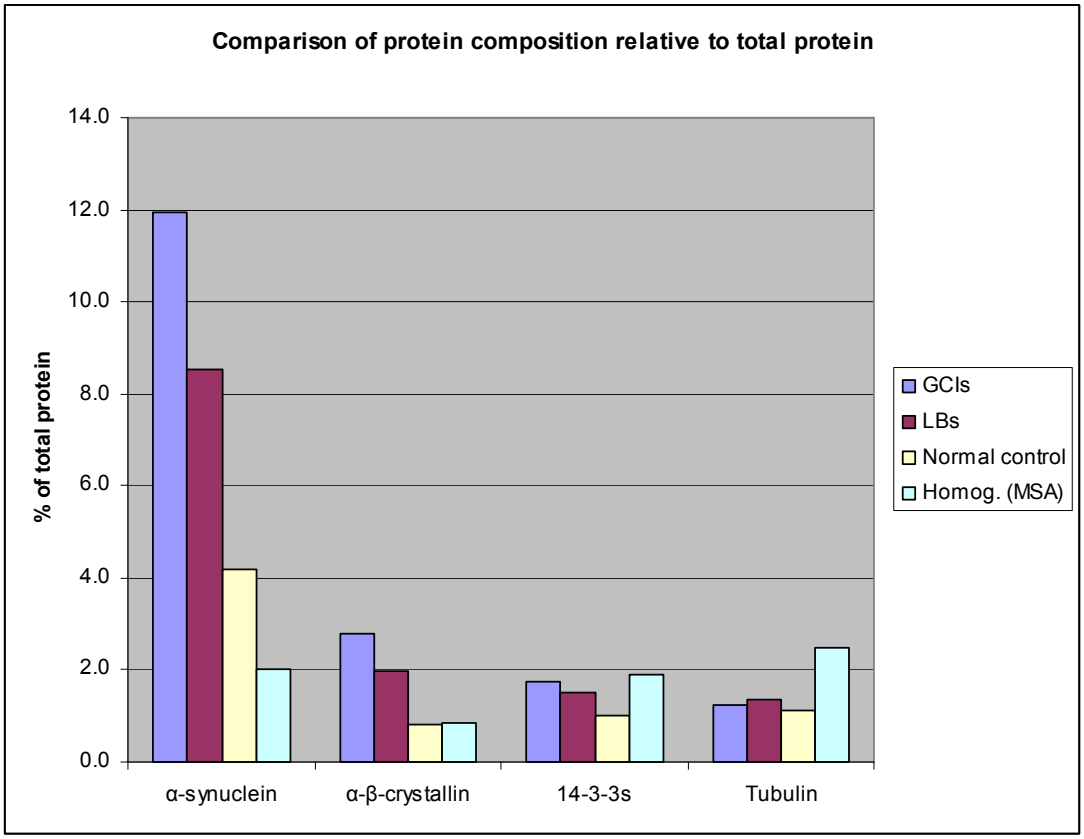

Figure 6-9: Comparison of protein composition of GCIs, LBs, normal control and MSA homogenate, relative to total protein

The relative quantities of α-synuclein, α-β-crystallin, 14-3-3 proteins and tubulin were quantified in a 2D-DIGE analysis of inclusions isolated from MSA cases (n=6), DLB cases (n=2) and a 'normal' control case where inclusions were discovered (n=1), and in MSA homogenate (n=1).

6.3.5 Western blot comparison of MSA, DLB and normal cases

A comparison of the α-synuclein content in inclusions purified from normal, DLB and MSA cases was performed by Western blotting (Figure 6.10) as an independent comparison to corroborate the α-synuclein quantification results from the 2D-DIGE experiments. α-synuclein is enriched in both GCIs and LBs (Lanes 6 and 5 respectively, Figure 6.10) compared to the crude brain homogenate (Lanes 3 and 2 respectively). There is a greater amount of α-synuclein per µg of total protein in both monomeric and higher molecular weight forms, present in GCIs than in LBs (Lane 6 compared to Lane 5). While 'normal' control brain homogenate (Lane 1) contains similar levels of α-synuclein to DLB and MSA tissue, very little α-synuclein is present in the immunocaptured fraction from this tissue (Lane 4).

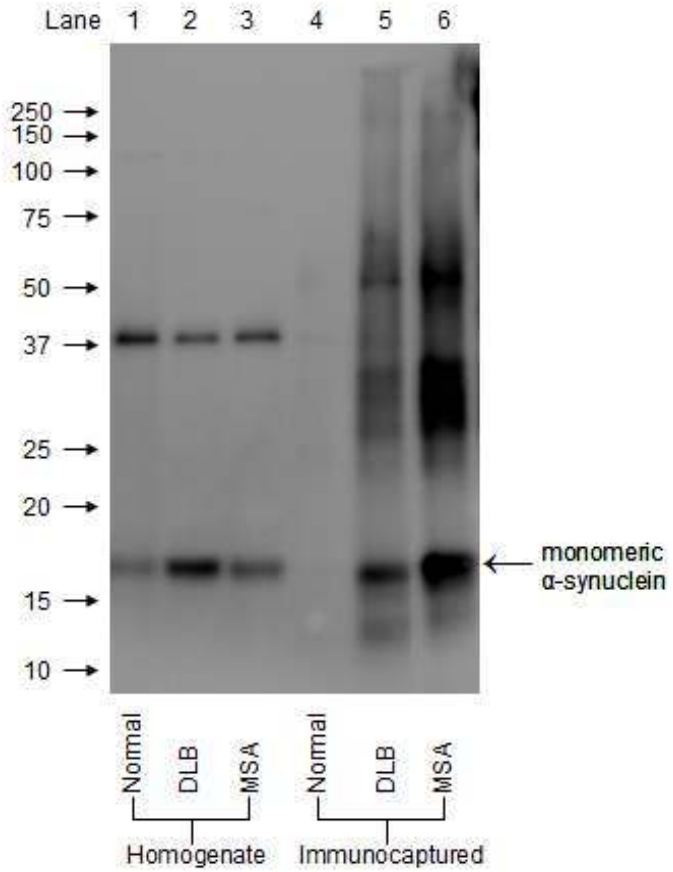

Figure 6-10: Comparison of α-synuclein present in immunocaptured fractions from normal control, DLB and MSA cases (n=1)
Brain tissue homogenate from normal (Lane 1), DLB (Lane 2) and MSA (Lane 3) cases was used for inclusion purification, with inclusions isolated in the immunocaptured fraction (Lanes 4, 5 and 6, respectively). The samples were solubilised in 1x sample buffer and 2 µg of each sample was separated by SDS-PAGE using a BioRad Mini-Protean TGX Any kD gel, transferred to PVDF and probed with an antibody against α-synuclein (antibody no. 2, Table 2.1). The blot was imaged on a Fujifilm LAS-4000 CCD imager for 5 minutes.

The amount of monomeric, polymeric and total α-synuclein was quantified for each lane and the results are shown in Figure 6.11. All three homogenates (MSA, DLB and normal control) contained similar levels of total α-synuclein. The immunocaptured sample from the normal control contained less α-synuclein than the corresponding homogenate, whereas an enrichment of α-synuclein was seen in both the LB and GCI samples.

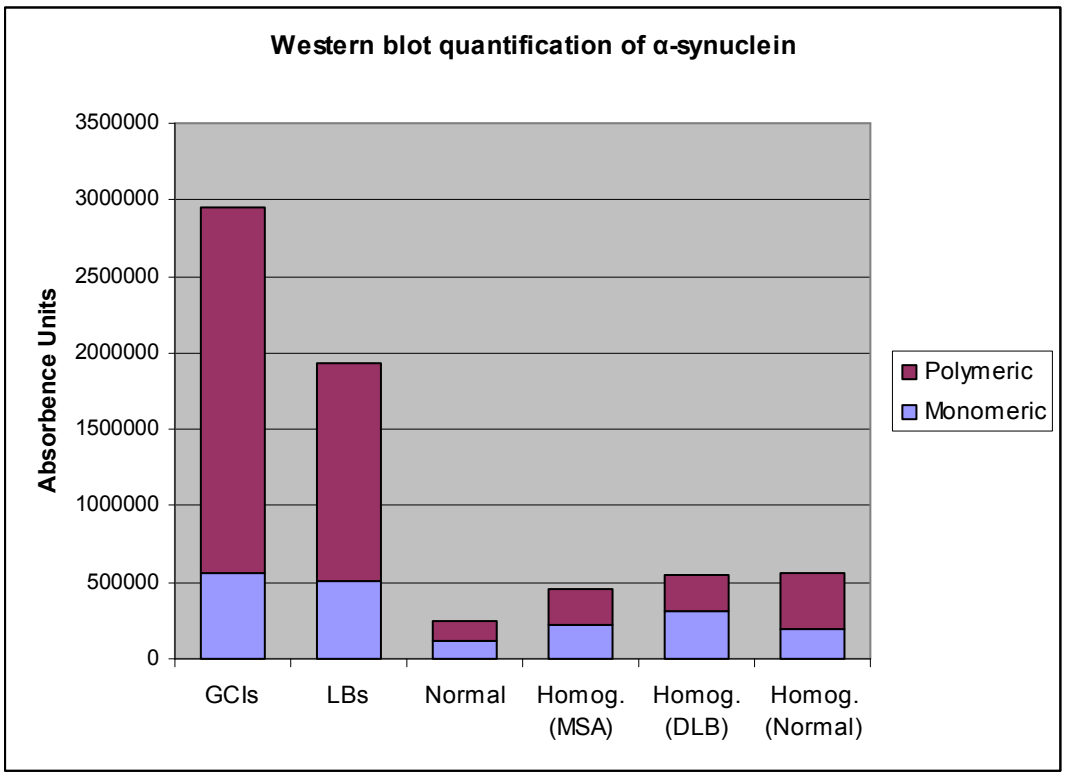

Figure 6-11: Western blot quantification of monomeric, polymeric and total α-synuclein in immunocaptured inclusions and matched homogenates
The Western blot in Figure 6.10 was analysed using Carestream Molecular Imaging Software Version 5.0.6.20 as described in section 6.2.5. The monomeric band (including truncated forms below it) between 10 and 18 kDa was selected for quantification in each lane and the polymeric forms from 18 kDa upwards were selected as a single region in each lane for quantification. The total was obtained from the sum of these two measurements in each lane. Background subtraction was performed using a representative blank section of the blot. All values presented have been normalised to the total µg of protein loaded in each lane.

The fold-enrichment of monomeric, polymeric and total α-synuclein for each immunocaptured sample from its respective crude homogenate is shown in Table 6.12, along with the ratio of enrichment of polymeric to monomeric forms. Polymeric α-synuclein is disproportionally enriched in GCIs and LBs, with an approximately 4-fold ratio of polymeric to monomeric forms enriched from the crude homogenate, suggesting a greater rate of incorporation of polymeric forms of α-synuclein into inclusions.

Table 6-12: Enrichment of α-synuclein in immunocaptured inclusions compared to matched brain homogenates

	Fold-enrichment from homogenate			
Sample	**Monomeric**	**Polymeric**	**Total**	**Poly:mono ratio**
GCIs	2.5	10.3	6.4	4.1
LBs	1.6	6.1	3.6	3.8
Normal	0.6	0.4	0.5	0.7

In this Western blot analysis, the GCI sample used (MSA 1), the LB sample (DLB 1) and the normal sample were all analysed by 2D-DIGE in the previous experiment, thus allowing the α-synuclein quantification from the two methods to be compared. An MSA homogenate was also analysed by 2D-DIGE in the previous experiment, although it is a different case (MSA 0) compared to the matched homogenate (MSA 1) used in the Western blot analysis. While the α-synuclein quantity for the specific cases (MSA 1 and DLB 1) were used in this comparison, when the comparison was repeated with the average α-synuclein quantity found for GCIs and LBs across multiple biological replicates, the results were not materially different (data not shown).

The α-synuclein quantification of each sample obtained by DIGE and Western blot analysis, relative to the α-synuclein content of GCIs, is shown in Table 6.13 and Figure 6.12. The relative quantities agree very closely between the two methods, with the exception of a lower amount of α-synuclein found in the normal sample with Western blotting compared to DIGE.

Table 6-13: Comparison of DIGE and Western Blot quantitation of α-synuclein content of inclusions

	% of protein relative to GCIs		Fold change relative to GCIs	
Sample	**DIGE**	**Western**	**DIGE**	**Western**
GCIs	100	100	1.0	1.0
LBs	69	66	-1.5	-1.5
Normal control	28	9	-3.6	-11.7
Homog. (MSA)	13	16	-7.5	-6.4

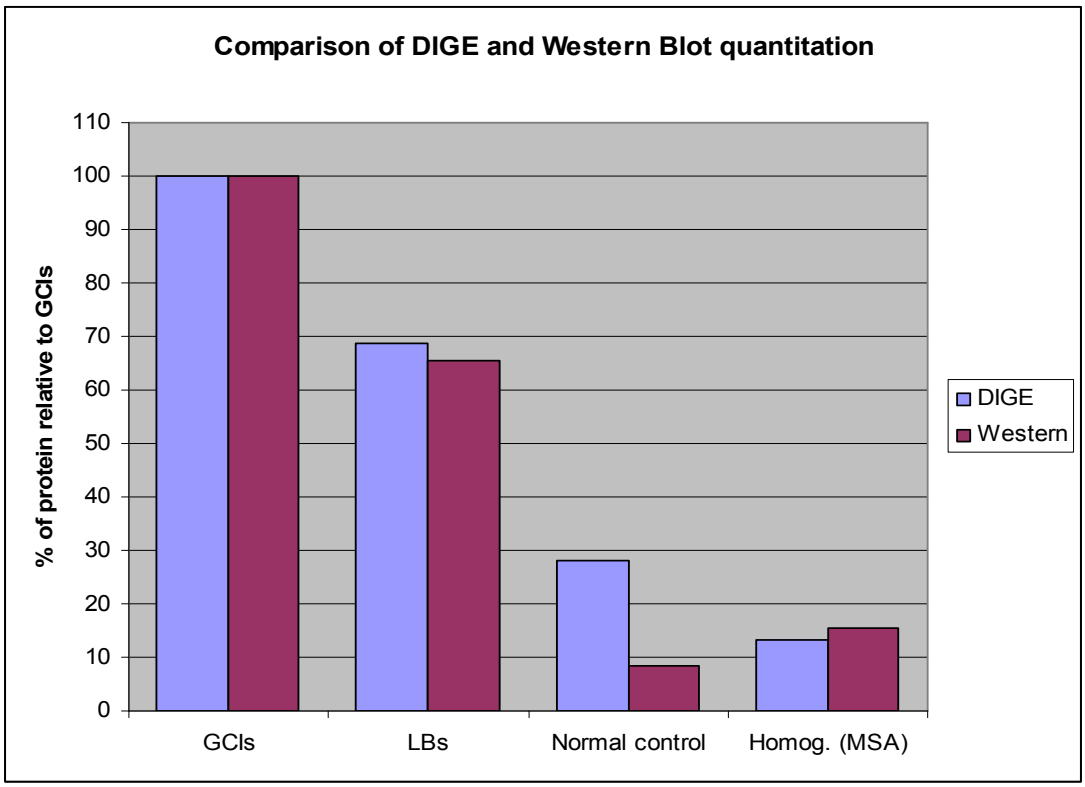

Figure 6-12: Comparison of 2D-DIGE and Western Blot quantification of α-synuclein content of inclusions
The relative quantity of α-synuclein was quantified by both 2D-DIGE analysis and Western blot analysis of inclusions isolated from an MSA case, a DLB case, a 'normal' control case where inclusions were discovered and an MSA homogenate prior to inclusion isolation. The relative quantifications from the two methods of analysis agree closely.

6.4 Discussion

6.4.1 Application of optimised GCI purification method for the purification of Lewy Bodies

The adaptation of the optimised GCI purification method to the purification of Lewy Bodies worked successfully. As evidenced by IF and IHC of purification fractions, the nuclei were removed via lysis and subsequent DNase digestion and tubulin was diminished in response to tryptic digestion. Abundant captured inclusions (LBs) were visualised in the immunomagnetically captured fraction, with minimal inclusions remaining in the wash fraction.

When the purification was subsequently repeated using the same two DLB cases (for DIGE analysis), there was less than 5% difference in the yield obtained from each purification replicate. The average yield per case was 39 μg per tube of homogenate (equivalent to 2g brain tissue), which is approximately $1/5^{th}$ of the yield of GCIs from the same amount of brain tissue (~200 μg), which agrees with the estimate of LBs being only $1/3^{rd}$ to $1/5^{th}$ as abundant as GCIs.

The enrichment of the major LB protein α-synuclein [179] was demonstrated in the immunocaptured fraction via Western blotting. This enrichment appears to be less than that in GCIs – these differences are discussed in the next section, when a quantitative comparison between the two was performed using 2D-DIGE and Western blotting. A wide variety of polymeric forms appear enriched compare to the monomeric form of α-synuclein. This is likely due to the aggregation of α-synuclein into fibrillar structures within LBs [59].

The tissue from both DLB cases used in this study was from the brainstem region. 'Classic' brainstem-type Lewy bodies have a dense, granular core surrounded by a less dense periphery and outer halo, whereas cortical-type LBs have a more uniform structure with less differentiation between the central and peripheral regions [181]. The morphological differences between brainstem-type and cortical-type LBs may arise from a difference in protein composition between the two types, which may be associated with the LB progression from the brainstem through to the cortex during the progression of the disease [108]. Thus, the results from this study may only

reflect the protein composition of the classic brainstem-type LBs and may not apply to LBs found in the cortex.

LBs and Lewy neurites (LNs) frequently co-exist [182], so α-synuclein-containing LNs will be immunocaptured from the brain tissue along with LBs during the purification process. Occasional α-synuclein-containing LNs were observed in the immunocaptured fractions from DLB cases via immunohistochemistry (data not shown). However, the capture of these infrequent LNs along with the LBs is unlikely to substantially alter results.

6.4.2 Identification of LB proteins by mass spectrometry

A total of 348 proteins were identified by mass spectrometry from trypsin-digested complex mixtures of solubilised immunocaptured LBs obtained from two different DLB cases. 174 of these proteins were present in both DLB cases, which supports the presence of these proteins being common to LBs, and thus related to their formation and function. However, the proteins identified in a single case may still be common to LBs, but at a lower abundance, thus eluding detection in complex mixture in both cases. Also, lower molecular weight proteins generate fewer peptides that and are more easily missed when performing MS analysis in complex mixtures. In the future this could be addressed by using targeted MS to identify specific proteins.

19 proteins previously reported to be in LBs, as summarised in reviews by Licker *et al.* [180] and Leverenz *et al.* [108], were identified. The identified proteins α-synuclein, α-β-crystallin, 14-3-3 proteins, tubulin, MAP1A, MAP1B, MAP2, and heat shock 70 kDa protein were discussed in Chapter 5.4.1, and the identified proteins neurofilament, alpha-internexin, tropomyosin, gelsolin, HSP90, UCH-L1, calcium/calmodulin-dependent protein kinase type II, agrin, synaptotagmin, GAPDH, and superoxide dismutase, are discussed below.

The neurofilament proteins – light, medium, and heavy chain subunits – are the intermediate filaments of the nervous system, found in neurons in both the central and peripheral nervous systems [183]. Alpha-internexin is an intermediate filament that is abundantly expressed alongside neurofilament in the central nervous system [183]. Tropomyosins are a family of actin-binding proteins that work in non-muscle

cells to stabilise actin filaments [184]. Gelsolin is another actin-binding protein, which caps the growing end of the actin filament, stimulates its nucleation and severs the actin filaments [185]. Gelsolin also binds to amyloid beta protein (Aβ, involved in Alzheimer's Disease) and can inhibit the fibrillisation of Aβ [185].

HSP90 is a molecular chaperone, which promotes correct protein conformation by reducing misfolding and aggregation [186]. It is believed to interact with the hydrophobic surfaces of substrate proteins and act in the late stages of folding [186]. UCH-L1 is involved in the ubiquitin-proteasome system and functions by hydrolysing polyubiquitin chains to generate re-usable ubiquitin monomers, thus promoting the ubiquitination and subsequent proteosomal degradation of α-synuclein [4, 8].

Calcium/calmodulin-dependent protein kinase type II (CaMKII) is a highly abundant neuronal serine/threonine kinase [187]. CaMKII is a multifunctional enzyme that is regulated by intracellular calcium levels, so its subcellular location is a predictor of its function [187]. Agrin is a large heparin sulphate glycoprotein that plays a role in stabilizing developing neuromuscular synapses [188].

Synaptotagmin is a transmembrane calcium sensor [150] involved in membrane fusion [153], as described in Chapter 5.4.2. GAPDH is a glycolytic enzyme, which is involved in many cellular processes apart from glycolysis [189]. It is involved in cytoskeletal dynamics, including tubulin bundling and actin polymerization, and has a role in membrane fusion and trafficking, where it may act as a scaffolding protein that mediates vesicular trafficking between different cellular compartments [189]. Superoxide dismutase (SOD) is an antioxidant that metabolises the superoxide anion [190]. There are three different families of SODs, which all utilise a unique metal ion [190]. The Cu-Zn family SOD was found in this experiment.

A comprehensive set of synaptic vesicle-associated proteins were identified by mass spectrometry, including 9 established synaptic vesicle proteins, 37 proteins transiently associated with the synaptic vesicle membrane, and 9 putative synaptic vesicle proteins (based on a review of the synaptic vesicle proteome by Burre and Volknandt (2007) [133]). These may be related to how the inclusion proteins are targeted to the LBs or GCIs. The functions of the established synaptic vesicle

proteins that were identified – SNAP25, VATPase (5 protein subunits), Synaptotagmin-1, VAMP2 and synaptic vesicle glycoprotein 2A – were previously described in Chapter 5.4.2.

6.4.3 Comparison of inclusion types using 2D-DIGE

Comparison of LB preparations from two different DLB cases revealed 85% of proteins displayed expression differences of less than 1.5-fold (97% of proteins at a 2-fold level). In Chapter 5.3.4.2, when GCI preparations from five different MSA cases were compared, there was 78% similarity at a 1.5-fold level (95% at a 2-fold level). When the LB samples (n=2) were compared to the GCI samples (n=3) in this experiment, 85% of proteins displayed expression differences of less than 1.5-fold (97% at a 2-fold level). Thus, a high degree of similarity between the protein composition of LBs and GCIs is suggested by this preliminary study, given that the differences between the two inclusion types are comparable to the case-to-case biological variation within each type. A larger number of samples are needed to differentiate between the biological variance between cases and the variance between inclusion types with statistical significance.

Four established inclusion proteins (α-synuclein, α-β-crystallin, 14-3-3 and tubulin) were quantified from the samples on the DIGE gels. This data was combined with quantifications performed on previous gel sets, as the comparison is performed in the DIA module of DeCyder and is therefore batch-independent. This allowed for comparison of the relative abundance of proteins of interest within and between sample types.

The technical variation in this analysis was low, with approximately 10% variation found in the quantification of α-synuclein and α-β-crystallin and approximately 20% variation for 14-3-3 and tubulin, as assessed by comparing the results from the same samples run on different gels. The sources of technical variation in this analysis may arise from differences in protein resolution or other physical factors during the gel electrophoresis; differences in the calculation of spot boundaries by the software algorithm in the DIA module of DeCyder; and differences in the selection of spots to be included in the quantification of each protein type. The larger number of isoforms (spots) present for α-synuclein and α-β-crystallin compared to 14-3-3 and tubulin

may explain the lower variance for the former two proteins. Any differences due to spot matching between gels, because of either the spot boundary definitions automatically defined by the DIA algorithm or the manual selection of spots to be included in the analysis, are more likely to be reduced with the greater number of spots selected.

The variation between biological replicates (of the same inclusion type) was approximately 30% for α-synuclein and tubulin in both GCIs and LBs. The variation for α-β-crystallin was also approximately 30% in GCIs, but only 12% in LBs. 14-3-3 proteins displayed a higher amount of variance, with approximately 50-60% variance in GCIs and LBs. A very strong positive linear relationship was found between the relative quantities of α-synuclein and α-β-crystallin in each case (Figure 6.8). No other statistically significant relationships were found between the four proteins quantified.

α-β-crystallin is a ubiquitous 175-residue protein belonging to the family of small heat shock proteins (sHsps) that act as molecular chaperones [191]. α-β-crystallin has been found to be a major component of GCIs [113, 118, 192] and to colocalise with α-synuclein in LBs and LNs [193]. The presence of α-β-crystallin in inclusions suggests that it may be produced by the cell in response to α-synuclein toxicity and aggregation [193, 194]. α-β-crystallin has been shown *in vitro* to protect against α-synuclein induced toxicity and aggregation [191, 193-195].

Bruinsma *et al.* (2011) [194] showed that the coincubation of α-synuclein with α-β-crystallin resulted in the formation of fewer α-synuclein fibrils. There are several proposed mechanisms for how this may occur. α-β-crystallin may bind to aggregating α-synuclein and prevent protein misfolding, or it may return misfolded α-synuclein to its normal conformation, or it may facilitate the transformation of oligomers into amorphous aggregates rather than into stable fibrils [194]. Rekas *et al.* (2004) [195] presented evidence for the latter mechanism, showing that α-β-crystallin interacts with α-synuclein to form large non-fibrillar aggregates, implying it redirects α-synuclein away from a pathway of stable fibril formation in favour of more easily degradable amorphous aggregates.

Rekas *et al.* (2004) [195] also showed a reduction in the number, but not length, of α-synuclein fibrils when coincubated with α-β-crystallin. It was shown that α-β-crystallin interrupted α-synuclein aggregation at its earliest pre-fibrillar stages, before the elongation process [196]. This most likely occurred by the binding of α-β-crystallin to partially folded α-synuclein monomers to prevent their aggregation into fibrils [196]. However, the authors did not exclude the possibility of further interaction between α-β-crystallin and fibrillar α-synuclein, finding that α-β-crystallin also prevented further fibrillisation when added during the growth stage of fibril formation [196].

More recently, Waudby *et al.* (2010) [191] have shown that α-β-crystallin binds along the lateral surface (length) of α-synuclein fibrils and inhibits further elongation. Binding in this fashion may be a protective mechanism to prevent further growth of α-synuclein fibrils before they can be cleared from the cell by other means [191]. This suggests there may be multiple mechanisms for the interaction of α-β-crystallin with α-synuclein. α-β-crystallin may assist in maintaining a balance between the aggregation and disaggregation of α-synuclein and may reduce the levels of the toxic oligomeric form of α-synuclein by controlling its folding state [194].

Expression of α-β-crystallin is induced by oxidative stress and it is recruited to α-synuclein aggregates under oxidative stress conditions [197]. An approximate binding ratio of 0.6:1 α-β-crystallin to α-synuclein was observed *in vitro* [191]. In this study, α-β-crystallin was found at a ratio of 0.23:1 to α-synuclein, suggesting that α-β-crystallin present in inclusions may be entirely bound to α-synuclein within inclusions. This could account for the linear relationship between the quantities of these two proteins within inclusions.

GCIs were shown to consist of approximately 12% α-synuclein, compared to 8.5% in LBs and 4% in the normal control. The amounts of α-β-crystallin and 14-3-3 proteins were also highest in GCIs, with less in LBs and less still in the normal control. Both α-synuclein and α-β-crystallin are greatly enriched (up to 6-fold and 3.3-fold respectively) in GCIs and LBs compared to MSA homogenate.

The amount of tubulin remains similar between inclusion types, with just over 1% tubulin present in each. It is not proportional to the amount of α-synuclein present in a sample, but rather to the total amount of protein present. One explanation is that tubulin is incorporated into inclusions in a consistent ratio to the total protein in the inclusion. An alternative explanation, proposed here, is that some of the cytoskeletal structure surrounding the inclusions remains attached after the immunocapture of isolated inclusions. Because the limited trypsin digestion is performed for each sample with a constant trypsin to total protein ratio, a similar amount of remaining tubulin surrounds each inclusion, thus giving a comparable amount of tubulin in each final immunocaptured preparation, regardless of the inclusion type.

6.4.4 Comparison of inclusion types using Western blotting

Western Blotting demonstrated that MSA, DLB and normal control brain homogenates all contain similar levels of α-synuclein. The immunocaptured sample from the normal control contains less α-synuclein than the corresponding homogenate, whereas an enrichment of α-synuclein is seen in both the immunocaptured GCI and LB samples relative to the MSA and DLB homogenates, respectively. Polymeric α-synuclein is disproportionally enriched in GCIs and LBs, with approximately 4-fold the amount of polymeric to monomeric forms enriched from the crude homogenate, suggesting a greater rate of incorporation of polymeric forms of α-synuclein into inclusions. The presence of modified and aggregated forms of α-synuclein in the inclusions from the immunocaptured fractions may explain the difference in the α-synuclein profile seen on the Western blot compared to the homogenate samples. The appearance of the α-synuclein profile in the immunocaptured samples may also differ from the homogenate samples due to technical reasons. There is a much higher proportion of α-synuclein the in 2 µg of immunocaptured sample compared to the 2 µg of homogenate loaded. Thus, while the total protein load is the same, the load of α-synuclein in the immunocaptured samples is much higher, which may affect its ability to focus on a 1-D gel.

The relative quantity of α-synuclein determined in each sample type (GCIs, LBs, normal control, and MSA homogenate), normalised to the quantity found in GCIs, agreed very closely between the DIGE and Western Blot quantification methods, as

shown in Figure 6.12. The correlation with the Western blot data supports the quantification technique used with the DIGE gels.

On a 2D gel, α-synuclein appears almost exclusively in monomeric form, including many truncated monomeric isoforms, with very few higher molecular weight aggregates identified. This is in contrast to its appearance on a Western blot, where the majority of α-synuclein is present as various polymeric aggregates (appearing as a high molecular weight smear between ~23 and ~300 kDa), with a smaller monomeric band appearing at ~16 kDa and various truncated monomeric forms appearing down to ~12 kDa.

One possibility is that the varying higher molecular weight forms of α-synuclein are distributed across such a large number of protein spots on a 2D gel that the amount of protein in each individual spot drops below the limit of detection or is masked by other more highly abundant proteins with the same pI and molecular weight. However, this would be difficult to account for the large amount of aggregated forms detected via Western blotting. Given that the total quantities of α-synuclein correlate between the 2D gels and the Western blot, it is more likely that α-synuclein remains aggregated during the 1-DE process prior to probing with the α-synuclein antibody (for Western blotting), but is disaggregated into its monomeric components by the 2-DE process (for DIGE).

This may be due to the presence of the chaotropic agents urea and thiourea and the detergent CHAPs in the 2D sample buffer (TUC) and denaturing under current during the isoelectric focusing step. After immunocapture, inclusions were solubilised into TUC buffer regardless of the intended downstream analysis method, then precipitated with a ReadyPrep 2D Clean-up Kit (BioRad) and resolubilised into either TUC (for 2D analysis) or 4x 1D Sample Buffer (for 1D analysis). While reduction and alkylation of the sample occurs in 2-DE as opposed to reduction alone in 1-DE, α-synuclein contains no cysteine residues [39], so the addition of an alkylation step is unlikely to contribute to this disaggregation of the protein. The presence of urea alone is also unlikely to be solely responsible, as the addition of urea to the 1D sample buffer has little affect on the aggregation state of α-synuclein (data not shown). The appearance of α-synuclein at a higher molecular weight on 1D gels may also be due to forming non-covalent bonds with other proteins, which

causes a shift in the apparent molecular weight. Thus, while the exact mechanism is not known, it appears that the aggregated α-synuclein apparent in 1-DE is disaggregated to appear in its monomeric form on 2D gels.

6.4.5 Critique of α-synuclein quantification from inclusion preparations

There are several explanations for why the relative quantity of α-synuclein was found to be greatest in the preparations of immunocaptured GCIs (12%), with less in LBs (8.5%) and less still in the normal control preparation (4%). Four possibilities include:

- The preparation consists of purified inclusions containing similar quantities of α-synuclein, with additional immunocapture of soluble α-synuclein occurring.

- The preparation consists of purified inclusions containing similar quantities of α-synuclein, with the additional immunocapture of insoluble α-synuclein or early stage inclusions consisting mostly of an α-synuclein core.

- The preparation consists of a consistent background of non-specific proteins that bound to the primary antibody during immunocapture, with a variable amount of captured inclusions consisting mostly of α-synuclein.

- An accurate reflection of the biology, with the preparation consisting of purified inclusions with differing incorporation of α-synuclein within the different inclusion types.

To prevent the immunocapture of soluble α-synuclein (hypothesis #1), the centrifugation steps of the purification procedure were designed to separate soluble α-synuclein from aggregates (inclusions) prior to the addition of the antibody. Given that the homogenates from MSA, DLB and normal cases all contained similar amounts of α-synuclein (as shown by Western blotting, Figure 6.10), if soluble α-synuclein was being captured in addition to aggregates, we would expect to see a much greater enrichment of α-synuclein in the normal control. Instead, we see less α-synuclein in the immunocaptured fraction of the normal control than in the matched homogenate, with very little monomeric α-synuclein present. Thus, it is unlikely that soluble α-synuclein is present in the immunocaptured preparations.

To prevent the immunocapture of insoluble α-synuclein and early-stage aggregates (hypothesis #2), the initial centrifugation step at 1,000x g in the purification procedure was designed to separate inclusions from smaller insoluble structures. This initial pelleting and series of following washes – after pelleting, after the density gradient, after the DNase digestion, and after the trypsin digestion – makes it unlikely that smaller aggregates of insoluble α-synuclein would remain by the time the antibody addition was performed and thus it is unlikely that these would appear in the immunocaptured preparation.

If only a small number of inclusions (consisting mostly of α-synuclein) were captured along with a large background of non-specific proteins (hypothesis #3), then we would expect a similar amount of protein to be captured from each preparation. However, the normal control gives a much lower protein yield per tube of homogenate (~35µg) compared to MSA (~200 µg) preparations, even when the same ratio of antibody to homogenate is used for the immunocapture, indicating specific binding of inclusions by the primary antibody. However, the presence of some non-inclusion proteins cannot be excluded, either due to non-specific binding to the primary or secondary antibodies or directly binding to the beads. Given the prior testing of the antibodies for specificity, direct binding to the beads is the most likely scenario and this may account for the small amount of protein capture (~15 µg) that occurred in a secondary-only control experiment in Chapter 5.3.3. Immunohistochemistry has also been used to show that the immunocaptured fractions consist mostly of inclusions with very little non-inclusion material (Figure 4.2). Thus, the large majority of proteins in the immunocaptured fractions are expected to arise from captured inclusions.

In summary, there is evidence for the presence of α-synuclein in higher relative abundance in GCIs compared to LBs (hypothesis #4). This may reflect a higher level of toxic α-synuclein present in MSA compared to DLB, or it may relate to how α-synuclein is sequestered into inclusions in these disease states. The direct transport of α-synuclein into LBs in DLB may require the presence of additional proteins, thus diluting the relative abundance of α-synuclein within LBs compared to GCIs.

6.5 Conclusion

The optimised GCI purification method, developed in Chapters 3 and 4, was successfully adapted to the purification of LBs from DLB brain tissue. Reproducible yields were obtained and the yield of LBs from the DLB cases was approximately 20% of the yield of GCIs from a comparable amount of MSA tissue. 348 protein identifications were made by mass spectrometry of trypsin-digested complex mixtures of solubilised immunocaptured LBs, including 55 vesicle-related proteins.

The biological variation in the protein composition between LBs purified from different DLB cases and between LBs and GCIs was similar (~85% similarity at the <1.5-fold differential expression level), thus a larger number of samples are needed to distinguish the overall biological variance between inclusion types from the biological variance between cases with statistical significance, or to determine whether in fact such a difference exists.

When the high abundance inclusion proteins – α-synuclein, α-β-crystallin, 14-3-3 and tubulin – were quantified from the DIGE gels, GCIs were shown to consist of approximately 12% α-synuclein, compared to 8.5% in LBs and 4% in the normal control. α-β-crystallin and 14-3-3 protein concentrations were also highest in GCIs, with less in LBs and less still in the normal control. However, the amount of tubulin remains similar between inclusion types, with just over 1% tubulin present in each, which may suggest a residual amount of cytoskeleton surrounding each inclusion after the immunocapture process, rather than its presence within the inclusion itself.. A positive linear relationship was found between the relative quantities of α-synuclein and the molecular chaperon α-β-crystallin that interacts with α-synuclein to prevent its fibrillisation, which may suggest that the α-β-crystallin present in inclusions is bound to the α-synuclein.

MSA, DLB and normal brain homogenates were all shown to contain similar levels of α-synuclein. The immunocaptured GCI and LB samples showed a 6.4- and 3.6-fold enrichment of α-synuclein, respectively, from the homogenate. A disproportional enrichment of polymeric to monomeric forms of α-synuclein (~4:1 ratio) was observed, suggesting a greater rate of incorporation of polymeric forms of α-synuclein into inclusions, which agrees with previous findings [39, 61]. The

relative quantities of α-synuclein in each sample type analysed by 2D-DIGE was verified by Western blotting. While several hypotheses can be proposed to account for why the relative quantity of α-synuclein is different between the immunocaptured preparations from different types of homogenate (MSA v DLB v normal), the data supports a biological difference in relative α-synuclein quantity between inclusion types.

7 Comparison of Lewy Bodies and Glial Cytoplasmic Inclusions

7.1 Introduction

In Chapters 5 and 6, the protein constituents of Glial Cytoplasmic Inclusions and Lewy Bodies were determined by mass spectrometry of solubilised inclusions. Thus, it is now possible to compare purified GCIs to purified LBs to determine which proteins are common to both inclusion types, and thus may be related to the inclusion formation process. The identification of GCI-specific inclusion proteins may also provide an insight into the mechanism whereby α-synuclein is sequestered into GCIs from its original neuronal origin.

One hypothesis behind the role of inclusions in the cell is that they are a protective mechanism that sequesters potentially toxic excess or misfolded α-synuclein that cannot be degraded by the cell [8, 38]. Identifying the proteome of LBs and GCIs may elucidate which proteins are involved in the packaging of α-synuclein into inclusions and potentially the pathway by which this occurs. While α-synuclein is present in neurons and thus may be incorporated into LBs through numerous mechanisms, α-synuclein is not expressed in oligodendrocytes [48] which supports the selective targeting of this protein to GCIs.

7.1.1 Hypotheses

The hypotheses supporting these experiments were:

- Lewy Bodies and GCIs will contain a set of proteins in common as well as proteins unique to each inclusion type. Identifying the common and unique proteins in both inclusion types may elucidate the formation process of these inclusions and reflect the toxic effects of the disease.

7.1.2 Aims

The aims of these experiments were:

- To identify inclusion proteins that are common to both GCIs and LBs and to relate them to the inclusion formation process.

- To validate the mass spectrometry identifications of vesicle-related inclusion proteins by immunohistochemistry.

7.2 Materials and Methods

7.2.1 Immunofluorescence

Immunofluorescence was performed on fixed sections of MSA tissue (case SA0101, superior temporal) and DLB tissue (Case SA0083, superior frontal) as described in Chapter 2.10.2 and imaged as described in Chapter 2.10.3. Dual staining was performed on both MSA and DLB sections using a sheep anti-α-synuclein primary antibody (antibody no. 1, Table 2.1) used at 1:1000 (1 µg/mL) with either A) a rabbit anti-SNAP25 primary antibody (antibody no. 6, Table 2.1) used at 1:500, B) a rabbit anti-VAMP2 primary antibody (antibody no. 7, Table 2.1) used at 1:500, A) a rabbit anti-synaptotagmin-1 primary antibody (antibody no. 8, Table 2.1) used at 1:250, or D) a rabbit anti-synaptophysin primary antibody (antibody no. 9, Table 2.1) used at 1:250. Anti-sheep Cy-3 conjugated secondary (antibody no. 19, Table 2.2) and anti-rabbit Alexa488 conjugated secondary (antibody no. 20, Table 2.2) were both used at 1:200 (3.75 µg/mL and 5 µg/mL, respectively). Nuclei were stained with DAPI in the mounting media. Samples were viewed and photographed on an Olympus BX50 Fluorescence microscope and channels were merged in Adobe Photoshop version CS5, as described in Chapter 2.10.3.

7.3 Results

7.3.1 Comparison of Lewy Body and Glial Cytoplasmic Inclusion proteins

160 GCI proteins were consistently identified by mass spectrometry, defined as being identified in at least 4 out of 5 MSA cases analysed, and 170 LB proteins were consistently identified, defined as being identified in 2 out of 2 DLB cases analysed. Four cytokeratin proteins that were identified in both groups were excluded as contaminants. There were 112 proteins identified consistently in both GCIs and LBs, giving an overlap of 68% between GCI and LB proteins. 25% of these proteins identified in common were vesicle-related and 22% were previously established components of LBs or GCIs (Figure 7.1).

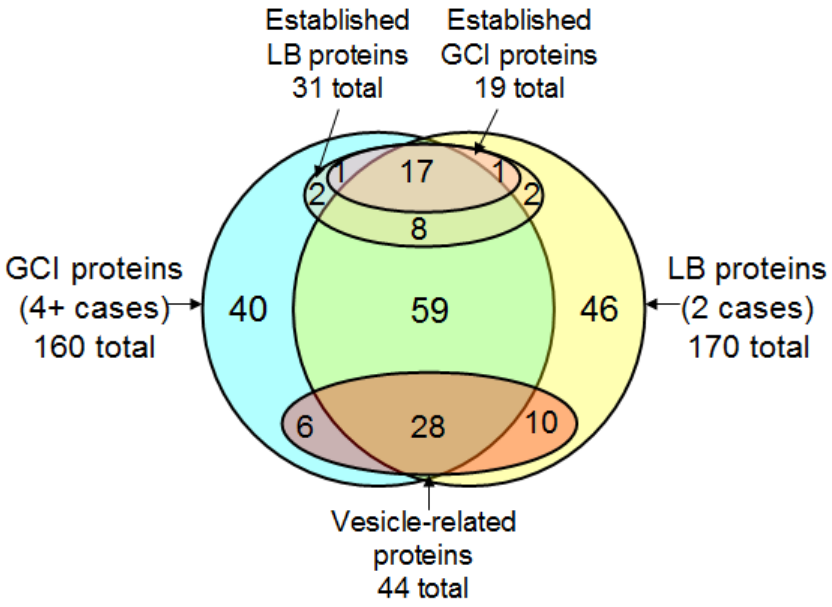

Figure 7-1: Venn diagram of GCI identifications from 4+ MSA cases and LB protein identifications from 2+ DLB cases
Solubilised Inclusions isolated from 5 MSA cases and 2 DLB cases were trypsin-digested and the digested peptides were analysed by LTQ Orbitrap XL mass spectrometry. 160 proteins were identified in 4 or more MSA cases (excluding keratins) and 170 proteins were identified in both DLB cases (excluding keratins). The overlap between the identification of established GCI and LB proteins and vesicle-related proteins with the total protein identifications is shown. Note: Overlap between vesicle-related proteins and established GCI and LB proteins has been omitted for the sake of clarity. See Figure 7.2 for these relationships.

The 112 proteins that were identified consistently in both GCIs and LBs are listed in Table 7.1, classified by functional groups. Further details from the MS identification of these proteins are listed in Appendix A (GCI proteins) and Appendix O (LB proteins). Of the 48 proteins that were identified consistently in GCIs but not LBs, 35 proteins were still identified in one DLB case (Table 7.2) and 13 proteins were not identified at all in LBs (Table 7.3). Of the 58 proteins that were identified consistently in LBs but not GCIs, 49 proteins were still identified in one to three MSA cases (Table 7.4) and 9 proteins were not identified at all in GCIs (Table 7.5).

The overlap between the synaptic vesicle-related proteins and established GCI and LB proteins that were consistently identified in both GCIs and LBs in this study is shown in Figure 7.2. The details of the 12 vesicle-related proteins that have not previously been established in GCIs or LBs are shown in Table 7.6.

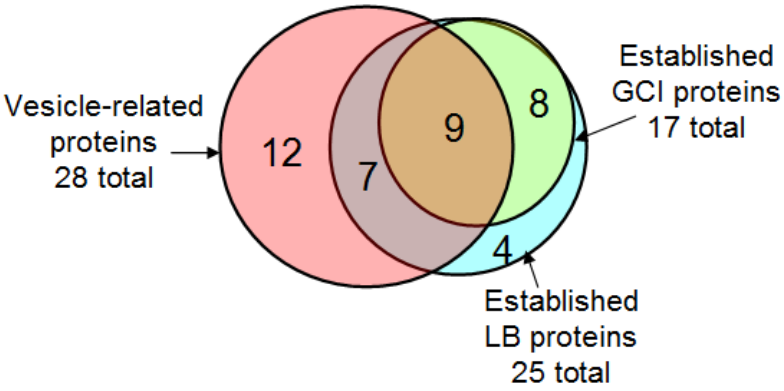

Figure 7-2: Venn diagram of vesicle-related proteins and established GCI and LB proteins identified in 4+ MSA cases and 2 DLB cases
The overlap between the vesicle-related proteins and the established GCI and LB proteins from Figure 7.1 is shown in the diagram.

Table 7-1: MS Identification of 112 proteins identified consistently in both GCIs (4+ cases) and LBs (2 cases)

Protein	Acc. No.[a]	Also found in: 1D gel[b]	Also found in: 2D gel[c]	Calc. pI	Calc. MW (Da)	Avg. No. of Peptides (GCI)[d]	Avg. No. of Peptides (LB)[e]
Established synaptic vesicle proteins							
Synaptosomal-associated protein 25	P60880			4.77	23300	3.9	3.8
V-type proton ATPase catalytic subunit A	P38606	X		5.52	68300	4.8	5.5
V-type proton ATPase subunit B, brain isoform	P21281			5.81	56465	3.6	3.3
V-type proton ATPase subunit d 1	P61421			5.00	40300	3.7	3.8
Transiently-associated synaptic vesicle proteins - cytoskeletal							
Actin, cytoplasmic 1	P60709	X	X	5.48	41700	7.6	7.0
Alpha-internexin	Q16352			5.40	55357	6.5	6.5
Neurofilament light polypeptide	P07196	X		4.65	61500	7.5	9.0
Neurofilament medium polypeptide	P07197			4.91	102400	8.4	14.3
Tubulin alpha-1A chain	Q71U36	X	X	5.06	50104	14.1	14.0
Tubulin alpha-4A chain	P68366		X	5.06	49900	10.3	11.0
Tubulin alpha-1B chain	P68363	X	X	5.06	50120	14.0	14.0
Tubulin beta chain	P07437		X	4.89	49639	15.0	16.3
Tubulin beta-2A chain	Q13885	X	X	4.89	49875	15.7	17.5
Tubulin beta-2C chain	P68371	X	X	4.89	49799	16.0	16.3
Tubulin beta-3 chain	Q13509	X	X	4.93	50400	11.9	13.3
Tubulin beta-4 chain	P04350	X	X	4.88	49554	16.3	16.8
Transiently-associated synaptic vesicle proteins - others							
Beta-soluble NSF attachment protein	Q9H115		X	5.47	33500	5.6	7.0
Calcium/calmodulin-dependent protein kinase II alpha	Q8IWE0			7.20	54054	4.5	2.7
Calcium/calmodulin-dependent protein kinase type II subunit delta	Q13557			7.25	56300	3.7	3.3
Clathrin heavy chain 1	Q00610	X		5.69	191500	8.8	10.3
Cytoplasmic dynein 1 heavy chain 1	Q14204	X		6.40	532072	12.8	8.5
Heat shock protein HSP 90-alpha	P07900		X	5.02	84607	11.8	12.0
Heat shock protein HSP 90-beta	P08238	X	X	5.03	83200	12.5	13.8
Microtubule-associated protein 1B	P46821			4.81	270500	8.6	13.5
Synapsin-1	P17600			9.83	74100	2.8	2.3

Protein	Acc. No.[a]	Also found in: 1D gel[b]	Also found in: 2D gel[c]	Calc. pI	Calc. MW (Da)	Avg. No. of Peptides (GCI)[d]	Avg. No. of Peptides (LB)[e]
Putative synaptic vesicle proteins							
Gamma-enolase	P09104			5.03	47200	4.4	4.3
L-lactate dehydrogenase B chain	P07195			6.05	36615	2.3	3.8
Reticulon-4	Q9NQC3			4.50	129900	3.1	2.3
Vesicle-related proteins – others							
Alpha-synuclein	P37840	X	X	4.70	14500	3.6	4.0
Syntaxin-binding protein 1	P61764	X		6.96	67500		7.3
Vesicle-fusing ATPase	P46459	X	X	6.95	82500	5.7	4.3
Chaperones							
60 kDa heat shock protein, mitochondrial	P10809	X	X	5.87	61000	5.5	6.8
78 kDa glucose-regulated protein	P11021	X	X	5.16	72288	11.5	11.5
Alpha-crystallin B chain	P02511		X	7.33	20100	4.7	4.3
Calnexin	P27824	X		4.60	67526	6.5	7.3
Calreticulin	P27797			4.44	48112	6.9	7.8
Clusterin	P10909			6.27	52500	2.8	4.3
Endoplasmin	P14625	X	X	4.84	92400	11.2	9.3
Prostaglandin E synthase 3	Q15185			4.54	18700	2.4	2.0
Protein disulfide-isomerase	P07237	X	X	4.87	57100	2.9	2.7
Protein disulfide-isomerase A3	P30101	X	X	6.35	56700	6.9	4.5
Cytoskeletal components & cytoskeletal-associated proteins							
Band 4.1-like protein 3	Q9Y2J2			5.19	120600	3.4	3.0
Glial fibrillary acidic protein	P14136	X	X	5.52	49800	12.8	14.0
Myristoylated alanine-rich C-kinase substrate	P29966	X		4.45	31500	3.8	4.0
Vimentin	P08670			5.12	53600	5.1	7.8
Basement membrane proteins							
Basement membrane-specific heparan sulfate proteoglycan core protein	P98160			6.51	468532	9.3	14.0
Collagen alpha-1(IV) chain	P02462			8.28	160500	2.1	2.0
Laminin subunit gamma-1	P11047	X		5.12	177489	8.1	12.8

Protein	Acc. No.[a]	Also found in: 1D gel[b]	Also found in: 2D gel[c]	Calc. pI	Calc. MW (Da)	Avg. No. of Peptides (GCI)[d]	Avg. No. of Peptides (LB)[e]
Cell membrane proteins							
2',3'-cyclic-nucleotide 3'-phosphodiesterase	P09543	X	X	9.07	47500	8.8	7.5
Adipocyte plasma membrane-associated protein	Q9HDC9			6.16	46451	2.2	2.0
Brain acid soluble protein 1	P80723			4.63	22680	4.6	3.8
Myelin proteolipid protein	P60201			8.35	30057	2.9	3.0
Mitochondrial proteins							
ATP synthase subunit alpha, mitochondrial	P25705	X	X	9.13	59714	8.8	7.8
ATP synthase subunit beta, mitochondrial	P06576	X	X	5.40	56500	12.6	10.8
Cytochrome b-c1 complex subunit 1, mitochondrial	P31930		X	6.37	52612	4.7	3.0
Mitochondrial inner membrane protein	Q16891	X		6.48	83600	2.0	2.3
NADH dehydrogenase [ubiquinone] iron-sulfur protein 3, mitochondrial	O75489		X	7.50	30223	2.9	2.7
ER proteins							
Erlin-2	O94905	X	X	5.62	37800	4.2	2.5
Glucosidase 2 subunit beta	P14314			4.41	59400	2.9	4.0
Membrane-associated progesterone receptor component 1	O00264			4.70	21658	3.4	3.5
Neutral alpha-glucosidase AB	Q14697	X		6.14	106807	3.1	3.0
Reticulocalbin-2	Q14257			4.40	36854	3.0	2.7
Thioredoxin domain-containing protein 5	Q8NBS9			5.97	47600	2.0	2.0
Secreted proteins							
Apolipoprotein E	P02649			5.73	36132	3.4	3.0
Calumenin	O43852			4.64	37100	3.6	2.0
Tubulointerstitial nephritis antigen-like	Q9GZM7			6.99	52353	5.3	7.8
Transporter proteins							
Serotransferrin	P02787	X	X	7.12	77014	5.2	3.7
Sodium/potassium-transporting ATPase subunit alpha-3	P13637	X		5.38	111700	7.5	11.8
Glycolysis							
Hexokinase-1	P19367	X		6.80	102400	3.9	3.3
Triosephosphate isomerase	P60174			6.90	26700	3.8	4.0

Protein	Acc. No.[a]	Also found in: 1D gel[b]	Also found in: 2D gel[c]	Calc. pI	Calc. MW (Da)	Avg. No. of Peptides (GCI)[d]	Avg. No. of Peptides (LB)[e]
Kinases							
Creatine kinase B-type	P12277	X	X	5.59	42600	10.3	9.3
Pyridoxal kinase	O00764			6.13	35100	2.7	3.3
Adaptor proteins							
14-3-3 protein beta/alpha	P31946	X	X	4.83	28100	4.6	4.3
14-3-3 protein epsilon	P62258	X	X	4.74	29155	5.1	4.3
14-3-3 protein eta	Q04917	X	X	4.84	28201	3.0	2.3
14-3-3 protein gamma	P61981	X	X	4.89	28285	4.1	4.0
14-3-3 protein theta	P27348	X	X	4.78	27747	5.0	4.8
14-3-3 protein zeta/delta	P63104	X	X	4.79	27728	5.7	5.3
G protein Signalling							
Guanine nucleotide-binding protein G(i) subunit alpha-2	P04899			5.54	40425	4.5	5.5
Guanine nucleotide-binding protein G(I)/G(S)/G(T) subunit beta-1	P62873			6.00	37400	5.6	4.8
Guanine nucleotide-binding protein G(I)/G(S)/G(T) subunit beta-2	P62879			6.00	37307	4.2	3.7
Isoform Alpha-2 of Guanine nucleotide-binding protein G(o) subunit alpha	P09471-2			5.90	40061	5.5	3.3
Protein degradation (UPS and ALP)							
26S protease regulatory subunit 7	P35998			5.95	48600	2.5	2.7
F-box only protein 2	Q9UK22			4.37	33300	3.2	2.3
Polyubiquitin-C	P0CG48			7.66	77000	2.3	2.3
Ubiquitin carboxyl-terminal hydrolase 5	P45974			5.03	95700	4.5	4.8
Ubiquitin carboxyl-terminal hydrolase isozyme L1	P09936			5.48	24808	2.5	3.0
Ubiquitin-like modifier-activating enzyme 1	P22314	X		5.76	117774	6.4	5.0
Neurogenesis							
Dihydropyrimidinase-related protein 2	Q16555			6.38	62255	6.8	6.5
Neural cell adhesion molecule 1	P13591	X		4.87	94500	5.8	4.0

Protein	Acc. No.[a]	Also found in: 1D gel[b]	Also found in: 2D gel[c]	Calc. pI	Calc. MW (Da)	Avg. No. of Peptides (GCI)[d]	Avg. No. of Peptides (LB)[e]
Nuclear and transcription proteins							
ATP-dependent RNA helicase A	Q08211			6.84	140869	4.5	3.3
Histone H4	P62805			11.36	11360	2.7	3.7
Lupus La protein	P05455			7.12	46800	3.5	3.3
Nucleolin	P19338			4.70	76600	4.6	4.3
Nucleophosmin	P06748			4.78	32600	3.0	3.3
Prohibitin	Q6PUJ7			5.76	29802	2.8	3.0
Prohibitin-2	Q99623	X		9.83	33300	3.7	2.3
Transcription intermediary factor 1-beta	Q13263			5.77	88500	4.7	2.0
X-ray repair cross-complementing protein 5	P13010			5.81	82652	4.3	3.5
X-ray repair cross-complementing protein 6	P12956	X		6.64	69800	3.1	2.7
Protein biosynthesis and ribosomal proteins							
Heterogeneous nuclear ribonucleoprotein A1	P09651	X	X	9.13	38700	3.6	2.0
Heterogeneous nuclear ribonucleoprotein H2	P55795			6.30	49232	3.2	2.0
Heterogeneous nuclear ribonucleoprotein K	P61978			5.54	50944	4.5	5.3
Heterogeneous nuclear ribonucleoprotein U-like protein 2	Q1KMD3			4.91	85052	3.0	2.0
Heterogeneous nuclear ribonucleoproteins A2/B1	P22626		X	8.95	37400	2.6	2.8
Heterogeneous nuclear ribonucleoproteins C1/C2	P07910	X		5.08	33600	2.9	3.0
Others							
Annexin A5	P08758			5.05	35900	4.0	6.3
Carbonyl reductase [NADPH] 1	P16152	X	X	8.32	30356	6.2	4.3
Ferritin heavy chain	P02794		X	5.55	21212	2.9	2.0
Glutathione S-transferase Mu 3	P21266		X	5.54	26500	3.5	2.3
Hemoglobin subunit beta	P68871	X	X	7.28	15988	4.5	4.8
Myosin light polypeptide 6	P60660			4.65	16919	2.8	3.5

[a] SwissProt accession number
[b] 1D gel slices of MSA case (Chapter 5.3.1.2)
[c] 2D gel spots of MSA case (Chapter 5.3.1.3)
[d] Average number of unique peptides sequenced in GCI samples
[e] Average number of unique peptides sequenced in LB samples

Table 7-2: MS Identification of 35 proteins consistently identified in GCIs (4+ cases) but not consistently in LBs (1 case only)

Protein	Acc. No.[a]	Also found in:		Calc. pI	Calc. MW (Da)	Avg. No. of Peptides (GCI)[d]	Avg. No. of Peptides (LB)[e]
		1D gel[b]	2D gel[c]				
Transiently-associated synaptic vesicle proteins - cytoskeletal							
Elongation factor 1-alpha 1	P68104	X	X	9.01	50109	3.7	3.5
Spectrin beta chain, brain 1	Q01082	X		5.57	274400	8.8	13.5
Transiently-associated synaptic vesicle proteins - others							
Isoform 2 of Dynamin-1	Q05193-2			6.87	97200	7.0	3.0
Glyceraldehyde-3-phosphate dehydrogenase	P04406	X	X	8.46	36000	2.6	2.0
Heat shock 70 kDa protein 12A	O43301			6.77	74900	3.6	2.0
Putative synaptic vesicle proteins							
Phosphoglycerate mutase 1	P18669			7.18	28800	3.6	3.5
Vesicle-related proteins – others							
Transmembrane emp24 domain-containing protein 2	Q15363		X	5.17	22700	2.0	2.0
Chaperones							
Heat shock-related 70 kDa protein 2	P54652			5.74	69978	6.3	9.5
Protein disulfide-isomerase A4	P13667	X		5.07	72887	3.5	3.0
Cytoskeletal-associated proteins							
Cofilin-1	P23528			8.09	18500	3.1	3.0
Microtubule-associated protein RP/EB family member 2	Q15555			5.57	37000	2.4	2.0
Tubulin-folding cofactor B	Q99426			5.15	27300	2.5	3.0
Mitochondrial proteins							
ATP synthase subunit d, mitochondrial	O75947	X		5.30	18500	2.9	3.0
CDGSH iron-sulfur domain-containing protein 1	Q9NZ45			9.09	12191	2.1	2.0
Complement component 1 Q subcomponent-binding protein, mitochondrial	Q07021	X		4.84	31300	2.8	2.5
Cytochrome b-c1 complex subunit 2, mitochondrial	P22695	X	X	8.63	48413	3.0	2.0
Isocitrate dehydrogenase [NADP], mitochondrial	P48735	X	X	8.69	50900	2.6	2.0
NADH-ubiquinone oxidoreductase 75 kDa subunit, mitochondrial	P28331	X	X	6.23	79400	3.9	3.5

Protein	Acc. No.[a]	Also found in:		Calc. pI	Calc. MW (Da)	Avg. No. of Peptides (GCI)[d]	Avg. No. of Peptides (LB)[e]
		1D gel[b]	2D gel[c]				
Transporter proteins							
Astrocytic phosphoprotein PEA-15	Q15121			5.02	15031	2.8	4.0
Chloride intracellular channel protein 4	Q9Y696			5.59	28800	2.8	2.0
Voltage-dependent anion-selective channel protein 1	P21796		X	8.54	30754	6.5	3.5
Voltage-dependent anion-selective channel protein 2	P45880			7.56	31500	4.0	2.0
Voltage-dependent anion-selective channel protein 3	Q9Y277			8.66	30639	4.4	2.5
Neurogenesis							
Neuromodulin	P17677			4.72	24788	3.2	2.0
Nuclear and transcription proteins							
Importin subunit beta-1	Q14974			4.78	97100	3.1	2.0
mRNA-related proteins							
Cold-inducible RNA-binding protein	Q14011			9.51	18600	2.4	2.5
Endonuclease domain-containing 1 protein	O94919			5.71	55000	2.2	2.5
Protein biosynthesis and ribosomal proteins							
Eukaryotic initiation factor 4A-I	P60842			5.48	46100	2.5	2.0
Heterogeneous nuclear ribonucleoprotein A3	P51991	X	X	9.01	39600	3.1	2.5
Others							
Albumin (Fragment)	F6KPG5			6.04	66488	5.1	9.0
D-3-phosphoglycerate dehydrogenase	O43175		X	6.71	56614	4.8	5.5
Ferritin light chain	P02792		X	5.78	20007	2.9	2.0
Neurochondrin	Q9UBB6			5.48	78800	3.9	2.0
Secernin-1	Q12765			4.75	46400	3.3	3.5
Serine/threonine-protein phosphatase 2A 65 kDa regulatory subunit A alpha isoform	P30153			5.11	65300	2.3	6.0

[a] SwissProt accession number
[b] 1D gel slices of MSA case (Chapter 5.3.1.2)
[c] 2D gel spots of MSA case (Chapter 5.3.1.3)
[d] Average number of unique peptides sequenced in GCI samples
[e] Average number of unique peptides sequenced in LB samples

Table 7-3: MS Identification of 13 proteins consistently identified in GCIs (4+ cases) but not in LBs (0 cases)

Protein	Acc. No.[a]	Also found in:		Calc. pI	Calc. MW (Da)	Avg. No. of Peptides (GCI)[d]
		1D gel[b]	2D gel[c]			
Vesicle-related proteins – others						
Transmembrane emp24 domain-containing protein 10	P49755		X	7.44	24960	3.2
Cell membrane proteins						
Creatine kinase U-type, mitochondrial	P12532	X	X	8.34	47007	2.3
Trans-Golgi network integral membrane protein 2	O43493			5.73	51100	2.7
Mitochondrial proteins						
ATP synthase subunit gamma, mitochondrial	P36542		X	9.22	33000	2.5
Cytochrome c oxidase subunit 4 isoform 1, mitochondrial	P13073			9.51	19600	2.3
Cytochrome c1, heme protein, mitochondrial	P08574			9.00	35400	2.3
NADH dehydrogenase [ubiquinone] 1 alpha subcomplex subunit 5	Q16718	X	X	5.99	13450	2.1
Secreted proteins						
Apolipoprotein D	P05090			5.15	21262	2.0
G-protein signalling						
Rho GTPase-activating protein 1	Q07960			6.29	50404	3.2
Protein degradation						
Lysosome membrane protein 2	Q14108			5.14	54255	2.7
Neurogenesis						
Contactin-1	Q12860	X		5.90	113200	2.7
Protein biosynthesis and ribosomal proteins						
Heterogeneous nuclear ribonucleoprotein U	Q00839	X		6.00	90500	4.7
Others						
Catechol O-methyltransferase	P21964			5.47	30000	2.4

[a] SwissProt accession number
[b] 1D gel slices of MSA case (Chapter 5.3.1.2)
[c] 2D gel spots of MSA case (Chapter 5.3.1.3)
[d] Average number of unique peptides sequenced

Table 7-4: MS Identification of 49 proteins consistently identified in LBs (2 cases) but not consistently in GCIs (≤3 cases)

Protein	Acc. No.[a]	Also found in:		Calc. pI	Calc. MW (Da)	Avg. No. of Peptides (LB)[d]	Avg. No. of Peptides (GCI)[e]
		1D gel[b]	2D gel[c]				
Established synaptic vesicle proteins							
Synaptic vesicle glycoprotein 2A	Q7L0J3			5.57	82600	2.0	2.3
Vesicle-associated membrane protein 2	P63027	X		8.13	12655	2.0	2.0
Transiently-associated synaptic vesicle proteins - cytoskeletal							
Neurofilament heavy polypeptide	P12036			6.18	112400	6.0	6.3
Spectrin alpha chain, brain	Q13813	X		5.35	284400	9.5	2.0
Isoform 2 of Spectrin alpha chain, brain	Q13813-2	X		5.35	284919	8.0	9.2
Transiently-associated synaptic vesicle proteins - others							
AP-2 complex subunit beta	P63010			5.38	104500	2.7	2.3
Dynamin-1	Q05193	X		7.17	97300	5.7	2.0
Putative synaptic vesicle proteins							
6-phosphofructokinase type C	Q01813			7.55	85500	5.5	5.3
Fructose-bisphosphate aldolase C	P09972			6.87	39400	3.3	2.0
Glucose-6-phosphate isomerase	P06744			8.32	63100	2.3	2.8
Chaperones							
Heat shock cognate 71 kDa protein	P11142		X	5.52	70900	7.0	5.0
Heat shock protein beta-1	P04792			6.40	22800	2.8	2.0
Hypoxia up-regulated protein 1	Q9Y4L1		X	5.22	111300	2.0	4.4
Small glutamine-rich tetratricopeptide repeat-containing protein alpha	O43765			4.87	34000	2.0	2.0
Stress-70 protein, mitochondrial	P38646		X	6.16	73600	3.0	2.0
Cytoskeletal-associated proteins							
Gamma-synuclein	O76070			4.86	13323	3.0	2.5
Microtubule-associated protein 2	P11137			4.91	199400	4.3	4.3

Protein	Acc. No.[a]	Also found in:		Calc. pI	Calc. MW (Da)	Avg. No. of Peptides (LB)[d]	Avg. No. of Peptides (GCI)[e]
		1D gel[b]	2D gel[c]				
Basement membrane proteins							
Collagen alpha-2(IV) chain	P08572			8.66	167400	2.0	4.0
Collagen, type I, alpha 1, isoform CRA_a	D3DTX7			6.24	84688	2.0	2.0
Integrin beta-1	P05556			5.39	88357	3.0	2.5
Laminin subunit alpha-2	P24043			6.40	343700	3.0	5.5
Laminin subunit alpha-5	O15230			7.02	399479	2.8	4.5
Laminin subunit beta-2	P55268	X		6.52	195854	12.0	15.0
Nidogen-1	P14543			5.29	136300	3.8	6.0
Nidogen-2	Q14112			5.29	151200	4.0	5.0
Cell membrane proteins							
Basigin	P35613			5.66	42200	3.0	2.0
Gamma-glutamyltransferase 5	P36269			7.55	62200	2.3	2.5
Myelin basic protein	P02686			9.79	33100	3.0	2.0
Mitochondrial proteins							
Glutamate dehydrogenase 1, mitochondrial	P00367			7.80	61400	2.3	2.5
Secreted proteins							
Agrin	O00468			6.40	214706	9.8	12.0
Galectin-1	P09382			5.50	14706	2.0	2.0
ProSAAS	Q9UHG2			6.62	27356	3.0	2.0
Transporter proteins							
4F2 cell-surface antigen heavy chain	P08195			5.01	68000	3.3	2.8
Sodium/potassium-transporting ATPase subunit alpha-1	P05023	X		5.49	112800	8.0	9.6
Sodium/potassium-transporting ATPase subunit alpha-2	P50993	X		5.66	112200	8.7	8.0
Sodium/potassium-transporting ATPase subunit beta-1	P05026	X		8.53	35000	2.0	2.0
Solute carrier family 2, facilitated glucose transporter member 1	P11166			8.72	54000	2.5	2.8
Vacuolar-type H(+)-ATPase	Q53X12			6.70	95689	2.0	2.5
Protein degradation							
Ubiquitin thioesterase OTUB1	Q96FW1			4.94	31300	2.0	2.5

Protein	Acc. No.[a]	Also found in:		Calc. pI	Calc. MW (Da)	Avg. No. of Peptides (LB)[d]	Avg. No. of Peptides (GCI)[e]
		1D gel[b]	2D gel[c]				
Cell adhesion, motility and shape							
Myosin-9	P35579			5.60	226392	20.3	13.3
Myosin regulatory light chain 12A	P19105			4.81	19781	4.0	2.3
Nuclear and transcription proteins							
Polymerase I and transcript release factor	Q6NZI2			5.60	43400	3.3	3.0
mRNA-related proteins							
Ribonuclease inhibitor	P13489			4.82	49941	4.3	5.3
Protein biosynthesis and ribosomal proteins							
60S acidic ribosomal protein P0	P05388		X	5.97	34300	2.0	2.0
Others							
Acidic leucine-rich nuclear phosphoprotein 32 family member E	Q9BTT0			3.85	30700	3.5	3.3
Nicotinamide phosphoribosyltransferase	P43490		X	7.15	55487	2.0	2.0
Protein S100-B	P04271			4.59	10706	2.0	2.0
Serum albumin	P02768	X	X	6.28	69300	10.3	7.5
Serum deprivation-response protein	O95810			5.21	47100	2.3	2.0

[a] SwissProt accession number
[b] 1D gel slices of MSA case (Chapter 5.3.1.2)
[c] 2D gel spots of MSA case (Chapter 5.3.1.3)
[d] Average number of unique peptides sequenced in LB samples
[e] Average number of unique peptides sequenced in GCI samples

Table 7-5: MS Identification of 9 proteins identified in LBs (2 cases) but not in GCIs (0 cases)

Protein	Acc. No.[a]	Calc. pI	Calc. MW (Da)	Avg. No. of Peptides[b]
Cell membrane proteins				
Erythrocyte band 7 integral membrane protein	P27105	7.88	31700	2.5
Secreted proteins				
Secretogranin-2	P13521	4.75	70897	2.0
Cell adhesion, motility and shape				
CD9 antigen	P21926	7.15	25400	2.0
Nuclear and transcription proteins				
Histone H2B type F-S	P57053	10.37	13900	2.0
mRNA-related proteins				
Ras GTPase-activating protein-binding protein 2	Q9UN86	5.55	54100	2.0
Protein biosynthesis and ribosomal proteins				
Eukaryotic initiation factor 4A-II	Q14240	5.48	46400	2.0
HNRPU protein	Q96BA7	7.87	79666	4.0
Others				
Paraneoplastic antigen MA2	Q5U5Z3	4.82	41414	2.3
Protein-glutamine gamma-glutamyltransferase 2	P21980	5.22	77300	2.3

[a] SwissProt accession number
[b] Average number of unique peptides sequenced

Table 7-6: MS Identification of 12 vesicle-related proteins in both GCIs and LBs, previously unestablished in inclusions

Vesicle classification[a]	Acc. No.[b]	Name	Calc. pI	Calc. MW (Da)	Avg. Xcorr[b]	Avg. No. of Peptides[c]	Avg. % Sequence Coverage[d]
Established	P60880	*Synaptosomal-associated protein 25	4.77	23300	19.8	3.8	25.1
Established	P38606	V-type proton ATPase catalytic subunit A	5.52	68300	39.1	5.1	13.9
Established	P61421	V-type proton ATPase subunit d 1	5.00	40300	27.5	3.7	20.8
Established	P21281	V-type proton ATPase subunit B, brain isoform	5.81	56465	21.1	3.4	10.9
Transient	P60709	Actin, cytoplasmic 1	5.48	41700	123.8	7.3	34.9
Transient	Q9H115	Beta-soluble NSF attachment protein	5.47	33500	33.8	6.3	31.7
Transient	Q00610	Clathrin heavy chain 1	5.69	191500	67.7	9.5	8.5
Transient	Q14204	Cytoplasmic dynein 1 heavy chain 1	6.40	532072	95.9	10.6	3.4
Transient	P17600	Synapsin-1	9.83	74100	19.5	2.6	6.1
Putative	Q9NQC3	Reticulon-4	4.50	129900	17.1	2.7	3.9
Putative	P07195	L-lactate dehydrogenase B chain	6.05	36615	13.8	3.0	11.2
Putative	P09104	Gamma-enolase	5.03	47200	21.7	4.3	16.7

[a] Classification as an established, transiently-associated or putative novel vesicle protein, according to Burre and Volknandt (2007) [133]
[b] SwissProt accession number
[c] Average Xcorr significance score
[d] Average number of unique peptides sequenced
[e] Average % of the full-length amino acid sequence covered by identified peptides
* Presence in GCIs and LBs validated with immunofluorescence (section 7.3.3)

7.3.2 Comparison of GCI and LB protein identifications to an independent study

The protein identifications made consistently from GCIs and from brainstem LBs that were purified using immunomagnetic capture in this study were compared to the protein identifications made from cortical LBs that were purified using laser capture microdissection in a study by Leverenz *et al.* [108]. Of the 156 protein identifications made by Leverenz *et al.* [108], 45 were in common with the 112 proteins consistently found in both GCIs and LBs in this study (Figure 7.3).

The protein identifications in common between the three groups include: the established synaptic vesicle proteins SNAP25 and VATPase; the transiently-associated synaptic vesicle proteins CamKII, clathrin, dynein, MAP1B, synapsin I, actin, alpha-internexin, neurofilament (light and medium chains) and tubulin; and the established inclusion proteins α-synuclein, α-β-crystallin, and the 14-3-3s.

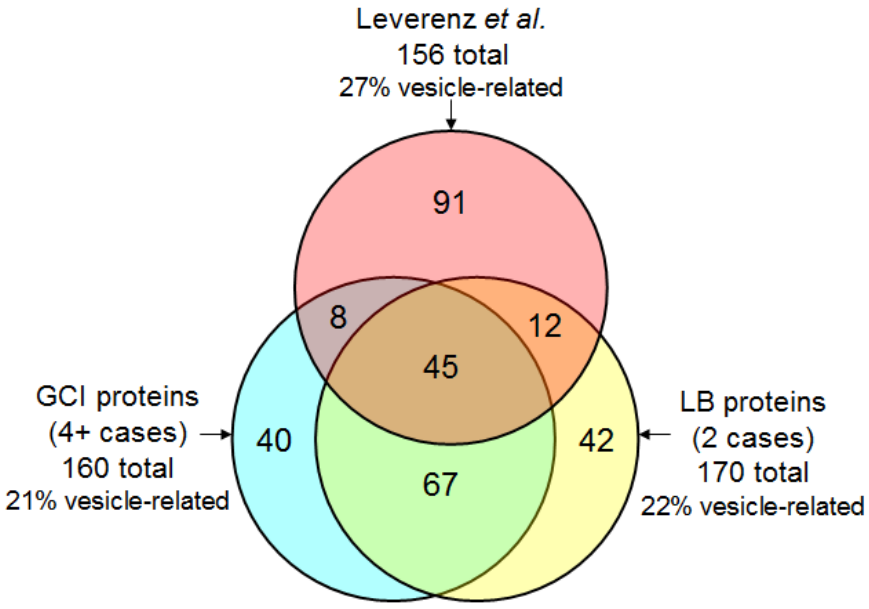

Figure 7-3: Venn diagram of GCI and brainstem LB identifications from this study with cortical LB identifications by Leverenz *et al.* [108]
Solubilised Inclusions isolated from 5 MSA cases and 2 DLB cases were trypsin-digested and the digested peptides were analysed by LTQ Orbitrap XL mass spectrometry. 160 proteins were identified in 4 or more MSA cases (excluding keratins) and 170 proteins were identified in both DLB cases (excluding keratins). The overlap between the identification of GCI and LB proteins in this study with the identification of LB proteins by Leverenz *et al.* [108] is shown,

7.3.3 Validation of selected vesicle-related protein identifications by immunofluorescence

Immunofluoresence was performed on fixed sections of tissue from MSA and DLB cases to confirm the mass spectrometry identifications of the established synaptic vesicle-related proteins synaptosomal-associated protein 25 (SNAP25), vesicle-associated membrane protein 2 (VAMP2), synaptotagmin-1 and synaptophysin in both GCIs and LBs (Table 7.7). These proteins were selected for validation based on their classification as established synaptic vesicle-related proteins and commercial antibody availability. The immunofluoresence performed in this section was courtesy of Fariba Chegini and Wei-Ping Gai.

The presence of all four of these vesicle-related proteins was confirmed in GCIs, as shown in Figure 7.4. The presence of all four proteins was also confirmed in LBs, as shown in Figure 7.5, although synaptophysin was not detected in the two DLB samples analysed by mass spectrometry.

Table 7-7: Established synaptic vesicle-related proteins chosen for validation

Protein	No. of cases protein was identified in[a]	
	MSA	DLB
SNAP25	5	2
VAMP2	2	2
Synaptotagmin-1	2	1
Synaptophysin	2	0

[a] by mass spectrometry of complex mixtures

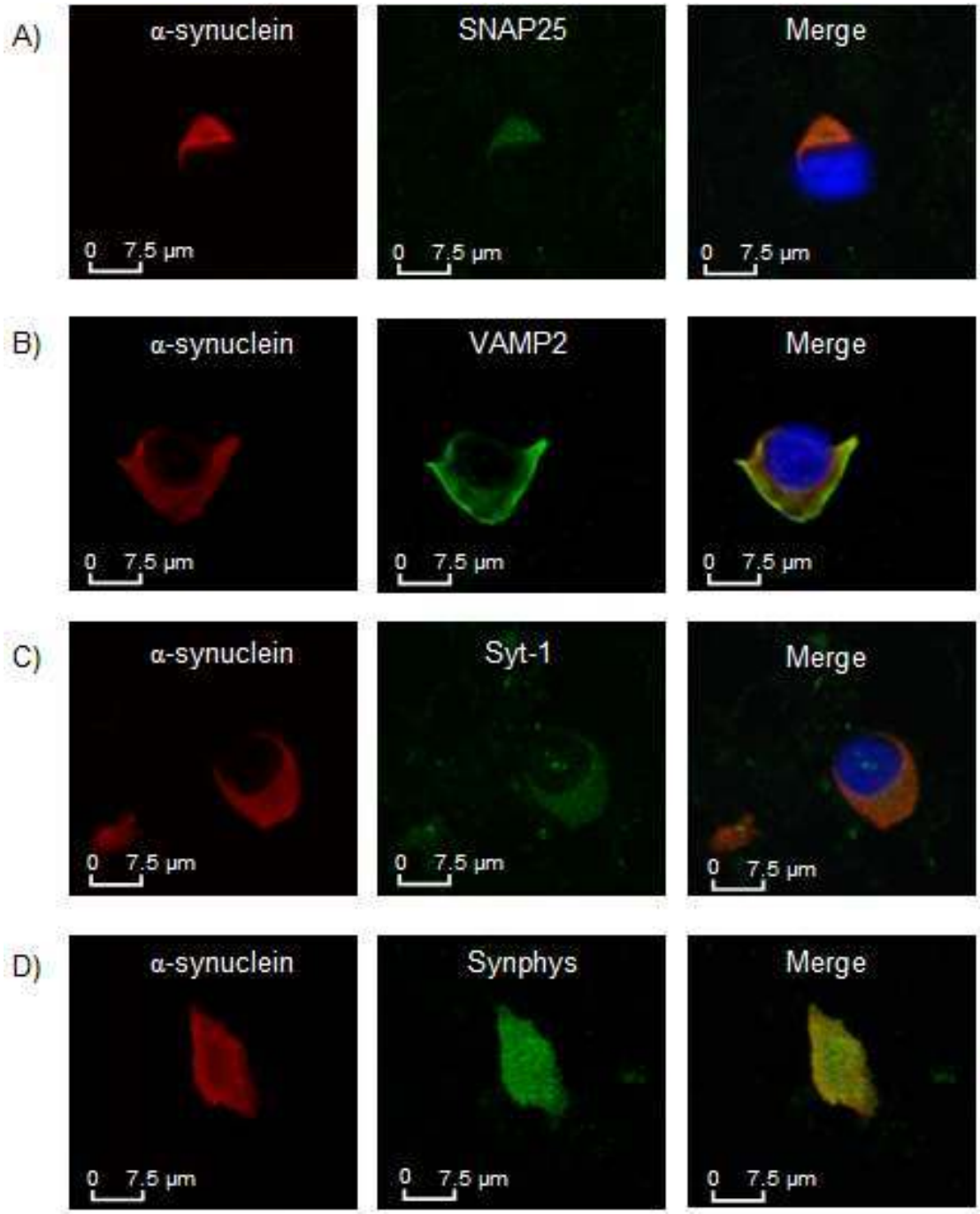

Figure 7-4: Immunofluorescence validation of the presence of synaptic vesicle-related proteins in GCIs
Fixed sections of MSA tissue were dual stained against α-synuclein and A) SNAP25, B) VAMP2, C) synaptotagmin 1 and D) synaptophysin, as described in section 7.2.1. A Cy-3-conjugated secondary antibody was used for α-synuclein, appearing red, and an Alexa-488-conjugated secondary antibody was used for the synaptic vesicle proteins, appearing green. Nuclei were stained with DAPI and appear blue.

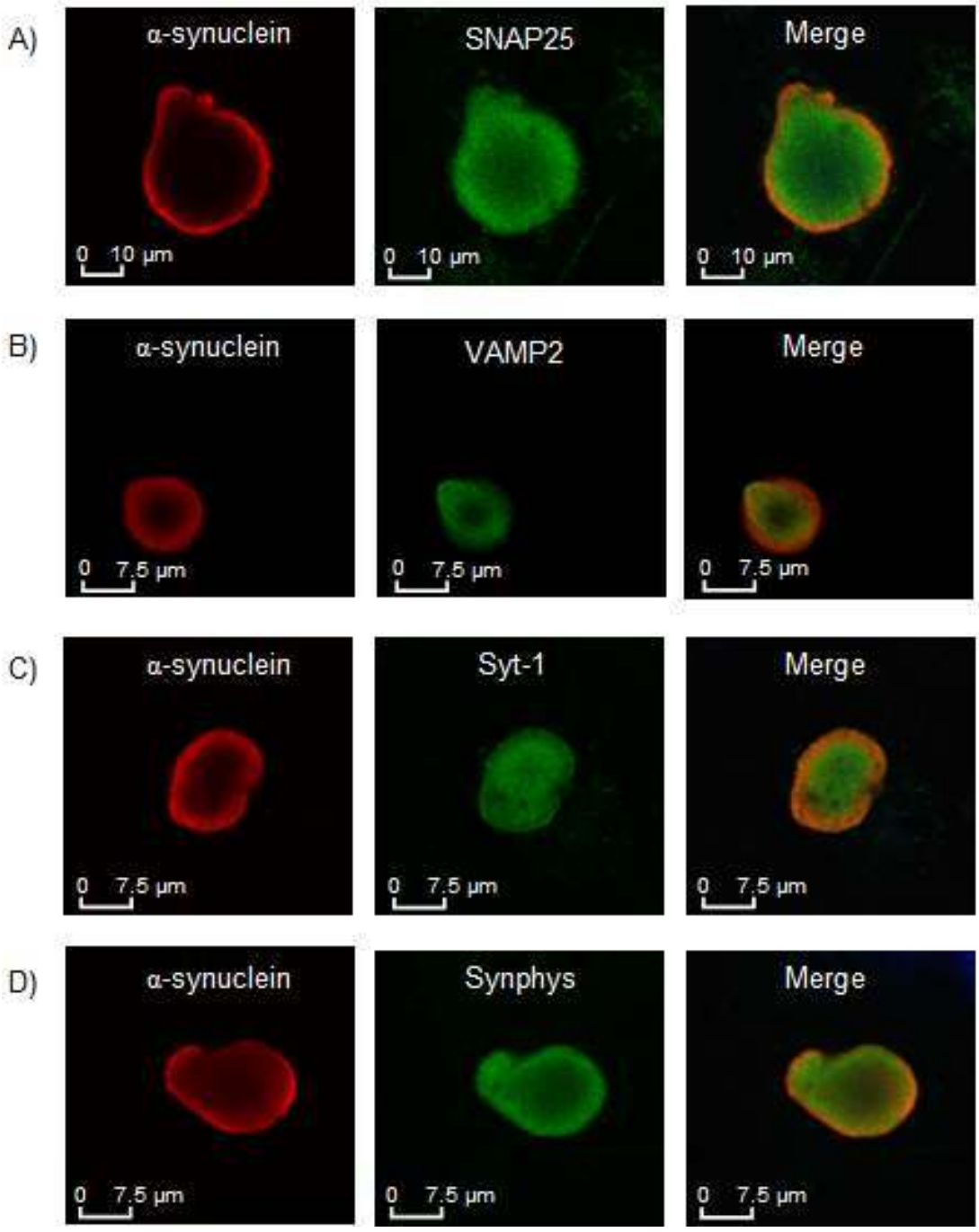

Figure 7-5: Immunofluorescence validation of the presence of synaptic vesicle-related proteins in LBs
Fixed sections of DLB tissue were dual stained against α-synuclein and A) SNAP25, B) VAMP2, C) synaptotagmin 1 and D) synaptophysin, as described in section 7.2.1. A Cy-3-conjugated secondary antibody was used for α-synuclein, appearing red, and an Alexa-488-conjugated secondary antibody was used for the synaptic vesicle proteins, appearing green.

7.4 Discussion

7.4.1 Protein identifications and overlaps

When the 160 consistently identified GCI proteins were compared to the 170 consistently identified LB proteins, 112 (68%) of the proteins were common to both GCIs and LBs. 28 of these 112 proteins in common (25%) were synaptic vesicle-related and 25 proteins (22%) had previously been established as components of LBs or GCIs. Of the 28 vesicle-related proteins found in common between GCIs and LBs, 12 proteins have not previously been established as GCI or LB proteins. The presence of one of these proteins, SNAP25, was validated in both GCIs and LBs using immunofluorescence, along with the established synaptic vesicle-related proteins VAMP2, synaptotagmin I and synaptophysin.

These proteins were selected for validation based on their classification as established synaptic vesicle-related proteins and commercial antibody availability. Synaptophysin was found in LBs via immunofluorescence despite not being detected in the two DLB samples analysed by mass spectrometry. It may have been absent or below the limit of detection for a complex mixture in the two samples analysed. As it was identified in only two out of the five MSA samples analysed, it may have been detected in LBs if a larger number of cases were analysed.

The enzyme trypsin was used to generate peptides for mass spectrometry analysis for all samples in this study. Trypsin cuts peptides after arginine and lysine residues (unless followed by a proline residue), thus all peptides generated by tryptic digestion will always carry a minimum of two positive charges. This provides a distinct advantage, as the high resolution capability of the Orbitrap analyser allows for the charge state of the precursor ion to be determined prior to MS/MS, thereby permitting rejection of all singly charged ions (which are mostly background ions) and analysing only the multiply charged ions generated by the tryptic digestion. This increases the number of peptides that the instrument can analyse, which is particularly valuable for complex mixtures of proteins. However, low molecular weight proteins with minimal lysine or arginine residues may not generate many suitable peptides for analysis. Another protease such as AspN or GluC could be used in addition to trypsin for the targeted identification of such proteins. These proteases

are not routinely used in place of trypsin as they can generate singly charged peptides.

Of the 112 proteins consistently identified between GCIs and brainstem LBs in this study, 45 proteins (40%) were also identified in cortical bodies in a study by Leverenz *et al.* [108]. The 91 proteins (out of 156) identified by Leverenz *et al.* that were not consistently identified in either GCIs or LBs in this study may arise for two reasons. Firstly, the sample analysed by Leverenz *et al.* was a single pooled sample from five DLB cases, so an identified protein may have arisen from only one or two of the contributing cases instead of being common to all cases. The data was not compared to the identifications made from single cases in this study. Secondly, these proteins may be present as contaminants from the surrounding tissue because of the laser capture process used for inclusion purification by Leverenz *et al*. As LBs were captured from 10 μm sections of tissue, and LBs are spherical in structure, the tissue immediately surrounding the LBs would also be captured and the proteins from this tissue identified in the sample alongside the genuine LB proteins.

7.4.2 The cause of neurodegenerative disorders

Overabundant or misfolded proteins would normally be degraded by either the Ubiquitin-Proteasome System (UPS) or the Autophagy-Lysosomal Pathway (ALP) (Chapter 1.4). Defects in any of the enzymes involved in either the UPS or ALP may lead to a reduction in capacity for clearing damaged proteins. If this is combined with an excess of aggregated α-synuclein, the aggregated α-synuclein may continue to form at a rate faster than which it can be cleared from the cytosol. UPS proteins identified in this study in both GCIs (≥4 out of 5 cases) and LBs (2 out of 2 cases) include the 26S protease regulatory subunit 7, UCH-L1 (also identified by Leverenz *et al.* [108]), ubiquitin-like modifier-activating enzyme 1 (also identified by Leverenz *et al.* [108]), ubiquitin carboxy-terminal hydrolase 5, and polyubiquitin C. The lysosomal marker lysosome membrane protein 2 (LAMP2) was identified in GCIs (≥4 out of 5 cases) but not in LBs.

There is also a proposed link between mitochondrial dysfunction and neurodegenerative disorders, with both chemical and genetic evidence for mitochondrial involvement in the pathogenesis of PD [98-102]. Eleven electron

transport chain proteins were identified in this study in GCIs (≥4 out of 5 cases), including components of Complex I/NADH dehydrogenase complex (3 proteins), Complex III/Cytochrome b complex (3 proteins), Complex IV/Cytochrome oxidase complex (1 protein) and Complex V/ATP synthase complex (4 proteins). Six of these proteins were also identified in LBs.

7.4.3 Potential mechanism of inclusion formation

So how does a neuron dispose of aggregated α-synuclein when its usual disposal systems fail? One possibility is that when degradation and clearance of α-synuclein is no longer possible, the aggregated α-synuclein is instead incorporated into inclusions, large insoluble aggregates of protein within the cell, to sequester potentially toxic proteins away from the remainder of the cell. How is α-synuclein, a presynaptic nerve terminal protein [38], targeted to a LB within the cell body of the neuron in PD and DLB? And in MSA, how is this neuronal protein targeted to a GCI within an oligodendrocyte?

One hypothesis for the formation of inclusions is that aggregated α-synuclein is selectively targeted to inclusions via vesicle-mediated transport. It is proposed that there is a pathway involving the release of toxic α-synuclein species from neurons, a re-uptake of α-synuclein from the extracellular space by neighbouring neurons (in PD and DLB) or oligodendrocytes (in MSA), and the targeting and intracellular trafficking of α-synuclein through retrograde vesicular transport to the inclusion within the cell body (Figure 7.6).

A vesicle-based trafficking mechanism could explain the presence of the wide range of vesicle-related proteins identified from inclusions in this study. The alternative hypothesis, which cannot be discounted, is that vesicle-related proteins are present in inclusions as a result of their interaction with α-synuclein.

7.4.3.1 Step 1: Release of extracellular α-synuclein

It is proposed that defective aggregated α-synuclein is selectively targeted into vesicles and released into the extracellular space. α-synuclein is present in human CSF and blood at low nanomolar concentrations in both normal and PD patients [198]. However, the mechanism and physiological and pathological roles that extracellular α-synuclein (eSNCA) play are not fully understood [199].

Figure 7-6: Potential mechanism of inclusion formation via vesicle-mediated transport of α-synuclein

Step 1: the release of external α-synuclein from the presynaptic nerve terminal is proposed to occur via either exocytosis of free α-synuclein, or via the release of α-synuclein-containing exosomes from a multi-vesicular body (MVB) (supported by the identification of exosomal marker CD9 in LBs)

Step 2: the re-uptake of extracellular α-synuclein into the cell body is proposed to occur by clathrin-mediated endocytosis (supported by the identification of clathrin, AP-2 complex subunits, and dynamin)

Step 3: specific targeting of α-synuclein to the inclusion is proposed to occur by retrograde vesicular transport along microtubule tracks (supported by the identification of dynein, α- and β-tubulin, dynactin and spectrin)

Step 4: the addition of α-synuclein and associated proteins to the inclusion is proposed to involve SNARE proteins, mechanism unknown (supported by the identification of Rab GTPases, SNAP25, VAMP2, syntaxin-1, VATPase and NSF)

Note: while the re-uptake of α-synuclein (steps 2-4) is shown in this diagram on the same neuron from which it is released (step 1) for the sake of clarity, the re-uptake is proposed to take place by neighbouring neurons (in DLB and PD) or oligodendrocytes (in MSA).

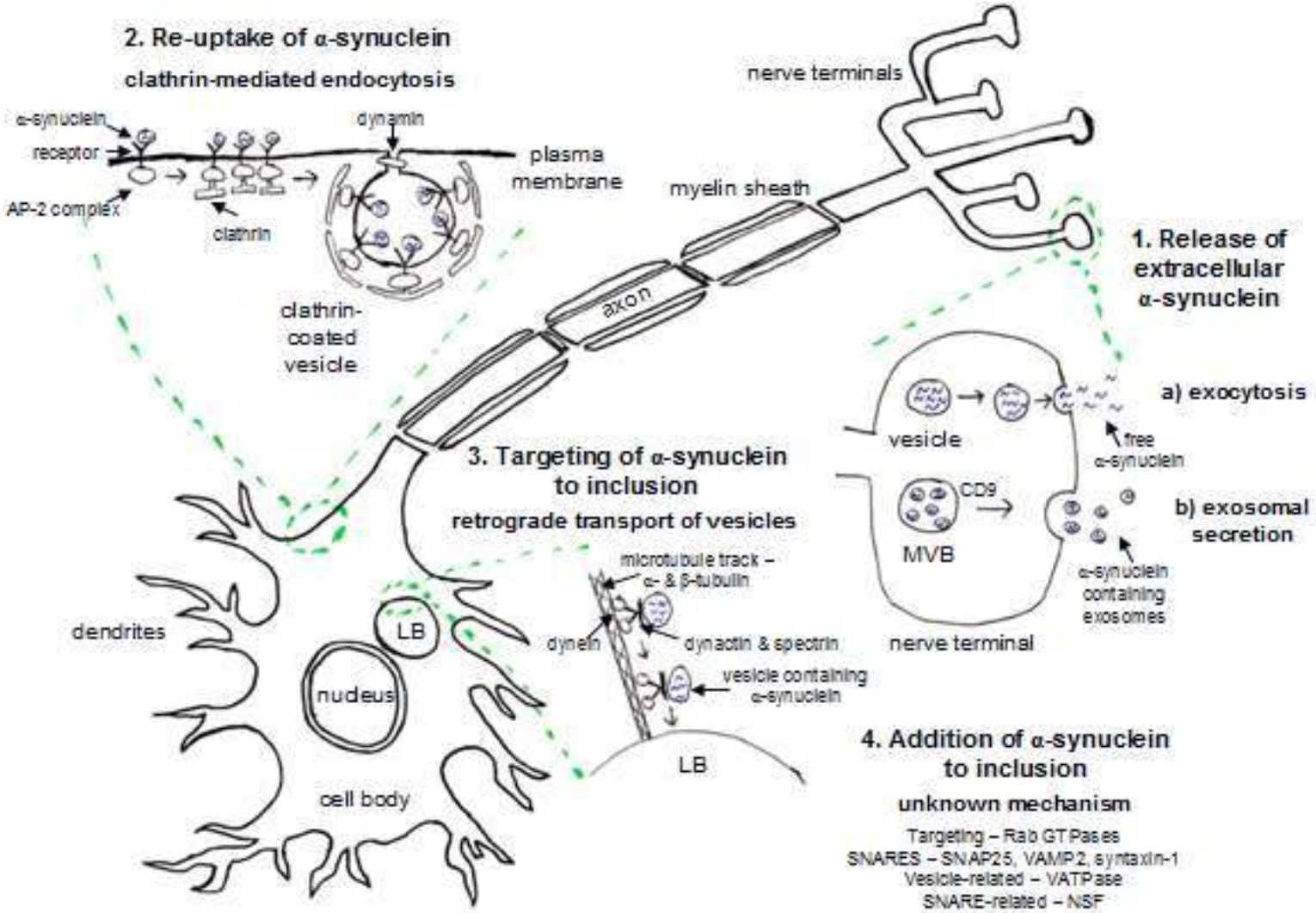
2. Re-uptake of α-synuclein
clathrin-mediated endocytosis
α-synuclein
receptor
AP-2 complex
clathrin
dynamin
plasma membrane
clathrin-coated vesicle
nerve terminals
myelin sheath
axon
1. Release of extracellular α-synuclein
a) exocytosis
vesicle
free α-synuclein
CD9
MVB
b) exosomal secretion
α-synuclein containing exosomes
nerve terminal
3. Targeting of α-synuclein to inclusion
retrograde transport of vesicles
microtubule track – α- & β-tubulin
dynein
dynactin & spectrin
vesicle containing α-synuclein
dendrites
LB
nucleus
cell body
LB
4. Addition of α-synuclein to inclusion
unknown mechanism
Targeting – Rab GTPases
SNARES – SNAP25, VAMP2, syntaxin-1
Vesicle-related – VATPase
SNARE-related – NSF

eSNCA is neurotoxic at high concentrations [200]. Some studies suggest fibrillar aggregates to be the toxic species, while others have suggested the protofibrillar or oligomeric forms [201]. eSNCA has also been shown to cause microglial activation, further contributing to neurotoxicity [200-202].

Only a small portion of cellular α-synuclein is translocated into vesicles and secreted, therefore it must be a selective process [201]. How this occurs is unknown. One hypothesis is that defective proteins are selected, translocated and subsequently discarded from cells by exocytosis [201, 203]. The highly aggregated nature of vesicular α-synuclein supports this [201]. Another hypothesis is that α-synuclein is targeted to vesicles by specific post-translational modifications [201]. The secretion of α-synuclein is enhanced when mitochondrial and proteasomal functions are impaired [202].

Lee *et al.* (2005) [199] over-expressed human α-synuclein in SH-SY5Y cells and examined the α-synuclein released into the media. An exocytotic mechanism of release was suspected, as the release of α-synuclein was inhibited at 18°C and low temperature is a classical blocker of vesicular exocytosis [199]. Vesicular α-synuclein is highly prone to aggregation, compared to that found in the cytosol, and the aggregated forms are also secreted from the cells. When proteasomal dysfunction was modeled, an increase in both aggregated and monomeric α-synuclein was found in the media [199].

Danzer *et al.* (2012) [204] demonstrated the presence of α-synuclein oligomers both inside and outside of exosomes from neurons. An exosomal mechanism of release for α-synuclein from neurons was proposed [204]. The exosomal marker CD9 was identified in both DLB cases in this study, but not in any of the five MSA cases. It is possible that different mechanisms of α-synuclein release from neurons occur in PD and DLB compared to in MSA, which may explain why the extracellular α-synuclein in these disorders is taken up by different cell types (neurons vs. oligodendrocytes).

7.4.3.2 Step 2: Re-uptake of extracellular α-synuclein

Two potential mechanisms exist for the clearance of extracellular α-synuclein. The first mechanism is degradation by extracellular proteolytic enzymes. α-synuclein has been shown to be cleaved by matrix metalloproteases, but fragments may have a

more toxic effect that the intact protein, so its unclear if this is helpful or harmful [201]. The second mechanism is re-uptake by neighbouring cells – which has been shown in both neurons and microglia in a cell culture model [201]. It is proposed here that re-uptake of eSNCA occurs in neurons in PD and DLB and in oligodendrocytes in MSA. The method by which this re-uptake occurs is controversial – some studies provide evidence for non-endocytic internalisation [205], whereas others support an endocytotic mechanism [202, 206, 207].

Liu *et al.* (2007) [202] used proteomics to discover novel cell surface and plasma membrane proteins on microglia that might be interacting with α-synuclein and mediating its internalisation. Of the 111 membrane-associated proteins they identified, clathrin and calnexin were validated with Western blotting, and clathrin was also shown to be co-localised with α-synuclein by confocal microscopy and co-IP analysis [202]. As clathrin is a key protein involved in endocytosis and protein trafficking, it is likely to play a major role in mediating the internalisation of eSNCA in microglia [202]. In this study, clathrin, AP-2 complex subunits and dynamin 1, which are involved in clathrin-mediated endocytosis (Figure 7.1), were all identified in ≥4 MSA cases and both DLB cases. They were also identified in cortical LBs by Leverenz *et al.* [108].

Liu *et al.* (2009) [200] showed that some internalised eSNCA is released through a recycling pathway (exocytosis) in addition to its degradation by the lysosomal pathway. Rab11a, which regulates the function of recycling endosomes, is physically associated with α-synuclein. HSP90 is associated with rab11a and is suggested to be involved in the cellular routing of internalised α-synuclein [200]. Rab11a was identified in a single MSA case in this study, whereas HSP90 was identified in five MSA cases and both DLB cases.

It is not known whether the internalised α-synuclein is then degraded by the cells where the reuptake has occurred, and if so, by what mechanism [201]. One hypothesis is that the internalised α-synuclein is degraded by the lysosomal pathway [203]. An alternative hypothesis is that the internalised α-synuclein is unable to be degraded by the cell and is instead sequestered into an inclusion, via vesicle-mediated transport. Neurons with LBs may internalise α-synuclein released from

other neurons, in a similar fashion to oligodendrocytes in MSA, either in addition to or instead of sequestering its natively expressed α synuclein.

In PD and DLB, it is also possible for retrograde transport of α-synuclein to occur directly from the presynaptic nerve terminal up the axon to the cell body of the neuron for addition to a LB, as opposed to a cycle of release and re-uptake. In MSA, there is also the possibility of direct transport from the neuron to the myelinating oligodendrocytes along the axon.

7.4.3.3 Step 3: Targeting of α-synuclein to the inclusion body

Oligodendrocytes have numerous membrane extensions that spirally wrap around neuronal axons to form a multilamellar myelin sheath. These contain an extensive cytoskeletal network of microtubules (heterodimers of α and β tubulin) and microfilaments (actin), while being devoid of intermediate filaments [136, 137]. While microtubules have a mesh-like organisation in the cell body, they are organized along the axis of the processes in the periphery [136, 137]. They are polarized structures, with a slow growing minus-end and a fast growing plus-end.

Proteins can be packaged in vesicles and transported from the cell body to the cell membrane (and vice-versa) along these microtubule "tracks" in the cytoskeletal framework. The current model of vesicular transport involves protruding cytoplasmic domains of transmembrane proteins interacting with kinesin and dynein motor proteins [208]. These cytoplasmic domains are likely to come from proteins bound into the vesicle, to be the sorting signal for transport [208]. The motor proteins then bind to the microtubules and move along them in an ATP-dependent process, pulling the vesicles with them. Soluble and vesicle-associated factors are required in addition to the motor proteins for vesicle transport, and it is not known whether the interaction between the vesicles and the motor proteins is direct or a via a mediating translocation protein [208].

The motor proteins that transport vesicles along microtubule tracks belong to the kinesin and dynein families. Transport is directed towards the plus-end by kinesins, with only a small subset exhibiting minus-end activity, and transport is directed towards the negative end by dyneins, in conjunction with the dynactin complex [209]. Thus, kinesins play an important role in post-Golgi transport and dyneins

facilitate the inward movement of endocytic vesicles [209]. The activation of motor activity depends upon the binding of the cargo structure to the motor, the assembly of cofactors and post-translational modifications of the proteins [209].

It is proposed that the aggregated α-synuclein internalised from the extracellular space is sequestered into an inclusion via vesicle-mediated retrograde transport along the microtubule "tracks" present in the cell, via the motor protein dynein. Both α- and β-tubulin were identified in all five MSA cases and both DLB cases in this study and also by Leverenz *et al.* [108]. The tubulin isoforms identified in both GCIs and LBs in this study are proposed to come not from the inclusions themselves but from immediately surrounding the inclusions. The motor protein dynein (associated with retrograde transport) was also identified in all five MSA cases and both DLB cases in this study, and also by Leverenz *et al.* [108]. Thus, it is hypothesised that this is the motor protein involved with the transport of α-synuclein-containing vesicles from the cell membrane towards the inclusion site in the cell body. The motor protein kinesin (associated with anterograde transport) was not found in any of the inclusion samples in this study. The dynein-associated protein spectrin was also identified in four MSA cases and both DLB cases in this study, and also by Leverenz *et al.* [108]. Dynactin was identified in two MSA cases and one DLB case.

7.4.3.4 Step 4: Addition of vesicle contents to inclusion body

The delivery of proteins to specific sites requires the targeting of transport vesicles and their fusion with the proper compartment. Two families of proteins, low molecular weight Rab GTPases and SNARE proteins, are involved in this targeting and fusion [209, 210]. SNARE proteins, present on both vesicles and targets, are essential in effecting the fusion of the vesicle with its target membranes. The two types of SNARE proteins are the arginine-containing R-SNAREs present on vesicles (originally called v-SNARES) and the glutamine-containing Q-SNAREs present on targets (originally called t-SNARES) [209, 210]. The docking and fusion of vesicles with a target membrane is mediated by the specific recognition of R-SNAREs and Q-SNAREs, which form a stable complex and pull together the vesicle and target membranes and provide the energy to fuse the lipid bilayers [209, 210]. Rab GTPases appear to work upstream in mediating the initial docking of the vesicle to the target, thus contributing to the specificity of vesicle docking by regulating

SNARE pairing [209, 210]. While this mechanism applies for the fusion of vesicles with other membrane-bound organelles, inclusions are not membrane-bound structures, so it is uncertain exactly how the contents of the α-synuclein-containing vesicles are added to the inclusions.

The target SNARE synaptosomal-associated protein 25 (SNAP25) was identified in all five MSA cases and both DLB cases in this study, and also by Leverenz *et al.* [108]. The vesicle SNARE VAMP2 was identified in two MSA cases and both DLB cases in this study. The target SNARE syntaxin-1 was identified in two MSA cases, with syntaxin-1 binding protein identified in all five MSA cases and both DLB cases in this study, and also by Leverenz *et al.* [108]. The SNARE-related protein NSF was identified in all five MSA cases and both DLB cases in this study.

The vesicle-related protein VATPase was identified in four MSA cases and both DLB cases in this study, and also by Leverenz *et al.* [108]. Other vesicle-related proteins identified in this study include synaptotagmin-1, synaptophysin, synaptogyrin-1, synaptic vesicle glycoprotein and synapsin. Rab proteins (including Rab1A, Rab2A, Rab3A, Rab5C and Rab11A) were identified in four MSA cases in this study, and also by Leverenz *et al.* [108].

7.4.4 Alternative mechanism of inclusion formation

While the mechanism for the addition of α-synuclein and other proteins to inclusions has been proposed in the previous section to involve retrograde vesicular transport of defective α-synuclein released from the presynaptic terminal, an alternative mechanism is that proteins are targeted to inclusions through anterograde transport through the ER system.

7.4.4.1 Quality control in the ER

The endoplasmic reticulum (ER) is the first organelle of the secretory pathway. Proteins destined for secretion are translated via ribosomes on the surface of the ER membrane and enter the ER lumen directly through a translocation pore. In the ER lumen, they undergo protein folding and maturation including glycosylation, disulphide bond formation and oligomerisation [211-214].

The ER quality control (ERQC) system monitors the folding and processing of the newly translated proteins before they exit the ER [214], utilising molecular chaperones and glycosylation events to recognise the incorrectly folded or assembled proteins [211]. The misfolded and defective proteins are then cleared by ER-associated degradation (ERAD), where the proteins are returned to the cytosol via the translocon to be ubiquitinated and degraded by the ubiquitin-proteasome system [212-215]. The exact mechanism for this retrotranslocation is not known, although the Sec61p translocation pore through which nascent polypeptides enter the ER has also been proposed to function as a retrotranslocation channel for proteins targeted by the ERAD [213]. It has been shown that some misfolded proteins are still trafficked to the Golgi instead of being retained in the ER, as they still present a functional ER export signal despite their misfolding [214].

The demands on the ERQC and ERAD systems are formidable, as up to a third of proteins are associated with the secretory pathway and up to 30% of proteins are aberrantly synthesised [213, 214], leaving the ER responsible for monitoring and targeting the degradation of up to 10% of the proteome. The ERQC system contributes to the development of a number of diseases by either depleting essential proteins required by the cell or by accumulating misfolded or defective proteins that it is unable to subsequently degrade [211].

78kDa glucose-related protein (GRP78), a resident ER Hsp70 chaperone, and protein disulfide-isomerase (PDI) are both involved in protein folding in the ER [213]. They may also play a role in the recognition and engagement of misfolded proteins by ERAD, including their retrotranslocation into the cytosol [213]. GRP78 was identified in all five MSA cases and both DLB cases in this study. PDI and three of its variants (A3, A4 and A6) were found in this study, with both PDI and its A3 variant found in ≥4 MSA cases and both DLB cases. The chaperones calnexin and calreticulin also aid in protein folding in the ER and are especially involved in binding glycoproteins [213]. Both calnexin and calreticulin were identified in all five MSA cases and both DLB cases in this study.

7.4.4.2 The unfolded protein response (UPR)

The accumulation of misfolded proteins activates the unfolded protein response (UPR), a complex signalling pathway to protect against ER stress [213, 216]. UPR

activation leads to a general decrease in the initiation of protein translation to reduce the protein load in the ER [213]. UPR activation also causes specific genes required for protein folding, ER-Golgi trafficking and ERAD to be transcriptionally upregulated, which acts to relieve the ER stress [213, 216]. Sustained UPR activation leads to cellular dysfunction and disease [213].

In humans there are three distinct pathways for UPR activation, modulated by three transmembrane sensors – IRE1 (inositol-requiring transmembrane kinase and endonuclease 1), ATF6 (activation of transcription factor 6) and PERK (protein kinase-like ER kinase) [213]. The proteins involved downstream of these pathways include: XBP-1 (X-box-binding protein 1) in the IRE1 pathway; S1P (site-1 protease), S2P (site-2 protease), SREBP (sterol response element-binding protein) and the general transcription factor NF-Y in the ATF6 pathway; and eIF2α (elongation translation-initiation factor 2), ATF4 (activation of transcription factor 4), and CHOP (C/EBP homologous protein) in the PERK pathway [213]. None of the three transmembrane sensors or any of their downstream targets described above were identified in this study.

The chaperone protein GRP78, discussed earlier, is also a downstream target in all three of the UPR activation pathways. The IRE1, ATF6 and PERK transmembrane sensors involved in the UPR normally bind GRP78 [213]. However, GRP78 preferentially binds to misfolded proteins, leading to the activation of the transmembrane sensors during times of ER stress as a result of their dissociation with GRP78 [213]. As GRP78 was found in this study but not the transmembrane sensor proteins, it is likely that GRP78 was found in association with misfolded proteins. GRP78 may bind to misfolded α-synuclein or other misfolded proteins that are packaged into inclusions.

7.4.4.3 ER to Golgi protein trafficking

Correctly folded proteins are packaged into coat protein complex II (COPII)-coated vesicles and transported from the ER to the Golgi for further modification and targeting to their final destination [212, 214, 217]. The COPII coat consists of five proteins – Sar1, Sec23, Sec24, Sec13 and Sec 31 [217]. The inner coat is comprised of heterodimers of Sec 23 and Sec 24 and the outer coat is comprised of heterotetramers of Sec13 and Sec31 [217, 218]. The small GTPase Sar1 is recruited

to the ER membrane to regulate the assembly of the COPII coat [217-219]. Proteins that are targeted to exit the ER via COPII-coated vesicles may contain a signal to bind directly to Sec24, or they may be included indirectly through binding to a transport adapter, or even enter the vesicles via passive diffusion [217]. Neither Sar1 nor any proteins from the Sec protein family were identified in inclusions in this study.

The family of ER vesicle (ERV) proteins are thought to function in the formation, loading and fusion of COPII-coated vesicles [212]. ERV proteins were not identified in inclusions in this study. The p24 family of transmembrane proteins are also associated with COPII-coated vesicles and are proposed to be involved in vesicle formation, cargo protein sorting and the regulation of vesicle transport [212]. The transmembrane emp24 domain-containing proteins 2, 4, 7, 9 and 10 were found in inclusions in this study, with protein 2 found in all five MSA cases and one DLB case and protein 10 found in four MSA cases.

7.4.4.4 Relationship between ER stress and inclusion formation

Smith *et al.* (2005) [220] showed that expression of the A53T α-synuclein mutant in a cell model caused decreased proteasome activity and increased oxidative stress, which led to both mitochondrial dysfunction and ER stress, leading to cell death. Neither wild type α-synuclein nor the A30P mutant had this effect [220]. The ER stress pathway appeared to be activated in response to a greater accumulation of unfolded proteins due to the proteasome dysfunction [220].

Sugeno *et al.* (2008) [221] showed that low-dose rotenone-treated cells over-expressing wild type α-synuclein, which is highly phosphorylated at serine 129, showed a much higher rate of UPR induction than cells overexpressing a unphosphorylated α-synuclein mutant. The wild-type expressing cells also showed higher levels of aggregate formation than the mutant-expressing cells [221]. This suggests a role for serine 129 phosphorylation in both aggregate formation and the induction of α-synuclein toxicity, leading to mitochondrial dysfunction and cell death [221].

Cooper *et al.* (2006) [215] identified the inhibition of trafficking from the ER to the Golgi to be a major component of α-synuclein-caused toxicity. They used a yeast

model to demonstrate that the accumulation of α-synuclein caused ER stress [215]. Both wild type and A53T mutant α-synuclein impaired vesicular transport from the ER to the Golgi, with a more rapid onset of impairment caused by the mutant strain [215]. The impairment of vesicular transport preceded the onset of ER stress [215]. The over-expression of genes that promote transport from the ER to the Golgi was shown to suppress α-synuclein toxicity [215]. Rab1, which plays an essential role in the tethering and docking of vesicles at the Golgi, was shown to protect against neurodegeneration in animal models [215]. The ER stress observed in models of PD may be caused by the accumulation of proteins in the ER as a result of the α-synuclein-induced reduction in ER-Golgi trafficking [215].

Taken together, these studies suggest that excess or defective α-synuclein may impair the ER-Golgi trafficking system, leading to a buildup of misfolded proteins and activating the UPR. Haynes *et al.* (2004) [216] have shown that sustained UPR activation is causative of oxidative stress via the generation of reactive oxygen species (ROS), which eventually leads to cell death. As Lewy Bodies have been shown to be associated with the ER [222], it is possible that the LB is an alternative destination for the trafficking of impaired proteins from the ER in an attempt to alleviate ER stress and subsequent cell death.

7.5 Conclusion

The proteins that were consistently identified in GCIs and LBs in this study have been used as the basis for developing two alternative hypotheses for how proteins are targeted to inclusions. Defective α-synuclein and associated proteins may be released extracellularly from the presynaptic terminal, for re-uptake by the target cell in clathrin-coated vesicles (neurons in PD or DLB, oligodendrocytes in MSA), where they are selectively targeted to an inclusion body via retrograde vesicular transport. Alternatively, misfolded or excess α-synuclein may lead to an inhibition of ER-Golgi trafficking and subsequent ER stress at the point of translation, where α-synuclein and associated proteins that subsequently fail to be degraded are targeted to a LB via anterograde transport in COPII-coated vesicles. It is unclear how the latter mechanism would relate to GCI formation in MSA, as the α-synuclein would still need to be targeted to the oligodendrocyte from a neuronal cell.

The identification of a large number of synaptic vesicle-related proteins in the purified GCI and LB samples in this study, including those associated with exosomes (CD9), clathrin-mediated endocytosis (clathrin, AP-2 complex, dynamin), retrograde transport (dynein, dynactin, spectrin) and synaptic vesicle fusion (SNAP25, VAMP2, syntaxin-1), support the former hypothesis. While the ER chaperone proteins GRP78, PDI, calnexin and calreticulin were identified in this study, proteins relating to the UPR signalling cascade and the formation of COPII-vesicles (with the exception of the supporting family of p24 proteins) were not identified in purified inclusions.

8 Final Discussion

8.1 Introduction

The primary aim of this thesis was to characterise the proteome of Glial Cytoplasmic Inclusions (GCIs) and Lewy Bodies (LBs) to elucidate clues as to the role and formation of these inclusions in neurodegenerative disorders. Inclusions purified from human post-mortem tissue were chosen for analysis, as animal models lack suitability for an ageing disease [6] with very few animal models able to produce inclusions [104]. To obtain a sufficient yield of high-purity inclusions for downstream analysis, a published method of GCI purification was redeveloped and the optimised method applied to multiple MSA and DLB cases. The purified inclusions were analysed by 2D-DIGE and protein identifications were made by LTQ Orbitrap XL mass spectrometry. The expected outcome of this work was that a comprehensive identification of the protein content of both GCIs and LBs would be made including the first relative quantification of their major protein constituents.

8.2 Optimisation of an inclusion purification technique

The published GCI purification method of Gai *et al.* [113], utilising Percoll density gradient centrifugation and α-synuclein-based immunomagnetic capture, was optimised with a series of modifications, including a limited tryptic digestion to separate the inclusions from the surrounding cytoskeleton. The optimised method delivered a 28-fold increase in soluble protein yield compared with the published method. The optimised method delivered a 3.8-fold enrichment of the major GCI protein α-synuclein while reducing tubulin contamination by 5.2-fold, when compared to the published method. The optimised method is extremely robust, as since its development, the laboratory of Gai *et al.* has adopted the developed modifications for their inclusion purifications and have obtained a similar degree of success with a different operator based in a different laboratory.

The original published method of Gai *et al.* [113] had already improved upon the previously published methods of Iwatsubo *et al.* [110] and Sian *et al.* [112]. While the subsequent method of Leverenz *et al.* [108] chose a 'direct' approach to isolating inclusions via laser capture microdissection (LCM) this still has high potential for contamination from surrounding structures due to the thickness of the sections used

for LCM, relative to the size of inclusions. In addition, the low yield obtained with the method of Leverenz *et al.* [108] (less than 1 ug in total from six pooled cases) limits the downstream analysis options for the enriched inclusions. The optimised method for inclusion purification developed in this study provides sufficient yield for subsequent analysis using proteomic techniques such as Western blotting and 2D-DIGE.

8.3 Proteomic analysis of inclusions

Inclusions from six MSA cases, two DLB cases and one normal control case were analysed via both 2D-DIGE and mass spectrometry. Relative protein quantifications were performed from the DIGE gels based on preparative gel matching of protein isoforms for four major known inclusions proteins. GCIs consisted of 11.9% α-synuclein, 2.8% α-β-crystallin, 1.7% 14-3-3 proteins, and 1.2% tubulin. LBs consisted of 8.5% α-synuclein, 2.0% α-β-crystallin, 1.5% 14-3-3 proteins, and 1.3% tubulin. There is a 6-fold enrichment of α-synuclein in GCIs compared to MSA homogenate (which consists of 2.0% α-synuclein). The DIGE quantification of α-synuclein enrichment in inclusions from the homogenate was verified by Western blotting.

From the nine cases analysed, a strong positive linear relationship was found between the quantity of α-synuclein and α-β-crystallin in each case. α-β-crystallin is a small heat shock protein that is recruited to α-synuclein aggregates under oxidative stress conditions [197]. α-β-crystallin has been shown *in vitro* to reduce the number of α-synuclein fibrils [194, 195] and to bind to α-synuclein monomers to prevent their fibrillisation [196] as well as binding to the lateral surface of α-synuclein fibrils to inhibit further elongation [191]. Thus, there may be multiple mechanisms for the interaction of α-β-crystallin with α-synuclein. α-β-crystallin may assist in maintaining a balance between the aggregation and disaggregation of α-synuclein and may reduce the levels of the potentially toxic oligomeric form of α-synuclein by controlling its folding state [194]. As α-β-crystallin was found at a ratio of 0.23:1 to α-synuclein in this study and it has a binding ratio to α-synuclein of up to 0.6:1 [191], it is suggested that the α-β-crystallin present in inclusions may be entirely bound to α-synuclein, which could account for the linear relationship between the quantities of these two proteins within inclusions.

Of the inclusion proteins identified by mass spectrometry, 160 GCI proteins were consistently identified (identified in at least 4 out of 5 MSA cases and 170 LB proteins were consistently identified (identified in 2 out of 2 DLB cases). 112 (68%) of these proteins were common to both GCIs and LBs, with 28 (25%) of these proteins identified in common being vesicle-related. This is similar to the percentage of vesicle-related proteins (27%) identified in LBs by Leverenz *et al.* [108] using LCM as a purification technique, Of the 28 vesicle-related proteins found in common between GCIs and LBs, 12 proteins have not previously been established as GCI or LB protein. These include synaptosomal-associated protein 25, V-type proton ATPase subunits, clathrin and dynein (Table 7.6). Less vesicle-related proteins were identified by 2-DE than by mass spectrometry, which may be due to the membrane-bound vesicle proteins focusing poorly via 2-DE due to their hydrophobic nature.

8.4 The formation of inclusions

The identification of a broad range of synaptic vesicle-related proteins led to the development of a hypothesis for the vesicle-mediated targeting of proteins to inclusions. It is proposed that excess or damaged α-synuclein is released into the extracellular space by neurons at the presynaptic terminal [201] and re-uptake occurs by either neighbouring neurons (in PD and DLB) or oligodendrocytes (in MSA) via endocytosis into clathrin-coated vesicles [202, 206]. These vesicles are then transported from the cell membrane into the cell body along the microtubule 'tracks', via the motor protein dynein [208], to be packaged into a GCI or LB. It is unknown what distinguishing factor between PD and MSA causes α-synuclein to be targeted to neurons or oligodendrocytes in these disease states, respectively.

An alternative hypothesis has been proposed for inclusion formation, which is that excess or damaged α-synuclein, at its point of translation at the ER, leads to an inhibition of ER-Golgi trafficking and subsequent ER stress [215]. As LBs have been shown to be associated with the ER [222], α-synuclein and associated proteins that subsequently fail to be degraded may be targeted to a LB via anterograde transport in COPII-coated vesicles to protect the cell from further stress. An alternative mechanism must be present for GCIs as oligodendrocytes do not natively express α-synuclein [48]

8.5 Critical review

This project was ambitious in terms of both the availability and cost of the resources required. The amount of human brain tissue available was a limiting factor for the project, with approximately 50% of the GCI-rich sections and up to 20% of the total available MSA tissue depleted from the SA Brain Bank during the course of the project. Purification of inclusions from this tissue was a time-intensive process, with one week required to obtain purified solubilised inclusions from 2-12g of tissue with a further week required for follow-up analysis with Western blotting and IHC.

The other resources required for this project were extensive. Over 4 mg of primary antibody was used in the inclusion purifications, plus 2 mL each of the Dynabeads M-280 and Dynabeads MyOne magnetic beads (Invitrogen) and 1 L of Percoll Plus (GE Healthcare). A 5 nmol CyDye DIGE Fluor minimal labelling kit (GE Healthcare) was used for the 12 DIGE gels run in this project in addition to the IPG strips, acrylamide, CHAPS, etc. required for both the DIGE and preparative 2D gels. Over 500 samples (single injection of one soluble sample or one 1D gel band or one 2D spot) were analysed by mass spectrometry. With approximately 2 hours of instrument time required per sample, six weeks of instrument time was invested in the analysis of samples for this project. This project was uniquely placed with access to the SA Brain Bank, locally produced α-synuclein antibody, and an in-house mass spectrometry facility, otherwise the extent of the experiments carried out in the course of this project would not have been feasible.

The generalisation of the results of this study needs to be considered in the context of the tissues used for analysis. The protein identifications and quantifications from classical brainstem LBs from DLB tissue in this study may differ from cortical LBs in DLB and from LBs in PD tissue. The MSA brain regions selected for GCI purifications may also have a bearing on the results obtained. The potential co-purification of Lewy neurites and other α-synuclein based aggregates with the immunocaptured samples cannot be excluded, and other factors such as the age of the cases when deceased, the duration and severity of the disease, and the post-mortem interval may have an impact on the results.

8.6 Future Directions

Potential future investigations related to the findings in this thesis include validation of further vesicle protein identifications, continued optimisation of the purification method, the relative quantification of the entire inclusion proteome using mass spectrometry, and investigation into the truncations and post-translational modifications of the α-synuclein contained within inclusions.

Further optimisation of the purification method could include trialling a low-pH elution of the inclusions from the magnetic beads. This would separate the magnetic beads and IgG from the inclusions prior to their solubilisation, to reduce any background profile of proteins obtained directly from the beads. While quantification of four main inclusion proteins was performed using 2D-DIGE gels in this study, relative quantification of all the protein components can be performed directly using mass spectrometry in the future if a quantitative mass spectrometer is obtained (the instrument used in this study was chosen for its high sensitivity).

The multitude of α-synuclein isoforms visualised by 2D-E of immunocaptured inclusions in this study (~50-100 2D gel spots) suggests a wide array of truncated and post-translationally modified forms. The high degree of α-synuclein enrichment with the optimised purification method may make the analysis of α-synuclein truncations and modifications from these gel spots possible.

Purified inclusions can be subjected to 2-DE on multiple gels and Western blotting performed with a series of antibodies raised against different portions of the α-synuclein amino acid sequence. An antibody against an n-terminal sequence will show α-synuclein of all lengths, whereas antibodies against c-terminal portions will not bind truncated forms that are too short to include the antibody recognition site. The negatively charged C-terminal region of α-synuclein hinders aggregation [61], so its is proposed that C-terminal truncations may promote the aggregation of α-synuclein into inclusions. Confirming the presence of truncated α-synuclein in inclusions would support this.

Further 2-DE of purified inclusions targeted to LMW proteins can be used to excise the α-synuclein gel spots for analysis of post-translational modifications, such as phosphorylation and ubiquitination, by targeted mass spectrometry. The existing

mass spectrometry data can also be analysed further using PEAKS mass spectrometry data analysis software (Bioinformatics Solutions Inc, Waterloo, Canada) to look for truncated peptides and to perform an extensive search of post-translational modifications present. Identifying the forms of α-synuclein present in inclusions will provide further information on the reason for its incorporation into inclusions as opposed to its degradation within the cell. Due to limitations in tissue availability, processing time and the expense of the resources, as outlined previously, these experiments have yet to be conducted.

8.7 Conclusion

In this study, a method for inclusion purification was optimised with a series of modifications to dramatically increase the yield and purity, allowing the comprehensive proteomic analysis of GCIs and LBs including the quantification of major inclusion proteins and a comparison between the two types of inclusions. A wide range of synaptic vesicle-related protein identifications were made, supporting a hypothesis for vesicle-mediated targeting of proteins to inclusions.

Appendix A

MS Identification of 164 GCI proteins identified in a minimum of 4 out of 5 MSA cases

Acc. No.[a]	Name	Calc. pI	Calc. MW (Da)	Avg. Xcorr[b]	Avg. No. of Peptides[c]	Avg. % Sequence Coverage[d]
P04350	*Tubulin beta-4 chain	4.88	49554	290.1	16.3	56.0
P68371	*Tubulin beta-2C chain	4.89	49799	250.8	16.0	54.0
Q13885	Tubulin beta-2A chain	4.89	49875	234.0	15.7	53.3
Q71U36	*Tubulin alpha-1A chain	5.06	50104	228.7	14.1	58.7
P07437	*Tubulin beta chain	4.89	49639	224.3	15.0	50.8
P68363	*Tubulin alpha-1B chain	5.06	50120	217.6	14.0	58.4
P68366	Tubulin alpha-4A chain	5.06	49900	195.3	10.3	40.0
P14136	*Glial fibrillary acidic protein	5.52	49800	131.8	12.8	33.6
P37840	*Alpha-synuclein	4.70	14500	128.7	3.6	37.5
Q13509	*Tubulin beta-3 chain	4.93	50400	119.0	11.9	37.9
P60709	*Actin, cytoplasmic 1	5.48	41700	113.9	7.6	34.2
P08238	*Heat shock protein HSP 90-beta	5.03	83200	100.7	12.5	21.7
P09543	*2',3'-cyclic-nucleotide 3'-phosphodiesterase	9.07	47500	100.4	8.8	28.8
P12277	*Creatine kinase B-type	5.59	42600	99.0	10.3	49.2
P06576	*ATP synthase subunit beta, mitochondrial	5.40	56500	97.4	12.6	40.5
Q14204	Cytoplasmic dynein 1 heavy chain 1	6.40	532072	95.9	12.8	3.9
P07900	*Heat shock protein HSP 90-alpha	5.02	84607	85.9	11.8	22.2
P04264	*Keratin, type II cytoskeletal 1	8.12	65999	82.0	10.4	20.7
P07197	*Neurofilament medium polypeptide	4.91	102400	78.0	8.4	13.2
P07196	*Neurofilament light polypeptide	4.65	61500	71.8	7.5	19.5
P98160	Basement membrane-specific heparan sulfate proteoglycan core protein	6.51	468532	71.0	9.3	3.1
P14625	*Endoplasmin	4.84	92400	68.4	11.2	19.6
P11021	78 kDa glucose-regulated protein	5.16	72288	67.3	11.5	25.4
P61764	*Syntaxin-binding protein 1	6.96	67500	63.3	9.6	22.7

Acc. No.[a]	Name	Calc. pI	Calc. MW (Da)	Avg. Xcorr[b]	Avg. No. of Peptides[c]	Avg. % Sequence Coverage[d]
P63104	*14-3-3 protein zeta/delta	4.79	27728	62.0	5.7	33.9
P27797	*Calreticulin	4.44	48112	60.5	6.9	28.9
Q01082	*Spectrin beta chain, brain 1	5.57	274400	60.2	8.8	5.4
Q00610	*Clathrin heavy chain 1	5.69	191500	60.2	8.8	7.7
Q16352	Alpha-internexin	5.40	55357	55.6	6.5	17.0
P25705	*ATP synthase subunit alpha, mitochondrial	9.13	59714	54.0	8.8	22.5
P62258	*14-3-3 protein epsilon	4.74	29155	53.2	5.1	30.2
P13645	*Keratin, type I cytoskeletal 10	5.21	58792	51.6	6.9	16.7
P13637	*Sodium/potassium-transporting ATPase subunit alpha-3	5.38	111700	49.5	7.5	11.8
Q05193-2	Isoform 2 of Dynamin-1	6.87	97200	49.4	7.0	12.3
P16152	*Carbonyl reductase [NADPH] 1	8.32	30356	49.0	6.2	34.0
P27824	Calnexin	4.60	67526	49.0	6.5	15.9
P62873	*Guanine nucleotide-binding protein G(I)/G(S)/G(T) subunit beta-1	6.00	37400	48.3	5.6	27.2
Q16555	*Dihydropyrimidinase-related protein 2	6.38	62255	48.0	6.8	20.7
P35908	*Keratin, type II cytoskeletal 2 epidermal	8.00	65393	47.9	7.8	16.5
P30101	Protein disulfide-isomerase A3	6.35	56700	45.0	6.9	19.8
P46459	*Vesicle-fusing ATPase	6.95	82500	43.2	5.7	10.1
P46821	*Microtubule-associated protein 1B	4.81	270500	43.0	8.6	5.1
P27348	*14-3-3 protein theta	4.78	27747	42.1	5.0	28.9
P02511	*Alpha-crystallin B chain	7.33	20100	41.9	4.7	37.0
Q00839	*Heterogeneous nuclear ribonucleoprotein U	6.00	90500	41.9	4.7	10.1
P31930	*Cytochrome b-c1 complex subunit 1, mitochondrial	6.37	52612	41.4	4.7	18.7
P11047	*Laminin subunit gamma-1	5.12	177489	40.8	8.1	7.5
P31946	*14-3-3 protein beta/alpha	4.83	28100	40.4	4.6	27.6
P35527	*Keratin, type I cytoskeletal 9	5.24	62027	38.9	5.4	16.1
P80723	Brain acid soluble protein 1	4.63	22680	37.9	4.6	36.4
P08670	*Vimentin	5.12	53600	37.2	5.1	14.5
F6KPG5	Albumin (Fragment)	6.04	66488	36.7	5.1	10.7
P21796	*Voltage-dependent anion-selective channel protein 1	8.54	30754	36.6	6.5	35.7
P09936	*Ubiquitin carboxyl-terminal hydrolase isozyme L1	5.48	24808	36.0	2.5	17.1

Acc. No.[a]	Name	Calc. pI	Calc. MW (Da)	Avg. Xcorr[b]	Avg. No. of Peptides[c]	Avg. % Sequence Coverage[d]
P38606	V-type proton ATPase catalytic subunit A	5.52	68300	35.6	4.8	12.3
P10809	*60 kDa heat shock protein, mitochondrial	5.87	61000	35.6	5.5	14.3
P61981	*14-3-3 protein gamma	4.89	28285	35.5	4.1	24.8
P02787	Serotransferrin	7.12	77014	35.4	5.2	10.0
P22314	*Ubiquitin-like modifier-activating enzyme 1	5.76	117774	34.9	6.4	9.6
P62879	Guanine nucleotide-binding protein G(I)/G(S)/G(T) subunit beta-2	6.00	37307	34.6	4.2	20.6
P54652	Heat shock-related 70 kDa protein 2	5.74	69978	34.5	6.3	13.6
P68104	*Elongation factor 1-alpha 1	9.01	50109	33.6	3.7	10.7
P09471-2	Isoform Alpha-2 of Guanine nucleotide-binding protein G(o) subunit alpha	5.90	40061	32.3	5.5	19.8
Q9GZM7	Tubulointerstitial nephritis antigen-like	6.99	52353	31.7	5.3	14.8
P13591	*Neural cell adhesion molecule 1	4.87	94500	31.5	5.8	8.7
P09651	*Heterogeneous nuclear ribonucleoprotein A1	9.13	38700	31.5	3.6	13.3
Q8IWE0	Calcium/calmodulin-dependent protein kinase II alpha	7.20	54054	30.9	4.5	16.0
Q08211	*ATP-dependent RNA helicase A	6.84	140869	30.4	4.5	5.0
P61978	*Heterogeneous nuclear ribonucleoprotein K	5.54	50944	30.1	4.5	17.3
P22626	*Heterogeneous nuclear ribonucleoproteins A2/B1	8.95	37400	29.2	2.6	10.2
Q9H115	*Beta-soluble NSF attachment protein	5.47	33500	29.1	5.6	28.0
P19338	*Nucleolin	4.70	76600	29.1	4.6	9.8
P45974	Ubiquitin carboxyl-terminal hydrolase 5	5.03	95700	29.0	4.5	9.2
P08758	Annexin A5	5.05	35900	28.5	4.0	20.5
P68871	Hemoglobin subunit beta	7.28	15988	28.2	4.5	43.3
P45880	*Voltage-dependent anion-selective channel protein 2	7.56	31500	27.8	4.0	25.2
P02794	Ferritin heavy chain	5.55	21212	27.6	2.9	24.3
Q9Y2J2	Band 4.1-like protein 3	5.19	120600	27.5	3.4	4.7
P17677	Neuromodulin	4.72	24788	27.2	3.2	22.4
P13010	*X-ray repair cross-complementing protein 5	5.81	82652	27.0	4.3	8.8
P28331	*NADH-ubiquinone oxidoreductase 75 kDa subunit, mitochondrial	6.23	79400	25.9	3.9	9.3
P07237	Protein disulfide-isomerase	4.87	57100	25.5	2.9	8.6
P04899	*Guanine nucleotide-binding protein G(i) subunit alpha-2	5.54	40425	24.8	4.5	16.2

Acc. No.[a]	Name	Calc. pI	Calc. MW (Da)	Avg. Xcorr[b]	Avg. No. of Peptides[c]	Avg. % Sequence Coverage[d]
P02792	Ferritin light chain	5.78	20007	24.7	2.9	23.1
O00264	Membrane-associated progesterone receptor component 1	4.70	21658	24.7	3.4	34.8
P61421	V-type proton ATPase subunit d 1	5.00	40300	24.5	3.7	20.1
Q04917	14-3-3 protein eta	4.84	28201	23.9	3.0	17.9
Q13263	Transcription intermediary factor 1-beta	5.77	88500	23.8	4.7	9.2
P06748	*Nucleophosmin	4.78	32600	23.7	3.0	18.0
P18669	*Phosphoglycerate mutase 1	7.18	28800	23.2	3.6	20.9
Q1KMD3	*Heterogeneous nuclear ribonucleoprotein U-like protein 2	4.91	85052	23.0	3.0	5.4
P17600	Synapsin-1	9.83	74100	22.7	2.8	7.2
O43301	Heat shock 70 kDa protein 12A	6.77	74900	22.4	3.6	7.0
P55795	Heterogeneous nuclear ribonucleoprotein H2	6.30	49232	22.4	3.2	11.4
O75947	ATP synthase subunit d, mitochondrial	5.30	18500	22.3	2.9	27.4
P12956	*X-ray repair cross-complementing protein 6	6.64	69800	22.3	3.1	7.3
O94905	Erlin-2	5.62	37800	22.2	4.2	16.9
Q13557	Calcium/calmodulin-dependent protein kinase type II subunit delta	7.25	56300	21.7	3.7	12.9
P30153	*Serine/threonine-protein phosphatase 2A 65 kDa regulatory subunit A alpha isoform	5.11	65300	21.6	2.3	5.8
P19367	Hexokinase-1	6.80	102400	21.6	3.9	5.1
P51991	*Heterogeneous nuclear ribonucleoprotein A3	9.01	39600	21.5	3.1	11.4
Q14697	Neutral alpha-glucosidase AB	6.14	106807	21.1	3.1	5.8
P21281	V-type proton ATPase subunit B, brain isoform	5.81	56465	21.0	3.6	11.6
P0CG48	Polyubiquitin-C	7.66	77000	20.8	2.3	34.5
P60174	*Triosephosphate isomerase	6.90	26700	20.8	3.8	20.2
Q9NQC3	Reticulon-4	4.50	129900	20.7	3.1	5.1
Q9Y696	Chloride intracellular channel protein 4	5.59	28800	20.6	2.8	17.6
O43852	Calumenin	4.64	37100	20.6	3.6	17.9
Q12860	Contactin-1	5.90	113200	20.4	2.7	3.7
P49755	Transmembrane emp24 domain-containing protein 10	7.44	24960	20.2	3.2	21.4
P60880	*Synaptosomal-associated protein 25	4.77	23300	20.2	3.9	25.5
Q9Y277	*Voltage-dependent anion-selective channel protein 3	8.66	30639	20.2	4.4	20.2

Acc. No.[a]	Name	Calc. pI	Calc. MW (Da)	Avg. Xcorr[b]	Avg. No. of Peptides[c]	Avg. % Sequence Coverage[d]
P09104	Gamma-enolase	5.03	47200	20.0	4.4	17.4
Q15121	*Astrocytic phosphoprotein PEA-15	5.02	15031	20.0	2.8	21.7
P13667	Protein disulfide-isomerase A4	5.07	72887	20.0	3.5	7.4
O43175	D-3-phosphoglycerate dehydrogenase	6.71	56614	19.7	4.8	12.2
P23528	*Cofilin-1	8.09	18500	19.5	3.1	26.7
P14314	Glucosidase 2 subunit beta	4.41	59400	18.8	2.9	6.9
Q9UBB6	Neurochondrin	5.48	78800	18.5	3.9	7.6
Q6PUJ7	Prohibitin	5.76	29802	17.8	2.8	15.5
P60201	Myelin proteolipid protein	8.35	30057	17.6	2.9	12.6
P29966	Myristoylated alanine-rich C-kinase substrate	4.45	31500	17.6	3.8	19.9
P22695	*Cytochrome b-c1 complex subunit 2, mitochondrial	8.63	48413	17.3	3.0	10.1
P07910	Heterogeneous nuclear ribonucleoproteins C1/C2	5.08	33600	17.3	2.9	11.7
Q07960	Rho GTPase-activating protein 1	6.29	50404	17.3	3.2	11.3
P02649	Apolipoprotein E	5.73	36132	16.8	3.4	13.9
Q14974	Importin subunit beta-1	4.78	97100	16.7	3.1	5.2
Q99623	Prohibitin-2	9.83	33300	16.7	3.7	16.4
P60842	Eukaryotic initiation factor 4A-I	5.48	46100	16.4	2.5	8.7
P60660	Myosin light polypeptide 6	4.65	16919	16.4	2.8	24.2
Q12765	*Secernin-1	4.75	46400	16.4	3.3	12.0
Q14108	Lysosome membrane protein 2	5.14	54255	16.2	2.7	8.2
P02462	Collagen alpha-1(IV) chain	8.28	160500	15.9	2.1	1.8
P21266	Glutathione S-transferase Mu 3	5.54	26500	15.8	3.5	19.8
P62805	*Histone H4	11.36	11360	15.7	2.7	25.8
Q15555	Microtubule-associated protein RP/EB family member 2	5.57	37000	15.6	2.4	8.8
Q9UK22	F-box only protein 2	4.37	33300	15.5	3.2	15.4
P12532	Creatine kinase U-type, mitochondrial	8.34	47007	15.5	2.3	10.8
P48735	Isocitrate dehydrogenase [NADP], mitochondrial	8.69	50900	15.4	2.6	7.8
P05090	Apolipoprotein D	5.15	21262	15.3	2.0	13.2
Q15185	Prostaglandin E synthase 3	4.54	18700	14.5	2.4	20.8
Q14257	Reticulocalbin-2	4.40	36854	14.2	3.0	16.8

Acc. No.[a]	Name	Calc. pI	Calc. MW (Da)	Avg. Xcorr[b]	Avg. No. of Peptides[c]	Avg. % Sequence Coverage[d]
O00764	Pyridoxal kinase	6.13	35100	13.8	2.7	13.2
O75489	NADH dehydrogenase [ubiquinone] iron-sulfur protein 3, mitochondrial	7.50	30223	13.8	2.9	16.3
P36542	ATP synthase subunit gamma, mitochondrial	9.22	33000	13.5	2.5	9.5
P05455	*Lupus La protein	7.12	46800	13.3	3.5	10.9
Q9HDC9	Adipocyte plasma membrane-associated protein	6.16	46451	13.2	2.2	7.8
Q07021	Complement component 1 Q subcomponent-binding protein, mitochondrial	4.84	31300	12.9	2.8	15.8
Q16718	NADH dehydrogenase [ubiquinone] 1 alpha subcomplex subunit 5	5.99	13450	12.8	2.1	26.4
P21964	Catechol O-methyltransferase	5.47	30000	12.6	2.4	13.9
P10909	Clusterin	6.27	52500	12.6	2.8	10.0
P07195	L-lactate dehydrogenase B chain	6.05	36615	12.4	2.3	8.4
Q14011	Cold-inducible RNA-binding protein	9.51	18600	11.8	2.4	21.7
Q99426	Tubulin-folding cofactor B	5.15	27300	11.7	2.5	13.9
P04406	Glyceraldehyde-3-phosphate dehydrogenase	8.46	36000	11.7	2.6	12.0
Q16891	Mitochondrial inner membrane protein	6.48	83600	11.6	2.0	3.7
O43493	Trans-Golgi network integral membrane protein 2	5.73	51100	11.3	2.7	8.2
P35998	26S protease regulatory subunit 7	5.95	48600	11.2	2.5	8.0
O94919	Endonuclease domain-containing 1 protein	5.71	55000	11.0	2.2	6.1
Q9NZ45	CDGSH iron-sulfur domain-containing protein 1	9.09	12191	10.3	2.1	27.0
Q15363	Transmembrane emp24 domain-containing protein 2	5.17	22700	9.9	2.0	12.4
P13073	Cytochrome c oxidase subunit 4 isoform 1, mitochondrial	9.51	19600	9.7	2.3	15.2
P08574	Cytochrome c1, heme protein, mitochondrial	9.00	35400	8.8	2.3	10.2
Q8NBS9	Thioredoxin domain-containing protein 5	5.97	47600	8.1	2.0	6.3

[a] SwissProt accession number
[b] Average Xcorr significance score
[c] Average number of unique peptides sequenced
[d] Average % of the full-length amino acid sequence covered by identified peptides
* Also identified in the secondary-only control preparation

Appendix B

MS Identification of 56 GCI proteins that are transiently associated with the synaptic vesicle membrane

Acc. No.[a]	Name	Calc. pI	Calc. MW (Da)	No. of cases[b]	Avg. Xcorr[b]	Avg. No. of Peptides[c]	Avg. % Sequence Coverage[d]
P04350	Tubulin beta-4 chain	4.88	49554	5	290.1	16.3	56.0
P68371	Tubulin beta-2C chain	4.89	49799	5	250.8	16.0	54.0
Q13885	Tubulin beta-2A chain	4.89	49875	5	234.0	15.7	53.3
Q71U36	Tubulin alpha-1A chain	5.06	50104	5	228.7	14.1	58.7
P07437	Tubulin beta chain	4.89	49639	5	224.3	15.0	50.8
P68363	Tubulin alpha-1B chain	5.06	50120	5	217.6	14.0	58.4
Q13509	Tubulin beta-3 chain	4.93	50400	5	119.0	11.9	37.9
P08238	Heat shock protein HSP 90-beta	5.03	83200	5	100.7	12.5	21.7
Q14204	Cytoplasmic dynein 1 heavy chain 1	6.40	532072	5	95.9	12.8	3.9
P07900	Heat shock protein HSP 90-alpha	5.02	84607	5	85.9	11.8	22.2
P07197	Neurofilament medium polypeptide	4.91	102400	5	78.0	8.4	13.2
P07196	Neurofilament light polypeptide	4.65	61500	5	71.8	7.5	19.5
Q00610	Clathrin heavy chain 1	5.69	191500	5	60.2	8.8	7.7
Q16352	Alpha-internexin	5.40	55357	5	55.6	6.5	17.0
P46821	Microtubule-associated protein 1B	4.81	270500	5	43.0	8.6	5.1
P68104	Elongation factor 1-alpha 1	9.01	50109	5	33.6	3.7	10.7
Q9H115	Beta-soluble NSF attachment protein	5.47	33500	5	29.1	5.6	28.0
P04406	Glyceraldehyde-3-phosphate dehydrogenase	8.46	36000	5	11.7	2.6	12.0
P68366	Tubulin alpha-4A chain	5.06	49900	4	195.3	10.3	40.0
P60709	Actin, cytoplasmic 1	5.48	41700	4	113.9	7.6	34.2
Q01082	Spectrin beta chain, brain 1	5.57	274400	4	60.2	8.8	5.4
Q05193-2	Isoform 2 of Dynamin-1	6.87	97200	4	49.4	7.0	12.3
Q8IWE0	Calcium/calmodulin-dependent protein kinase II alpha	7.20	54054	4	30.9	4.5	16.0
P17600	Synapsin-1	9.83	74100	4	22.7	2.8	7.2

Acc. No.[a]	Name	Calc. pI	Calc. MW (Da)	No. of cases[b]	Avg. Xcorr[b]	Avg. No. of Peptides[c]	Avg. % Sequence Coverage[d]
Q13557	Calcium/calmodulin-dependent protein kinase type II subunit delta	7.25	56300	4	21.7	3.7	12.9
Q13813-2	Isoform 2 of Spectrin alpha chain, brain	5.35	284919	3	62.9	9.2	6.0
P12036	Neurofilament heavy polypeptide	6.18	112400	3	50.2	6.3	7.7
A8K9C4	Elongation factor 1-alpha	9.01	50169	3	44.8	4.3	13.9
P31150	Rab GDP dissociation inhibitor alpha	5.14	50550	3	31.5	6.2	22.4
Q13554	Calcium/calmodulin-dependent protein kinase type II subunit beta	7.27	72600	3	24.2	3.3	7.6
P63010	AP-2 complex subunit beta	5.38	104500	3	15.8	2.3	4.3
O95782	AP-2 complex subunit alpha-1	7.03	107500	3	9.6	2.0	3.2
O94811	Tubulin polymerization-promoting protein	9.44	23679	3	9.2	2.0	17.8
Q53G99	Beta actin variant (Fragment)	5.59	41738	2	87.5	6.7	31.5
Q9UQ16	Dynamin-3	8.35	97700	2	21.8	3.0	4.3
Q13557-8	Isoform Delta 6 of Calcium/calmodulin-dependent protein kinase type II subunit delta	7.25	54093	2	21.1	2.5	10.6
P78559	Microtubule-associated protein 1A	4.92	305298	2	20.1	3.5	1.7
Q13554-8	Isoform 8 of Calcium/calmodulin-dependent protein kinase type II subunit beta	7.28	57901	2	17.5	3.5	11.7
P29692	Elongation factor 1-delta	5.01	31100	2	10.8	2.3	9.8
Q9BUF5	Tubulin beta-6 chain	4.88	49800	1	179.6	8.0	23.7
P07900-2	Isoform 2 of Heat shock protein HSP 90-alpha	5.16	98099	1	125.4	17.0	26.0
Q53G85	Elongation factor 1-alpha (Fragment)	9.01	50081	1	27.4	3.0	9.7
P50570	Dynamin-2	7.44	98000	1	25.0	4.0	5.3
Q05193	Dynamin-1	7.17	97300	1	19.6	2.0	3.4
Q13813	Spectrin alpha chain, brain	5.35	284400	1	18.6	2.0	1.4
Q14203	Dynactin subunit 1	5.81	141600	1	14.8	2.0	2.7
Q92777	Synapsin-2	8.41	62800	1	14.1	3.0	9.6
P07737	Profilin-1	8.27	15045	1	13.6	2.0	21.4
Q59GI5	Dynamin 1 isoform 2 variant (Fragment)	7.68	68820	1	13.0	2.0	4.0
O00429	Dynamin-1-like protein	6.81	81800	1	12.3	2.0	3.5
P26641	Elongation factor 1-gamma	6.67	50100	1	10.6	2.0	7.1

Acc. No.[a]	Name	Calc. pI	Calc. MW (Da)	No. of cases[b]	Avg. Xcorr[b]	Avg. No. of Peptides[c]	Avg. % Sequence Coverage[d]
P54920	Alpha-soluble NSF attachment protein	5.36	33211	1	10.1	3.0	14.2
B4DM45	Highly similar to Dynactin-1	5.40	136735	1	9.2	2.0	2.4
O94973	AP-2 complex subunit alpha-2	6.96	103900	1	9.0	2.0	3.3
P63167	Dynein light chain 1, cytoplasmic	7.40	10359	1	8.2	2.0	37.1
E5KLK2	Mitochondrial dynamin-like 120 kDa protein	7.99	107501	1	7.4	2.0	3.4

[a] SwissProt accession number
[b] Number of MSA cases protein was identified in
[c] Average Xcorr significance score
[d] Average number of unique peptides sequenced
[e] Average % of the full-length amino acid sequence covered by identified peptides

Appendix C

MS Identification of 19 GCI proteins that are putative synaptic vesicle proteins

Acc. No.[a]	Name	Calc. pI	Calc. MW (Da)	No. of cases[b]	Avg. Xcorr[b]	Avg. No. of Peptides[c]	Avg. % Sequence Coverage[d]
P18669	Phosphoglycerate mutase 1	7.18	28800	4	23.2	3.6	20.9
Q9NQC3	Reticulon-4	4.50	129900	4	20.7	3.1	5.1
P09104	Gamma-enolase	5.03	47200	4	20.0	4.4	17.4
P07195	L-lactate dehydrogenase B chain	6.05	36615	4	12.4	2.3	8.4
Q01813	6-phosphofructokinase type C	7.55	85500	3	26.8	5.3	10.5
P52306	Rap1 GTPase-GDP dissociation stimulator 1	5.31	66300	3	24.5	4.0	9.8
P06733	Alpha-enolase	7.39	47139	3	20.6	3.5	13.4
P08237	6-phosphofructokinase, muscle type	7.99	85100	3	18.0	3.6	5.8
P61019	Ras-related protein Rab-2A	6.54	23531	3	12.1	2.3	14.6
P17858	6-phosphofructokinase, liver type	7.50	84964	2	24.8	4.7	8.2
P04216	Thy-1 membrane glycoprotein	8.73	17900	2	13.5	2.0	18.0
O95197-3	Isoform 3 of Reticulon-3	8.51	25593	2	10.7	2.0	11.0
P62760	Visinin-like protein 1	5.15	22128	1	16.2	4.0	24.6
P62820	Ras-related protein Rab-1A	6.21	22700	1	14.0	3.0	22.4
P14618	Pyruvate kinase isozymes M1/M2	7.84	57900	1	11.8	2.0	5.7
P62491	Ras-related protein Rab-11A	6.57	24400	1	9.8	2.0	11.1
Q16181	Septin-7	8.63	50600	1	9.0	2.0	6.5
P51148	Ras-related protein Rab-5C	8.41	23468	1	8.4	2.0	10.7
P09972	Fructose-bisphosphate aldolase C	6.87	39400	1	7.5	2.0	8.5

[a] SwissProt accession number
[b] Number of MSA cases protein was identified in
[c] Average Xcorr significance score
[d] Average number of unique peptides sequenced
[e] Average % of the full-length amino acid sequence covered by identified peptides

Appendix D

MS Identification of 81 GCI proteins identified in a single fraction from 1-DE fractionation

Fraction	Acc. No.[a]	Name	Calc. pI	Calc. MW (Da)	Xcorr[b]	No. of Peptides[c]	% Sequence Coverage[d]
2	P13637	Sodium/potassium-transporting ATPase subunit alpha-3	5.38	111700	69.1	11	14.8
2	P50993	Sodium/potassium-transporting ATPase subunit alpha-2	5.66	112200	58.8	9	12.6
2	Q13813-2	Isoform 2 of Spectrin alpha chain, brain	5.35	284919	55.0	6	3.4
2	Q12860	Contactin-1	5.90	113200	28.6	4	5.3
2	P11047	Laminin subunit gamma-1	5.12	177489	20.6	3	2.7
2	P16615	Sarcoplasmic/endoplasmic reticulum calcium ATPase 2	5.34	114700	20.0	2	2.8
2	P31944	*Caspase-14	5.58	27700	14.3	2	11.6
2	O75396	*Vesicle-trafficking protein SEC22b	6.92	24578	10.1	2	12.1
2	P04406	Glyceraldehyde-3-phosphate dehydrogenase	8.46	36000	8.1	2	8.4
2	P08123	*Collagen alpha-2(I) chain	8.95	129235	7.9	2	2.4
2	P12273	*Prolactin-inducible protein	8.05	16562	6.5	2	15.1
3	P11021	78 kDa glucose-regulated protein	5.16	72288	75.6	13	27.1
3	Q13813	Spectrin alpha chain, brain	5.35	284400	70.1	8	4.9
3	P14625	Endoplasmin	4.84	92400	58.0	5	8.3
3	P28331	NADH-ubiquinone oxidoreductase 75 kDa subunit, mitochondrial	6.23	79400	39.0	4	9.6
3	P13667	Protein disulfide-isomerase A4	5.07	72887	34.2	5	11.0
3	Q14643	*Inositol 1,4,5-trisphosphate receptor type 1	6.04	313700	33.0	3	1.4
3	P19367	Hexokinase-1	6.80	102400	32.8	4	5.9
3	Q14683	*Structural maintenance of chromosomes protein 1A	7.64	143144	30.7	4	4.0
3	Q92896	*Golgi apparatus protein 1	6.90	134464	30.2	8	8.9
3	Q14697	Neutral alpha-glucosidase AB	6.14	106807	29.5	5	8.5
3	P40939	*Trifunctional enzyme subunit alpha, mitochondrial	9.04	82947	28.1	5	9.6

Fraction	Acc. No.[a]	Name	Calc. pI	Calc. MW (Da)	Xcorr[b]	No. of Peptides[c]	% Sequence Coverage[d]
3	P35580	Myosin-10	5.54	228858	26.1	5	3.7
3	P55268	Laminin subunit beta-2	6.52	195854	24.3	3	2.5
3	O75746	Calcium-binding mitochondrial carrier protein Aralar1	8.38	74700	21.3	2	3.7
3	B7Z4T3	*Highly similar to Stress-70 protein, mitochondrial	6.34	69908	20.5	3	5.5
3	P38606	V-type proton ATPase catalytic subunit A	5.52	68300	19.3	3	8.1
3	P29401	Transketolase	7.66	67800	18.7	3	9.3
3	P02787	Serotransferrin	7.12	77014	18.3	2	3.0
3	P13591	Neural cell adhesion molecule 1	4.87	94500	17.8	2	3.6
3	P43304	*Glycerol-3-phosphate dehydrogenase, mitochondrial	7.69	80800	17.1	2	3.9
3	Q6P2Q9	*Pre-mRNA-processing-splicing factor 8	8.84	273427	16.8	2	0.9
3	P36776	*Lon protease homolog, mitochondrial	6.39	106400	16.6	3	3.3
3	P35606	*Coatomer subunit beta	5.27	102400	15.1	3	3.4
3	P49327	Fatty acid synthase	6.44	273254	14.4	2	1.1
3	P51659	Peroxisomal multifunctional enzyme type 2	8.84	79600	10.6	2	3.7
3	P29966	Myristoylated alanine-rich C-kinase substrate	4.45	31500	9.5	2	11.1
3	Q16891	Mitochondrial inner membrane protein	6.48	83600	8.6	2	3.7
3	O94856-4	*Isoform 4 of Neurofascin	6.28	119395	6.0	2	3.2
4	P30101	Protein disulfide-isomerase A3	6.35	56700	39.7	3	6.5
4	P10809	60 kDa heat shock protein, mitochondrial	5.87	61000	25.4	3	9.4
4	P07237	Protein disulfide-isomerase	4.87	57100	23.3	3	11.4
4	P49748	*Very long-chain specific acyl-CoA dehydrogenase, mitochondrial	8.75	70300	17.4	2	4.1
4	P46459	Vesicle-fusing ATPase	6.95	82500	14.6	2	3.6
4	Q9UHG3	Prenylcysteine oxidase 1	6.18	56600	11.9	2	5.0
4	Q9Y265	*RuvB-like 1	6.42	50200	10.6	2	5.9
4	P14618	Pyruvate kinase isozymes M1/M2	7.84	57900	6.9	2	5.5
4	Q15084	Protein disulfide-isomerase A6	5.08	48100	6.3	2	8.4
5	P22695	Cytochrome b-c1 complex subunit 2, mitochondrial	8.63	48413	52.2	8	30.0
5	P15311	*Ezrin	6.27	69370	33.9	3	7.9

Fraction	Acc. No.a	Name	Calc. pI	Calc. MW (Da)	Xcorrb	No. of Peptidesc	% Sequence Coveraged
5	P21579	Synaptotagmin-1	8.12	47543	31.0	3	10.7
5	Q99623	Prohibitin-2	9.83	33300	28.4	3	14.7
5	P12532	Creatine kinase U-type, mitochondrial	8.34	47007	23.4	3	18.2
5	P48735	Isocitrate dehydrogenase [NADP], mitochondrial	8.69	50900	21.7	3	9.1
5	O94905	Erlin-2	5.62	37800	13.8	3	11.5
5	P28845	Corticosteroid 11-beta-dehydrogenase isozyme 1	8.56	32380	13.0	2	8.6
5	P49411	*Elongation factor Tu, mitochondrial	7.61	49510	12.7	2	5.8
5	O43427	*Acidic fibroblast growth factor intracellular-binding protein	6.48	41900	11.1	3	9.3
6	P62258	14-3-3 protein epsilon	4.74	29155	78.0	6	27.8
6	P61981	14-3-3 protein gamma	4.89	28285	49.5	5	25.1
6	P31946	14-3-3 protein beta/alpha	4.83	28100	47.0	6	33.3
6	Q04917	14-3-3 protein eta	4.84	28201	31.3	3	11.8
6	Q07021	Complement component 1 Q subcomponent-binding protein, mitochondrial	4.84	31300	16.5	3	22.7
7	Q53GE9	*Elongation factor 1-alpha (Fragment)	9.01	50079	21.6	2	8.7
7	O75947	ATP synthase subunit d, mitochondrial	5.30	18500	17.6	2	21.7
7	P24539	ATP synthase subunit b, mitochondrial	9.36	28900	14.5	2	9.4
8	Q9BVA1	*Tubulin beta-2B chain	4.89	49921	102.5	8	22.7
8	Q13509	Tubulin beta-3 chain	4.93	50400	63.3	8	22.4
8	P12956	X-ray repair cross-complementing protein 6	6.64	69800	23.6	4	6.7
8	P68104	Elongation factor 1-alpha 1	9.01	50109	19.3	2	8.7
8	P30044	Peroxiredoxin-5, mitochondrial	8.70	22100	17.1	2	13.1
8	P51991	Heterogeneous nuclear ribonucleoprotein A3	9.01	39600	14.6	2	6.9
8	P63027	Vesicle-associated membrane protein 2	8.13	12655	13.0	2	28.5
8	P09651	Heterogeneous nuclear ribonucleoprotein A1	9.13	38700	9.8	2	7.0
8	P17568	*Fatty acid synthase	8.92	16391	7.7	2	12.4
9	P68371	Tubulin beta-2C chain	4.89	49799	89.5	7	20.0
9	P22626	Heterogeneous nuclear ribonucleoproteins A2/B1	8.95	37400	22.1	2	4.8

Fraction	Acc. No.a	Name	Calc. pI	Calc. MW (Da)	Xcorrb	No. of Peptidesc	% Sequence Coveraged
9	Q16718	NADH dehydrogenase [ubiquinone] 1 alpha subcomplex subunit 5	5.99	13450	19.6	2	31.0
9	P07910	Heterogeneous nuclear ribonucleoproteins C1/C2	5.08	33600	11.0	2	8.8
9	P08237	6-phosphofructokinase, muscle type	7.99	85100	10.2	2	4.0
10	P04083	*Annexin A1	7.02	38700	11.2	2	10.1

[a] SwissProt accession number
[b] Xcorr significance score
[c] Number of unique peptides sequenced
[d] % of the full-length amino acid sequence covered by identified peptides
* not previously identified by direct injection analysis

Appendix E

MS Identification of 36 GCI proteins identified in multiple fractions from 1-DE fractionation

Fractions	Acc. No.[a]	Name	Calc. pI	Calc. MW (Da)	Avg. Xcorr[b]	Avg. No. of Peptides[c]	Avg. % Sequence Coverage[d]
1-10	Q15582	*Transforming growth factor-beta-induced protein ig-h3	7.71	74634	98.6	2.8	8.0
4,6	Q13885	Tubulin beta-2A chain	4.89	49875	85.1	7.0	21.8
2-10	P04350	Tubulin beta-4 chain	4.88	49554	81.1	7.1	22.5
4-6	Q71U36	Tubulin alpha-1A chain	5.06	50104	79.4	5.7	23.6
2-5,7-9	P14136	Glial fibrillary acidic protein	5.52	49800	53.8	5.0	12.7
2,3	Q01082	Spectrin beta chain, brain 1	5.57	274400	51.0	6.5	3.9
6,8,9	P37840	Alpha-synuclein	4.70	14500	49.0	3.7	32.6
2,3	P12111	Collagen alpha-3(VI) chain	6.68	343500	48.8	4.5	1.8
1-3	P05023	Sodium/potassium-transporting ATPase subunit alpha-1	5.49	112800	48.3	8.0	12.0
3,4	Q86VX4	Structural maintenance of chromosomes 3	7.18	141400	48.2	6.0	6.9
2,3	Q00610	Clathrin heavy chain 1	5.69	191500	45.8	5.5	4.2
4,5	P25705	ATP synthase subunit alpha, mitochondrial	9.13	59714	43.8	5.5	16.6
2,3,7-9	P68363	Tubulin alpha-1B chain	5.06	50120	42.1	3.2	13.1
5-7	P60709	Actin, cytoplasmic 1	5.48	41700	39.5	3.3	18.0
3,4,7	Q14204	Cytoplasmic dynein 1 heavy chain 1	6.40	532072	39.5	4.0	1.3
2,4-9	P12277	Creatine kinase B-type	5.59	42600	38.1	3.9	17.7
4-6,8	P06576	ATP synthase subunit beta, mitochondrial	5.40	56500	36.7	5.3	16.9
5-7,9	P09543	2',3'-cyclic-nucleotide 3'-phosphodiesterase	9.07	47500	35.8	4.0	14.5
6-9	P63104	14-3-3 protein zeta/delta	4.79	27728	32.4	3.3	18.3
5-7,9	P27348	14-3-3 protein theta	4.78	27747	30.6	4.0	21.9
6-9	P16152	Carbonyl reductase [NADPH] 1	8.32	30356	27.7	2.3	11.5
8,9	P08238	Heat shock protein HSP 90-beta	5.03	83200	26.7	3.0	5.5
2,5	P09471	Guanine nucleotide-binding protein G(o) subunit alpha	5.53	40000	22.6	3.0	10.2
4,5,8	P61764	Syntaxin-binding protein 1	6.96	67500	20.7	2.0	4.5

Fractions	Acc. No.[a]	Name	Calc. pI	Calc. MW (Da)	Avg. Xcorr[b]	Avg. No. of Peptides[c]	Avg. % Sequence Coverage[d]
3,4	P27824	Calnexin	4.60	67526	18.7	2.5	4.9
4,5,8	Q00839	Heterogeneous nuclear ribonucleoprotein U	6.00	90500	16.2	2.3	4.2
2,3	P02768	Serum albumin	6.28	69300	15.8	2.5	4.4
3,5	P78527	DNA-dependent protein kinase catalytic subunit	7.12	468800	14.8	2.0	0.6
4,5	P07196	Neurofilament light polypeptide	4.65	61500	14.2	2.0	3.9
6-8	P31943	Heterogeneous nuclear ribonucleoprotein H	6.30	49200	13.0	2.3	9.0
3,7	P22314	Ubiquitin-like modifier-activating enzyme 1	5.76	117774	12.7	2.5	3.4
6,7	P47985	*Cytochrome b-c1 complex subunit Rieske, mitochondrial	8.32	29649	11.5	2.0	12.8
3-5	P11216	Glycogen phosphorylase, brain form	6.86	96600	11.5	2.0	3.5
3,5	Q05193	Dynamin-1	7.17	97300	11.4	2.0	3.4
8,9	P68871	Hemoglobin subunit beta	7.28	15988	9.0	2.0	21.8
3,4	P05026	Sodium/potassium-transporting ATPase subunit beta-1	8.53	35000	7.9	2.0	8.9

[a] SwissProt accession number
[b] Average Xcorr significance score
[c] Average number of unique peptides sequenced
[d] Average % of the full-length amino acid sequence covered by identified peptides
* not previously identified by direct injection analysis

Appendix F

MS Identification of 135 variants of 99 GCI proteins from 209 spots from 2-DE fractionation

Spot No.	Acc. No.[a]	Name	Calc. pI[b]	Calc. MW (Da)[c]	App. pI[d]	App. MW (Da)[e]	Xcorr[f]	No. Peptides[g]	% Sequence Coverage[h]
1	P10809	60 kDa heat shock protein, mitochondrial	5.87	61000	5.30	60000	443.1	15	39.6
2	P11021	78 kDa glucose-regulated protein	5.16	72300	5.10	85000	826.6	26	42.2
3	P02511	Alpha-crystallin B chain	7.33	20100	6.10	20000	19.0	2	19.4
4	P02511	Alpha-crystallin B chain	7.33	20100	6.00	19000	18.6	2	19.4
5	P02511	Alpha-crystallin B chain	7.33	20100	6.10	15000	20.1	3	25.7
6	P02511	Alpha-crystallin B chain	7.33	20100	6.20	12000	175.0	3	24.0
7	P02511	Alpha-crystallin B chain	7.33	20100	6.30	20000	30.3	3	24.0
8	P02511	Alpha-crystallin B chain	7.33	20100	6.50	20000	40.3	4	30.3
9	P02511	Alpha-crystallin B chain	7.33	20100	6.50	18000	60.3	6	38.3
10	P02511	Alpha-crystallin B chain	7.33	20100	6.50	15000	55.6	2	21.1
11	P02511	Alpha-crystallin B chain	7.33	20100	6.60	15000	28.7	2	21.1
12	P02511	Alpha-crystallin B chain	7.33	20100	6.90	20000	60.3	6	38.9
13	P02511	Alpha-crystallin B chain	7.33	20100	6.90	19000	60.3	6	38.9
14	P02511	Alpha-crystallin B chain	7.33	20100	7.20	20000	91.3	8	53.1
15	P02511	Alpha-crystallin B chain	7.33	20100	7.40	20000	91.3	8	53.1
16	P02511	Alpha-crystallin B chain	7.33	20100	7.50	13000	13.8	2	21.1
17	P02511	Alpha-crystallin B chain	7.33	20100	7.50	12000	11.1	2	21.1
18	Q9UBS4	DnaJ homolog subfamily B member 11	6.18	40500	6.10	43000	119.1	4	20.1
19	P14625	Endoplasmin	4.84	92400	5.00	120000	378.7	17	26.7
20	P11142	Heat shock cognate 71 kDa protein	5.52	70900	5.40	80000	248.8	16	34.1
21	P08238	Heat shock protein HSP 90-beta	5.03	83200	5.10	110000	134.7	7	13.0
	P07900	Heat shock protein HSP 90-alpha	5.02	84600	5.10	110000	130.8	7	11.8
22	P08238	Heat shock protein HSP 90-beta	5.03	83200	5.20	95000	31.1	5	9.1
23	Q9Y4L1	Hypoxia up-regulated protein 1	5.22	111300	5.20	170000	372.7	18	31.0

Spot No.	Acc. No.[a]	Name	Calc. pI[b]	Calc. MW (Da)[c]	App. pI[d]	App. MW (Da)[e]	Xcorr[f]	No. Peptides[g]	% Sequence Coverage[h]
24	P30101	Protein disulfide-isomerase A3	6.35	56700	5.60	60000	542.6	16	36.8
25	P30101	Protein disulfide-isomerase A3	6.35	56700	5.70	60000	493.2	11	26.1
26	P07237	Protein disulfide-isomerase	4.87	57100	5.00	60000	163.0	9	25.6
27	Q15084	Protein disulfide-isomerase A6	5.08	48100	5.20	52000	349.5	9	24.6
	Q71U36	Tubulin alpha-1A chain	5.06	50100	5.20	52000	186.8	9	34.4
	P04350	Tubulin beta-4 chain	4.88	49600	5.20	52000	77.3	8	25.5
28	P38646	Stress-70 protein, mitochondrial	6.16	73600	5.50	85000	457.8	20	39.0
29	Q99832	T-complex protein 1 subunit eta	7.65	59300	8.20	60000	76.2	5	14.6
30	P04350	Tubulin beta-4 chain	4.88	49600	5.10	55000	483.7	14	41.4
	P68371	Tubulin beta-2C chain	4.89	49800	5.10	55000	412.9	14	40.5
	Q13885	Tubulin beta-2A chain	4.89	49900	5.10	55000	398.4	13	34.4
31	P68363	Tubulin alpha-1B chain	5.06	50100	5.20	58000	451.0	10	39.0
	P68366	Tubulin alpha-4A chain	5.06	49900	5.20	58000	265.3	8	30.1
	Q9NY65	Tubulin alpha-8 chain	5.06	50100	5.20	58000	189.0	6	21.2
32	Q71U36	Tubulin alpha-1A chain	5.06	50100	5.20	58000	408.4	11	41.2
33	Q71U36	Tubulin alpha-1A chain	5.06	50100	5.20	52000	212.9	11	42.6
	P04350	Tubulin beta-4 chain	4.88	49600	5.20	52000	61.0	7	20.3
	Q15084	Protein disulfide-isomerase A6	5.08	48100	5.20	52000	59.0	7	21.4
34	P04350	Tubulin beta-4 chain	4.88	49600	5.30	52000	173.4	11	33.6
	Q71U36	Tubulin alpha-1A chain	5.06	50100	5.30	52000	109.9	6	21.7
	P10644	cAMP-dependent protein kinase type I-alpha regulatory subunit	5.35	43000	5.30	52000	53.9	5	16.0
35	Q71U36	Tubulin alpha-1A chain	5.06	50100	5.30	50000	190.8	9	35.3
	P04350	Tubulin beta-4 chain	4.88	49600	5.30	50000	50.8	4	11.9

Spot No.	Acc. No.[a]	Name	Calc. pI[b]	Calc. MW (Da)[c]	App. pI[d]	App. MW (Da)[e]	Xcorr[f]	No. Peptides[g]	% Sequence Coverage[h]
36	Q71U36	Tubulin alpha-1A chain	5.06	50100	5.30	48000	177.7	9	33.9
	P04350	Tubulin beta-4 chain	4.88	49600	5.30	48000	65.5	4	11.0
	P14136	Glial fibrillary acidic protein	5.52	49800	5.30	48000	55.5	9	23.2
	Q5VWJ9	Sorting nexin-30	5.35	49600	5.30	48000	39.4	2	5.7
	P54578	Ubiquitin carboxyl-terminal hydrolase 14	5.30	56000	5.30	48000	21.9	3	8.7
	Q02790	Peptidyl-prolyl cis-trans isomerase FKBP4	5.43	51800	5.30	48000	14.0	3	11.3
37	P04350	Tubulin beta-4 chain	4.88	49600	5.30	52000	266.2	13	36.3
	P68371	Tubulin beta-2C chain	4.89	49800	5.30	52000	204.6	10	29.9
	Q13885	Tubulin beta-2A chain	4.89	49900	5.30	52000	188.0	11	32.6
	P07437	Tubulin beta chain	4.89	49600	5.30	52000	140.2	10	29.3
	Q16401	26S proteasome non-ATPase regulatory subunit 5	5.48	56200	5.30	52000	59.3	5	19.4
	P52306	Rap1 GTPase-GDP dissociation stimulator 1	5.31	66300	5.30	52000	48.0	5	12.4
	P68363	Tubulin alpha-1B chain	5.06	50100	5.30	52000	47.0	5	18.6
38	Q71U36	Tubulin alpha-1A chain	5.06	50100	5.30	50000	164.6	2	9.1
39	P04350	Tubulin beta-4 chain	4.88	49600	5.70	45000	41.3	2	5.0
40	P04350	Tubulin beta-4 chain	4.88	49600	5.60	41000	159.6	10	29.7
	Q13885	Tubulin beta-2A chain	4.89	49900	5.60	41000	94.2	7	18.7
	P09471-2	Isoform Alpha-2 of Guanine nucleotide-binding protein G(o) subunit alpha	5.90	40100	5.60	41000	84.1	5	18.9
	P68363	Tubulin alpha-1B chain	5.06	50100	5.60	41000	47.6	3	12.4
41	P04350	Tubulin beta-4 chain	4.88	49600	5.20	39000	139.0	9	23.9
	P14136	Glial fibrillary acidic protein	5.52	49800	5.20	39000	50.9	5	12.0
	P68363	Tubulin alpha-1B chain	5.06	50100	5.20	39000	24.7	4	15.3
42	P04350	Tubulin beta-4 chain	4.88	49600	5.20	37000	193.1	11	36.0
	P68371	Tubulin beta-2C chain	4.89	49800	5.20	37000	161.5	9	28.3
	Q13885	Tubulin beta-2A chain	4.89	49900	5.20	37000	155.4	9	28.3
	Q71U36	Tubulin alpha-1A chain	5.06	50100	5.20	37000	37.7	4	15.5

Spot No.	Acc. No.[a]	Name	Calc. pI[b]	Calc. MW (Da)[c]	App. pI[d]	App. MW (Da)[e]	Xcorr[f]	No. Peptides[g]	% Sequence Coverage[h]
43	P04350	Tubulin beta-4 chain	4.88	49600	5.20	36000	189.5	10	30.4
	P68371	Tubulin beta-2C chain	4.89	49800	5.20	36000	126.9	9	26.7
	Q13885	Tubulin beta-2A chain	4.89	49900	5.20	36000	105.8	8	23.4
	Q71U36	Tubulin alpha-1A chain	5.06	50100	5.20	36000	42.3	4	15.5
44	P04350	Tubulin beta-4 chain	4.88	49600	4.80	20000	15.1	2	6.1
45	P68371	Tubulin beta-2C chain	4.89	49800	4.90	19000	26.4	4	12.1
	P04350	Tubulin beta-4 chain	4.88	49600	4.90	19000	26.0	4	12.2
46	P68371	Tubulin beta-2C chain	4.89	49800	4.90	19000	54.4	3	9.4
	P04350	Tubulin beta-4 chain	4.88	49600	4.90	19000	51.2	4	12.2
47	P04350	Tubulin beta-4 chain	4.88	49600	4.90	19000	71.2	5	15.5
48	P04350	Tubulin beta-4 chain	4.88	49600	4.90	19000	79.9	4	12.4
49	P68371	Tubulin beta-2C chain	4.89	49800	5.00	20000	34.2	3	9.4
50	P68363	Tubulin alpha-1B chain	5.06	50100	5.00	20000	5.5	2	6.2
51	P68363	Tubulin alpha-1B chain	5.06	50100	5.10	20000	18.8	2	6.2
52	P68363	Tubulin alpha-1B chain	5.06	50100	5.10	20000	27.1	2	6.2
53	P04350	Tubulin beta-4 chain	4.88	49600	5.20	22000	30.7	4	11.0
54	P68363	Tubulin alpha-1B chain	5.06	50100	5.40	22000	23.4	2	7.8
	P27348	14-3-3 protein theta	4.78	27700	5.40	22000	19.1	2	13.1
55	P68363	Tubulin alpha-1B chain	5.06	50100	5.40	20000	36.9	2	7.8
56	P04350	Tubulin beta-4 chain	4.88	49600	5.00	17000	39.6	3	10.4
	P68363	Tubulin alpha-1B chain	5.06	50100	5.00	17000	16.6	2	6.2
57	P04350	Tubulin beta-4 chain	4.88	49600	4.80	15000	49.2	3	11.0
	P37840	Alpha-synuclein	4.70	14500	4.80	15000	27.9	2	25.7
58	P68363	Tubulin alpha-1B chain	5.06	50100	5.40	17000	11.5	2	7.8
59	P04350	Tubulin beta-4 chain	4.88	49600	5.30	14000	36.8	2	4.5
60	P04350	Tubulin beta-4 chain	4.88	49600	5.60	15000	12.5	2	5.6
61	P04350	Tubulin beta-4 chain	4.88	49600	5.60	12000	32.8	2	4.5
	P37840	Alpha-synuclein	4.70	14500	5.60	12000	13.0	2	25.7

Spot No.	Acc. No.[a]	Name	Calc. pI[b]	Calc. MW (Da)[c]	App. pI[d]	App. MW (Da)[e]	Xcorr[f]	No. Peptides[g]	% Sequence Coverage[h]
62	P04350	Tubulin beta-4 chain	4.88	49600	6.00	10000	31.1	2	4.5
63	P60709	Actin, cytoplasmic 1	5.48	41700	5.20	45000	139.1	7	28.3
64	P60709	Actin, cytoplasmic 1	5.48	41700	5.30	45000	261.1	8	31.2
65	P60709	Actin, cytoplasmic 1	5.48	41700	5.30	45000	242.4	7	28.5
66	P60709	Actin, cytoplasmic 1	5.48	41700	5.50	41000	147.3	6	25.9
67	P60709	Actin, cytoplasmic 1	5.48	41700	5.50	37000	87.9	6	25.6
68	P60709	Actin, cytoplasmic 1	5.48	41700	5.80	41000	83.8	6	20.5
69	P14136	Glial fibrillary acidic protein	5.52	49800	5.40	52000	166.0	11	29.2
	Q13885	Tubulin beta-2A chain	4.89	49900	5.40	52000	146.0	10	29.4
	P68371	Tubulin beta-2C chain	4.89	49800	5.40	52000	135.2	9	26.7
	P04350	Tubulin beta-4 chain	4.88	49600	5.40	52000	133.8	10	30.4
	P07437	Tubulin beta chain	4.89	49600	5.40	52000	119.2	10	29.5
	P68363	Tubulin alpha-1B chain	5.06	50100	5.40	52000	27.3	3	10.2
70	P14136	Glial fibrillary acidic protein	5.52	49800	5.50	52000	224.1	15	38.2
	Q13885	Tubulin beta-2A chain	4.89	49900	5.50	52000	143.0	10	29.4
	P68371	Tubulin beta-2C chain	4.89	49800	5.50	52000	133.6	9	26.1
	P04350	Tubulin beta-4 chain	4.88	49600	5.50	52000	133.2	9	27.0
	Q13509	Tubulin beta-3 chain	4.93	50400	5.50	52000	125.4	9	26.4
	P07437	Tubulin beta chain	4.89	49600	5.50	52000	112.1	9	26.1
	P68363	Tubulin alpha-1B chain	5.06	50100	5.50	52000	34.8	4	14.6
71	P14136	Glial fibrillary acidic protein	5.52	49800	5.10	42000	247.7	11	28.5
72	P14136	Glial fibrillary acidic protein	5.52	49800	5.10	39000	216.7	15	31.3
	Q13885	Tubulin beta-2A chain	4.89	49900	5.10	39000	155.5	7	19.8
	P04350	Tubulin beta-4 chain	4.88	49600	5.10	39000	150.3	8	23.4
	Q13509	Tubulin beta-3 chain	4.93	50400	5.10	39000	128.0	7	19.6
73	P14136	Glial fibrillary acidic protein	5.52	49800	5.00	38000	331.2	11	28.2
74	P14136	Glial fibrillary acidic protein	5.52	49800	4.80	39000	56.4	3	7.2
	P04350	Tubulin beta-4 chain	4.88	49600	4.80	39000	44.8	4	11.7
75	P12277	Creatine kinase B-type	5.59	42600	5.20	42000	207.9	7	32.8

Spot No.	Acc. No.[a]	Name	Calc. pI[b]	Calc. MW (Da)[c]	App. pI[d]	App. MW (Da)[e]	Xcorr[f]	No. Peptides[g]	% Sequence Coverage[h]
76	P12277	Creatine kinase B-type	5.59	42600	5.30	43000	333.8	7	32.8
77	P12277	Creatine kinase B-type	5.59	42600	5.30	43000	270.5	9	38.9
78	P12277	Creatine kinase B-type	5.59	42600	5.30	42000	289.7	8	36.2
79	P12277	Creatine kinase B-type	5.59	42600	5.30	41000	176.1	6	24.4
80	P12277	Creatine kinase B-type	5.59	42600	5.40	45000	474.7	9	41.2
81	P12277	Creatine kinase B-type	5.59	42600	5.50	45000	614.9	12	48.8
82	P12277	Creatine kinase B-type	5.59	42600	5.60	45000	29.7	3	14.2
	O94905	Erlin-2	5.62	37800	5.60	45000	21.5	3	11.5
83	P12277	Creatine kinase B-type	5.59	42600	5.40	41000	308.7	7	27.0
84	P12277	Creatine kinase B-type	5.59	42600	5.80	39000	66.5	3	18.6
	P21695	Glycerol-3-phosphate dehydrogenase [NAD+], cytoplasmic	6.18	37500	5.80	39000	33.7	5	16.3
	P68363	Tubulin alpha-1B chain	5.06	50100	5.80	39000	26.1	4	14.2
	P62140	Serine/threonine-protein phosphatase PP1-beta catalytic subunit	6.19	37200	5.80	39000	17.1	3	10.1
	P53365	Arfaptin-2	6.04	37800	5.80	39000	10.9	2	7.9
	P04350	Tubulin beta-4 chain	4.88	49600	5.80	39000	7.9	2	4.5
85	P12277	Creatine kinase B-type	5.59	42600	5.90	37000	84.1	5	24.2
86	P12277	Creatine kinase B-type	5.59	42600	6.20	35000	152.6	8	34.9
87	P12277	Creatine kinase B-type	5.59	42600	5.70	25000	106.6	4	18.1
88	P12277	Creatine kinase B-type	5.59	42600	5.80	22000	8.3	3	11.6
89	P12277	Creatine kinase B-type	5.59	42600	6.10	23000	47.4	3	13.9
90	P12532	Creatine kinase U-type, mitochondrial	8.34	47000	7.90	48000	34.7	2	13.2
91	P00558	Phosphoglycerate kinase 1	8.10	44600	9.20	47000	104.8	8	29.3
	P09543	2',3'-cyclic-nucleotide 3'-phosphodiesterase	9.07	47500	9.20	47000	91.2	9	26.6
	P68104	Elongation factor 1-alpha 1	9.01	50100	9.20	47000	43.5	3	10.0
92	P14618-2	Isoform M1 of Pyruvate kinase isozymes M1/M2	7.71	58000	8.10	60000	118.9	7	20.5
93	P30085	UMP-CMP kinase	5.57	22200	5.50	22000	37.1	2	12.8
	P32119	Peroxiredoxin-2	5.97	21900	5.50	22000	26.5	2	8.6
	Q9UBI1	COMM domain-containing protein 3	5.99	22100	5.50	22000	7.9	2	12.3

Spot No.	Acc. No.[a]	Name	Calc. pI[b]	Calc. MW (Da)[c]	App. pI[d]	App. MW (Da)[e]	Xcorr[f]	No. Peptides[g]	% Sequence Coverage[h]
94	P16152	Carbonyl reductase [NADPH] 1	8.32	30400	9.00	34000	12.7	2	9.8
95	P16152	Carbonyl reductase [NADPH] 1	8.32	30400	9.30	32000	137.4	7	40.8
96	P16152	Carbonyl reductase [NADPH] 1	8.32	30400	9.20	30000	53.4	6	28.9
	Q8TB37	Iron-sulfur protein NUBPL	9.04	34100	9.20	30000	30.1	4	20.1
	P05388	60S acidic ribosomal protein P0	5.97	34300	9.20	30000	11.4	2	8.5
97	P16152	Carbonyl reductase [NADPH] 1	8.32	30400	9.30	28000	35.3	3	14.4
	Q0KKI6	Immunoblobulin light chain (Fragment)	8.06	24000	9.30	28000	30.6	4	29.2
98	P16152	Carbonyl reductase [NADPH] 1	8.32	30400	9.30	26000	37.9	5	26.0
	Q0KKI6	Immunoblobulin light chain (Fragment)	8.06	24000	9.30	26000	27.4	3	22.8
99	P16152	Carbonyl reductase [NADPH] 1	8.32	30400	10.20	26000	19.4	2	10.1
100	P28845	Corticosteroid 11-beta-dehydrogenase isozyme 1	8.56	32400	9.00	37000	24.2	2	8.6
	P51991	Heterogeneous nuclear ribonucleoprotein A3	9.01	39600	9.00	37000	9.2	2	6.9
101	O43175	D-3-phosphoglycerate dehydrogenase	6.71	56600	6.40	55000	20.4	2	5.1
	P14868	Aspartyl-tRNA synthetase, cytoplasmic	6.55	57100	6.40	55000	18.9	2	6.0
	P05166	Propionyl-CoA carboxylase beta chain, mitochondrial	7.64	58200	6.40	55000	15.5	2	5.2
102	Q02338	D-beta-hydroxybutyrate dehydrogenase, mitochondrial	8.95	38100	9.10	30000	48.9	4	18.4
	P16152	Carbonyl reductase [NADPH] 1	8.32	30400	9.10	30000	20.5	3	15.9
103	P04406	Glyceraldehyde-3-phosphate dehydrogenase	8.46	36000	9.00	38000	64.6	6	39.4
	P28845	Corticosteroid 11-beta-dehydrogenase isozyme 1	8.56	32400	9.00	38000	8.5	2	8.6
104	P04406	Glyceraldehyde-3-phosphate dehydrogenase	8.46	36000	9.40	38000	39.0	4	23.9
105	Q6FHB5	HMOX2 protein (Fragment)	5.41	36000	5.80	32000	109.5	6	33.9
106	Q02252	Methylmalonate-semialdehyde dehydrogenase [acylating], mitochondrial	8.50	57800	8.10	55000	31.8	3	10.5
107	Q02252	Methylmalonate-semialdehyde dehydrogenase [acylating], mitochondrial	8.50	57800	8.90	55000	135.6	3	10.5
108	P51659	Peroxisomal multifunctional enzyme type 2	8.84	79600	9.10	37000	74.7	7	15.8
	P40926	Malate dehydrogenase, mitochondrial	8.68	35500	9.10	37000	34.9	5	21.3
	Q68Y55	Poly(RC) binding protein 2	8.00	34900	9.10	37000	17.6	2	10.0

Spot No.	Acc. No.[a]	Name	Calc. pI[b]	Calc. MW (Da)[c]	App. pI[d]	App. MW (Da)[e]	Xcorr[f]	No. Peptides[g]	% Sequence Coverage[h]
109	P06576	ATP synthase subunit beta, mitochondrial	5.40	56500	5.10	52000	676.2	22	68.6
	Q71U36	Tubulin alpha-1A chain	5.06	50100	5.10	52000	128.6	7	26.2
	P04350	Tubulin beta-4 chain	4.88	49600	5.10	52000	92.1	7	21.4
110	P25705	ATP synthase subunit alpha, mitochondrial	9.13	59700	7.50	55000	51.7	7	18.3
	Q02252	Methylmalonate-semialdehyde dehydrogenase [acylating], mitochondrial	8.50	57800	7.50	55000	46.4	5	13.8
	P43490	Nicotinamide phosphoribosyltransferase	7.15	55500	7.50	55000	40.8	5	15.3
111	P25705	ATP synthase subunit alpha, mitochondrial	9.13	59700	8.10	55000	85.3	7	19.0
112	P25705	ATP synthase subunit alpha, mitochondrial	9.13	59700	8.80	55000	539.1	14	36.9
113	P25705	ATP synthase subunit alpha, mitochondrial	9.13	59700	9.20	55000	240.1	9	24.4
114	P25705	ATP synthase subunit alpha, mitochondrial	9.13	59700	9.50	43000	50.8	6	16.5
	P04075	Fructose-bisphosphate aldolase A	8.09	39400	9.50	43000	37.5	3	12.9
	P09543	2',3'-cyclic-nucleotide 3'-phosphodiesterase	9.07	47500	9.50	43000	23.9	2	5.5
115	P25705	ATP synthase subunit alpha, mitochondrial	9.13	59700	10.20	42000	84.2	4	12.5
116	P31930	Cytochrome b-c1 complex subunit 1, mitochondrial	6.37	52600	5.50	50000	125.0	8	27.5
	P14136	Glial fibrillary acidic protein	5.52	49800	5.50	50000	93.1	10	25.9
	P04350	Tubulin beta-4 chain	4.88	49600	5.50	50000	59.0	6	18.0
	Q9Y230	RuvB-like 2	5.64	51100	5.50	50000	43.7	5	13.2
	P68363	Tubulin alpha-1B chain	5.06	50100	5.50	50000	37.5	4	14.2
	Q02790	Peptidyl-prolyl cis-trans isomerase FKBP4	5.43	51800	5.50	50000	25.1	3	11.3
117	P31930	Cytochrome b-c1 complex subunit 1, mitochondrial	6.37	52600	5.50	50000	226.0	8	26.5
	P06576	ATP synthase subunit beta, mitochondrial	5.40	56500	5.50	50000	61.5	5	24.0
118	P22695	Cytochrome b-c1 complex subunit 2, mitochondrial	8.63	48400	8.20	48000	135.8	7	29.8
119	P47985	Cytochrome b-c1 complex subunit Rieske, mitochondrial	8.32	29600	6.40	27000	40.4	2	12.8
120	P47985	Cytochrome b-c1 complex subunit Rieske, mitochondrial	8.32	29600	6.40	25000	21.1	2	12.8
121	P20674	Cytochrome c oxidase subunit 5A, mitochondrial	6.79	16800	5.10	12000	12.0	2	16.0
	P37840	Alpha-synuclein	4.70	14500	5.10	12000	7.1	2	25.7
122	P38117	Electron transfer flavoprotein subunit beta	8.10	27800	9.10	28000	41.0	3	14.9
	O14818	Proteasome subunit alpha type-7	8.46	27900	9.10	28000	17.1	2	11.7

Spot No.	Acc. No.[a]	Name	Calc. pI[b]	Calc. MW (Da)[c]	App. pI[d]	App. MW (Da)[e]	Xcorr[f]	No. Peptides[g]	% Sequence Coverage[h]
123	Q16718	NADH dehydrogenase [ubiquinone] 1 alpha subcomplex subunit 5	5.99	13500	5.60	11000	16.0	2	16.4
	P37840	Alpha-synuclein	4.70	14500	5.60	11000	6.4	2	25.7
124	P49821	NADH dehydrogenase [ubiquinone] flavoprotein 1, mitochondrial	8.21	50800	8.20	52000	67.0	3	10.8
125	O75489	NADH dehydrogenase [ubiquinone] iron-sulfur protein 3, mitochondrial	7.50	30200	5.60	26000	81.2	6	26.5
126	P28331	NADH-ubiquinone oxidoreductase 75 kDa subunit, mitochondrial	6.23	79400	5.40	90000	268.5	15	32.3
127	Q6PJF2	IGK@protein	6.55	25500	5.30	25000	27.6	4	22.1
128	Q6PJF2	IGK@protein	6.55	25500	5.40	25000	31.2	2	15.3
129	P01834	Ig kappa chain C region	5.87	11600	6.40	28000	8.8	2	34.0
130	P01834	Ig kappa chain C region	5.87	11600	9.00	16000	5.5	2	34.9
131	Q6PJF2	IGK@protein	6.55	25500	10.10	55000	46.9	4	28.9
	P01857	Ig gamma-1 chain C region	8.19	36100	10.10	55000	38.5	2	10.0
132	P01857	Ig gamma-1 chain C region	8.19	36100	10.30	55000	30.9	2	9.4
	Q6PJF2	IGK@protein	6.55	25500	10.30	55000	28.5	4	30.2
133	P01857	Ig gamma-1 chain C region	8.19	36100	8.80	42000	38.3	3	16.7
	P09543	2',3'-cyclic-nucleotide 3'-phosphodiesterase	9.07	47500	8.80	42000	25.3	2	5.5
134	P01857	Ig gamma-1 chain C region	8.19	36100	10.10	32000	39.9	4	19.4
	P36542	ATP synthase subunit gamma, mitochondrial	9.22	33000	10.10	32000	39.0	4	15.8
	P16152	Carbonyl reductase [NADPH] 1	8.32	30400	10.10	32000	13.5	2	9.8
135	Q0KKI6	Immunoblobulin light chain (Fragment)	8.06	24000	9.30	28000	33.7	3	23.3
	P16152	Carbonyl reductase [NADPH] 1	8.32	30400	9.30	28000	32.3	2	11.9
136	Q6PIL8	IGK@protein	6.55	25800	9.70	28000	34.3	3	23.3
	P16152	Carbonyl reductase [NADPH] 1	8.32	30400	9.70	28000	25.3	4	20.6
137	Q6PIL8	IGK@protein	6.55	25800	9.70	26000	33.6	3	23.3
138	Q0KKI6	Immunoblobulin light chain (Fragment)	8.06	24000	9.30	25000	35.9	4	31.1
	P16152	Carbonyl reductase [NADPH] 1	8.32	30400	9.30	25000	21.4	2	8.7

Spot No.	Acc. No.[a]	Name	Calc. pI[b]	Calc. MW (Da)[c]	App. pI[d]	App. MW (Da)[e]	Xcorr[f]	No. Peptides[g]	% Sequence Coverage[h]
139	P01857	Ig gamma-1 chain C region	8.19	36100	10.20	29000	30.5	2	10.0
	Q6P5S8	IGK@protein	6.33	25800	10.20	29000	26.4	2	14.4
140	P01857	Ig gamma-1 chain C region	8.19	36100	10.10	29000	37.4	2	10.9
	P16152	Carbonyl reductase [NADPH] 1	8.32	30400	10.10	29000	10.9	2	9.8
141	Q6PJF2	IGK@protein	6.55	25500	10.10	27000	15.2	3	21.3
142	P54920	Alpha-soluble NSF attachment protein	5.36	33200	5.20	36000	118.3	11	48.1
143	Q9H115	Beta-soluble NSF attachment protein	5.47	33500	5.30	36000	113.8	8	40.6
144	P49755	Transmembrane emp24 domain-containing protein 10	7.44	24960	6.30	18000	27.5	2	14.6
145	Q15363	Transmembrane emp24 domain-containing protein 2	5.17	22700	5.30	20000	10.3	2	14.4
146	O75832	26S proteasome non-ATPase regulatory subunit 10	6.10	24400	5.70	25000	43.5	4	19.9
147	Q9UNM6	26S proteasome non-ATPase regulatory subunit 13	5.81	42900	5.70	42000	79.3	5	17.6
148	P09471	Guanine nucleotide-binding protein G(o) subunit alpha	5.53	40000	5.30	40000	123.3	4	16.1
149	P07355	Annexin A2	7.75	38600	9.00	37000	17.4	2	6.2
150	Q9UJS0	Calcium-binding mitochondrial carrier protein Aralar2	8.62	74100	9.80	80000	15.3	3	6.4
151	Q02818	Nucleobindin-1	5.25	53800	5.20	60000	95.6	6	16.1
	P10809	60 kDa heat shock protein, mitochondrial	5.87	61000	5.20	60000	75.1	5	16.6
152	P51571	Translocon-associated protein subunit delta	6.15	19000	5.60	18000	54.3	3	19.7
153	Q99798	Aconitate hydratase, mitochondrial	7.61	85400	7.40	100000	146.2	9	19.0
	O95479	GDH/6PGL endoplasmic bifunctional protein	7.30	88800	7.40	100000	38.1	3	5.4
154	Q99798	Aconitate hydratase, mitochondrial	7.61	85400	7.30	100000	240.2	15	26.3
	O95479	GDH/6PGL endoplasmic bifunctional protein	7.30	88800	7.30	100000	18.7	3	4.9
155	P51553	Isocitrate dehydrogenase [NAD] subunit gamma, mitochondrial	8.50	42800	9.10	43000	43.3	2	13.7
	P04075	Fructose-bisphosphate aldolase A	8.09	39400	9.10	43000	41.9	3	12.9
	P09543	2',3'-cyclic-nucleotide 3'-phosphodiesterase	9.07	47500	9.10	43000	18.2	2	7.1
156	P48735	Isocitrate dehydrogenase [NADP], mitochondrial	8.69	50900	8.80	48000	147.4	6	18.4
	P68104	Elongation factor 1-alpha 1	9.01	50100	8.80	48000	45.0	2	7.6

Spot No.	Acc. No.[a]	Name	Calc. pI[b]	Calc. MW (Da)[c]	App. pI[d]	App. MW (Da)[e]	Xcorr[f]	No. Peptides[g]	% Sequence Coverage[h]
157	P48735	Isocitrate dehydrogenase [NADP], mitochondrial	8.69	50900	9.20	48000	202.5	12	28.5
	P68104	Elongation factor 1-alpha 1	9.01	50100	9.20	48000	43.5	4	13.2
	P09543	2',3'-cyclic-nucleotide 3'-phosphodiesterase	9.07	47500	9.20	48000	35.9	3	10.5
158	P40926	Malate dehydrogenase, mitochondrial	8.68	35500	10.10	38000	91.5	7	31.1
	P01857	Ig gamma-1 chain C region	8.19	36100	10.10	38000	38.9	2	10.0
159	P09543	2',3'-cyclic-nucleotide 3'-phosphodiesterase	9.07	47500	9.50	60000	31.3	4	12.8
	Q53HR5	Elongation factor 1-alpha (Fragment)	9.01	50100	9.50	60000	25.1	2	4.8
160	P09543	2',3'-cyclic-nucleotide 3'-phosphodiesterase	9.07	47500	9.50	55000	12.0	2	8.3
161	P09543	2',3'-cyclic-nucleotide 3'-phosphodiesterase	9.07	47500	9.70	55000	9.9	2	8.3
162	P09543	2',3'-cyclic-nucleotide 3'-phosphodiesterase	9.07	47500	9.50	47000	129.8	8	21.1
	Q6IPT9	Elongation factor 1-alpha	9.07	50200	9.50	47000	48.9	2	7.8
163	P09543	2',3'-cyclic-nucleotide 3'-phosphodiesterase	9.07	47500	9.60	47000	125.7	8	19.5
164	Q96IU4	Abhydrolase domain-containing protein 14B	6.40	22300	5.80	23000	38.1	4	26.2
165	Q96KP4	Cytosolic non-specific dipeptidase	5.97	52800	5.70	55000	29.3	4	10.7
166	Q96KP4	Cytosolic non-specific dipeptidase	5.97	52800	5.80	55000	84.2	5	13.5
167	B4DJ30	cDNA FLJ61290, highly similar to Neutral alpha-glucosidase AB	6.06	112900	5.80	120000	181.3	9	13.0
	E5KMI6	Mitochondrial lon protease-like protein	6.39	106400	5.80	120000	107.3	12	18.4
	Q9NZ08	Endoplasmic reticulum aminopeptidase 1	6.46	107200	5.80	120000	26.8	4	5.4
168	P21266	Glutathione S-transferase Mu 3	5.54	26500	5.30	26000	122.8	8	34.7
169	Q08188	Protein-glutamine gamma-glutamyltransferase E	5.86	76600	6.00	110000	82.9	11	28.4
	P22735	Protein-glutamine gamma-glutamyltransferase K	6.04	89700	6.00	110000	36.8	3	5.5
170	P29401	Transketolase	7.66	67800	7.80	80000	197.8	10	25.0
171	P29401	Transketolase	7.66	67800	8.20	80000	289.0	11	29.1
172	B7ZAF6	Succinate-CoA ligase, ADP-forming, beta subunit, isoform CRA_d	5.87	43800	5.80	46000	160.6	11	39.3
	P60709	Actin, cytoplasmic 1	5.48	41700	5.80	46000	61.7	5	25.3
	P68371	Tubulin beta-2C chain	4.89	49800	5.80	46000	48.9	7	20.5
	P68363	Tubulin alpha-1B chain	5.06	50100	5.80	46000	44.1	6	23.1

Spot No.	Acc. No.[a]	Name	Calc. pI[b]	Calc. MW (Da)[c]	App. pI[d]	App. MW (Da)[e]	Xcorr[f]	No. Peptides[g]	% Sequence Coverage[h]
173	P02675	Fibrinogen beta chain	8.27	55900	8.30	55000	109.9	5	18.5
174	P68871	Hemoglobin subunit beta	7.28	16000	7.40	11000	14.4	2	21.8
175	P02787	Serotransferrin	7.12	77000	7.00	90000	129.1	10	21.8
	P46459	Vesicle-fusing ATPase	6.95	82500	7.00	90000	77.8	7	12.6
	Q96RQ3	Methylcrotonoyl-CoA carboxylase subunit alpha, mitochondrial	7.78	80400	7.00	90000	35.3	2	5.1
	O43143	Putative pre-mRNA-splicing factor ATP-dependent RNA helicase DHX15	7.46	90900	7.00	90000	34.2	4	6.5
176	Q53H26	Transferrin variant (Fragment)	7.03	77000	7.40	90000	136.3	8	15.9
	P46459	Vesicle-fusing ATPase	6.95	82500	7.40	90000	98.3	12	19.4
	Q13616	Cullin-1	8.00	89600	7.40	90000	52.3	5	12.6
	O43143	Putative pre-mRNA-splicing factor ATP-dependent RNA helicase DHX15	7.46	90900	7.40	90000	51.1	6	9.9
	P17858	6-phosphofructokinase, liver type	7.50	85000	7.40	90000	41.8	4	8.0
177	P02768	Serum albumin	6.28	69300	5.70	80000	103.1	7	13.8
178	P02768	Serum albumin	6.28	69300	5.70	80000	108.6	7	13.0
179	Q5JPH6	Probable glutamyl-tRNA synthetase, mitochondrial	8.76	58700	9.30	55000	29.9	2	6.7
180	P22626	Heterogeneous nuclear ribonucleoproteins A2/B1	8.95	37400	9.00	35000	29.6	3	7.7
181	P22626	Heterogeneous nuclear ribonucleoproteins A2/B1	8.95	37400	9.00	35000	57.2	7	26.1
	P09651	Heterogeneous nuclear ribonucleoprotein A1	9.13	38700	9.00	35000	11.3	2	7.0
182	P09651	Heterogeneous nuclear ribonucleoprotein A1	9.13	25930	8.50	22000	372.0	3	11.0
183	P35232	Prohibitin	5.76	29800	5.50	28000	168.9	7	30.5
184	Q13838	Spliceosome RNA helicase DDX39B	5.67	49000	5.60	52000	183.6	6	19.2
	P02679	Fibrinogen gamma chain	5.62	51500	5.60	52000	71.0	4	13.9
	P68363	Tubulin alpha-1B chain	5.06	50100	5.60	52000	41.8	5	18.6
	Q6NT72	UNC84B protein (Fragment)	5.72	49400	5.60	52000	34.5	2	8.8
	Q02790	Peptidyl-prolyl cis-trans isomerase FKBP4	5.43	51800	5.60	52000	31.9	3	10.0
185	P62258	14-3-3 protein epsilon	4.74	29200	4.80	30000	113.6	2	12.6
186	P61981	14-3-3 protein gamma	4.89	28300	4.90	28000	107.7	3	17.4
	P27348	14-3-3 protein theta	4.78	27700	4.90	28000	65.5	4	25.7

Spot No.	Acc. No.[a]	Name	Calc. pI[b]	Calc. MW (Da)[c]	App. pI[d]	App. MW (Da)[e]	Xcorr[f]	No. Peptides[g]	% Sequence Coverage[h]
187	P63104	14-3-3 protein zeta/delta	4.79	27700	4.90	27000	95.1	4	25.7
	Q04917	14-3-3 protein eta	4.84	28200	4.90	27000	62.8	2	13.4
	P27348	14-3-3 protein theta	4.78	27700	4.90	27000	60.7	3	20.8
	P31946	14-3-3 protein beta/alpha	4.83	28100	4.90	27000	56.7	3	21.1
188	P37840	Alpha-synuclein	4.70	14500	5.20	22000	6.8	2	25.7
189	P37840	Alpha-synuclein	4.70	14500	4.60	16000	31.4	2	25.7
190	P37840	Alpha-synuclein	4.70	14500	4.70	16000	225.6	4	36.4
191	P37840	Alpha-synuclein	4.70	14500	4.80	16000	119.2	4	36.4
192	P37840	Alpha-synuclein	4.70	14500	4.80	16000	51.8	2	25.7
193	P37840	Alpha-synuclein	4.70	14500	4.80	16000	66.5	2	25.7
	P68363	Tubulin alpha-1B chain	5.06	50100	4.80	16000	23.5	2	6.2
	P04350	Tubulin beta-4 chain	4.88	49600	4.80	16000	20.7	2	7.7
194	P37840	Alpha-synuclein	4.70	14500	4.80	16000	33.8	2	25.7
	P68363	Tubulin alpha-1B chain	5.06	50100	4.80	16000	15.6	2	6.2
195	P37840	Alpha-synuclein	4.70	14500	4.80	15000	41.7	2	25.7
	P04350	Tubulin beta-4 chain	4.88	49600	4.80	15000	41.5	3	11.0
196	P37840	Alpha-synuclein	4.70	14500	4.90	15000	34.5	2	25.7
	Q13885	Tubulin beta-2A chain	4.89	49900	4.90	15000	17.6	2	6.1
	P04350	Tubulin beta-4 chain	4.88	49600	4.90	15000	16.2	2	7.0
197	P37840	Alpha-synuclein	4.70	14500	5.10	14000	24.1	2	25.7
198	P37840	Alpha-synuclein	4.70	14500	5.20	14000	28.4	2	25.7
199	P37840	Alpha-synuclein	4.70	14500	5.30	12000	14.5	2	25.7
200	P37840	Alpha-synuclein	4.70	14500	5.30	12000	42.5	2	25.7
201	P37840	Alpha-synuclein	4.70	14500	5.50	12000	140.0	2	25.7
202	P37840	Alpha-synuclein	4.70	14500	5.60	12000	13.4	2	25.7
203	P02794	Ferritin heavy chain	5.55	21200	5.20	20000	14.2	2	14.2
204	P02792	Ferritin light chain	5.78	20000	5.50	19000	61.9	2	17.1
205	P09455	Retinol-binding protein 1	5.11	15800	5.10	13000	62.7	2	15.6
	P37840	Alpha-synuclein	4.70	14500	5.10	13000	22.6	2	25.7

Spot No.	Acc. No.[a]	Name	Calc. pI[b]	Calc. MW (Da)[c]	App. pI[d]	App. MW (Da)[e]	Xcorr[f]	No. Peptides[g]	% Sequence Coverage[h]
206	P21796	Voltage-dependent anion-selective channel protein 1	8.54	30800	8.80	32000	25.2	3	14.8
	P16152	Carbonyl reductase [NADPH] 1	8.32	30400	8.80	32000	10.7	2	9.8
207	P21796	Voltage-dependent anion-selective channel protein 1	8.54	30754	9.00	32000	74.9	6	27.6
	P16152	Carbonyl reductase [NADPH] 1	8.32	30356	9.00	32000	32.9	5	32.1
208	P21796	Voltage-dependent anion-selective channel protein 1	8.54	30800	8.80	30000	17.1	2	14.8
	P16152	Carbonyl reductase [NADPH] 1	8.32	30400	8.80	30000	8.6	2	9.8
209	P21796	Voltage-dependent anion-selective channel protein 1	8.54	30800	9.40	32000	112.8	6	27.6

[a] SwissProt accession number
[b] Calculated isoelectric point
[c] Calculated molecular weight, Da **or 'theoretical'
[d] Apparent isoelectric point
[e] Apparent molecular weight, Da ** or 'observed'
[f] Xcorr significance score
[g] Number of unique peptides sequenced
[h] % of the full-length amino acid sequence covered by identified peptides

Appendix G

MS Identification of 51 GCI-adherent proteins from carbonate stripping experiment (present in adherent fraction but not core fraction)

Acc. No.[a]	Name	Calc. pI	Calc. MW (Da)	Xcorr[b]	No. of Peptides[c]	% Sequence Coverage[d]
Q13885	*Tubulin beta-2A chain	4.89	49875	127.7	14	55.1
B3KML9	Highly similar to Tubulin beta-2C chain	4.93	44574	101.1	10	35.5
P62805	*Histone H4	11.36	11360	98.7	7	52.4
P14136-3	Isoform 3 of Glial fibrillary acidic protein	6.13	49500	93.8	9	27.6
Q53G99	Beta actin variant (Fragment)	5.59	41738	76.3	9	37.6
Q13509	*Tubulin beta-3 chain	4.93	50400	75.9	9	28.4
Q13813-2	Isoform 2 of Spectrin alpha chain, brain	5.35	284919	68.0	13	8.3
P62873	*Guanine nucleotide-binding protein G(I)/G(S)/G(T) subunit beta-1	6.00	37400	31.7	4	22.9
Q02818	*Nucleobindin-1	5.25	53800	28.9	5	14.1
P07196	*Neurofilament light polypeptide	4.65	61500	28.4	2	4.6
P36957	Dihydrolipoyllysine-residue succinyltransferase component of 2-oxoglutarate dehydrogenase complex, mitochondrial	8.95	48724	27.1	5	17.9
P62937	Peptidyl-prolyl cis-trans isomerase A	7.81	18000	25.6	5	39.4
P02768	Serum albumin	6.28	69300	24.3	5	13.3
O43390	Heterogeneous nuclear ibonucleoproteins R	8.13	70900	22.7	3	6.0
Q03252	Lamin-B2	5.35	67647	21.6	3	5.8
P11142	*Heat shock cognate 71 kDa protein	5.52	70900	17.4	4	9.6
A8K6K8	cDNA FLJ77325	5.88	55008	17.0	2	7.4
Q13200	26S proteasome non-ATPase regulatory subunit 2	5.20	100100	16.9	2	3.4
P40926	Malate dehydrogenase, mitochondrial	8.68	35500	16.8	3	16.9
Q15393	Splicing factor 3B subunit 3	5.26	135500	16.3	4	4.9
P00505	Aspartate aminotransferase, mitochondrial	9.01	47500	14.8	4	13.5

Acc. No.[a]	Name	Calc. pI	Calc. MW (Da)	Xcorr[b]	No. of Peptides[c]	% Sequence Coverage[d]
Q9Y2J2	*Band 4.1-like protein 3	5.19	120600	14.8	2	3.2
O75400	Pre-mRNA-processing factor 40 homolog A	7.56	108700	14.4	2	3.5
P04792	Heat shock protein beta-1	6.40	22800	14.3	2	22.9
P05090	Apolipoprotein D	5.15	21262	13.8	2	13.2
P52565	Rho GDP-dissociation inhibitor 1	5.11	23193	13.6	3	22.1
Q13501	Sequestosome-1	5.22	47700	13.2	3	13.0
P18859	ATP synthase-coupling factor 6, mitochondrial	9.52	12580	12.8	3	44.4
Q5TB20	Acidic (Leucine-rich) nuclear phosphoprotein 32 family, member E	3.74	25110	12.5	2	15.0
Q16352	Alpha-internexin	5.40	55357	12.4	2	5.2
P10809	*60 kDa heat shock protein, mitochondrial	5.87	61000	12.2	2	4.7
Q9Y2B0	Protein canopy homolog 2	4.92	20639	11.9	2	17.6
Q9Y3E1	Hepatoma-derived growth factor-related protein 3	7.99	22606	11.7	2	8.4
P28331	*NADH-ubiquinone oxidoreductase 75 kDa subunit, mitochondrial	6.23	79400	11.2	2	4.5
P12036	Neurofilament heavy polypeptide	6.18	112400	11.1	2	2.8
Q14257	*Reticulocalbin-2	4.40	36854	10.6	3	15.8
O14979	Heterogeneous nuclear ribonucleoprotein D-like	9.57	46400	10.3	3	6.9
Q96FW1	*Ubiquitin thioesterase OTUB1	4.94	31300	10.2	2	17.0
P60880	Synaptosomal-associated protein 25	4.77	23300	10.1	2	14.1
Q07021	Complement component 1 Q subcomponent-binding protein, mitochondrial	4.84	31300	9.8	2	15.6
P30040	Endoplasmic reticulum resident protein 29	7.31	28975	9.4	2	11.5
P60660	Myosin light polypeptide 6	4.65	16919	9.0	2	20.5
P04271	Protein S100-B	4.59	10706	8.9	2	40.2
P07910	Heterogeneous nuclear ribonucleoproteins C1/C2	5.08	33600	8.9	2	9.2
Q16718	NADH dehydrogenase [ubiquinone] 1 alpha subcomplex subunit 5	5.99	13450	8.8	2	21.6
Q13185	Chromobox protein homolog 3	5.33	20798	8.6	3	22.4
O94811	Tubulin polymerization-promoting protein	9.44	23679	8.1	2	11.0

Acc. No.[a]	Name	Calc. pI	Calc. MW (Da)	Xcorr[b]	No. of Peptides[c]	% Sequence Coverage[d]
P14854	Cytochrome c oxidase subunit 6B1	7.05	10186	8.1	2	26.7
Q16891	Mitochondrial inner membrane protein	6.48	83600	7.8	2	4.8
P21281	V-type proton ATPase subunit B, brain isoform	5.81	56465	7.5	2	6.9
Q08380	Galectin-3-binding protein	5.27	65300	6.7	2	4.4

[a] SwissProt accession number
[b] Xcorr significance score
[c] Number of unique peptides sequenced
[d] % of the full-length amino acid sequence covered by identified peptides
* also identified in the total GCI protein fraction

Appendix H

MS Identification of 94 core GCI proteins from carbonate stripping experiment (present in core fraction but not adherent fraction)

Acc. No.[a]	Name	Calc. pI	Calc. MW (Da)	Xcorr[b]	No. of Peptides[c]	% Sequence Coverage[d]
P07437	*Tubulin beta chain	4.89	49639	145.5	16	61.9
Q9BVA1	Tubulin beta-2B chain	4.89	49921	144.6	16	61.8
P60709	*Actin, cytoplasmic 1	5.48	41700	57.1	7	37.6
Q14204	*Cytoplasmic dynein 1 heavy chain 1	6.40	532072	55.2	4	1.1
P49327	*Fatty acid synthase	6.44	273254	40.5	7	4.3
P49411	Elongation factor Tu, mitochondrial	7.61	49510	38.9	6	19.5
P21796	*Voltage-dependent anion-selective channel protein 1	8.54	30754	37.7	7	46.3
P14136	*Glial fibrillary acidic protein	5.52	49800	37.3	5	13.9
P27824	*Calnexin	4.60	67526	31.6	6	14.9
O43175	*D-3-phosphoglycerate dehydrogenase	6.71	56614	31.3	6	16.1
Q08211	*ATP-dependent RNA helicase A	6.84	140869	30.8	5	5.5
Q16658	Fascin	7.24	54500	30.1	5	16.4
Q05639	Elongation factor 1-alpha 2	9.03	50438	29.6	4	13.4
P31930	*Cytochrome b-c1 complex subunit 1, mitochondrial	6.37	52612	27.8	4	13.8
P23528	*Cofilin-1	8.09	18500	27.5	5	37.4
P06744	*Glucose-6-phosphate isomerase	8.32	63100	26.0	4	10.9
P45880	*Voltage-dependent anion-selective channel protein 2	7.56	31500	24.6	4	26.5
Q02790	*Peptidyl-prolyl cis-trans isomerase FKBP4	5.43	51800	23.9	3	11.1
P22695	*Cytochrome b-c1 complex subunit 2, mitochondrial	8.63	48413	23.6	4	13.9
P52306	*Rap1 GTPase-GDP dissociation stimulator 1	5.31	66300	23.1	3	7.6
Q2L7G6	*Heterogeneous nuclear ribonucleoprotein-R2	8.29	66900	22.4	4	11.6
Q13838	*Spliceosome RNA helicase DDX39B	5.67	48960	22.2	3	9.1
Q8WXF7	*Atlastin-1	6.18	63500	21.8	3	8.2
Q9NQC3	*Reticulon-4	4.50	129900	20.5	3	3.7

Acc. No.[a]	Name	Calc. pI	Calc. MW (Da)	Xcorr[b]	No. of Peptides[c]	% Sequence Coverage[d]
P23246	*Splicing factor, proline- and glutamine-rich	9.44	76100	20.5	3	5.8
Q9UQ16	Dynamin-3	8.35	97700	18.6	2	3.0
P50570	Dynamin-2	7.44	98000	18.2	2	2.9
Q1KMD3	*Heterogeneous nuclear ribonucleoprotein U-like protein 2	4.91	85052	18.1	3	5.5
Q9Y277	*Voltage-dependent anion-selective channel protein 3	8.66	30639	17.4	3	21.9
Q04917	*14-3-3 protein eta	4.84	28201	17.4	3	18.3
Q53GQ0	Estradiol 17-beta-dehydrogenase 12	9.32	34300	17.2	3	13.8
O00264	*Membrane-associated progesterone receptor component 1	4.70	21658	17.1	2	26.2
Q05193-2	Isoform 2 of Dynamin-1	6.87	97200	17.0	2	4.2
P35232	Prohibitin	5.76	29800	16.7	3	23.9
P08237	*6-phosphofructokinase, muscle type	7.99	85100	16.3	4	7.3
P30044	*Peroxiredoxin-5, mitochondrial	8.70	22100	16.2	3	22.9
P14866	*Heterogeneous nuclear ribonucleoprotein L	8.22	64100	15.9	2	8.7
Q96KP4	*Cytosolic non-specific dipeptidase	5.97	52800	15.8	3	9.9
Q13148	TAR DNA-binding protein 43	6.19	44700	15.4	2	8.7
P48735	*Isocitrate dehydrogenase [NADP], mitochondrial	8.69	50900	14.7	2	6.6
Q9HDC9	Adipocyte plasma membrane-associated protein	6.16	46451	14.7	3	10.8
P13637	*Sodium/potassium-transporting ATPase subunit alpha-3	5.38	111700	14.6	3	5.1
P78527	*DNA-dependent protein kinase catalytic subunit	7.12	468800	14.4	2	0.7
P17858	*6-phosphofructokinase, liver type	7.50	84964	13.9	4	8.2
P28845	*Corticosteroid 11-beta-dehydrogenase isozyme 1	8.56	32380	13.8	2	8.2
Q92499	ATP-dependent RNA helicase DDX1	7.23	82400	13.7	3	5.1
Q14240	*Eukaryotic initiation factor 4A-II	5.48	46400	13.6	2	6.9
P52597	Heterogeneous nuclear ribonucleoprotein F	5.58	45600	13.4	3	12.1
P30042	*ES1 protein homolog, mitochondrial	8.27	28200	13.2	2	13.8
Q15185	*Prostaglandin E synthase 3	4.54	18700	13.1	3	26.3
Q15363	*Transmembrane emp24 domain-containing protein 2	5.17	22700	13.0	3	18.4
Q14697	*Neutral alpha-glucosidase AB	6.14	106807	12.8	3	4.6
P08133	*Annexin A6	5.60	75800	12.5	2	4.2
P02792	*Ferritin light chain	5.78	20007	12.1	2	17.1

Acc. No.[a]	Name	Calc. pI	Calc. MW (Da)	Xcorr[b]	No. of Peptides[c]	% Sequence Coverage[d]
Q9NZ45	*CDGSH iron-sulfur domain-containing protein 1	9.09	12191	12.1	2	25.9
P60981	*Destrin	7.85	18500	11.7	2	17.6
P11216	Glycogen phosphorylase, brain form	6.86	96600	11.6	2	3.9
P21964	Catechol O-methyltransferase	5.47	30000	11.6	3	19.6
Q99623	Prohibitin-2	9.83	33300	11.3	2	10.0
P07910-2	*Isoform C1 of Heterogeneous nuclear ribonucleoproteins C1/C2	5.08	32300	11.2	3	15.0
P60201	Myelin proteolipid protein	8.35	30057	11.1	2	9.4
P31150	*Rab GDP dissociation inhibitor alpha	5.14	50550	10.8	3	10.5
Q05469	Hormone-sensitive lipase	6.70	116500	9.8	2	3.3
Q27J81	Inverted formin-2	5.38	135500	9.7	2	2.2
O94919	*Endonuclease domain-containing 1 protein	5.71	55000	9.7	3	8.2
P46459	Vesicle-fusing ATPase	6.95	82500	9.7	2	2.8
P26641	Elongation factor 1-gamma	6.67	50100	9.7	2	6.4
P07099	Epoxide hydrolase 1	7.25	52900	9.6	2	7.0
E9PS42	Uncharacterized protein	8.50	16569	9.5	2	20.9
P30519	Heme oxygenase 2	5.41	36000	9.5	2	10.1
P26885	Peptidyl-prolyl cis-trans isomerase FKBP2	9.13	15639	9.4	2	19.0
O43852	Calumenin	4.64	37100	9.4	2	9.8
Q9H307	Pinin	7.14	81600	9.0	3	5.3
P05455	*Lupus La protein	7.12	46800	8.9	2	7.4
Q13875	Myelin-associated oligodendrocyte basic protein	11.34	20900	8.7	2	16.9
Q9Y696	*Chloride intracellular channel protein 4	5.59	28800	8.6	2	14.2
Q9H115	*Beta-soluble NSF attachment protein	5.47	33500	8.6	2	8.7
Q07002	Cyclin-dependent kinase 18	8.66	54100	8.6	2	5.5
O75947	ATP synthase subunit d, mitochondrial	5.30	18500	8.2	2	16.8
Q6E0B2	*Small intestine SPAK-like kinase	6.70	52594	8.1	2	5.5
O00764	*Pyridoxal kinase	6.13	35100	8.0	2	9.0
P00918	Carbonic anhydrase 2	7.40	29228	7.7	2	11.2
P19367	Hexokinase-1	6.80	102400	7.5	2	2.7
Q14103	*Heterogeneous nuclear ribonucleoprotein D0	7.81	38400	7.2	2	6.8

Acc. No.[a]	Name	Calc. pI	Calc. MW (Da)	Xcorr[b]	No. of Peptides[c]	% Sequence Coverage[d]
Q99426	Tubulin-folding cofactor B	5.15	27300	7.0	2	12.7
P48444	Coatomer subunit delta	6.21	57174	6.7	2	4.5
P51674	*Neuronal membrane glycoprotein M6-a	5.27	31200	6.5	2	5.0
Q12860	Contactin-1	5.90	113200	6.5	2	2.7
P04406	*Glyceraldehyde-3-phosphate dehydrogenase	8.46	36000	6.4	2	11.3
P55265	Double-stranded RNA-specific adenosine deaminase	8.65	136000	6.1	2	2.1
Q96QK1	Vacuolar protein sorting-associated protein 35	5.49	91600	5.9	2	3.5
A5YM72	Carnosine synthase 1	6.21	88428	5.9	2	3.6
O43237	*Cytoplasmic dynein 1 light intermediate chain 2	6.38	54100	5.7	2	5.9
P02462	Collagen alpha-1(IV) chain	8.28	160500	5.4	2	1.7

[a] SwissProt accession number
[b] Xcorr significance score
[c] Number of unique peptides sequenced
[d] % of the full-length amino acid sequence covered by identified peptides
* also identified in the total GCI protein fraction

Appendix I

MS Identification of 64 GCI proteins present in both core and adherent fractions from carbonate stripping experiment

Acc. No.[a]	Name	Calc. pI	Calc. MW (Da)	Avg. Xcorr[b]	Avg. No. of Peptides[c]	Avg. % Sequence Coverage[d]
P37840	*Alpha-synuclein	4.70	14500	179.9	6.5	46.1
P04350	*Tubulin beta-4 chain	4.88	49554	179.3	16.5	60.0
P68371	*Tubulin beta-2C chain	4.89	49799	151.8	16.0	59.9
P12277	*Creatine kinase B-type	5.59	42600	98.8	12.0	56.0
Q71U36	*Tubulin alpha-1A chain	5.06	50104	98.4	11.0	43.6
P08238	*Heat shock protein HSP 90-beta	5.03	83200	70.7	11.5	21.1
P07900	*Heat shock protein HSP 90-alpha	5.02	84607	63.8	11.0	20.8
P09543	*2',3'-cyclic-nucleotide 3'-phosphodiesterase	9.07	47500	56.9	9.0	25.9
P02511	*Alpha-crystallin B chain	7.33	20100	56.8	6.5	47.7
P11021	*78 kDa glucose-regulated protein	5.16	72288	53.0	9.5	23.0
P14625	*Endoplasmin	4.84	92400	49.2	8.5	15.0
P22626	*Heterogeneous nuclear ribonucleoproteins A2/B1	8.95	37400	48.4	5.5	17.4
P06576	*ATP synthase subunit beta, mitochondrial	5.40	56500	47.9	8.5	23.8
P62258	*14-3-3 protein epsilon	4.74	29155	46.7	5.0	30.8
P25705	*ATP synthase subunit alpha, mitochondrial	9.13	59714	43.2	7.0	22.2
P61981	*14-3-3 protein gamma	4.89	28285	41.6	5.0	36.6
P16152	*Carbonyl reductase [NADPH] 1	8.32	30356	41.3	9.0	40.3
P02787	*Serotransferrin	7.12	77014	39.4	8.0	17.1
P06396	*Gelsolin	6.28	85600	38.5	7.0	16.7
P09651	*Heterogeneous nuclear ribonucleoprotein A1	9.13	38700	37.9	4.5	15.2
Q96BA7	HNRPU protein	7.87	79666	35.9	7.5	13.2
P19338	*Nucleolin	4.70	76600	34.4	4.5	9.7
P51991	*Heterogeneous nuclear ribonucleoprotein A3	9.01	39600	32.9	4.0	13.8
Q00610	*Clathrin heavy chain 1	5.69	191500	32.7	6.5	6.5

Acc. No.[a]	Name	Calc. pI	Calc. MW (Da)	Avg. Xcorr[b]	Avg. No. of Peptides[c]	Avg. % Sequence Coverage[d]
P27797	*Calreticulin	4.44	48112	32.4	4.5	16.9
P27348	*14-3-3 protein theta	4.78	27747	31.2	2.5	19.2
P68104	*Elongation factor 1-alpha 1	9.01	50109	30.9	3.5	13.6
P46821	*Microtubule-associated protein 1B	4.81	270500	29.6	6.5	4.0
P22314	*Ubiquitin-like modifier-activating enzyme 1	5.76	117774	29.4	5.5	7.7
Q16555	*Dihydropyrimidinase-related protein 2	6.38	62255	28.9	6.0	19.2
P09936	*Ubiquitin carboxyl-terminal hydrolase isozyme L1	5.48	24808	26.4	4.0	26.0
P30101	*Protein disulfide-isomerase A3	6.35	56700	26.2	3.0	9.9
P31946	14-3-3 protein beta/alpha	4.83	28100	25.8	3.0	22.6
P61978	*Heterogeneous nuclear ribonucleoprotein K	5.54	50944	25.7	5.0	18.5
P63104	*14-3-3 protein zeta/delta	4.79	27728	24.9	3.5	22.9
P13667	*Protein disulfide-isomerase A4	5.07	72887	24.4	3.5	8.6
P06748	*Nucleophosmin	4.78	32600	24.1	4.0	23.3
P29401	Transketolase	7.66	67800	23.5	3.0	8.3
P54652	*Heat shock-related 70 kDa protein 2	5.74	69978	22.6	5.0	11.5
P04264	*Keratin, type II cytoskeletal 1	8.12	65999	21.9	4.5	9.0
P13010	*X-ray repair cross-complementing protein 5	5.81	82652	21.3	2.5	4.6
P13489	*Ribonuclease inhibitor	4.82	49941	20.6	4.0	14.4
P60174	*Triosephosphate isomerase	6.90	26700	19.6	5.0	28.5
P61764	Syntaxin-binding protein 1	6.96	67500	19.2	3.5	8.7
P18669	*Phosphoglycerate mutase 1	7.18	28800	19.1	3.5	21.7
Q9C040	*Tripartite motif-containing protein 2	6.96	81479	18.8	3.5	7.8
P31943	*Heterogeneous nuclear ribonucleoprotein H	6.30	49200	18.2	3.5	13.0
P07197	*Neurofilament medium polypeptide	4.91	102400	17.9	3.0	6.7
P23284	Peptidyl-prolyl cis-trans isomerase B	9.41	23728	16.7	3.5	21.8
P07237	Protein disulfide-isomerase	4.87	57100	16.4	2.0	6.0
P12956	*X-ray repair cross-complementing protein 6	6.64	69800	16.3	3.0	7.2
P14314	Glucosidase 2 subunit beta	4.41	59400	15.8	2.5	5.9
Q12765	*Secernin-1	4.75	46400	15.5	3.0	10.4
P35527	*Keratin, type I cytoskeletal 9	5.24	62027	15.5	3.5	10.0

Acc. No.[a]	Name	Calc. pI	Calc. MW (Da)	Avg. Xcorr[b]	Avg. No. of Peptides[c]	Avg. % Sequence Coverage[d]
Q15233	*Non-POU domain-containing octamer-binding protein	8.95	54200	15.5	2.0	5.2
Q6NZI2	*Polymerase I and transcript release factor	5.60	43400	13.3	2.5	10.5
P09471	Guanine nucleotide-binding protein G(o) subunit alpha	5.53	40000	12.5	3.5	13.6
P09972	*Fructose-bisphosphate aldolase C	6.87	39400	11.3	2.5	11.3
Q13263	*Transcription intermediary factor 1-beta	5.77	88500	10.8	2.0	3.7
P02686	Myelin basic protein	9.79	33100	10.2	2.0	6.9
Q15121	*Astrocytic phosphoprotein PEA-15	5.02	15031	10.1	3.0	26.9
Q13151	*Heterogeneous nuclear ribonucleoprotein A0	9.29	30822	9.4	2.5	14.3
P68871	*Hemoglobin subunit beta	7.28	15988	9.4	2.5	24.8
Q92841	Probable ATP-dependent RNA helicase DDX17	8.59	72300	9.1	2.0	4.0

[a] SwissProt accession number
[b] Average Xcorr significance score from core and peripheral fractions
[c] Average number of unique peptides sequenced from core and peripheral fractions
[d] Average % of the full-length amino acid sequence covered by identified peptides from the core and peripheral fractions
* also identified in the total GCI protein fraction

Appendix J

MS Identification of 97 core GCI proteins identified in a single fraction from 1-DE fractionation

Fraction	Acc. No.[a]	Name	Calc. pI	Calc. MW (Da)	Xcorr[b]	No. of Peptides[c]	% Sequence Coverage[d]	Reps[e]
1	P16615	Sarcoplasmic/endoplasmic reticulum calcium ATPase 2	5.34	114700	26.6	3.0	3.9	1
2	Q6PJF2	IGK@ protein	6.55	25505	60.6	5.0	30.2	1
2	Q01082	Spectrin beta chain, brain 1	5.57	274400	36.7	3.0	1.7	1
2	Q9NYU2	UDP-glucose:glycoprotein glucosyltransferase 1	5.63	177100	29.7	2.0	2.5	1
2	Q6IPN0	RTN4 protein	4.81	36900	13.4	2.0	8.2	1
2	P25311	Zinc-alpha-2-glycoprotein	6.05	34237	12.2	2.0	7.4	1
2	P05089	Arginase-1	7.21	34700	8.2	2.0	9.0	1
2	Q8TEM1	Nuclear pore membrane glycoprotein 210	6.81	204983	7.9	2.0	1.8	1
3	P11021	78 kDa glucose-regulated protein	5.16	72288	83.5	8.0	17.8	2
3	P13667	Protein disulfide-isomerase A4	5.07	72887	46.7	4.0	9.4	2
3	Q14697	Neutral alpha-glucosidase AB	6.14	106800	31.1	2.5	4.0	2
3	P55060	Exportin-2	5.77	110300	29.2	2.5	4.2	2
3	P02787	Serotransferrin	7.12	77000	19.4	2.0	3.0	1
3	P14314	Glucosidase 2 subunit beta	4.41	59400	17.7	2.0	4.4	2
3	O14980	Exportin-1	6.06	123306	17.1	2.0	3.1	2
3	A5YM72	Carnosine synthase 1	6.21	88428	14.0	2.0	3.3	1
3	Q16891	Mitochondrial inner membrane protein	6.48	83600	13.8	2.0	3.4	1
3	P28331	NADH-ubiquinone oxidoreductase 75 kDa subunit, mitochondrial	6.23	79417	13.4	2.0	4.8	2
3	P38646	Stress-70 protein, mitochondrial	6.16	73600	13.3	3.0	5.4	2
3	P01871	Ig mu chain C region	6.77	49300	12.3	2.0	6.9	1
3	O43866	CD5 antigen-like	5.47	38063	11.5	2.0	10.4	1
3	O00116	Alkyldihydroxyacetonephosphate synthase, peroxisomal	7.34	72900	11.3	3.0	7.1	2
4	P29401	Transketolase	7.66	67800	49.4	4.5	11.1	2
4	P04406	Glyceraldehyde-3-phosphate dehydrogenase	8.46	36000	42.2	3.0	7.2	1

Fraction	Acc. No.[a]	Name	Calc. pI	Calc. MW (Da)	Xcorr[b]	No. of Peptides[c]	% Sequence Coverage[d]	Reps[e]
4	P10809	60 kDa heat shock protein, mitochondrial	5.87	61000	13.5	2.0	5.1	1
4	Q6PYX1	Hepatitis B virus receptor binding protein (Fragment)	8.03	38138	10.4	2.0	4.8	1
4	P04040	Catalase	7.39	59719	10.3	2.0	10.5	1
4	Q08188	Protein-glutamine gamma-glutamyltransferase E	5.86	76584	6.9	2.0	7.1	1
5	Q9HDC9	Adipocyte plasma membrane-associated protein	6.16	46451	44.7	5.5	19.4	2
5	P62987	Ubiquitin-60S ribosomal protein L40	9.83	14719	38.7	3.0	28.9	1
5	P07900	Heat shock protein HSP 90-alpha	5.02	84600	38.1	4.0	6.8	1
5	P49411	Elongation factor Tu, mitochondrial	7.61	49510	31.0	2.5	7.7	2
5	P48735	Isocitrate dehydrogenase [NADP], mitochondrial	8.69	50877	30.7	3.0	9.1	2
5	Q5FWF9	IGL@ protein	5.59	24779	26.6	2.0	14.7	1
5	P17844	Probable ATP-dependent RNA helicase DDX5	8.92	69100	20.2	2.0	3.8	1
5	P22695	Cytochrome b-c1 complex subunit 2, mitochondrial	8.63	48413	20.1	2.5	9.5	2
5	O00571	ATP-dependent RNA helicase DDX3X	7.18	73200	20.0	3.0	5.3	2
5	P55084	Trifunctional enzyme subunit beta, mitochondrial	9.41	51300	18.4	2.5	6.2	2
5	P39656	Dolichyl-diphosphooligosaccharide--protein glycosyltransferase 48 kDa subunit	6.55	50800	14.0	3.0	7.2	2
5	Q9P2R7	Succinyl-CoA ligase [ADP-forming] subunit beta, mitochondrial	7.42	50300	13.6	2.0	4.3	1
5	A0MZ66	Shootin-1	5.33	71600	13.0	2.0	3.0	1
5	O94905	Erlin-2	5.62	37800	12.6	2.0	7.1	2
5	P04181	Ornithine aminotransferase, mitochondrial	7.03	48504	11.1	2.0	6.8	1
5	O43852	Calumenin	4.64	37100	10.9	2.0	7.6	1
5	Q7L099	Protein RUFY3	5.49	52900	10.6	2.3	5.5	2
5	P52597	Heterogeneous nuclear ribonucleoprotein F	5.58	45643	10.6	2.0	8.2	1
5	Q15276	Rab GTPase-binding effector protein 1	5.01	99200	8.8	2.0	3.5	1
5	P13489	Ribonuclease inhibitor	4.82	49941	8.5	2.0	6.5	2
5	Q07960	Rho GTPase-activating protein 1	6.29	50400	8.4	2.0	5.2	1
5	P07954	Fumarate hydratase, mitochondrial	8.76	54600	6.0	2.0	5.9	1
6	Q9BUF5	Tubulin beta-6 chain	4.88	49825	71.1	5.0	15.0	1
6	Q99623	Prohibitin-2	9.83	33300	35.2	5.0	23.7	2
6	P68104	Elongation factor 1-alpha 1	9.01	50109	26.6	2.0	7.6	1

Fraction	Acc. No.[a]	Name	Calc. pI	Calc. MW (Da)	Xcorr[b]	No. of Peptides[c]	% Sequence Coverage[d]	Reps[e]
6	P21796	Voltage-dependent anion-selective channel protein 1	8.54	30754	25.5	2.5	13.8	2
6	P28845	Corticosteroid 11-beta-dehydrogenase isozyme 1	8.56	32380	20.1	2.0	8.6	1
6	O75746	Calcium-binding mitochondrial carrier protein Aralar1	8.38	74700	13.1	2.0	3.0	1
6	P00387	NADH-cytochrome b5 reductase 3	7.59	34200	11.0	2.0	8.8	2
6	Q05193	Dynamin-1	7.17	97300	9.8	2.0	2.2	1
6	P31942	Heterogeneous nuclear ribonucleoprotein H3	6.87	36900	9.2	2.0	8.4	1
6	P09471	Guanine nucleotide-binding protein G(o) subunit alpha	5.53	40000	8.8	2.0	6.5	1
6	Q9Y2S2	Lambda-crystallin homolog	6.18	35400	8.7	2.0	6.9	1
7	Q6PIL8	IGK@ protein	6.55	25818	58.9	5.5	30.5	2
7	P31946	14-3-3 protein beta/alpha	4.83	28100	33.8	2.5	17.3	2
7	P61981	14-3-3 protein gamma	4.89	28300	30.4	2.5	15.4	2
7	Q04917	14-3-3 protein eta	4.84	28201	26.9	2.5	12.6	2
7	Q99714	3-hydroxyacyl-CoA dehydrogenase type-2	7.78	26906	23.3	3.5	26.2	2
7	P24539	ATP synthase subunit b, mitochondrial	9.36	28900	15.0	2.0	9.4	1
7	P31943	Heterogeneous nuclear ribonucleoprotein H	6.30	49200	13.8	2.0	7.6	1
7	P60842	Eukaryotic initiation factor 4A-I	5.48	46100	9.1	2.0	5.7	1
8	P18085	ADP-ribosylation factor 4	7.14	20498	20.3	2.0	17.2	2
8	P23284	Peptidyl-prolyl cis-trans isomerase B	9.41	23728	20.0	2.0	11.1	1
8	P01859	Ig gamma-2 chain C region	7.59	35878	20.0	2.0	14.4	1
8	P49755	Transmembrane emp24 domain-containing protein 10	7.44	24960	18.2	2.5	19.4	2
8	Q15126	Phosphomevalonate kinase	5.73	21981	8.1	2.0	10.9	1
8	Q12765	Secernin-1	4.75	46400	6.0	2.0	6.5	1
9	Q7Z3Y4	Putative uncharacterized protein	7.59	25686	64.2	6.0	30.1	1
9	P60880	Synaptosomal-associated protein 25	4.77	23300	10.8	2.0	13.1	1
9	P63027	Vesicle-associated membrane protein 2	8.13	12655	8.8	2.0	28.5	1
10	P62805	Histone H4	11.36	11360	17.5	2.0	19.4	2
10	P62937	Peptidyl-prolyl cis-trans isomerase A	7.81	18000	17.4	2.0	10.9	1
10	Q15366	Poly(rC)-binding protein 2	6.79	38600	15.7	2.0	6.6	1
10	P08237	6-phosphofructokinase, muscle type	7.99	85100	13.9	2.0	3.2	1
10	Q92841	Probable ATP-dependent RNA helicase DDX17	8.59	72326	13.5	2.5	4.5	2

Fraction	Acc. No.[a]	Name	Calc. pI	Calc. MW (Da)	Xcorr[b]	No. of Peptides[c]	% Sequence Coverage[d]	Reps[e]
10	P19338	Nucleolin	4.70	76600	13.0	2.0	3.2	1
10	P07737	Profilin-1	8.27	15045	12.0	2.0	21.4	1
10	Q5SSJ5	Heterochromatin protein 1-binding protein 3	9.67	61200	11.9	2.0	3.6	1
10	P78371	T-complex protein 1 subunit beta	6.46	57500	10.7	3.0	7.1	1
10	P52272	Heterogeneous nuclear ribonucleoprotein M	8.70	77500	9.9	2.0	4.1	1
10	P00568	Adenylate kinase isoenzyme 1	8.63	21621	9.8	2.0	13.4	1
10	P61604	10 kDa heat shock protein, mitochondrial	8.92	10900	8.4	2.0	23.5	1
10	P61204	ADP-ribosylation factor 3	7.43	20600	8.0	2.0	9.9	1
10	P68871	Hemoglobin subunit beta	7.28	15988	8.0	2.0	21.8	2
10	O00429	Dynamin-1-like protein	6.81	81800	8.0	2.0	4.1	1
10	Q9P2K5	Myelin expression factor 2	8.75	64081	7.4	2.0	3.8	1
10	P00505	Aspartate aminotransferase, mitochondrial	9.01	47500	5.8	2.0	6.7	1
10	Q9P0J0	NADH dehydrogenase [ubiquinone] 1 alpha subcomplex subunit 13	8.43	16700	5.7	2.0	13.9	1
10	Q86UE4	Protein LYRIC	9.32	63799	5.7	2.0	4.0	1

[a] SwissProt accession number
[b] Xcorr significance score (average score if identified in replicate injections)
[c] Number of unique peptides sequenced (average number if identified in replicate injections)
[d] % of the full-length amino acid sequence covered by identified peptides (average coverage if identified in replicate injections)
[e] Number of replicate injections in which protein was identified

Appendix K

MS Identification of 76 core GCI proteins identified in multiple fractions from 1-DE fractionation

Fractions	Acc. No.[a]	Name	Calc. pI	Calc. MW (Da)	Avg. Xcorr[b]	Avg. No. of Peptides[c]	Avg. % Sequence Coverage[d]
9-10	Q13885	Tubulin beta-2A chain	4.89	49875	83.7	7.0	20.2
5-8,10	P68371	Tubulin beta-2C chain	4.89	49800	80.3	7.1	19.8
1-3,6,8,10	Q0KKI6	Immunoblobulin light chain (Fragment)	8.06	24015	78.4	6.8	38.9
4-5,9-10	Q6P5S8	IGK@ protein	6.33	25757	68.2	5.3	26.7
1-10	P04350	Tubulin beta-4 chain	4.88	49600	67.5	6.3	18.5
4-7	Q71U36	Tubulin alpha-1A chain	5.06	50104	64.9	4.8	17.9
3,7-8	Q6N096	Putative uncharacterized protein DKFZp686I15196	8.06	50895	54.7	4.0	14.5
2-3,5,10	Q14204	Cytoplasmic dynein 1 heavy chain 1	6.40	532072	54.0	3.6	1.1
1-10	P37840	Alpha-synuclein	4.70	14500	52.3	2.8	25.6
3-6,8	P01834	Ig kappa chain C region	5.87	11602	47.9	4.8	59.4
1-10	P02768	Serum albumin	6.28	69300	47.8	3.8	7.5
2-3,5	P14625	Endoplasmin	4.84	92400	46.3	4.8	8.1
3,5-10	P12277	Creatine kinase B-type	5.59	42600	46.3	3.9	17.6
1-3,5-10	A0A5E4	Putative uncharacterized protein	5.94	24731	42.7	2.7	18.6
6-10	P16152	Carbonyl reductase [NADPH] 1	8.32	30356	41.0	4.1	21.1
2-3	Q9Y4L1	Hypoxia up-regulated protein 1	5.22	111266	39.6	3.3	5.5
4-5	Q15084	Protein disulfide-isomerase A6	5.08	48100	39.3	4.0	19.4
1-3,5-6,9-10	P01857	Ig gamma-1 chain C region	8.19	36083	39.1	2.9	14.8
3-4,8-10	P68363	Tubulin alpha-1B chain	5.06	50100	38.8	3.5	12.7
5-10	P08238	Heat shock protein HSP 90-beta	5.03	83200	37.4	3.5	6.1
2-3	P78527	DNA-dependent protein kinase catalytic subunit	7.12	468800	36.9	3.3	1.2
3,5	Q5RKT7	Ribosomal protein S27a	9.60	17893	35.6	2.0	18.0
7-10	P02511	Alpha-crystallin B chain	7.33	20100	34.4	2.4	22.2
2-3	Q00610	Clathrin heavy chain 1	5.69	191500	33.8	2.5	2.0

Fractions	Acc. No.[a]	Name	Calc. pI	Calc. MW (Da)	Avg. Xcorr[b]	Avg. No. of Peptides[c]	Avg. % Sequence Coverage[d]
4-10	P14136	Glial fibrillary acidic protein	5.52	49800	32.7	4.4	10.5
6-7,10	P62258	14-3-3 protein epsilon	4.74	29200	32.1	2.7	14.2
4-5,10	P06576	ATP synthase subunit beta, mitochondrial	5.40	56500	31.9	3.2	8.0
7,10	P63104	14-3-3 protein zeta/delta	4.79	27728	31.7	3.8	21.6
4,6	Q8N5F4	IGL@ protein	5.34	24945	31.2	3.0	11.0
4-6	P52306	Rap1 GTPase-GDP dissociation stimulator 1	5.31	66300	30.9	3.7	11.1
2-3,6	P49327	Fatty acid synthase	6.44	273254	29.0	2.8	1.5
2,6-7	P0CG48	Polyubiquitin-C	7.66	77000	28.7	2.0	35.5
5-7,10	P60709	Actin, cytoplasmic 1	5.48	41700	27.5	2.0	8.7
3,5-6,8	P09543	2',3'-cyclic-nucleotide 3'-phosphodiesterase	9.07	47500	25.5	2.3	6.9
3,10	P40939	Trifunctional enzyme subunit alpha, mitochondrial	9.04	82947	25.3	2.3	4.0
5-6	Q14240	Eukaryotic initiation factor 4A-II	5.48	46400	25.1	3.3	10.3
4-6	P30101	Protein disulfide-isomerase A3	6.35	56700	25.0	2.8	5.5
1-2	P13637	Sodium/potassium-transporting ATPase subunit alpha-3	5.38	111700	24.5	3.5	5.9
4-5,8-10	Q5SZU1	Phosphoglycerate dehydrogenase	6.92	53100	24.1	3.1	9.3
3-5	P27824	Calnexin	4.60	67526	23.6	2.5	12.7
2,10	Q6N092	Putative uncharacterized protein DKFZp686K18196 (Fragment)	6.93	56400	23.6	2.5	8.3
1,8	Q9NQC3	Reticulon-4	4.50	129900	23.5	3.0	3.4
1-2,5,7-10	P02766	Transthyretin	5.76	15877	22.7	3.1	40.2
9-10	P30044	Peroxiredoxin-5, mitochondrial	8.70	22100	22.5	2.3	16.0
6-8,10	P27348	14-3-3 protein theta	4.78	27747	21.9	3.0	18.1
1,5,8	P01876	Ig alpha-1 chain C region	6.51	37631	21.4	2.0	7.5
1-2,4	O94919	Endonuclease domain-containing 1 protein	5.71	55000	20.2	2.7	14.8
4-6,10	P25705	ATP synthase subunit alpha, mitochondrial	9.13	59714	19.1	2.6	6.8
6-8,10	P09651	Heterogeneous nuclear ribonucleoprotein A1	9.13	38700	18.9	2.0	7.0
3,6	P51659	Peroxisomal multifunctional enzyme type 2	8.84	79600	18.9	4.0	7.5
6,8	P08758	Annexin A5	5.05	35914	18.4	2.8	10.9
9-10	P07910	Heterogeneous nuclear ribonucleoproteins C1/C2	5.08	33600	17.7	2.8	11.6

Fractions	Acc. No.[a]	Name	Calc. pI	Calc. MW (Da)	Avg. Xcorr[b]	Avg. No. of Peptides[c]	Avg. % Sequence Coverage[d]
5-6	Q00839	Heterogeneous nuclear ribonucleoprotein U	6.00	90500	16.7	2.3	4.5
5-6,8	P12956	X-ray repair cross-complementing protein 6	6.64	69800	16.7	2.3	4.6
9-10	P23246	Splicing factor, proline- and glutamine-rich	9.44	76100	16.2	2.0	3.8
2-3,5-7,9	P02763	Alpha-1-acid glycoprotein 1	5.02	23497	16.0	2.4	15.1
6,8,10	P51991	Heterogeneous nuclear ribonucleoprotein A3	9.01	39600	15.8	2.0	6.9
6-7	P35232	Prohibitin	5.76	29800	15.2	2.0	9.2
5-7,10	P54652	Heat shock-related 70 kDa protein 2	5.74	69978	15.2	3.3	6.5
5-6	Q27J81	Inverted formin-2	5.38	135500	14.5	2.0	2.4
1-4,6-10	P02749	Beta-2-glycoprotein 1	7.97	38300	14.3	2.1	10.2
7,10	P22314	Ubiquitin-like modifier-activating enzyme 1	5.76	117774	14.2	2.5	3.1
5,7	P07196	Neurofilament light polypeptide	4.65	61500	14.1	2.0	3.9
5-7	P61978	Heterogeneous nuclear ribonucleoprotein K	5.54	50900	13.9	2.0	6.3
5-10	P06744	Glucose-6-phosphate isomerase	8.32	63100	13.7	2.0	5.7
6-7	P25686	DnaJ homolog subfamily B member 2	5.95	35600	13.6	2.0	7.1
6,8	P22626	Heterogeneous nuclear ribonucleoproteins A2/B1	8.95	37400	13.6	2.0	7.4
3,5	P11216	Glycogen phosphorylase, brain form	6.86	96600	12.8	2.0	3.3
5,10	P17858	6-phosphofructokinase, liver type	7.50	84964	12.7	3.0	5.2
6-7	P06396	Gelsolin	6.28	85600	12.3	2.0	3.6
7,10	Q16555	Dihydropyrimidinase-related protein 2	6.38	62300	11.8	2.0	4.6
5-6,10	P61764	Syntaxin-binding protein 1	6.96	67500	11.1	2.3	4.9
5,8,10	Q92499	ATP-dependent RNA helicase DDX1	7.23	82400	10.5	2.0	2.8
5-6,10	Q9Y617	Phosphoserine aminotransferase	7.66	40397	9.9	2.0	6.1
9-10	P23528	Cofilin-1	8.09	18491	9.2	3.0	27.1
1-2,8-9	O75396	Vesicle-trafficking protein SEC22b	6.92	24578	8.6	2.0	11.9

[a] SwissProt accession number
[b] Average Xcorr significance score
[c] Average number of unique peptides sequenced
[d] Average % of the full-length amino acid sequence covered by identified peptides

Appendix L

MS Identification of 74 proteins present in both the secondary-only control fraction and the matched immunocaptured GCI fraction

Acc. No.[a]	Name	Calc. pI	Calc. MW (Da)	No. of Peptides[b]	% Sequence Coverage[c]	Control Xcorr[d]	Matched Xcorr[e]
P04350	Tubulin beta-4 chain	4.88	49554	22	70.5	190.1	210.3
P68371	Tubulin beta-2C chain	4.89	49799	22	68.5	173.9	191.9
Q9BVA1	Tubulin beta-2B chain	4.89	49921	23	74.6	161.1	159.2
P07437	Tubulin beta chain	4.89	49639	24	74.8	158.7	179.0
P14136	Glial fibrillary acidic protein	5.52	49800	16	43.5	138.7	100.9
P68363	Tubulin alpha-1B chain	5.06	50120	17	59.4	115.3	123.5
Q71U36	Tubulin alpha-1A chain	5.06	50104	16	59.4	112.8	126.6
P12277	Creatine kinase B-type	5.59	42600	14	57.2	100.4	104.9
Q13509	Tubulin beta-3 chain	4.93	50400	15	36.7	96.4	93.1
P04264	Keratin, type II cytoskeletal 1	8.12	65999	12	23.0	81.6	16.1
P07900	Heat shock protein HSP 90-alpha	5.02	84607	12	21.9	76.4	85.1
P08238	Heat shock protein HSP 90-beta	5.03	83200	12	25.7	75.2	103.4
P60709	Actin, cytoplasmic 1	5.48	41700	10	45.3	75.0	68.3
P06576	ATP synthase subunit beta, mitochondrial	5.40	56500	10	35.0	66.0	64.6
P25705	ATP synthase subunit alpha, mitochondrial	9.13	59714	12	34.5	65.7	45.9
P07197	Neurofilament medium polypeptide	4.91	102400	10	17.1	65.2	47.8
P13637	Sodium/potassium-transporting ATPase subunit alpha-3	5.38	111700	8	11.6	46.1	20.7
P09651	Heterogeneous nuclear ribonucleoprotein A1	9.13	38700	7	22.0	45.6	42.2
Q00839	Heterogeneous nuclear ribonucleoprotein U	6.00	90500	9	17.8	43.6	44.7
P07196	Neurofilament light polypeptide	4.65	61500	7	24.7	43.4	27.8
P62258	14-3-3 protein epsilon	4.74	29155	8	34.9	43.1	35.4
P62805	Histone H4	11.36	11360	5	44.7	37.8	23.0
P21796	Voltage-dependent anion-selective channel protein 1	8.54	30754	4	29.3	33.8	24.6
P19338	Nucleolin	4.70	76600	6	13.7	33.8	26.7

Acc. No.[a]	Name	Calc. pI	Calc. MW (Da)	No. of Peptides[b]	% Sequence Coverage[c]	Control Xcorr[d]	Matched Xcorr[e]
Q00610	Clathrin heavy chain 1	5.69	191500	4	3.5	33.3	40.5
P12036	Neurofilament heavy polypeptide	6.18	112400	3	4.3	32.6	21.5
P61764	Syntaxin-binding protein 1	6.96	67500	7	16.8	32.4	36.7
P22314	Ubiquitin-like modifier-activating enzyme 1	5.76	117774	6	8.4	32.3	48.2
P31930	Cytochrome b-c1 complex subunit 1, mitochondrial	6.37	52612	6	18.5	31.9	21.4
P31943	Heterogeneous nuclear ribonucleoprotein H	6.30	49200	7	26.7	31.3	28.5
P63104	14-3-3 protein zeta/delta	4.79	27728	4	25.7	31.0	23.5
P37840	Alpha-synuclein	4.70	14500	4	38.6	30.2	255.9
P13010	X-ray repair cross-complementing protein 5	5.81	82652	4	5.2	29.4	38.9
P27348	14-3-3 protein theta	4.78	27747	4	18.4	28.5	40.6
P51991	Heterogeneous nuclear ribonucleoprotein A3	9.01	39600	5	17.2	28.3	35.3
Q16555	Dihydropyrimidinase-related protein 2	6.38	62255	6	17.1	27.5	44.4
Q08211	ATP-dependent RNA helicase A	6.84	140869	2	1.7	27.5	23.5
P61981	14-3-3 protein gamma	4.89	28285	5	31.2	26.3	37.8
P11142	Heat shock cognate 71 kDa protein	5.52	70900	6	12.5	25.4	30.1
P46821	Microtubule-associated protein 1B	4.81	270500	2	1.3	25.0	40.1
P62873	Guanine nucleotide-binding protein G(I)/G(S)/G(T) subunit beta-1	6.00	37400	3	15.9	24.2	33.0
P06744	Glucose-6-phosphate isomerase	8.32	63100	6	15.6	24.2	14.7
P27797	Calreticulin	4.44	48112	5	20.6	23.3	50.2
P09972	Fructose-bisphosphate aldolase C	6.87	39400	3	18.4	23.1	17.9
P06396	Gelsolin	6.28	85600	4	10.0	22.4	54.3
P60174	Triosephosphate isomerase	6.90	26700	4	16.1	21.3	24.5
P14625	Endoplasmin	4.84	92400	4	8.2	21.1	61.4
Q2L7G6	Heterogeneous nuclear ribonucleoprotein-R2	8.29	66900	4	7.6	20.1	32.4
P12956	X-ray repair cross-complementing protein 6	6.64	69800	3	7.6	19.4	35.0
P61978	Heterogeneous nuclear ribonucleoprotein K	5.54	50944	3	10.6	19.2	46.9
P22695	Cytochrome b-c1 complex subunit 2, mitochondrial	8.63	48413	4	14.4	18.6	18.6
P02686	Myelin basic protein	9.79	33100	2	6.6	18.5	35.5
O75367	Core histone macro-H2A.1	9.79	39600	4	21.5	18.2	8.9
P02511	Alpha-crystallin B chain	7.33	20100	3	18.3	18.0	71.2

Acc. No.[a]	Name	Calc. pI	Calc. MW (Da)	No. of Peptides[b]	% Sequence Coverage[c]	Control Xcorr[d]	Matched Xcorr[e]
P18669	Phosphoglycerate mutase 1	7.18	28800	2	12.6	16.7	21.1
P16152	Carbonyl reductase [NADPH] 1	8.32	30356	4	20.6	15.6	34.7
Q15121	Astrocytic phosphoprotein PEA-15	5.02	15031	3	30.8	14.0	14.6
P13489	Ribonuclease inhibitor	4.82	49941	3	9.5	13.5	17.3
Q9H115	Beta-soluble NSF attachment protein	5.47	33500	3	17.1	13.1	14.1
P23528	Cofilin-1	8.09	18500	2	18.7	12.8	20.6
P43243	Matrin-3	6.25	94600	2	4.7	12.2	31.1
P04271	Protein S100-B	4.59	10706	2	40.2	12.0	11.4
Q05193	Dynamin-1	7.17	97300	3	4.3	11.0	16.9
P05455	Lupus La protein	7.12	46800	3	9.6	10.6	12.1
P09543	2',3'-cyclic-nucleotide 3'-phosphodiesterase	9.07	47500	2	6.2	10.0	72.1
P52272	Heterogeneous nuclear ribonucleoprotein M	8.70	77500	2	4.0	9.8	18.4
Q9Y277	Voltage-dependent anion-selective channel protein 3	8.66	30639	2	12.7	9.6	12.5
Q1KMD3	Heterogeneous nuclear ribonucleoprotein U-like protein 2	4.91	85052	2	3.8	9.4	15.9
Q9Y383	Putative RNA-binding protein Luc7-like 2	10.01	46500	2	7.7	9.1	9.8
P14866	Heterogeneous nuclear ribonucleoprotein L	8.22	64100	2	5.4	8.9	15.9
P30153	Serine/threonine-protein phosphatase 2A 65 kDa regulatory subunit A alpha isoform	5.11	65300	2	4.2	8.7	12.6
Q13151	Heterogeneous nuclear ribonucleoprotein A0	9.29	30822	2	10.2	8.4	17.5
P08133	Annexin A6	5.60	75800	2	4.6	6.8	7.0
P06748	Nucleophosmin	4.78	32600	2	11.6	6.7	11.6

[a] SwissProt accession number
[b] Number of unique peptides sequenced in secondary-only control fraction
[c] % of the full-length amino acid sequence covered by identified peptides in secondary-only control fraction
[d] Xcorr significance score of identification in secondary-only control fraction
[e] Xcorr significance score of identification in matched immunocaptured fraction

Appendix M

MS Identification of 64 proteins present in only the matched immunocaptured fraction (but not the secondary-only control fraction)

Acc. No.[a]	Name	Calc. pI	Calc. MW (Da)	Xcorr[b]	No. of Peptides[c]	% Sequence Coverage[d]
B3KML9	Highly similar to Tubulin beta-2C chain	4.93	44574	136.4	17	57.9
P22626-2	Isoform A2 of Heterogeneous nuclear ribonucleoproteins A2/B1	8.65	35984	48.1	7	21.4
Q14204	Cytoplasmic dynein 1 heavy chain 1	6.40	532072	42.8	6	1.6
Q53G85	Elongation factor 1-alpha (Fragment)	9.01	50081	42.8	6	24.7
P11021	78 kDa glucose-regulated protein	5.16	72288	41.6	6	13.6
P54652	Heat shock-related 70 kDa protein 2	5.74	69978	40.0	8	18.0
P30101	Protein disulfide-isomerase A3	6.35	56700	36.2	5	17.0
P27824	Calnexin	4.60	67526	35.6	5	12.5
Q15233	Non-POU domain-containing octamer-binding protein	8.95	54200	33.8	5	13.8
D6R956	Uncharacterized protein	5.81	26823	29.3	4	29.5
Q9NQC3	Reticulon-4	4.50	129900	26.0	5	6.5
O00264	Membrane-associated progesterone receptor component 1	4.70	21658	23.1	4	43.6
P69905	Hemoglobin subunit alpha	8.68	15248	21.4	3	41.6
P09471	Guanine nucleotide-binding protein G(o) subunit alpha	5.53	40000	20.9	6	23.7
O43175	D-3-phosphoglycerate dehydrogenase	6.71	56614	20.5	3	8.6
P60842	Eukaryotic initiation factor 4A-I	5.48	46100	20.1	3	10.6
Q16658	Fascin	7.24	54500	19.8	2	6.3
P68871	Hemoglobin subunit beta	7.28	15988	18.9	3	25.9
P04406	Glyceraldehyde-3-phosphate dehydrogenase	8.46	36000	18.6	3	15.5
P52306	Rap1 GTPase-GDP dissociation stimulator 1	5.31	66300	18.4	4	10.4
Q13263	Transcription intermediary factor 1-beta	5.77	88500	17.5	3	5.9
P52597	Heterogeneous nuclear ribonucleoprotein F	5.58	45600	17.5	3	13.3
P49327	Fatty acid synthase	6.44	273254	17.4	3	1.7
P02787	Serotransferrin	7.12	77014	17.0	2	3.9

Acc. No.[a]	Name	Calc. pI	Calc. MW (Da)	Xcorr[b]	No. of Peptides[c]	% Sequence Coverage[d]
P23246	Splicing factor, proline- and glutamine-rich	9.44	76100	16.3	2	4.2
Q14697	Neutral alpha-glucosidase AB	6.14	106807	16.0	3	4.9
P09874	Poly [ADP-ribose] polymerase 1	8.88	113000	14.5	2	2.9
P50570	Dynamin-2	7.44	98000	14.1	2	2.9
P23284	Peptidyl-prolyl cis-trans isomerase B	9.41	23728	14.0	2	12.5
Q9NZ45	CDGSH iron-sulfur domain-containing protein 1	9.09	12191	13.6	2	25.9
P00734	Prothrombin	5.90	70000	13.2	2	4.8
Q9Y2J2	Band 4.1-like protein 3	5.19	120600	13.2	2	3.7
Q16891	Mitochondrial inner membrane protein	6.48	83600	13.2	2	4.8
P29966	Myristoylated alanine-rich C-kinase substrate	4.45	31500	13.1	3	15.4
Q02790	Peptidyl-prolyl cis-trans isomerase FKBP4	5.43	51800	12.6	2	4.1
Q9C040	Tripartite motif-containing protein 2	6.96	81479	12.4	2	4.2
P13667	Protein disulfide-isomerase A4	5.07	72887	11.4	2	4.7
P31942	Heterogeneous nuclear ribonucleoprotein H3	6.87	36900	11.4	4	16.5
Q8N9I0	Synaptotagmin-2	7.99	46800	11.2	3	8.8
P30050	60S ribosomal protein L12	9.42	17808	11.0	2	19.4
P45974	Ubiquitin carboxyl-terminal hydrolase 5	5.03	95700	10.9	2	4.1
P78371	T-complex protein 1 subunit beta	6.46	57500	10.8	2	5.8
P00367	Glutamate dehydrogenase 1, mitochondrial	7.80	61400	10.7	2	6.3
P05090	Apolipoprotein D	5.15	21262	10.3	2	13.8
P0CG48	Polyubiquitin-C	7.66	77000	9.9	2	27.6
P26885	Peptidyl-prolyl cis-trans isomerase FKBP2	9.13	15639	9.6	2	19.0
P21964	Catechol O-methyltransferase	5.47	30000	9.3	2	14.0
Q12860	Contactin-1	5.90	113200	8.9	2	2.7
Q14257	Reticulocalbin-2	4.40	36854	8.8	3	13.6
Q96FW1	Ubiquitin thioesterase OTUB1	4.94	31300	8.6	2	9.2
P30042	ES1 protein homolog, mitochondrial	8.27	28200	8.5	2	13.8
P30519	Heme oxygenase 2	5.41	36000	8.5	2	9.8
Q15363	Transmembrane emp24 domain-containing protein 2	5.17	22700	8.5	3	18.4
Q9Y617	Phosphoserine aminotransferase	7.66	40400	7.8	2	6.8

Acc. No.[a]	Name	Calc. pI	Calc. MW (Da)	Xcorr[b]	No. of Peptides[c]	% Sequence Coverage[d]
Q6E0B2	Small intestine SPAK-like kinase	6.70	52594	7.7	2	5.5
P61088	Ubiquitin-conjugating enzyme E2 N	6.57	17127	7.5	2	17.1
P19367	Hexokinase-1	6.80	102400	7.3	2	2.5
P36542	ATP synthase subunit gamma, mitochondrial	9.22	33000	7.3	2	7.7
Q6NZI2	Polymerase I and transcript release factor	5.60	43400	7.2	2	9.0
Q8WXF1	Paraspeckle component 1	6.67	58700	7.1	2	5.2
Q9Y3B3	Transmembrane emp24 domain-containing protein 7	6.89	25200	6.0	2	13.0
Q9BTT0	Acidic leucine-rich nuclear phosphoprotein 32 family member E	3.85	30700	5.9	2	11.6
P14406	Cytochrome c oxidase subunit 7A2, mitochondrial	9.76	9400	5.9	2	27.7
P14314	Glucosidase 2 subunit beta	4.41	59400	5.1	2	4.7

[a] SwissProt accession number
[b] Xcorr significance score
[c] Number of unique peptides sequenced
[d] % of the full-length amino acid sequence covered by identified peptides

Appendix N

MS Identification of 39 proteins present in only the secondary-only control fraction (but not the matched immunocaptured fraction)

Acc. No.[a]	Name	Calc. pI	Calc. MW (Da)	Xcorr[b]	No. of Peptides[c]	% Sequence Coverage[d]
Q13813-2	Isoform 2 of Spectrin alpha chain, brain	5.35	284919	53.1	9	5.1
P22626	Heterogeneous nuclear ribonucleoproteins A2/B1	8.95	37400	51.8	6	18.7
P13645	Keratin, type I cytoskeletal 10	5.21	58792	47.2	9	24.7
P09936	Ubiquitin carboxyl-terminal hydrolase isozyme L1	5.48	24808	44.1	6	43.1
P35908	Keratin, type II cytoskeletal 2 epidermal	8.00	65393	34.9	4	9.4
Q01082	Spectrin beta chain, brain 1	5.57	274400	33.7	5	3.6
P08670	Vimentin	5.12	53600	32.3	4	10.9
P31946	14-3-3 protein beta/alpha	4.83	28100	31.9	4	24.8
P35527	Keratin, type I cytoskeletal 9	5.24	62027	30.3	6	17.7
P09471-2	Isoform Alpha-2 of Guanine nucleotide-binding protein G(o) subunit alpha	5.90	40061	27.7	6	22.6
P02533	Keratin, type I cytoskeletal 14	5.16	51529	23.9	3	9.5
P45880	Voltage-dependent anion-selective channel protein 2	7.56	31500	23.6	3	21.1
P04899	Guanine nucleotide-binding protein G(i) subunit alpha-2	5.54	40425	23.3	6	22.5
P02538	Keratin, type II cytoskeletal 6A	8.00	60000	22.1	3	6.4
P0C0S8	Histone H2A type 1	10.90	14100	20.6	3	28.5
P62937	Peptidyl-prolyl cis-trans isomerase A	7.81	18000	20.1	3	24.2
P68104	Elongation factor 1-alpha 1	9.01	50109	19.0	3	8.4
Q12765	Secernin-1	4.75	46400	18.7	4	14.7
P60880	Synaptosomal-associated protein 25	4.77	23300	17.1	4	28.2
P46459	Vesicle-fusing ATPase	6.95	82500	16.7	4	7.5
P02768	Serum albumin	6.28	69300	14.6	2	4.4
P20674	Cytochrome c oxidase subunit 5A, mitochondrial	6.79	16752	13.3	2	16.7
P13591	Neural cell adhesion molecule 1	4.87	94500	12.4	2	3.5
P10809	60 kDa heat shock protein, mitochondrial	5.87	61000	12.2	2	5.2

Acc. No.[a]	Name	Calc. pI	Calc. MW (Da)	Xcorr[b]	No. of Peptides[c]	% Sequence Coverage[d]
Q14240	Eukaryotic initiation factor 4A-II	5.48	46400	11.9	2	7.4
Q5TB20	Acidic (Leucine-rich) nuclear phosphoprotein 32 family, member E	3.74	25110	10.4	2	15.0
P06702	Protein S100-A9	6.13	13200	10.0	2	26.3
P36957	Dihydrolipoyllysine-residue succinyltransferase component of 2-oxoglutarate dehydrogenase complex, mitochondrial	8.95	48724	9.6	3	9.5
Q92841	Probable ATP-dependent RNA helicase DDX17	8.59	72300	9.6	2	4.0
Q14103	Heterogeneous nuclear ribonucleoprotein D0	7.81	38400	8.9	3	11.0
P08107	Heat shock 70 kDa protein 1A/1B	5.66	70000	8.8	3	5.5
P63241	Eukaryotic translation initiation factor 5A-1	5.24	16821	8.1	2	22.7
P61266	Syntaxin-1B	5.38	33200	7.6	2	10.1
Q9Y639	Neuroplastin	7.99	44400	7.4	2	8.3
O75531	Barrier-to-autointegration factor	6.09	10052	6.6	2	29.2
O76070	Gamma-synuclein	4.86	13323	6.6	2	24.4
P28331	NADH-ubiquinone oxidoreductase 75 kDa subunit, mitochondrial	6.23	79400	6.3	2	5.0
Q99962	Endophilin-A1	5.45	39900	6.2	2	8.8
P11047	Laminin subunit gamma-1	5.12	177489	5.2	2	1.7

[a] SwissProt accession number
[b] Xcorr significance score
[c] Number of unique peptides sequenced
[d] % of the full-length amino acid sequence covered by identified peptides

Appendix O

MS Identification of 174 LB proteins identified in 2 out of 2 DLB cases

Acc. No.[a]	Name	Calc. pI	Calc. MW (Da)	Avg. Xcorr[b]	Avg. No. of Peptides[c]	Avg. % Sequence Coverage[d]
P68371	Tubulin beta-2C chain	4.89	49799	269.5	16.3	60.8
P04350	Tubulin beta-4 chain	4.88	49554	268.6	16.8	62.8
Q13885	Tubulin beta-2A chain	4.89	49875	249.7	17.5	62.8
P07437	Tubulin beta chain	4.89	49639	236.5	16.3	60.4
Q71U36	Tubulin alpha-1A chain	5.06	50104	226.9	14.0	58.5
P68363	Tubulin alpha-1B chain	5.06	50120	222.7	14.0	58.5
P68366	Tubulin alpha-4A chain	5.06	49900	177.4	11.0	41.4
P14136	Glial fibrillary acidic protein	5.52	49800	175.0	14.0	35.0
Q13509	Tubulin beta-3 chain	4.93	50400	138.9	13.3	44.2
P35579	Myosin-9	5.60	226392	137.2	20.3	15.7
P04264	Keratin, type II cytoskeletal 1	8.12	65999	137.2	11.0	24.0
P07197	Neurofilament medium polypeptide	4.91	102400	134.8	14.3	25.7
P60709	Actin, cytoplasmic 1	5.48	41700	133.7	7.0	35.6
P08238	Heat shock protein HSP 90-beta	5.03	83200	121.9	13.8	24.1
P07196	Neurofilament light polypeptide	4.65	61500	108.6	9.0	22.9
P98160	Basement membrane-specific heparan sulfate proteoglycan core protein	6.51	468532	105.0	14.0	4.8
P07900	Heat shock protein HSP 90-alpha	5.02	84607	97.9	12.0	20.6
Q14204	Cytoplasmic dynein 1 heavy chain 1	6.40	532072	95.8	8.5	2.9
P12277	Creatine kinase B-type	5.59	42600	87.2	9.3	45.9
P46821	Microtubule-associated protein 1B	4.81	270500	86.2	13.5	8.7
P06576	ATP synthase subunit beta, mitochondrial	5.40	56500	85.5	10.8	34.4
P37840	Alpha-synuclein	4.70	14500	83.0	4.0	36.4
P02768	Serum albumin	6.28	69300	79.5	10.3	24.8
P13637	Sodium/potassium-transporting ATPase subunit alpha-3	5.38	111700	79.2	11.8	18.0

Acc. No.[a]	Name	Calc. pI	Calc. MW (Da)	Avg. Xcorr[b]	Avg. No. of Peptides[c]	Avg. % Sequence Coverage[d]
P55268	Laminin subunit beta-2	6.52	195854	76.3	12.0	10.1
Q16352	Alpha-internexin	5.40	55357	76.2	6.5	17.1
Q00610	Clathrin heavy chain 1	5.69	191500	75.3	10.3	9.4
P11021	78 kDa glucose-regulated protein	5.16	72288	71.7	11.5	24.0
P12036	Neurofilament heavy polypeptide	6.18	112400	71.2	6.0	7.9
Q13813	Spectrin alpha chain, brain	5.35	284400	70.4	9.5	6.0
P62258	14-3-3 protein epsilon	4.74	29155	69.8	4.3	26.6
Q13813-2	Isoform 2 of Spectrin alpha chain, brain	5.35	284919	69.6	8.0	6.0
P63104	14-3-3 protein zeta/delta	4.79	27728	67.2	5.3	31.6
P50993	Sodium/potassium-transporting ATPase subunit alpha-2	5.66	112200	66.3	8.7	13.2
P14625	Endoplasmin	4.84	92400	64.9	9.3	16.8
O00468	Agrin	6.40	214706	62.5	9.8	8.6
P11047	Laminin subunit gamma-1	5.12	177489	61.9	12.8	12.1
P08670	Vimentin	5.12	53600	60.0	7.8	20.0
P27797	Calreticulin	4.44	48112	57.7	7.8	32.6
P27824	Calnexin	4.60	67526	56.4	7.3	16.7
P09543	2',3'-cyclic-nucleotide 3'-phosphodiesterase	9.07	47500	55.9	7.5	21.7
P35527	Keratin, type I cytoskeletal 9	5.24	62027	55.4	7.3	21.8
P25705	ATP synthase subunit alpha, mitochondrial	9.13	59714	53.8	7.8	22.0
P05023	Sodium/potassium-transporting ATPase subunit alpha-1	5.49	112800	52.7	8.0	12.6
P02511	Alpha-crystallin B chain	7.33	20100	52.0	4.3	34.3
P31946	14-3-3 protein beta/alpha	4.83	28100	49.8	4.3	26.3
P61764	Syntaxin-binding protein 1	6.96	67500	48.5	7.3	16.8
P61981	14-3-3 protein gamma	4.89	28285	47.4	4.0	25.4
P13645	Keratin, type I cytoskeletal 10	5.21	58792	47.3	6.5	16.0
P27348	14-3-3 protein theta	4.78	27747	47.2	4.8	27.8
Q16555	Dihydropyrimidinase-related protein 2	6.38	62255	46.3	6.5	20.0
Q14112	Nidogen-2	5.29	151200	46.1	4.0	4.5
P38606	V-type proton ATPase catalytic subunit A	5.52	68300	42.6	5.5	15.6
Q9GZM7	Tubulointerstitial nephritis antigen-like	6.99	52353	42.5	7.8	22.6

Acc. No.[a]	Name	Calc. pI	Calc. MW (Da)	Avg. Xcorr[b]	Avg. No. of Peptides[c]	Avg. % Sequence Coverage[d]
P09936	Ubiquitin carboxyl-terminal hydrolase isozyme L1	5.48	24808	42.4	3.0	20.9
P08758	Annexin A5	5.05	35900	42.4	6.3	30.4
P35908	Keratin, type II cytoskeletal 2 epidermal	8.00	65393	39.3	5.0	9.6
P10809	60 kDa heat shock protein, mitochondrial	5.87	61000	38.6	6.8	18.0
Q9H115	Beta-soluble NSF attachment protein	5.47	33500	38.4	7.0	35.4
P30101	Protein disulfide-isomerase A3	6.35	56700	36.9	4.5	13.2
P46459	Vesicle-fusing ATPase	6.95	82500	36.7	4.3	7.7
P11142	Heat shock cognate 71 kDa protein	5.52	70900	36.5	7.0	15.6
P11137	Microtubule-associated protein 2	4.91	199400	35.4	4.3	3.3
P68871	Hemoglobin subunit beta	7.28	15988	34.4	4.8	45.1
P13591	Neural cell adhesion molecule 1	4.87	94500	34.0	4.0	5.7
P62873	Guanine nucleotide-binding protein G(I)/G(S)/G(T) subunit beta-1	6.00	37400	32.9	4.8	24.8
P04792	Heat shock protein beta-1	6.40	22800	32.8	2.8	25.7
Q96BA7	HNRPU protein	7.87	79666	32.1	4.0	11.3
Q05193	Dynamin-1	7.17	97300	31.9	5.7	9.7
P22626	Heterogeneous nuclear ribonucleoproteins A2/B1	8.95	37400	31.9	2.8	10.6
P80723	Brain acid soluble protein 1	4.63	22680	31.5	3.8	30.0
P05556	Integrin beta-1	5.39	88357	31.1	3.0	5.0
P61421	V-type proton ATPase subunit d 1	5.00	40300	30.5	3.8	21.6
P45974	Ubiquitin carboxyl-terminal hydrolase 5	5.03	95700	30.5	4.8	9.5
P31930	Cytochrome b-c1 complex subunit 1, mitochondrial	6.37	52612	29.9	3.0	11.1
P19338	Nucleolin	4.70	76600	29.8	4.3	9.2
P02787	Serotransferrin	7.12	77014	29.7	3.7	7.5
P13010	X-ray repair cross-complementing protein 5	5.81	82652	29.6	3.5	7.9
P14543	Nidogen-1	5.29	136300	29.6	3.8	3.7
P16152	Carbonyl reductase [NADPH] 1	8.32	30356	29.3	4.3	23.9
P22314	Ubiquitin-like modifier-activating enzyme 1	5.76	117774	29.0	5.0	7.2
P04899	Guanine nucleotide-binding protein G(i) subunit alpha-2	5.54	40425	28.7	5.5	21.1
P0CG48	Polyubiquitin-C	7.66	77000	28.3	2.3	34.6
P61978	Heterogeneous nuclear ribonucleoprotein K	5.54	50944	27.9	5.3	19.3

Acc. No.[a]	Name	Calc. pI	Calc. MW (Da)	Avg. Xcorr[b]	Avg. No. of Peptides[c]	Avg. % Sequence Coverage[d]
P60660	Myosin light polypeptide 6	4.65	16919	27.7	3.5	31.3
Q9Y2J2	Band 4.1-like protein 3	5.19	120600	27.2	3.0	4.2
Q01813	6-phosphofructokinase type C	7.55	85500	27.1	5.5	11.4
O00264	Membrane-associated progesterone receptor component 1	4.70	21658	27.1	3.5	37.2
P62805	Histone H4	11.36	11360	26.8	3.7	36.9
O15230	Laminin subunit alpha-5	7.02	399479	26.7	2.8	1.1
Q04917	14-3-3 protein eta	4.84	28201	26.0	2.3	14.5
P13521	Secretogranin-2	4.75	70897	25.8	2.0	5.0
P02686	Myelin basic protein	9.79	33100	25.7	3.0	11.2
P35613	Basigin	5.66	42200	25.7	3.0	15.2
P19105	Myosin regulatory light chain 12A	4.81	19781	25.3	4.0	31.1
P09651	Heterogeneous nuclear ribonucleoprotein A1	9.13	38700	25.2	2.0	8.3
P62879	Guanine nucleotide-binding protein G(I)/G(S)/G(T) subunit beta-2	6.00	37307	25.2	3.7	19.9
P08195	4F2 cell-surface antigen heavy chain	5.01	68000	25.1	3.3	7.4
P07237	Protein disulfide-isomerase	4.87	57100	24.6	2.7	7.1
Q5U5Z3	Paraneoplastic antigen MA2	4.82	41414	24.3	2.3	12.9
P09104	Gamma-enolase	5.03	47200	23.4	4.3	16.1
P10909	Clusterin	6.27	52500	23.4	4.3	14.8
P14314	Glucosidase 2 subunit beta	4.41	59400	23.0	4.0	10.4
Q13557	Calcium/calmodulin-dependent protein kinase type II subunit delta	7.25	56300	22.7	3.3	11.5
Q6NZI2	Polymerase I and transcript release factor	5.60	43400	22.5	3.3	12.1
P24043	Laminin subunit alpha-2	6.40	343700	22.0	3.0	1.5
P60174	Triosephosphate isomerase	6.90	26700	21.7	4.0	22.2
P00367	Glutamate dehydrogenase 1, mitochondrial	7.80	61400	21.5	2.3	7.0
P21281	V-type proton ATPase subunit B, brain isoform	5.81	56465	21.1	3.3	10.2
P09471-2	Isoform Alpha-2 of Guanine nucleotide-binding protein G(o) subunit alpha	5.90	40061	20.4	3.3	12.0
P06748	Nucleophosmin	4.78	32600	20.0	3.3	19.2
P13489	Ribonuclease inhibitor	4.82	49941	20.0	4.3	14.7
P08572	Collagen alpha-2(IV) chain	8.66	167400	19.8	2.0	1.7

Acc. No.[a]	Name	Calc. pI	Calc. MW (Da)	Avg. Xcorr[b]	Avg. No. of Peptides[c]	Avg. % Sequence Coverage[d]
P07910	Heterogeneous nuclear ribonucleoproteins C1/C2	5.08	33600	19.8	3.0	12.3
P29966	Myristoylated alanine-rich C-kinase substrate	4.45	31500	19.7	4.0	20.7
P60201	Myelin proteolipid protein	8.35	30057	19.6	3.0	13.4
P60880	Synaptosomal-associated protein 25	4.77	23300	19.4	3.8	24.6
P19367	Hexokinase-1	6.80	102400	19.3	3.3	4.5
P05026	Sodium/potassium-transporting ATPase subunit beta-1	8.53	35000	19.0	2.0	9.9
Q08211	ATP-dependent RNA helicase A	6.84	140869	18.1	3.3	3.3
P57053	Histone H2B type F-S	10.37	13900	18.1	2.0	19.8
Q1KMD3	Heterogeneous nuclear ribonucleoprotein U-like protein 2	4.91	85052	18.0	2.0	4.4
P21980	Protein-glutamine gamma-glutamyltransferase 2	5.22	77300	17.5	2.3	5.0
O00764	Pyridoxal kinase	6.13	35100	17.3	3.3	17.1
Q8IWE0	Calcium/calmodulin-dependent protein kinase II alpha	7.20	54054	17.3	2.7	10.5
P12956	X-ray repair cross-complementing protein 6	6.64	69800	17.2	2.7	5.6
Q9UK22	F-box only protein 2	4.37	33300	17.0	2.3	12.8
Q53X12	Vacuolar-type H(+)-ATPase	6.70	95689	16.9	2.0	3.8
Q14697	Neutral alpha-glucosidase AB	6.14	106807	16.8	3.0	4.8
P63010	AP-2 complex subunit beta	5.38	104500	16.3	2.7	5.7
Q9UHG2	ProSAAS	6.62	27356	16.2	3.0	18.5
P17600	Synapsin-1	9.83	74100	16.2	2.3	5.0
P38646	Stress-70 protein, mitochondrial	6.16	73600	16.0	3.0	5.8
P35998	26S protease regulatory subunit 7	5.95	48600	15.8	2.7	9.4
P05455	Lupus La protein	7.12	46800	15.8	3.3	10.1
P21266	Glutathione S-transferase Mu 3	5.54	26500	15.7	2.3	13.1
P02794	Ferritin heavy chain	5.55	21212	15.7	2.0	17.2
Q14240	Eukaryotic initiation factor 4A-II	5.48	46400	15.6	2.0	6.6
Q9HDC9	Adipocyte plasma membrane-associated protein	6.16	46451	15.3	2.0	10.5
P07195	L-lactate dehydrogenase B chain	6.05	36615	15.1	3.8	13.9
P09382	Galectin-1	5.50	14706	14.9	2.0	20.7
P02462	Collagen alpha-1(IV) chain	8.28	160500	14.6	2.0	1.7
O76070	Gamma-synuclein	4.86	13323	14.4	3.0	34.8

Acc. No.[a]	Name	Calc. pI	Calc. MW (Da)	Avg. Xcorr[b]	Avg. No. of Peptides[c]	Avg. % Sequence Coverage[d]
P36269	Gamma-glutamyltransferase 5	7.55	62200	14.3	2.3	8.2
O43852	Calumenin	4.64	37100	14.3	2.0	7.4
Q13263	Transcription intermediary factor 1-beta	5.77	88500	14.3	2.0	3.8
P09972	Fructose-bisphosphate aldolase C	6.87	39400	14.1	3.3	13.0
Q9NQC3	Reticulon-4	4.50	129900	13.5	2.3	2.7
Q14257	Reticulocalbin-2	4.40	36854	13.5	2.7	15.7
Q9BTT0	Acidic leucine-rich nuclear phosphoprotein 32 family member E	3.85	30700	13.2	3.5	20.5
P11166	Solute carrier family 2, facilitated glucose transporter member 1	8.72	54000	13.2	2.5	6.1
O94905	Erlin-2	5.62	37800	12.5	2.5	10.6
P27105	Erythrocyte band 7 integral membrane protein	7.88	31700	12.2	2.5	13.0
O43765	Small glutamine-rich tetratricopeptide repeat-containing protein alpha	4.87	34000	12.2	2.0	8.8
Q16891	Mitochondrial inner membrane protein	6.48	83600	11.8	2.3	4.3
P02649	Apolipoprotein E	5.73	36132	11.7	3.0	10.7
Q96FW1	Ubiquitin thioesterase OTUB1	4.94	31300	11.6	2.0	10.5
O75489	NADH dehydrogenase [ubiquinone] iron-sulfur protein 3, mitochondrial	7.50	30223	11.1	2.7	15.4
P55795	Heterogeneous nuclear ribonucleoprotein H2	6.30	49232	10.6	2.0	7.6
Q6PUJ7	Prohibitin	5.76	29802	10.4	3.0	15.4
Q99623	Prohibitin-2	9.83	33300	10.4	2.3	11.0
O95810	Serum deprivation-response protein	5.21	47100	10.3	2.3	8.4
Q9Y4L1	Hypoxia up-regulated protein 1	5.22	111300	10.3	2.0	3.0
P04271	Protein S100-B	4.59	10706	10.1	2.0	32.6
P63027	Vesicle-associated membrane protein 2	8.13	12655	9.8	2.0	28.5
Q15185	Prostaglandin E synthase 3	4.54	18700	9.8	2.0	15.6
D3DTX7	Collagen, type I, alpha 1, isoform CRA_a	6.24	84688	9.4	2.0	3.7
P06744	Glucose-6-phosphate isomerase	8.32	63100	9.4	2.3	6.6
P43490	Nicotinamide phosphoribosyltransferase	7.15	55487	8.9	2.0	7.7
Q7L0J3	Synaptic vesicle glycoprotein 2A	5.57	82600	8.8	2.0	3.1
P05388	60S acidic ribosomal protein P0	5.97	34300	8.7	2.0	10.4

Acc. No.[a]	Name	Calc. pI	Calc. MW (Da)	Avg. Xcorr[b]	Avg. No. of Peptides[c]	Avg. % Sequence Coverage[d]
Q9UN86	Ras GTPase-activating protein-binding protein 2	5.55	54100	7.9	2.0	5.8
Q8NBS9	Thioredoxin domain-containing protein 5	5.97	47600	7.1	2.0	6.0
P21926	CD9 antigen	7.15	25400	6.8	2.0	15.4

[a] SwissProt accession number
[b] Average Xcorr significance score
[c] Average number of unique peptides sequenced
[d] Average % of the full-length amino acid sequence covered by identified pepti

References

1. Wood-Kaczmar, A., S. Gandhi, and N.W. Wood, *Understanding the molecular causes of Parkinson's disease.* Trends in Molecular Medicine, 2006. **12**(11): p. 521-528.
2. Fahn, S., *Description of Parkinson's disease as a clinical syndrome.* Ann N Y Acad Sci, 2003. **991**: p. 1-14.
3. Takahashi, H. and K. Wakabayashi, *Controversy: is Parkinson's disease a single disease entity? Yes.* Parkinsonism & Related Disorders, 2005. **11 Suppl 1**: p. S31-37.
4. Tan, E.K., *The role of common genetic risk variants in Parkinson disease.* Clinical Genetics, 2007. **72**(5): p. 387-393.
5. Alves, G., E.B. Forsaa, K.F. Pedersen, M. Dreetz Gjerstad, and J.P. Larsen, *Epidemiology of Parkinson's disease.* J Neurol, 2008. **255 Suppl 5**: p. 18-32.
6. Klein, C. and M.G. Schlossmacher, *Parkinson disease, 10 years after its genetic revolution: multiple clues to a complex disorder.* Neurology, 2007. **69**(22): p. 2093-2104.
7. Elbaz, A., J.H. Bower, D.M. Maraganore, S.K. McDonnell, B.J. Peterson, J.E. Ahlskog, D.J. Schaid, and W.A. Rocca, *Risk tables for parkinsonism and Parkinson's disease.* J Clin Epidemiol, 2002. **55**(1): p. 25-31.
8. Cordato, D.J. and D.K. Chan, *Genetics and Parkinson's disease.* Journal of Clinical Neuroscience, 2004. **11**(2): p. 119-123.
9. Sidransky, E., M.A. Nalls, J.O. Aasly, J. Aharon-Peretz, G. Annesi, E.R. Barbosa, A. Bar-Shira, D. Berg, J. Bras, A. Brice, C.M. Chen, L.N. Clark, C. Condroyer, E.V. De Marco, A. Durr, M.J. Eblan, S. Fahn, M.J. Farrer, H.C. Fung, Z. Gan-Or, T. Gasser, R. Gershoni-Baruch, N. Giladi, A. Griffith, T. Gurevich, C. Januario, P. Kropp, A.E. Lang, G.J. Lee-Chen, S. Lesage, K. Marder, I.F. Mata, A. Mirelman, J. Mitsui, I. Mizuta, G. Nicoletti, C. Oliveira, R. Ottman, A. Orr-Urtreger, L.V. Pereira, A. Quattrone, E. Rogaeva, A. Rolfs, H. Rosenbaum, R. Rozenberg, A. Samii, T. Samaddar, C. Schulte, M. Sharma, A. Singleton, M. Spitz, E.K. Tan, N. Tayebi, T. Toda, A.R. Troiano, S. Tsuji, M. Wittstock, T.G. Wolfsberg, Y.R. Wu, C.P. Zabetian, Y. Zhao, and S.G. Ziegler, *Multicenter analysis of*

glucocerebrosidase mutations in Parkinson's disease. N Engl J Med, 2009. **361**(17): p. 1651-1661.

10. Ascherio, A., H. Chen, M.G. Weisskopf, E. O'Reilly, M.L. McCullough, E.E. Calle, M.A. Schwarzschild, and M.J. Thun, *Pesticide exposure and risk for Parkinson's disease.* Ann Neurol, 2006. **60**(2): p. 197-203.
11. Ritz, B. and F. Yu, *Parkinson's disease mortality and pesticide exposure in California 1984-1994.* Int J Epidemiol, 2000. **29**(2): p. 323-329.
12. Priyadarshi, A., S.A. Khuder, E.A. Schaub, and S.S. Priyadarshi, *Environmental risk factors and Parkinson's disease: a metaanalysis.* Environ Res, 2001. **86**(2): p. 122-127.
13. Hernan, M.A., B. Takkouche, F. Caamano-Isorna, and J.J. Gestal-Otero, *A meta-analysis of coffee drinking, cigarette smoking, and the risk of Parkinson's disease.* Ann Neurol, 2002. **52**(3): p. 276-284.
14. Gorell, J.M., B.A. Rybicki, C.C. Johnson, and E.L. Peterson, *Smoking and Parkinson's disease: a dose-response relationship.* Neurology, 1999. **52**(1): p. 115-119.
15. Eller, T., *Deep brain stimulation for Parkinson's disease, essential tremor, and dystonia.* Dis Mon, 2011. **57**(10): p. 638-646.
16. Date, I. and T. Yasuhara, *Neurological disorders and neural regeneration, with special reference to Parkinson's disease and cerebral ischemia.* J Artif Organs, 2009. **12**(1): p. 11-16.
17. Freed, C.R., P.E. Greene, R.E. Breeze, W.Y. Tsai, W. DuMouchel, R. Kao, S. Dillon, H. Winfield, S. Culver, J.Q. Trojanowski, D. Eidelberg, and S. Fahn, *Transplantation of embryonic dopamine neurons for severe Parkinson's disease.* N Engl J Med, 2001. **344**(10): p. 710-719.
18. Olanow, C.W., C.G. Goetz, J.H. Kordower, A.J. Stoessl, V. Sossi, M.F. Brin, K.M. Shannon, G.M. Nauert, D.P. Perl, J. Godbold, and T.B. Freeman, *A double-blind controlled trial of bilateral fetal nigral transplantation in Parkinson's disease.* Ann Neurol, 2003. **54**(3): p. 403-414.
19. Arjona, V., A. Minguez-Castellanos, R.J. Montoro, A. Ortega, F. Escamilla, J.J. Toledo-Aral, R. Pardal, S. Mendez-Ferrer, J.M. Martin, M. Perez, M.J. Katati, E. Valencia, T. Garcia, and J. Lopez-Barneo, *Autotransplantation of human carotid body cell aggregates for treatment of Parkinson's disease.* Neurosurgery, 2003. **53**(2): p. 321-328; discussion 328-330.

20. Iwatsubo, T., *Pathological biochemistry of alpha-synucleinopathy.* Neuropathology, 2007. **27**(5): p. 474-478.
21. Geldmacher, D.S., *Dementia with Lewy bodies: diagnosis and clinical approach.* Cleve Clin J Med, 2004. **71**(10): p. 789-790, 792-784, 797-788 passim.
22. McKeith, I., J. Mintzer, D. Aarsland, D. Burn, H. Chiu, J. Cohen-Mansfield, D. Dickson, B. Dubois, J.E. Duda, H. Feldman, S. Gauthier, G. Halliday, B. Lawlor, C. Lippa, O.L. Lopez, J. Carlos Machado, J. O'Brien, J. Playfer, and W. Reid, *Dementia with Lewy bodies.* Lancet Neurol, 2004. **3**(1): p. 19-28.
23. Josif, S. and K. Graham, *Diagnosis and treatment of dementia with Lewy bodies.* JAAPA, 2008. **21**(5): p. 22-26.
24. Bonifati, V., *Recent advances in the genetics of dementia with lewy bodies.* Curr Neurol Neurosci Rep, 2008. **8**(3): p. 187-189.
25. Goldmann Gross, R., A. Siderowf, and H.I. Hurtig, *Cognitive impairment in Parkinson's disease and dementia with lewy bodies: a spectrum of disease.* Neurosignals, 2008. **16**(1): p. 24-34.
26. Korczyn, A.D. and H. Reichmann, *Dementia with Lewy bodies.* J Neurol Sci, 2006. **248**(1-2): p. 3-8.
27. Inoue, M., S. Yagishita, M. Ryo, K. Hasegawa, N. Amano, and M. Matsushita, *The distribution and dynamic density of oligodendroglial cytoplasmic inclusions (GCIs) in multiple system atrophy: a correlation between the density of GCIs and the degree of involvement of striatonigral and olivopontocerebellar systems.* Acta Neuropathol, 1997. **93**(6): p. 585-591.
28. Ozawa, T., *Pathology and genetics of multiple system atrophy: an approach to determining genetic susceptibility spectrum.* Acta Neuropathol, 2006. **112**(5): p. 531-538.
29. Vanacore, N., *Epidemiological evidence on multiple system atrophy.* J Neural Transm, 2005. **112**(12): p. 1605-1612.
30. Wakabayashi, K. and H. Takahashi, *Cellular pathology in multiple system atrophy.* Neuropathology, 2006. **26**(4): p. 338-345.
31. Wenning, G.K., N. Stefanova, K.A. Jellinger, W. Poewe, and M.G. Schlossmacher, *Multiple system atrophy: a primary oligodendrogliopathy.* Ann Neurol, 2008. **64**(3): p. 239-246.

32. Vanacore, N., V. Bonifati, G. Fabbrini, C. Colosimo, G. De Michele, R. Marconi, D. Nicholl, N. Locuratolo, G. Talarico, S. Romano, F. Stocchi, U. Bonuccelli, M. De Mari, P. Vieregge, and G. Meco, *Epidemiology of multiple system atrophy. ESGAP Consortium. European Study Group on Atypical Parkinsonisms.* Neurol Sci, 2001. **22**(1): p. 97-99.
33. Wenning, G.K., F. Tison, Y. Ben Shlomo, S.E. Daniel, and N.P. Quinn, *Multiple system atrophy: a review of 203 pathologically proven cases.* Mov Disord, 1997. **12**(2): p. 133-147.
34. Yoshida, M., *Multiple system atrophy: alpha-synuclein and neuronal degeneration.* Neuropathology, 2007. **27**(5): p. 484-493.
35. Scholz, S.W., H. Houlden, C. Schulte, M. Sharma, A. Li, D. Berg, A. Melchers, R. Paudel, J.R. Gibbs, J. Simon-Sanchez, C. Paisan-Ruiz, J. Bras, J. Ding, H. Chen, B.J. Traynor, S. Arepalli, R.R. Zonozi, T. Revesz, J. Holton, N. Wood, A. Lees, W. Oertel, U. Wullner, S. Goldwurm, M.T. Pellecchia, T. Illig, O. Riess, H.H. Fernandez, R.L. Rodriguez, M.S. Okun, W. Poewe, G.K. Wenning, J.A. Hardy, A.B. Singleton, F. Del Sorbo, S. Schneider, K.P. Bhatia, and T. Gasser, *SNCA variants are associated with increased risk for multiple system atrophy.* Ann Neurol, 2009. **65**(5): p. 610-614.
36. Vanacore, N., V. Bonifati, G. Fabbrini, C. Colosimo, G. De Michele, R. Marconi, F. Stocchi, D. Nicholl, U. Bonuccelli, M. De Mari, P. Vieregge, and G. Meco, *Case-control study of multiple system atrophy.* Mov Disord, 2005. **20**(2): p. 158-163.
37. Vanacore, N., V. Bonifati, G. Fabbrini, C. Colosimo, R. Marconi, D. Nicholl, U. Bonuccelli, F. Stocchi, P. Lamberti, G. Volpe, G. De Michele, I. Iavarone, P. Bennett, P. Vieregge, and G. Meco, *Smoking habits in multiple system atrophy and progressive supranuclear palsy. European Study Group on Atypical Parkinsonisms.* Neurology, 2000. **54**(1): p. 114-119.
38. Wakabayashi, K., K. Tanji, F. Mori, and H. Takahashi, *The Lewy body in Parkinson's disease: molecules implicated in the formation and degradation of alpha-synuclein aggregates.* Neuropathology, 2007. **27**(5): p. 494-506.
39. Uversky, V.N. and D. Eliezer, *Biophysics of Parkinson's disease: structure and aggregation of alpha-synuclein.* Curr Protein Pept Sci, 2009. **10**(5): p. 483-499.

40. Anderson, J.P., D.E. Walker, J.M. Goldstein, R. de Laat, K. Banducci, R.J. Caccavello, R. Barbour, J. Huang, K. Kling, M. Lee, L. Diep, P.S. Keim, X. Shen, T. Chataway, M.G. Schlossmacher, P. Seubert, D. Schenk, S. Sinha, W.P. Gai, and T.J. Chilcote, *Phosphorylation of Ser-129 is the dominant pathological modification of alpha-synuclein in familial and sporadic Lewy body disease.* J Biol Chem, 2006. **281**(40): p. 29739-29752.

41. Zhu, X., S.L. Siedlak, M.A. Smith, G. Perry, and S.G. Chen, *LRRK2 protein is a component of Lewy bodies.* Ann Neurol, 2006. **60**(5): p. 617-618; author reply 618-619.

42. Gandhi, S., M.M. Muqit, L. Stanyer, D.G. Healy, P.M. Abou-Sleiman, I. Hargreaves, S. Heales, M. Ganguly, L. Parsons, A.J. Lees, D.S. Latchman, J.L. Holton, N.W. Wood, and T. Revesz, *PINK1 protein in normal human brain and Parkinson's disease.* Brain, 2006. **129**(Pt 7): p. 1720-1731.

43. Schlossmacher, M.G., M.P. Frosch, W.P. Gai, M. Medina, N. Sharma, L. Forno, T. Ochiishi, H. Shimura, R. Sharon, N. Hattori, J.W. Langston, Y. Mizuno, B.T. Hyman, D.J. Selkoe, and K.S. Kosik, *Parkin localizes to the Lewy bodies of Parkinson disease and dementia with Lewy bodies.* Am J Pathol, 2002. **160**(5): p. 1655-1667.

44. Bandopadhyay, R., A.E. Kingsbury, M.M. Muqit, K. Harvey, A.R. Reid, L. Kilford, S. Engelender, M.G. Schlossmacher, N.W. Wood, D.S. Latchman, R.J. Harvey, and A.J. Lees, *Synphilin-1 and parkin show overlapping expression patterns in human brain and form aggresomes in response to proteasomal inhibition.* Neurobiol Dis, 2005. **20**(2): p. 401-411.

45. Ozawa, T., D. Paviour, N.P. Quinn, K.A. Josephs, H. Sangha, L. Kilford, D.G. Healy, N.W. Wood, A.J. Lees, J.L. Holton, and T. Revesz, *The spectrum of pathological involvement of the striatonigral and olivopontocerebellar systems in multiple system atrophy: clinicopathological correlations.* Brain, 2004. **127**(Pt 12): p. 2657-2671.

46. Richter-Landsberg, C., M. Gorath, J.Q. Trojanowski, and V.M. Lee, *alpha-synuclein is developmentally expressed in cultured rat brain oligodendrocytes.* J Neurosci Res, 2000. **62**(1): p. 9-14.

47. Culvenor, J.G., R.L. Rietze, P.F. Bartlett, C.L. Masters, and Q.X. Li, *Oligodendrocytes from neural stem cells express alpha-synuclein: increased*

numbers from presenilin 1 deficient mice. Neuroreport, 2002. **13**(10): p. 1305-1308.

48. Miller, D.W., J.M. Johnson, S.M. Solano, Z.R. Hollingsworth, D.G. Standaert, and A.B. Young, *Absence of alpha-synuclein mRNA expression in normal and multiple system atrophy oligodendroglia.* J Neural Transm, 2005. **112**(12): p. 1613-1624.
49. Ozawa, T., K. Okuizumi, T. Ikeuchi, K. Wakabayashi, H. Takahashi, and S. Tsuji, *Analysis of the expression level of alpha-synuclein mRNA using postmortem brain samples from pathologically confirmed cases of multiple system atrophy.* Acta Neuropathol, 2001. **102**(2): p. 188-190.
50. Borghi, R., R. Marchese, A. Negro, L. Marinelli, G. Forloni, D. Zaccheo, G. Abbruzzese, and M. Tabaton, *Full length alpha-synuclein is present in cerebrospinal fluid from Parkinson's disease and normal subjects.* Neurosci Lett, 2000. **287**(1): p. 65-67.
51. Lindersson, E., D. Lundvig, C. Petersen, P. Madsen, J.R. Nyengaard, P. Hojrup, T. Moos, D. Otzen, W.P. Gai, P.C. Blumbergs, and P.H. Jensen, *p25alpha Stimulates alpha-synuclein aggregation and is co-localized with aggregated alpha-synuclein in alpha-synucleinopathies.* J Biol Chem, 2005. **280**(7): p. 5703-5715.
52. Braak, H., D. Sandmann-Keil, W. Gai, and E. Braak, *Extensive axonal Lewy neurites in Parkinson's disease: a novel pathological feature revealed by alpha-synuclein immunocytochemistry.* Neurosci Lett, 1999. **265**(1): p. 67-69.
53. Ono, K., M. Hirohata, and M. Yamada, *Alpha-synuclein assembly as a therapeutic target of Parkinson's disease and related disorders.* Curr Pharm Des, 2008. **14**(30): p. 3247-3266.
54. Sandmann-Keil, D., H. Braak, M. Okochi, C. Haass, and E. Braak, *Alpha-synuclein immunoreactive Lewy bodies and Lewy neurites in Parkinson's disease are detectable by an advanced silver-staining technique.* Acta Neuropathol, 1999. **98**(5): p. 461-464.
55. Baker, K.G., Y. Huang, H. McCann, W.P. Gai, P.H. Jensen, and G.M. Halliday, *P25alpha immunoreactive but alpha-synuclein immunonegative neuronal inclusions in multiple system atrophy.* Acta Neuropathol, 2006. **111**(2): p. 193-195.

56. Nishie, M., F. Mori, H. Fujiwara, M. Hasegawa, M. Yoshimoto, T. Iwatsubo, H. Takahashi, and K. Wakabayashi, *Accumulation of phosphorylated alpha-synuclein in the brain and peripheral ganglia of patients with multiple system atrophy.* Acta Neuropathol, 2004. **107**(4): p. 292-298.

57. Proukakis, C., C.G. Dudzik, T. Brier, D.S. MacKay, J.M. Cooper, G.L. Millhauser, H. Houlden, and A.H. Schapira, *A novel alpha-synuclein missense mutation in Parkinson disease.* Neurology, 2013. **80**(11): p. 1062-1064.

58. Kiely, A.P., Y.T. Asi, E. Kara, P. Limousin, H. Ling, P. Lewis, C. Proukakis, N. Quinn, A.J. Lees, J. Hardy, T. Revesz, H. Houlden, and J.L. Holton, *alpha-Synucleinopathy associated with G51D SNCA mutation: a link between Parkinson's disease and multiple system atrophy?* Acta Neuropathol, 2013. **125**(5): p. 753-769.

59. Bisaglia, M., S. Mammi, and L. Bubacco, *Structural insights on physiological functions and pathological effects of alpha-synuclein.* FASEB J, 2009. **23**(2): p. 329-340.

60. Bartels, T., J.G. Choi, and D.J. Selkoe, *alpha-Synuclein occurs physiologically as a helically folded tetramer that resists aggregation.* Nature, 2011. **477**(7362): p. 107-110.

61. Waxman, E.A. and B.I. Giasson, *Molecular mechanisms of alpha-synuclein neurodegeneration.* Biochim Biophys Acta, 2009. **1792**(7): p. 616-624.

62. Tofaris, G.K. and M.G. Spillantini, *Physiological and pathological properties of alpha-synuclein.* Cellular & Molecular Life Sciences, 2007. **64**(17): p. 2194-2201.

63. Cabin, D.E., K. Shimazu, D. Murphy, N.B. Cole, W. Gottschalk, K.L. McIlwain, B. Orrison, A. Chen, C.E. Ellis, R. Paylor, B. Lu, and R.L. Nussbaum, *Synaptic vesicle depletion correlates with attenuated synaptic responses to prolonged repetitive stimulation in mice lacking alpha-synuclein.* J Neurosci, 2002. **22**(20): p. 8797-8807.

64. Abeliovich, A., Y. Schmitz, I. Farinas, D. Choi-Lundberg, W.H. Ho, P.E. Castillo, N. Shinsky, J.M. Verdugo, M. Armanini, A. Ryan, M. Hynes, H. Phillips, D. Sulzer, and A. Rosenthal, *Mice lacking alpha-synuclein display functional deficits in the nigrostriatal dopamine system.* Neuron, 2000. **25**(1): p. 239-252.

65. McCormack, A.L. and D.A. Di Monte, *Enhanced alpha-synuclein expression in human neurodegenerative diseases: pathogenetic and therapeutic implications.* Curr Protein Pept Sci, 2009. **10**(5): p. 476-482.
66. Anand, V.S. and S.P. Braithwaite, *LRRK2 in Parkinson's disease: biochemical functions.* FEBS J, 2009. **276**(22): p. 6428-6435.
67. Galter, D., M. Westerlund, A. Carmine, E. Lindqvist, O. Sydow, and L. Olson, *LRRK2 expression linked to dopamine-innervated areas.* Ann Neurol, 2006. **59**(4): p. 714-719.
68. McCray, B.A. and J.P. Taylor, *The role of autophagy in age-related neurodegeneration.* Neurosignals, 2008. **16**(1): p. 75-84.
69. Martinez-Vicente, M. and A.M. Cuervo, *Autophagy and neurodegeneration: when the cleaning crew goes on strike.* Lancet Neurol, 2007. **6**(4): p. 352-361.
70. McNaught, K.S., C.W. Olanow, B. Halliwell, O. Isacson, and P. Jenner, *Failure of the ubiquitin-proteasome system in Parkinson's disease.* Nat Rev Neurosci, 2001. **2**(8): p. 589-594.
71. Rubinsztein, D.C., *The roles of intracellular protein-degradation pathways in neurodegeneration.* Nature, 2006. **443**(7113): p. 780-786.
72. Wooten, M.W., X. Hu, J.R. Babu, M.L. Seibenhener, T. Geetha, M.G. Paine, and M.C. Wooten, *Signaling, Polyubiquitination, Trafficking, and Inclusions: Sequestosome 1/p62's Role in Neurodegenerative Disease.* J Biomed Biotechnol, 2006. **2006**(3): p. 62079.
73. Alves-Rodrigues, A., L. Gregori, and M.E. Figueiredo-Pereira, *Ubiquitin, cellular inclusions and their role in neurodegeneration.* Trends Neurosci, 1998. **21**(12): p. 516-520.
74. Buchberger, A., *From UBA to UBX: new words in the ubiquitin vocabulary.* Trends Cell Biol, 2002. **12**(5): p. 216-221.
75. Wolf, D.H., *From lysosome to proteasome: the power of yeast in the dissection of proteinase function in cellular regulation and waste disposal.* Cell Mol Life Sci, 2004. **61**(13): p. 1601-1614.
76. Lim, K.L. and J.M. Tan, *Role of the ubiquitin proteasome system in Parkinson's disease.* BMC Biochemistry, 2007. **8 Suppl 1**: p. S13.

77. DeMartino, G.N. and C.A. Slaughter, *The proteasome, a novel protease regulated by multiple mechanisms.* J Biol Chem, 1999. **274**(32): p. 22123-22126.

78. Bedford, L., D. Hay, S. Paine, N. Rezvani, M. Mee, J. Lowe, and R.J. Mayer, *Is malfunction of the ubiquitin proteasome system the primary cause of alpha-synucleinopathies and other chronic human neurodegenerative disease?* Biochim Biophys Acta, 2008. **1782**(12): p. 683-690.

79. Lim, K.L., *Ubiquitin-proteasome system dysfunction in Parkinson's disease: current evidence and controversies.* Expert Rev Proteomics, 2007. **4**(6): p. 769-781.

80. McNaught, K.S. and P. Jenner, *Proteasomal function is impaired in substantia nigra in Parkinson's disease.* Neurosci Lett, 2001. **297**(3): p. 191-194.

81. Cook, C. and L. Petrucelli, *A critical evaluation of the ubiquitin-proteasome system in Parkinson's disease.* Biochim Biophys Acta, 2009. **1792**(7): p. 664-675.

82. Chin, L.S., J.A. Olzmann, and L. Li, *Parkin-mediated ubiquitin signalling in aggresome formation and autophagy.* Biochem Soc Trans. **38**(Pt 1): p. 144-149.

83. Yue, Z., L. Friedman, M. Komatsu, and K. Tanaka, *The cellular pathways of neuronal autophagy and their implication in neurodegenerative diseases.* Biochim Biophys Acta, 2009. **1793**(9): p. 1496-1507.

84. Cuervo, A.M., *Autophagy: in sickness and in health.* Trends Cell Biol, 2004. **14**(2): p. 70-77.

85. Hara, T., K. Nakamura, M. Matsui, A. Yamamoto, Y. Nakahara, R. Suzuki-Migishima, M. Yokoyama, K. Mishima, I. Saito, H. Okano, and N. Mizushima, *Suppression of basal autophagy in neural cells causes neurodegenerative disease in mice.* Nature, 2006. **441**(7095): p. 885-889.

86. Komatsu, M., S. Waguri, T. Chiba, S. Murata, J. Iwata, I. Tanida, T. Ueno, M. Koike, Y. Uchiyama, E. Kominami, and K. Tanaka, *Loss of autophagy in the central nervous system causes neurodegeneration in mice.* Nature, 2006. **441**(7095): p. 880-884.

87. Kim, I., S. Rodriguez-Enriquez, and J.J. Lemasters, *Selective degradation of mitochondria by mitophagy.* Arch Biochem Biophys, 2007. **462**(2): p. 245-253.

88. Nixon, R.A., *Autophagy in neurodegenerative disease: friend, foe or turncoat?* Trends Neurosci, 2006. **29**(9): p. 528-535.

89. Lee, J.A., *Autophagy in neurodegeneration: two sides of the same coin.* BMB Rep, 2009. **42**(6): p. 324-330.

90. Cuervo, A.M., L. Stefanis, R. Fredenburg, P.T. Lansbury, and D. Sulzer, *Impaired degradation of mutant alpha-synuclein by chaperone-mediated autophagy.* Science, 2004. **305**(5688): p. 1292-1295.

91. Kabuta, T., R. Setsuie, T. Mitsui, A. Kinugawa, M. Sakurai, S. Aoki, K. Uchida, and K. Wada, *Aberrant molecular properties shared by familial Parkinson's disease-associated mutant UCH-L1 and carbonyl-modified UCH-L1.* Hum Mol Genet, 2008. **17**(10): p. 1482-1496.

92. Chu, C.T., *Autophagic stress in neuronal injury and disease.* J Neuropathol Exp Neurol, 2006. **65**(5): p. 423-432.

93. Xue, L., G.C. Fletcher, and A.M. Tolkovsky, *Autophagy is activated by apoptotic signalling in sympathetic neurons: an alternative mechanism of death execution.* Mol Cell Neurosci, 1999. **14**(3): p. 180-198.

94. Lemasters, J.J., *Selective mitochondrial autophagy, or mitophagy, as a targeted defense against oxidative stress, mitochondrial dysfunction, and aging.* Rejuvenation Res, 2005. **8**(1): p. 3-5.

95. Ding, W.X. and X.M. Yin, *Mitophagy: mechanisms, pathophysiological roles, and analysis.* Biol Chem, 2012. **393**(7): p. 547-564.

96. Narendra, D., A. Tanaka, D.F. Suen, and R.J. Youle, *Parkin is recruited selectively to impaired mitochondria and promotes their autophagy.* J Cell Biol, 2008. **183**(5): p. 795-803.

97. Matsuda, N., S. Sato, K. Shiba, K. Okatsu, K. Saisho, C.A. Gautier, Y.S. Sou, S. Saiki, S. Kawajiri, F. Sato, M. Kimura, M. Komatsu, N. Hattori, and K. Tanaka, *PINK1 stabilized by mitochondrial depolarization recruits Parkin to damaged mitochondria and activates latent Parkin for mitophagy.* J Cell Biol, 2010. **189**(2): p. 211-221.

98. Onyango, I.G., *Mitochondrial dysfunction and oxidative stress in Parkinson's disease.* Neurochem Res, 2008. **33**(3): p. 589-597.

99. Bender, A., K.J. Krishnan, C.M. Morris, G.A. Taylor, A.K. Reeve, R.H. Perry, E. Jaros, J.S. Hersheson, J. Betts, T. Klopstock, R.W. Taylor, and D.M. Turnbull, *High levels of mitochondrial DNA deletions in substantia nigra neurons in aging and Parkinson disease.* Nat Genet, 2006. **38**(5): p. 515-517.

100. Kraytsberg, Y., E. Kudryavtseva, A.C. McKee, C. Geula, N.W. Kowall, and K. Khrapko, *Mitochondrial DNA deletions are abundant and cause functional impairment in aged human substantia nigra neurons.* Nat Genet, 2006. **38**(5): p. 518-520.

101. Chen, H. and D.C. Chan, *Mitochondrial dynamics--fusion, fission, movement, and mitophagy--in neurodegenerative diseases.* Hum Mol Genet, 2009. **18**(R2): p. R169-176.

102. Smeyne, R.J. and V. Jackson-Lewis, *The MPTP model of Parkinson's disease.* Brain Res Mol Brain Res, 2005. **134**(1): p. 57-66.

103. Dodson, M.W. and M. Guo, *Pink1, Parkin, DJ-1 and mitochondrial dysfunction in Parkinson's disease.* Curr Opin Neurobiol, 2007. **17**(3): p. 331-337.

104. Jin, J., G.E. Meredith, L. Chen, Y. Zhou, J. Xu, F.S. Shie, P. Lockhart, and J. Zhang, *Quantitative proteomic analysis of mitochondrial proteins: relevance to Lewy body formation and Parkinson's disease.* Brain Res Mol Brain Res, 2005. **134**(1): p. 119-138.

105. Jin, J., C. Hulette, Y. Wang, T. Zhang, C. Pan, R. Wadhwa, and J. Zhang, *Proteomic identification of a stress protein, mortalin/mthsp70/GRP75: relevance to Parkinson disease.* Mol Cell Proteomics, 2006. **5**(7): p. 1193-1204.

106. Basso, M., S. Giraudo, D. Corpillo, B. Bergamasco, L. Lopiano, and M. Fasano, *Proteome analysis of human substantia nigra in Parkinson's disease.* Proteomics, 2004. **4**(12): p. 3943-3952.

107. Werner, C.J., R. Heyny-von Haussen, G. Mall, and S. Wolf, *Proteome analysis of human substantia nigra in Parkinson's disease.* Proteome Sci, 2008. **6**: p. 8.

108. Leverenz, J.B., I. Umar, Q. Wang, T.J. Montine, P.J. McMillan, D.W. Tsuang, J. Jin, C. Pan, J. Shin, D. Zhu, and J. Zhang, *Proteomic identification of novel proteins in cortical lewy bodies.* Brain Pathol, 2007. **17**(2): p. 139-145.

109. Xia, Q., L. Liao, D. Cheng, D.M. Duong, M. Gearing, J.J. Lah, A.I. Levey, and J. Peng, *Proteomic identification of novel proteins associated with Lewy bodies.* Front Biosci, 2008. **13**: p. 3850-3856.

110. Iwatsubo, T., H. Yamaguchi, M. Fujimuro, H. Yokosawa, Y. Ihara, J.Q. Trojanowski, and V.M. Lee, *Purification and characterization of Lewy bodies from the brains of patients with diffuse Lewy body disease.* Am J Pathol, 1996. **148**(5): p. 1517-1529.

111. Pollanen, M.S., C. Bergeron, and L. Weyer, *Deposition of detergent-resistant neurofilaments into Lewy body fibrils.* Brain Res, 1993. **603**(1): p. 121-124.

112. Sian, J., R. Hensiek, D. Senitz, G. Muench, K. Jellinger, P. Riederer, and M. Gerlach, *A novel technique for the isolation of Lewy bodies in brain.* Acta Neuropathol, 1998. **96**(2): p. 111-115.

113. Gai, W.P., J.H. Power, P.C. Blumbergs, J.G. Culvenor, and P.H. Jensen, *Alpha-synuclein immunoisolation of glial inclusions from multiple system atrophy brain tissue reveals multiprotein components.* J Neurochem, 1999. **73**(5): p. 2093-2100.

114. Jensen, P.H., K. Islam, J. Kenney, M.S. Nielsen, J. Power, and W.P. Gai, *Microtubule-associated protein 1B is a component of cortical Lewy bodies and binds alpha-synuclein filaments.* J Biol Chem, 2000. **275**(28): p. 21500-21507.

115. Jin, L.T., S.Y. Hwang, G.S. Yoo, and J.K. Choi, *A mass spectrometry compatible silver staining method for protein incorporating a new silver sensitizer in sodium dodecyl sulfate-polyacrylamide electrophoresis gels.* Proteomics, 2006. **6**(8): p. 2334-2337.

116. Link, A.J. and J. LaBaer, *Proteomics: A Cold Spring Harbor Laboratory Course Manual.* 2009, Cold Spring Harbor, New York: Cold Spring Harbor Laboratory Press.

117. Wilson, C.H., S. Zeile, T. Chataway, V.B. Nieuwenhuijs, R.T. Padbury, and G.J. Barritt, *Increased expression of peroxiredoxin 1 and identification of a novel lipid-metabolizing enzyme in the early phase of liver ischemia reperfusion injury.* Proteomics, 2011. **11**(22): p. 4385-4396.

118. Pountney, D.L., T.M. Treweek, T. Chataway, Y. Huang, F. Chegini, P.C. Blumbergs, M.J. Raftery, and W.P. Gai, *Alpha B-crystallin is a major*

component of glial cytoplasmic inclusions in multiple system atrophy. Neurotox Res, 2005. **7**(1-2): p. 77-85.

119. Wakabayashi, K., M. Yoshimoto, S. Tsuji, and H. Takahashi, *Alpha-synuclein immunoreactivity in glial cytoplasmic inclusions in multiple system atrophy.* Neurosci Lett, 1998. **249**(2-3): p. 180-182.
120. Sluchanko, N.N. and N.B. Gusev, *14-3-3 proteins and regulation of cytoskeleton.* Biochemistry (Mosc), 2010. **75**(13): p. 1528-1546.
121. Iwai, A., E. Masliah, M. Yoshimoto, N. Ge, L. Flanagan, H.A. de Silva, A. Kittel, and T. Saitoh, *The precursor protein of non-A beta component of Alzheimer's disease amyloid is a presynaptic protein of the central nervous system.* Neuron, 1995. **14**(2): p. 467-475.
122. Boston, P.F., P. Jackson, P.A. Kynoch, and R.J. Thompson, *Purification, properties, and immunohistochemical localisation of human brain 14-3-3 protein.* J Neurochem, 1982. **38**(5): p. 1466-1474.
123. Perry, R.H., R.G. Cooks, and R.J. Noll, *Orbitrap mass spectrometry: instrumentation, ion motion and applications.* Mass Spectrom Rev, 2008. **27**(6): p. 661-699.
124. Tucker, A.M., L.O. Driskell, L.K. Pannell, and D.O. Wood, *Differential proteomic analysis of Rickettsia prowazekii propagated in diverse host backgrounds.* Appl Environ Microbiol, 2011. **77**(14): p. 4712-4718.
125. Sun, X., C.L. Xiao, R. Ge, X. Yin, H. Li, N. Li, X. Yang, Y. Zhu, X. He, and Q.Y. He, *Putative copper- and zinc-binding motifs in Streptococcus pneumoniae identified by immobilized metal affinity chromatography and mass spectrometry.* Proteomics, 2011. **11**(16): p. 3288-3298.
126. Yang, Y., X. Qiang, K. Owsiany, S. Zhang, T.W. Thannhauser, and L. Li, *Evaluation of different multidimensional LC-MS/MS pipelines for isobaric tags for relative and absolute quantitation (iTRAQ)-based proteomic analysis of potato tubers in response to cold storage.* J Proteome Res, 2011. **10**(10): p. 4647-4660.
127. Helmy, M., M. Tomita, and Y. Ishihama, *OryzaPG-DB: rice proteome database based on shotgun proteogenomics.* BMC Plant Biol, 2011. **11**: p. 63.
128. Baycin-Hizal, D., Y. Tian, I. Akan, E. Jacobson, D. Clark, J. Chu, K. Palter, H. Zhang, and M.J. Betenbaugh, *GlycoFly: a database of Drosophila N-*

linked glycoproteins identified using SPEG--MS techniques. J Proteome Res, 2011. **10**(6): p. 2777-2784.

129. Tang, W., Y.Q. Shi, J.J. Zou, X.F. Chen, J.Y. Zheng, S.W. Zhao, and Z.M. Liu, *Serum biomarker of diabetic peripheral neuropathy indentified by differential proteomics.* Front Biosci, 2012. **17**: p. 2671-2681.
130. Kaempfer, T., E. Duerst, P. Gehrig, B. Roschitzki, D. Rutishauser, J. Grossmann, G. Schoedon, F. Vallelian, and D.J. Schaer, *Extracellular hemoglobin polarizes the macrophage proteome toward Hb-clearance, enhanced antioxidant capacity and suppressed HLA class 2 expression.* J Proteome Res, 2011. **10**(5): p. 2397-2408.
131. Stoop, M.P., L. Coulier, T. Rosenling, S. Shi, A.M. Smolinska, L. Buydens, K. Ampt, C. Stingl, A. Dane, B. Muilwijk, R.L. Luitwieler, P.A. Sillevis Smitt, R.Q. Hintzen, R. Bischoff, S.S. Wijmenga, T. Hankemeier, A.J. van Gool, and T.M. Luider, *Quantitative proteomics and metabolomics analysis of normal human cerebrospinal fluid samples.* Mol Cell Proteomics, 2010. **9**(9): p. 2063-2075.
132. Molloy, M.P., *Isolation of bacterial cell membranes proteins using carbonate extraction.* Methods Mol Biol, 2008. **424**: p. 397-401.
133. Burre, J. and W. Volknandt, *The synaptic vesicle proteome.* J Neurochem, 2007. **101**(6): p. 1448-1462.
134. Laudanski, K. and D. Wyczechowska, *The distinctive role of small heat shock proteins in oncogenesis.* Arch Immunol Ther Exp (Warsz), 2006. **54**(2): p. 103-111.
135. Tischfield, M.A. and E.C. Engle, *Distinct alpha- and beta-tubulin isotypes are required for the positioning, differentiation and survival of neurons: new support for the 'multi-tubulin' hypothesis.* Biosci Rep, 2010. **30**(5): p. 319-330.
136. Richter-Landsberg, C., *The oligodendroglia cytoskeleton in health and disease.* J Neurosci Res, 2000. **59**(1): p. 11-18.
137. Richter-Landsberg, C., *The cytoskeleton in oligodendrocytes. Microtubule dynamics in health and disease.* J Mol Neurosci, 2008. **35**(1): p. 55-63.
138. Ovadi, J. and F. Orosz, *An unstructured protein with destructive potential: TPPP/p25 in neurodegeneration.* Bioessays, 2009. **31**(6): p. 676-686.

139. Lu, T.Z., Y. Quan, and Z.P. Feng, *Multifaceted role of heat shock protein 70 in neurons.* Mol Neurobiol, 2010. **42**(2): p. 114-123.
140. Segovia-Silvestre, T., A.V. Neutzsky-Wulff, M.G. Sorensen, C. Christiansen, J. Bollerslev, M.A. Karsdal, and K. Henriksen, *Advances in osteoclast biology resulting from the study of osteopetrotic mutations.* Hum Genet, 2009. **124**(6): p. 561-577.
141. Muramatsu, T., *Midkine, a heparin-binding cytokine with multiple roles in development, repair and diseases.* Proc Jpn Acad Ser B Phys Biol Sci, 2010. **86**(4): p. 410-425.
142. Le Novere, N., L. Li, and J.A. Girault, *DARPP-32: molecular integration of phosphorylation potential.* Cell Mol Life Sci, 2008. **65**(14): p. 2125-2127.
143. Huang, Y., J. Niwa, G. Sobue, and G.E. Breitwieser, *Calcium-sensing receptor ubiquitination and degradation mediated by the E3 ubiquitin ligase dorfin.* J Biol Chem, 2006. **281**(17): p. 11610-11617.
144. Cargnello, M. and P.P. Roux, *Activation and function of the MAPKs and their substrates, the MAPK-activated protein kinases.* Microbiol Mol Biol Rev, 2011. **75**(1): p. 50-83.
145. Hall, P.A. and S.E. Russell, *Mammalian septins: dynamic heteromers with roles in cellular morphogenesis and compartmentalization.* J Pathol, 2012. **226**(2): p. 287-299.
146. Montecucco, C., G. Schiavo, and S. Pantano, *SNARE complexes and neuroexocytosis: how many, how close?* Trends Biochem Sci, 2005. **30**(7): p. 367-372.
147. Sorensen, J.B., *SNARE complexes prepare for membrane fusion.* Trends Neurosci, 2005. **28**(9): p. 453-455.
148. Matteoli, M., D. Pozzi, C. Grumelli, S.B. Condliffe, C. Frassoni, T. Harkany, and C. Verderio, *The synaptic split of SNAP-25: different roles in glutamatergic and GABAergic neurons?* Neuroscience, 2009. **158**(1): p. 223-230.
149. Brunger, A.T., K. Weninger, M. Bowen, and S. Chu, *Single-molecule studies of the neuronal SNARE fusion machinery.* Annu Rev Biochem, 2009. **78**: p. 903-928.

150. Ybe, J.A., D.E. Wakeham, F.M. Brodsky, and P.K. Hwang, *Molecular structures of proteins involved in vesicle fusion.* Traffic, 2000. **1**(6): p. 474-479.

151. Greaves, J., G.R. Prescott, O.A. Gorleku, and L.H. Chamberlain, *Regulation of SNAP-25 trafficking and function by palmitoylation.* Biochem Soc Trans, 2010. **38**(Pt 1): p. 163-166.

152. Valtorta, F., M. Pennuto, D. Bonanomi, and F. Benfenati, *Synaptophysin: leading actor or walk-on role in synaptic vesicle exocytosis?* Bioessays, 2004. **26**(4): p. 445-453.

153. Chapman, E.R., *How does synaptotagmin trigger neurotransmitter release?* Annu Rev Biochem, 2008. **77**: p. 615-641.

154. Sasaki, T., H. Shirataki, H. Nakanishi, and Y. Takai, *Rab3A-rabphilin-3A system in neurotransmitter release.* Adv Second Messenger Phosphoprotein Res, 1997. **31**: p. 279-294.

155. Gonzalez, L., Jr. and R.H. Scheller, *Regulation of membrane trafficking: structural insights from a Rab/effector complex.* Cell, 1999. **96**(6): p. 755-758.

156. Beyenbach, K.W. and H. Wieczorek, *The V-type H+ ATPase: molecular structure and function, physiological roles and regulation.* J Exp Biol, 2006. **209**(Pt 4): p. 577-589.

157. El Far, O. and M. Seagar, *A role for V-ATPase subunits in synaptic vesicle fusion?* J Neurochem, 2011. **117**(4): p. 603-612.

158. Marshansky, V. and M. Futai, *The V-type H+-ATPase in vesicular trafficking: targeting, regulation and function.* Curr Opin Cell Biol, 2008. **20**(4): p. 415-426.

159. Vautrin, J., *SV2 frustrating exocytosis at the semi-diffusor synapse.* Synapse, 2009. **63**(4): p. 319-338.

160. Belizaire, R., C. Komanduri, K. Wooten, M. Chen, C. Thaller, and R. Janz, *Characterization of synaptogyrin 3 as a new synaptic vesicle protein.* J Comp Neurol, 2004. **470**(3): p. 266-281.

161. Jahn, R. and R.H. Scheller, *SNAREs--engines for membrane fusion.* Nat Rev Mol Cell Biol, 2006. **7**(9): p. 631-643.

162. Ochs, D., *Protein contaminants of sodium dodecyl sulfate-polyacrylamide gels.* Anal Biochem, 1983. **135**(2): p. 470-474.

163. Lyngholm, M., H. Vorum, K. Nielsen, N. Ehlers, and B. Honore, *Attempting to distinguish between endogenous and contaminating cytokeratins in a corneal proteomic study.* BMC Ophthalmol, 2011. **11**: p. 3.

164. Zhao, C., J.T. Slevin, and S.W. Whiteheart, *Cellular functions of NSF: not just SNAPs and SNAREs.* FEBS Lett, 2007. **581**(11): p. 2140-2149.

165. Teasdale, R.D. and B.M. Collins, *Insights into the PX (phox-homology) domain and SNX (sorting nexin) protein families: structures, functions and roles in disease.* Biochem J, 2012. **441**(1): p. 39-59.

166. Strating, J.R. and G.J. Martens, *The p24 family and selective transport processes at the ER-Golgi interface.* Biol Cell, 2009. **101**(9): p. 495-509.

167. Shiotani, M., K. Nakano, E. Yamauchi, Y. Oda, S. Hosokawa, and T. Aoki, *Proteomic analysis for neuronal vacuolation induced by MK-801 in rat retrosplenial cortex.* J Toxicol Sci, 2011. **36**(1): p. 131-133.

168. Fujishiro, H., T.B. Ahn, R. Frigerio, A. DelleDonne, K.A. Josephs, J.E. Parisi, J. Eric Ahlskog, and D.W. Dickson, *Glial cytoplasmic inclusions in neurologically normal elderly: prodromal multiple system atrophy?* Acta Neuropathol, 2008. **116**(3): p. 269-275.

169. Uchikado, H., A. DelleDonne, R. Uitti, and D.W. Dickson, *Coexistence of PSP and MSA: a case report and review of the literature.* Acta Neuropathol, 2006. **111**(2): p. 186-192.

170. Parkkinen, L., P. Hartikainen, and I. Alafuzoff, *Abundant glial alpha-synuclein pathology in a case without overt clinical symptoms.* Clin Neuropathol, 2007. **26**(6): p. 276-283.

171. Gibb, W.R. and A.J. Lees, *The relevance of the Lewy body to the pathogenesis of idiopathic Parkinson's disease.* J Neurol Neurosurg Psychiatry, 1988. **51**(6): p. 745-752.

172. Parkkinen, L., T. Pirttila, and I. Alafuzoff, *Applicability of current staging/categorization of alpha-synuclein pathology and their clinical relevance.* Acta Neuropathol, 2008. **115**(4): p. 399-407.

173. Adler, C.H., D.J. Connor, J.G. Hentz, M.N. Sabbagh, J.N. Caviness, H.A. Shill, B. Noble, and T.G. Beach, *Incidental Lewy body disease: clinical comparison to a control cohort.* Mov Disord, 2010. **25**(5): p. 642-646.

174. Milber, J.M., J.V. Noorigian, J.F. Morley, H. Petrovitch, L. White, G.W. Ross, and J.E. Duda, *Lewy pathology is not the first sign of degeneration in*

vulnerable neurons in Parkinson disease. Neurology, 2012. **79**(24): p. 2307-2314.

175. Halliday, G.M., K. Del Tredici, and H. Braak, *Critical appraisal of brain pathology staging related to presymptomatic and symptomatic cases of sporadic Parkinson's disease.* J Neural Transm Suppl, 2006(70): p. 99-103.
176. Trinkle-Mulcahy, L., S. Boulon, Y.W. Lam, R. Urcia, F.M. Boisvert, F. Vandermoere, N.A. Morrice, S. Swift, U. Rothbauer, H. Leonhardt, and A. Lamond, *Identifying specific protein interaction partners using quantitative mass spectrometry and bead proteomes.* J Cell Biol, 2008. **183**(2): p. 223-239.
177. Arima, K., K. Ueda, N. Sunohara, K. Arakawa, S. Hirai, M. Nakamura, H. Tonozuka-Uehara, and M. Kawai, *NACP/alpha-synuclein immunoreactivity in fibrillary components of neuronal and oligodendroglial cytoplasmic inclusions in the pontine nuclei in multiple system atrophy.* Acta Neuropathol, 1998. **96**(5): p. 439-444.
178. Jaros, E. and D.J. Burn, *The pathogenesis of multiple system atrophy: past, present, and future.* Mov Disord, 2000. **15**(5): p. 784-788.
179. Spillantini, M.G., M.L. Schmidt, V.M. Lee, J.Q. Trojanowski, R. Jakes, and M. Goedert, *Alpha-synuclein in Lewy bodies.* Nature, 1997. **388**(6645): p. 839-840.
180. Licker, V., E. Kovari, D.F. Hochstrasser, and P.R. Burkhard, *Proteomics in human Parkinson's disease research.* J Proteomics, 2009. **73**(1): p. 10-29.
181. Brion, J.P. and A.M. Couck, *Cortical and brainstem-type Lewy bodies are immunoreactive for the cyclin-dependent kinase 5.* Am J Pathol, 1995. **147**(5): p. 1465-1476.
182. Kanazawa, T., T. Uchihara, A. Takahashi, A. Nakamura, S. Orimo, and H. Mizusawa, *Three-layered structure shared between Lewy bodies and lewy neurites-three-dimensional reconstruction of triple-labeled sections.* Brain Pathol, 2008. **18**(3): p. 415-422.
183. Liem, R.K. and A. Messing, *Dysfunctions of neuronal and glial intermediate filaments in disease.* J Clin Invest, 2009. **119**(7): p. 1814-1824.
184. Wang, C.L. and L.M. Coluccio, *New insights into the regulation of the actin cytoskeleton by tropomyosin.* Int Rev Cell Mol Biol, 2010. **281**: p. 91-128.

185. Chauhan, V., L. Ji, and A. Chauhan, *Anti-amyloidogenic, anti-oxidant and anti-apoptotic role of gelsolin in Alzheimer's disease.* Biogerontology, 2008. **9**(6): p. 381-389.

186. Krukenberg, K.A., T.O. Street, L.A. Lavery, and D.A. Agard, *Conformational dynamics of the molecular chaperone Hsp90.* Q Rev Biophys, 2011. **44**(2): p. 229-255.

187. Liu, X.B. and K.D. Murray, *Neuronal excitability and calcium/calmodulin-dependent protein kinase type II: location, location, location.* Epilepsia, 2012. **53 Suppl 1**: p. 45-52.

188. Ngo, S.T., P.G. Noakes, and W.D. Phillips, *Neural agrin: a synaptic stabiliser.* Int J Biochem Cell Biol, 2007. **39**(5): p. 863-867.

189. Tristan, C., N. Shahani, T.W. Sedlak, and A. Sawa, *The diverse functions of GAPDH: views from different subcellular compartments.* Cell Signal, 2011. **23**(2): p. 317-323.

190. Miller, A.F., *Superoxide dismutases: ancient enzymes and new insights.* FEBS Lett, 2012. **586**(5): p. 585-595.

191. Waudby, C.A., T.P. Knowles, G.L. Devlin, J.N. Skepper, H. Ecroyd, J.A. Carver, M.E. Welland, J. Christodoulou, C.M. Dobson, and S. Meehan, *The interaction of alphaB-crystallin with mature alpha-synuclein amyloid fibrils inhibits their elongation.* Biophys J, 2010. **98**(5): p. 843-851.

192. Chin, S.S. and J.E. Goldman, *Glial inclusions in CNS degenerative diseases.* J Neuropathol Exp Neurol, 1996. **55**(5): p. 499-508.

193. Outeiro, T.F., J. Klucken, K.E. Strathearn, F. Liu, P. Nguyen, J.C. Rochet, B.T. Hyman, and P.J. McLean, *Small heat shock proteins protect against alpha-synuclein-induced toxicity and aggregation.* Biochem Biophys Res Commun, 2006. **351**(3): p. 631-638.

194. Bruinsma, I.B., K.A. Bruggink, K. Kinast, A.A. Versleijen, I.M. Segers-Nolten, V. Subramaniam, H.B. Kuiperij, W. Boelens, R.M. de Waal, and M.M. Verbeek, *Inhibition of alpha-synuclein aggregation by small heat shock proteins.* Proteins, 2011. **79**(10): p. 2956-2967.

195. Rekas, A., C.G. Adda, J. Andrew Aquilina, K.J. Barnham, M. Sunde, D. Galatis, N.A. Williamson, C.L. Masters, R.F. Anders, C.V. Robinson, R. Cappai, and J.A. Carver, *Interaction of the molecular chaperone alphaB-*

crystallin with alpha-synuclein: effects on amyloid fibril formation and chaperone activity. J Mol Biol, 2004. **340**(5): p. 1167-1183.

196. Rekas, A., L. Jankova, D.C. Thorn, R. Cappai, and J.A. Carver, *Monitoring the prevention of amyloid fibril formation by alpha-crystallin. Temperature dependence and the nature of the aggregating species.* FEBS J, 2007. **274**(24): p. 6290-6304.
197. Riedel, M., O. Goldbaum, and C. Richter-Landsberg, *alpha-Synuclein promotes the recruitment of tau to protein inclusions in oligodendroglial cells: effects of oxidative and proteolytic stress.* J Mol Neurosci, 2009. **39**(1-2): p. 226-234.
198. El-Agnaf, O.M., S.A. Salem, K.E. Paleologou, L.J. Cooper, N.J. Fullwood, M.J. Gibson, M.D. Curran, J.A. Court, D.M. Mann, S. Ikeda, M.R. Cookson, J. Hardy, and D. Allsop, *Alpha-synuclein implicated in Parkinson's disease is present in extracellular biological fluids, including human plasma.* FASEB J, 2003. **17**(13): p. 1945-1947.
199. Lee, H.J., S. Patel, and S.J. Lee, *Intravesicular localization and exocytosis of alpha-synuclein and its aggregates.* J Neurosci, 2005. **25**(25): p. 6016-6024.
200. Liu, J., J.P. Zhang, M. Shi, T. Quinn, J. Bradner, R. Beyer, S. Chen, and J. Zhang, *Rab11a and HSP90 regulate recycling of extracellular alpha-synuclein.* J Neurosci, 2009. **29**(5): p. 1480-1485.
201. Lee, S.J., *Origins and effects of extracellular alpha-synuclein: implications in Parkinson's disease.* J Mol Neurosci, 2008. **34**(1): p. 17-22.
202. Liu, J., Y. Zhou, Y. Wang, H. Fong, T.M. Murray, and J. Zhang, *Identification of proteins involved in microglial endocytosis of alpha-synuclein.* J Proteome Res, 2007. **6**(9): p. 3614-3627.
203. Kim, C. and S.J. Lee, *Controlling the mass action of alpha-synuclein in Parkinson's disease.* J Neurochem, 2008. **107**(2): p. 303-316.
204. Danzer, K.M., L.R. Kranich, W.P. Ruf, O. Cagsal-Getkin, A.R. Winslow, L. Zhu, C.R. Vanderburg, and P.J. McLean, *Exosomal cell-to-cell transmission of alpha synuclein oligomers.* Mol Neurodegener, 2012. **7**(1): p. 42.
205. Ahn, K.J., S.R. Paik, K.C. Chung, and J. Kim, *Amino acid sequence motifs and mechanistic features of the membrane translocation of alpha-synuclein.* J Neurochem, 2006. **97**(1): p. 265-279.

206. Sung, J.Y., J. Kim, S.R. Paik, J.H. Park, Y.S. Ahn, and K.C. Chung, *Induction of neuronal cell death by Rab5A-dependent endocytosis of alpha-synuclein.* J Biol Chem, 2001. **276**(29): p. 27441-27448.

207. Konno, M., T. Hasegawa, T. Baba, E. Miura, N. Sugeno, A. Kikuchi, F.C. Fiesel, T. Sasaki, M. Aoki, Y. Itoyama, and A. Takeda, *Suppression of dynamin GTPase decreases alpha-synuclein uptake by neuronal and oligodendroglial cells: a potent therapeutic target for synucleinopathy.* Mol Neurodegener, 2012. **7**(1): p. 38.

208. Kalwy, S.A. and R. Smith, *Mechanisms of myelin basic protein and proteolipid protein targeting in oligodendrocytes (review).* Mol Membr Biol, 1994. **11**(2): p. 67-78.

209. Larocca, J.N. and A.G. Rodriguez-Gabin, *Myelin biogenesis: vesicle transport in oligodendrocytes.* Neurochem Res, 2002. **27**(11): p. 1313-1329.

210. Kramer, E.M., A. Schardt, and K.A. Nave, *Membrane traffic in myelinating oligodendrocytes.* Microsc Res Tech, 2001. **52**(6): p. 656-671.

211. Haynes, C.M., S. Caldwell, and A.A. Cooper, *An HRD/DER-independent ER quality control mechanism involves Rsp5p-dependent ubiquitination and ER-Golgi transport.* J Cell Biol, 2002. **158**(1): p. 91-101.

212. Caldwell, S.R., K.J. Hill, and A.A. Cooper, *Degradation of endoplasmic reticulum (ER) quality control substrates requires transport between the ER and Golgi.* J Biol Chem, 2001. **276**(26): p. 23296-23303.

213. Kincaid, M.M. and A.A. Cooper, *ERADicate ER stress or die trying.* Antioxid Redox Signal, 2007. **9**(12): p. 2373-2387.

214. Kincaid, M.M. and A.A. Cooper, *Misfolded proteins traffic from the endoplasmic reticulum (ER) due to ER export signals.* Mol Biol Cell, 2007. **18**(2): p. 455-463.

215. Cooper, A.A., A.D. Gitler, A. Cashikar, C.M. Haynes, K.J. Hill, B. Bhullar, K. Liu, K. Xu, K.E. Strathearn, F. Liu, S. Cao, K.A. Caldwell, G.A. Caldwell, G. Marsischky, R.D. Kolodner, J. Labaer, J.C. Rochet, N.M. Bonini, and S. Lindquist, *Alpha-synuclein blocks ER-Golgi traffic and Rab1 rescues neuron loss in Parkinson's models.* Science, 2006. **313**(5785): p. 324-328.

216. Haynes, C.M., E.A. Titus, and A.A. Cooper, *Degradation of misfolded proteins prevents ER-derived oxidative stress and cell death.* Mol Cell, 2004. **15**(5): p. 767-776.

217. Jensen, D. and R. Schekman, *COPII-mediated vesicle formation at a glance.* J Cell Sci, 2011. **124**(Pt 1): p. 1-4.

218. Szul, T. and E. Sztul, *COPII and COPI traffic at the ER-Golgi interface.* Physiology (Bethesda), 2011. **26**(5): p. 348-364.

219. Miller, E.A. and C. Barlowe, *Regulation of coat assembly--sorting things out at the ER.* Curr Opin Cell Biol, 2010. **22**(4): p. 447-453.

220. Smith, W.W., H. Jiang, Z. Pei, Y. Tanaka, H. Morita, A. Sawa, V.L. Dawson, T.M. Dawson, and C.A. Ross, *Endoplasmic reticulum stress and mitochondrial cell death pathways mediate A53T mutant alpha-synuclein-induced toxicity.* Hum Mol Genet, 2005. **14**(24): p. 3801-3811.

221. Sugeno, N., A. Takeda, T. Hasegawa, M. Kobayashi, A. Kikuchi, F. Mori, K. Wakabayashi, and Y. Itoyama, *Serine 129 phosphorylation of alpha-synuclein induces unfolded protein response-mediated cell death.* J Biol Chem, 2008. **283**(34): p. 23179-23188.

222. Turnbull, L. and J.H.T. Power. *Peroxiredoxin 4 is confined to the endoplasmic reticulum in human brain and associated with Lewy body formation in Parkinson's disease and dementia with Lewy bodies*. in *Proceedings of the Australian Physiological Society*. 2010.